FAST ROOM-TEMPERATURE CURING POLYURETHANE-BASED HYDROGELS FOR MEDICAL APPLICATIONS

Inaugural-Dissertation

zur

Erlangung des Doktorgrades

Der Mathematisch-Naturwissenschaftlichen Fakultät

der Universität zu Köln

vorgelegt von

Lana Kortenbrede

aus Köln

Köln, 2024

Erstgutachter:	Prof. Dr. Axel G. Griesbeck
Zweitgutachterin:	Prof. Dr. Annette Schmidt
Drittgutachter:	Prof. Dr. Marc Leimenstoll

Tag der mündlichen Prüfung: 06.09.2024

Abstract

Postoperative adhesions represent a frequent complication after intra-abdominal surgeries and are associated with long-term side effects such as chronic pain, infertility in women, and life-threatening intestinal obstructions. Available adhesion prophylaxis products often show limitations in applicability or efficacy. In this dissertation, hydrogels that cure rapidly (<60 sec) at room temperature were developed, fulfilling the requirements for such a sensitive application. Their application is enabled by spraying a two-component (2K) system. A hexamethylene diisocyanate (HDI) terminated prepolymer (**prepolymer-1**) was selected as the starting material to identify a suitable crosslinking reaction for producing rapidly curing 2K hydrogels. Corresponding synthetic modifications were carried out to investigate four different crosslinking technologies with respect to their reaction kinetics. The isocyanate-amine reaction, forming urea, was identified as a suitable crosslinking technology. Various hydrogel formulations were optimized in terms of viscosity, adhesion behavior, biocompatibility and biodegradability. The latter required the implementation of biodegradable groups into the polyol backbone. Using a design of experiments (DoE), formulation parameters were varied to establish a structure-property relationship with important analytical target variables. This allowed the identification of an optimized formulation, which was further characterized regarding the curing reaction, resulting viscoelastic properties, hydrolytic degradation and mechanical properties such as tensile strength, compression behavior, molecular weight between crosslinks, and resulting mesh size. Biochemical properties such as cytotoxicity, cell adhesion, invasion and migration were investigated as measurable parameters to determine the effectiveness as an adhesion barrier. The formulation was adapted for sprayability with CO_2 and investigated in an *in vivo* efficacy model, revealing a lack of barrier effect and a suspected lack of biocompatibility. The latter was confirmed in a further study. Subsequent cytotoxicity investigations reflected this effect in gel extracts from day 8 onwards, consisting predominantly of degradation products, as well as in the hydrogels on day 14. Non-biodegradable systems based on **prepolymer-1** displayed no cytotoxic effect, supporting the hypothesis that the observed toxicity was caused by the degradation products. Therefore, the hydrogels presented here are initially limited to the use of non-biodegradable systems.

Kurzfassung

Postoperative Adhäsionen stellen eine häufige Komplikation nach intraabdominalen Eingriffen dar und sind mit Langzeitfolgen wie chronischen Schmerzen, Unfruchtbarkeit bei Frauen, sowie lebensbedrohlichen Darmverschlüssen assoziiert. Verfügbare Adhäsionsprophylaxe-Produkte weisen oft Einschränkungen in der Anwendbarkeit oder Wirksamkeit auf. Im Rahmen der vorliegenden Dissertation wurden bei Raumtemperatur schnell aushärtende Hydrogele entwickelt, welche die Anforderungen für eine derartig sensible Anwendung erfüllen und deren Applikation durch Versprühen eines Zwei-Komponenten(2K)-Systems ermöglicht wird. Als Startsubstanz wurde ein Hexamethylendiisocyanat (HDI) terminiertes Präpolymer (**Präpolymer-1**) ausgewählt, um eine geeignete Vernetzungsreaktion zu identifizieren, welche die Herstellung von schnell härtenden (<60 sec.), 2K Hydrogelen ermöglicht. Entsprechende synthetische Modifikationen wurden durchgeführt um vier unterschiedliche Vernetzungstechnologien hinsichtlich ihrer Reaktionsgeschwindigkeit zu untersuchen. Die Isocyanat-Amin-Reaktion unter Bildung einer Harnstoffgruppe wurde als geeignete Vernetzungstechnologie identifiziert. Verschiedene Hydrogel-Formulierungen wurden hinsichtlich Viskosität, Adhäsion, Biokompatibilität und Abbaubarkeit optimiert. Letzteres erforderte die Implementierung abbaubarer Gruppen in das Polyol-Grundgerüst. In der Verwendung eines statistischen Versuchsplans (DoE) wurden Parameter der Formulierung variiert, um eine Strukturwirkungsbeziehung zwischen diesen und wichtigen analytischen Zielgrößen herzustellen. Hierdurch konnte eine optimierte Formulierung identifiziert werden, welche weiterhin hinsichtlich der Aushärtungsreaktion, der resultierenden viskoelastischen Eigenschaften, des hydrolytischen Abbaus sowie der mechanischen Eigenschaften wie Zugfestigkeit, Kompressionsverhalten, Molekulargewicht zwischen Vernetzungspunkten und der daraus folgenden Maschenweite charakterisiert wurde. Zudem wurden die biochemischen Eigenschaften wie Zytotoxizität, Zelladhäsion sowie -invasion und -migration als messbare Parameter zur Bestimmung der Effektivität als Adhäsionsbarriere untersucht. Die Formulierung auf die Versprühbarkeit mit CO_2 angepasst und in einem *in vivo* Effektivitätsmodell untersucht. Hierin wurde eine fehlende Barrierewirkung festgestellt, sowie eine mangelnde Biokompatibilität vermutet. Letzteres konnte in einer weiteren Studie bestätigt werden. Nachträgliche Zytotoxizitätsuntersuchungen spiegelten diesen Effekt in Gelextrakten ab dem achten Tag und in den Hydrogelen am vierzehnten Tag wider. Nicht-abbaubare Systeme, basierend auf **Präpolymer-1**, zeigten keinen zytotoxischen Effekt. Dies unterstützt die Hypothese, dass die aufgetretene Toxizität durch die Abbauprodukte hervorgerufen wurde. Daher sind die hier präsentierten Hydrogele zunächst auf die Verwendung von nicht-abbaubaren Systemen beschränkt.

Table of Content

List of Abbreviations

(α-) STP	(Alpha-) silane terminated prepolymer
L_0	Length of an initial sample
$MW_{crosslinker}$	Molecular weight crosslinker
$MW_{prepolymer}$	Molecular weight prepolymer
$P_x(\mathrm{NCO})$	Molecular amount of x-mer
V_0	Volume KOH for blank sample
V_{sample}	Volume KOH for sample titration
f_{NCO}	Functionality NCO component
f_{OH}	Functionality OH component
$l_{C-\mathrm{C}}$	Length C-C bond
l_{C-O}	Length C-O bond
l_{chain}	Length of a polymer chain
$m_{initial}$	Mass of an initial hydrogel sample
$m_{swollen}$	Mass of a swollen hydrogel sample
n_{C-C}	Amount of C-C bonds
n_{C-O}	Amount of C-O bonds
n_{NCO}	Mol NCO
n_{OH}	Mol OH
1K	One component
2K	Two component
3D	Three-dimensional
A	Area
ANOVA	Analysis of variance
ATR	Attenuated total reflection
AV	Amine value
BSA	Bovine serum albumine
C	Concentration
Ca^{2+}	Calcium ion
C_n	Flory characteristic ratio
CO_2	Carbon dioxide
CTR	Control
d	Diameter
Đ	Dispersity
D_2O	Deuterium oxide

DBA	Dibutyl amine
DBP	Dibutyl phosphate
dH_2O	Distilled H_2O
DLS	Dynamic light scattering
DMA	Dynamic mechanical analysis
DMC	Double metal cyanide
DoE	Design of experiments
E	E modulus
EO	Ethylene oxide
Eq.	Equivalent
ε	Strain
f	Functionality
F	Force
G’	Storage modulus
G’’	Loss modulus
GAG	Glycosaminoglycan
GPC	Gel permeation chromatography
h	Hours
HA	Hyaluronic Acid
HCl	Hydrochloride acid
HDI	Hexamethylene diisocyanate
HEMA	Hydroxyethyl methacrylate
HOMO	Highest occupied molecule orbital
HPC	Hydroxypropyl cellulose
Hz	Hertz
IAP	Intraabdominal pressure
KOH	Potassium hydroxide
kPa	Kilo pascal
K_w	Equilibrium constant of water
L	Liter
L	Length of a stretched sample
LCST	Lower Critical Solution Temperature
LUMO	Lowest unoccupied molecule orbital
LVER	Linear viscoelastic region
M	Molar concentration Mol/L
m	Mass

M_c	Molecular weight between two crosslinks
MHz	Mega Hertz
min.	Minute
mL	Milliliter
mm	Milimeter
Mol.%	Mole percent
mPa*s	Millipascal second
M_r	Molecular weight of repeating unit
MTT-assay	Metabolic activity assay
M_W	Molecular weight
n.d.	Not determined
N/mm²	Newton per square milimeter
N_2	Nitrogen
NaCl	Sodium chloride
NaOH	Sodium hydroxide
NCO	Isocyanate group
NH_2	Primary amine group
NL	Normliter
nm	Nanometer
NMR	Nuclear magnetic resonance
OFAT	One factor at a time
OH	Hydroxy group
OHZ	Hydroxy number
PBD	Posphate buffered saline
PEG	Polyethylene glycol
pH	Potential of hydrogen
PLA	Poly lactic acid
PNIPAM	Poly N-isopropyl acrylamide
PO	Propylene oxide
pOH	Potential of hydroxide
PPG	Polypropylene glycol
ppm	Parts per million
PU	Polyurethane
PU-U	Polyurethane-urea
PVME	Poly (vinyl methyl ether)
R	Universal gas constant

r	Molar ratio OH/NCO
R/R²	Regression/squared regression
RG	Reactive Group
RSD	Relative standard deviation
RT	Room temperature
SD	Standard deviation
sec.	Seconds
SPE	Short path evaporator
T	Temperature
Tanδ	Loss factor
TAV	Total acidic value
T_g	Glass transition temperature
TI	Test item
UCST	Upper critical solution Temperature
v	wavenumber
$v_{2,r}$	Polymer volume fraction in the relaxed state
$v_{2,s}$	Polymer volume fraction in the swollen state
v_e	Crosslink density
Wt.-%	Weight percent
XRD	X-ray diffraction
ξ	Mesh size
ρ	Density
σ	Stress
X_1	Polymer solvent interaction parameter
γ	Shear rate

1 Introduction

The human body represents an excellently coordinated system, remarkably adapted to its environment. Within this complex system, one observes impressive processes and materials. A prime example is the human eye, a highly sensitive apparatus. The vitreous humor, the principal component of the eye, consists of 98-99.7% water, our physiological solvent.[1,2] The remaining 2-0.3% is occupied by fibrillar proteins, predominantly collagen fibers in mammals, providing a fibrillar structure. Additionally, glycosaminoglycans (GAG), predominant hyaluronic acid (HA), are present introducing chargeable sites and therefore leading to a swelling of the whole system. This renders the vitreous humor a form of hydrogel. Remarkably, upon closer inspection of the eyeball, one would not suspect its solid content to be at 2%. Interestingly, this eyeball also exhibits certain mechanical properties that would not be expected from a network at such a low concentration.

Hydrogels are encountered in many other areas of the body such as extracellular matrices or as tendons. Therefore hydrogels are also available as a natural material class, based on the macromolecules providing a swelling pressure, like HA or gelatin.[3] According to the classic definition a hydrogel is a three-dimensional (3D) network capable of storing a large amount of water without getting into solution itself.[4] Due to the 3D arrangement, hydrogels also have certain mechanical properties as we can observe them in the eyeball. This makes hydrogels ideal materials that can get by with little solid content and still comprising mechanical stability.

They are used in various applications, such as wound dressings, contact lenses or for drug delivery systems, as well as tissue engineering and regenerative medicine.[3,5–7] In the swollen state, hydrogels are spongy materials and thus facilitate the diffusion of potentially embedded drugs. This property represents a further advantage, as it is particularly useful in medical applications.[8] Both, contact lenses and wound dressings, are already widely used as drug delivery systems.[9–11]

Adhesion prophylaxis is a special form of wound dressing and can be regarded as an implant. It is applied to the patient after a surgery and is intended to reduce the formation of postoperative adhesions. The formation of adhesions is induced by the wound healing cascade itself, illustrated in Figure 1.

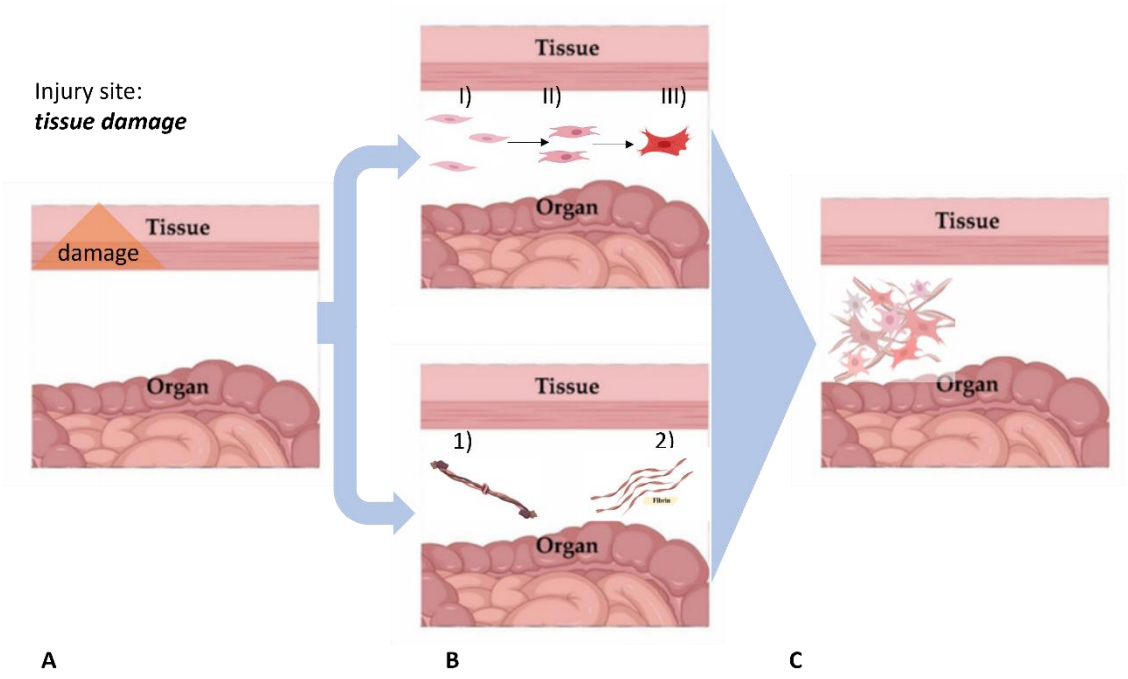

Figure 1 Illustration of the wound healing process after tissue injury caused by the surgery process itself. A) Arrangement of the abdomen under normal conditions. The orange triangle depicts the tissue injuring site. B) above: the tissue injuring site leads to a release of hormones and interleukins responsible for the growth of fibroblasts (I) and further on activation of fibroblasts (II) and differentiation to myofibroblasts (III). Below: fibrinogen (1) is synthesized as a result of the proinflammatory surrounding which is split by thrombin to fibrin (2), representing a physiological glue. Both processes take place in parallel. As depicted in C) a complex of myofibroblasts and fibrin is formed, responsible for the wound healing, but is not limited to seal wounds inflicted by the surgery processes. The complex can also adhere to other tissue and therefore leads to formation of postoperative adhesions. Illustration modified and adapted from Ref. [12] (CC BY license).

The tissue injury induced by the surgery process itself leads to the release of hormones and proinflammatory interleukins like cytokines, which activate the growth of fibroblasts and myofibroblasts (connective tissue cells). These cell types are the building blocks of wound closure and form the subsequent scar tissue. In addition, fibrinogen, a precursor of our physiological adhesive, is released and split by thrombin into fibrin. A complex consisting of fibroblasts, myofibroblasts as well as fibrin can form outgrowths which do not only seal the wound but also occur between tissue and organ, or organ and organ which represents the adhesion formation process, as illustrated in Figure 1.[12] Depending on the study, the prevalence of outgrowth of postoperative adhesions varied between 63-97% of all surgeries in which the abdomen is opened (laparotomy).[13–15] These adhesions partially recede. Nevertheless, the majority of patients with adhesions are affected by long-term side effects such as chronic pain, infertility in women or intestinal obstruction.[13] Although there are products on the market, they show insufficient efficacy or are cumbersome in their handling.[16,17] In addition to the synthesis and characterization of chemically and physically crosslinked hydrogels, a subordinate objective of this work is to establish a system which can be used as an *in situ* crosslinking hydrogel and thus serves as adhesion prophylaxis.

2 Task Definition and Solution Strategy

Postoperative adhesions are defined as bonds that occur between surfaces within body cavities which range from thin films of connective tissue to thick fibrous bridges that comprise blood vessels and nerve tissue.[18,19] The formation process has been described in more detail in chapter 1. Less invasive surgical methods such as laparoscopic procedures are not sufficient to completely prevent the occurrence of postoperative adhesions. Thus, adhesion prophylaxis is required and can be provided by a barrier material which is placed between the affected tissue and adjacent organs to prevent them from growing together. If possible, laparoscopic procedures are favored in surgical practice, as their use is less intrusive to patients.[20] Thus, a sprayable adhesion prophylaxis is favored which can be designed suitable for laparoscopic procedures. Several products serving as adhesion prophylaxis are available on the market, but are cumbersome in their handling[17], limited in their efficacy[21] or unsuitable for laparoscopic practice.[16] The aim of this thesis is the development of a sprayable, polyurethane based and fast curing hydrogel formulation and moreover the investigation thereof regarding the chemical crosslinking concept and important properties of the resulting material for its use as a laparoscopic adhesion prophylaxis product. Requirements for such a system will be described in detail in chapter 3.3, Table 5. A general concept for the development approach is presented in Figure 2, wherein RG represents a chemical reactive group.

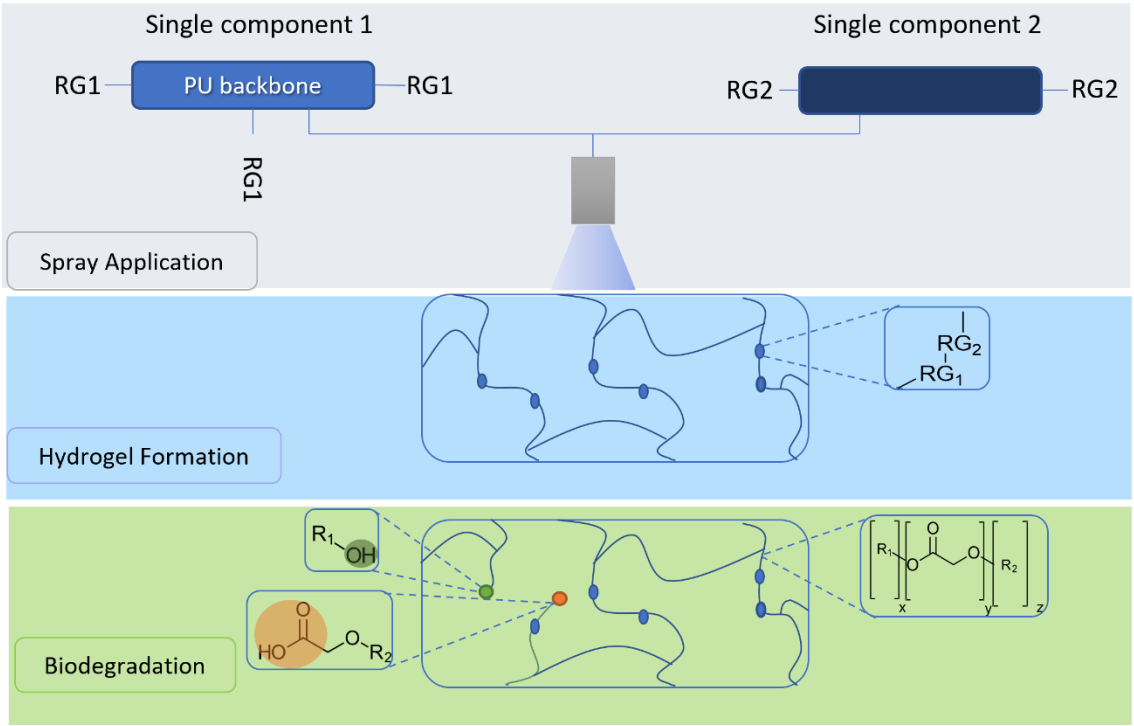

Figure 2 Illustration of a general concept for an *in situ* fast room temperature crosslinking hydrogel network divided in three stages. *Spray Application*: single component (SC) 1 and SC 2 will be provided in single aqueous solutions which will be applied on the surface *via* spray application using spray nozzles with overlapping spray jets as mixing area. *Hydrogel formation*: mixing of SC1 and SC2 is provided by the overlapping spray jets to allow a fast curing of both reactants to form the 3D network by the reaction of RG1 and RG2 *in situ*. Biodegradation: in the backbone of either SC1 and or SC2 hydrolysable groups will be implemented to design the system as biodegradable. Most common groups are ester units which will be hydrolyzed into carboxylic acids and alcohols. By a hydrolysis of the covalent bonds, the network starts to degrade and will be fully dissolved at a certain point in time.

The process of applying a sprayable barrier can be divided into three stages: *spray application, hydrogel formation* and *biodegradation*.

To accomplish crosslinking, at least one of the single components needs to feature a functionality (*f*) >2. It was decided to use a prepolymer, which exhibits *f*=3 as a starting point for all further modifications.

The material class of polyurethanes is described as highly biocompatible and safe for different biomedical applications[22–24] and was therefore chosen as the basic structure for a hydrogel system. For each approach, pathways were developed to combine the respective crosslinking chemistry of RG1 and RG2 with polyurethane chemistry. All reaction routes start from a trifunctional hexamethylene diisocyanate (HDI)-capped-prepolymer (**prepolymer-1**) which is based on a polyether polyol with *f*=3. Starting on glycerol (2wt.-%) this polyether (**polyether-3**) is synthesized *via* ring-opening polymerization of ethylene oxide (EO) (71wt.-%) and propylene oxide (27wt.-%). This chemical composition was chosen to allow the swelling in water by incorporating a high amount of EO groups as they are known to provide a huge swelling.[25] To avoid crystallization effects, a defined amount of PO was also imbedded into the polyol. Due to toxicological concerns, it was decided to use exclusively aliphatic diisocyanates. Residual aromatic diisocyanate monomers may hydrolyze to the corresponding amines, which are known to be toxic and cancerogenic.[26] It was decided to start with HDI.

The prepolymer is synthesized as described in chapter 6.3 and the general structure is reported in Figure 3.

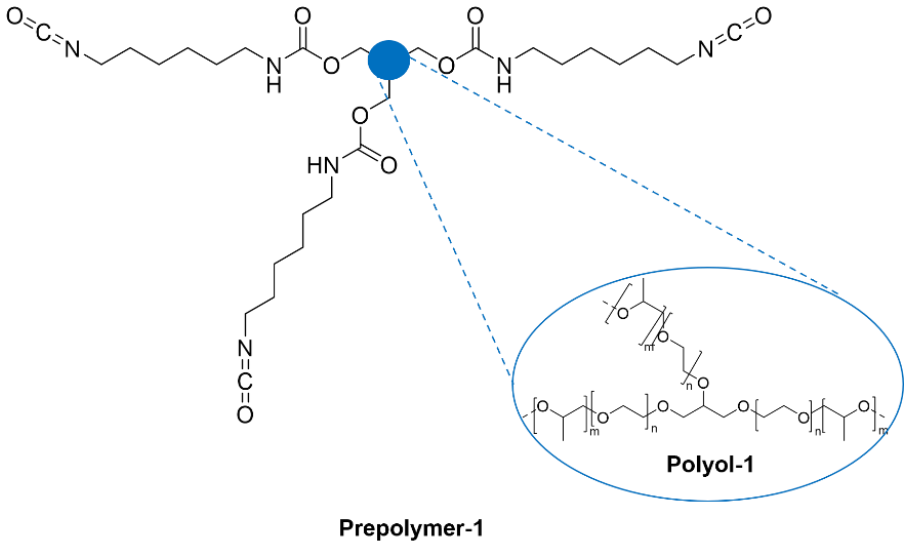

Figure 3 Illustration of the general structure of an aliphatic based **prepolymer-1** as initial reactant for further chemical modifications. The blue sphere depicts the polyol backbone of the prepolymer **polyol-1** which consists of glycerol as starter added in main parts to EO units (n) to obtain a high water solubility and additionally a small amount of PO units (m) to avoid crystallization between the EO segments.

Spray application

To allow an application *via* spraying, the viscosity of the initial single components is limited to max. 9 mPa*s. Since only a few compounds comprise such a low viscosity as a raw material, single components need to be diluted in aqueous systems. Therefore, the substances need to comprise a certain water solubility which is also necessary to absorb a large amount of water in the hydrogel network. Single components in aqueous solutions are prepared separately. Afterwards they will be mixed by an outer mixing spray applicator system as depicted schematically in Figure 4.

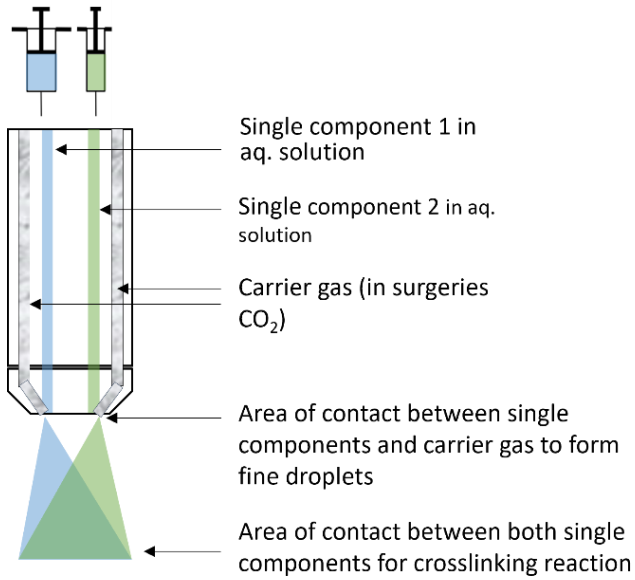

Figure 4 Illustration of a spray applicator used for applying the hydrogel formulation on a surface. Single component 1 and 2 provided in aqueous solutions, are forwarded to the spray nozzles and are then formed into fine droplets by support of a carrier gas. Both spray nozzles are arranged so that both spray nebulas are overlapping. This process depicts the mixing of the two components. As a result, the crosslinking takes place on the surface. By this, blockages by precuring of the gel within the channels are avoided.

Both single components are provided in aqueous solutions and are forwarded by single channels to the spray nozzles. By the use of a carrier gas the solutions are dispersed into very fine droplets. In surgeries CO_2 is used exclusively since it is known to avoid formation of embolisms, a sudden blocking of an artery.[27] The spray nozzles are arranged in a way that both spray jets are overlapping to allow a mixing and therefore a crosslinking of both single components.

In the subsequent development process of the hydrogel formulations, spray experiments with the use of carbon dioxide (CO_2) as carrier gas have been conducted. The use of CO_2 as carrier gas strongly influences the physico-chemical properties of the hydrogel formulations, which is why they had to be adapted for spraying with CO_2. This special feature will be discussed in chapter 4.2.6. All other formulations are adjusted to the use of inert gases (here: nitrogen, compressed air).

Hydrogel formation

One of the main requirements, which will be presented in chapter 3.3, addresses the curing time, which needs to be in the range of sec. (<60 sec.). Fast curing reactions from the group of cycloadditions, click-chemistry, condensations and/or polyadditions and physical crosslinking will be described in detail in chapter 3.4. The four main categories which will be considered for crosslinking reactions were *imine formation*, *alkoxy silane condensation*, *polyaddition* and *thermoresponsive curing*. These four testing approaches were named approaches HYGEL1-4. A brief summary of each chemical concept is presented in Figure 5.

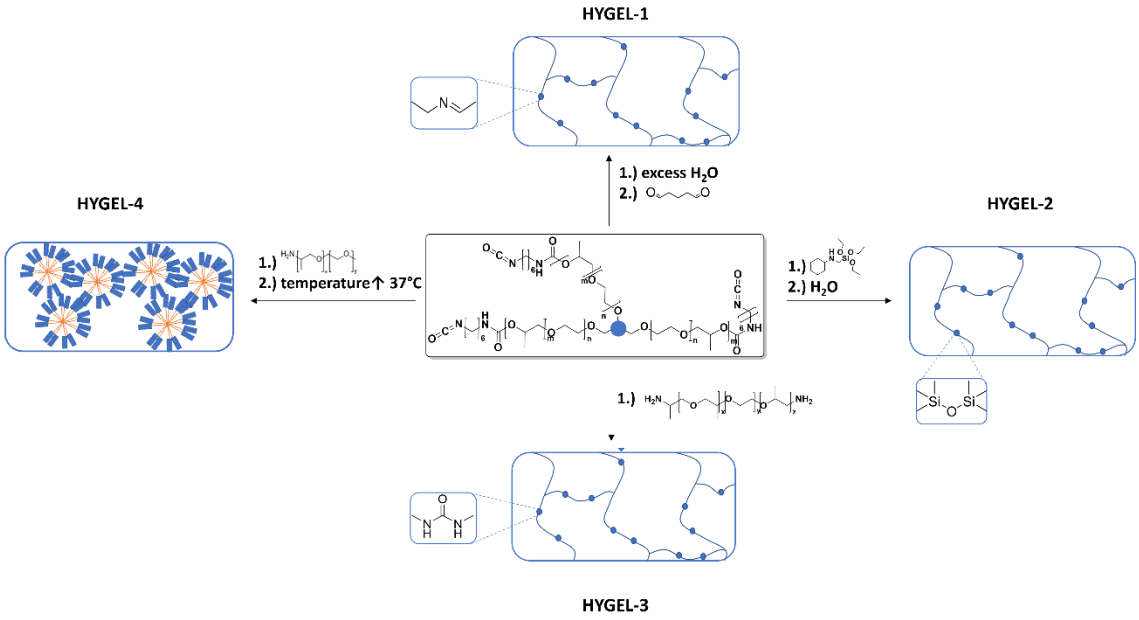

Figure 5 Illustration of the different curing approaches (HYGEL1-4) derived from **prepolymer-1**. Modification agents and/or crosslinks, if applicable, are listed on the arrows.

The underlying chemical concepts and the resulting networks are described in more detail below.

HYGEL-1: crosslinking via imine formation

Starting from **prepolymer-1**, an amine can be generated by a highly diluted solution of **prepolymer-1** in water. The NCO groups undergo hydrolysis, yielding the unstable carbamic acid intermediate, which subsequently decomposes with the elimination of CO_2 to afford the primary amine. High dilution prevents further reaction of the primary amines with residual NCO groups forming crosslinked urea. Subsequently, water can be removed from the aqueous solution in order to concentrate the resulting primary amine, for the crosslinking reaction with glutaraldehyde, as presented in Figure 6, which is known for its fast reaction speed.[28]

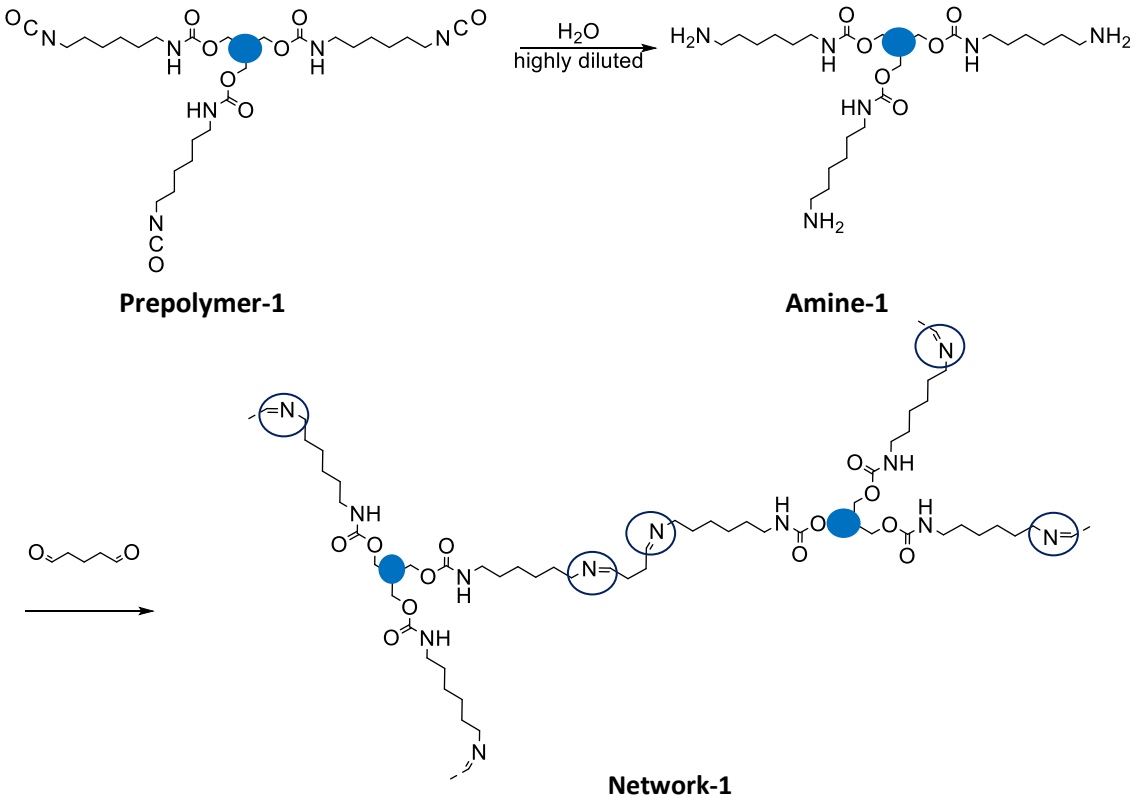

Figure 6 Reaction pathway to obtain primary **amine-1** with *f*=3 from **prepolymer-1** as starting point. **Prepolymer-1** will be highly diluted (2wt.-%) in water to avoid crosslinking of already hydrolyzed primary amines (NH_2 groups) to remaining NCO groups to predominantly obtain **amine-1**. After a concentration step of **amine-1**, glutaraldehyde (**COO-1**) will be added to induce the crosslinking reaction by an imine formation. Imine crosslinks are circled in blue.

The hydrogel formation *via* imine crosslinking is illustrated in Figure 7. A primary amine with *f*=3 derived from **prepolymer-1** is used herein with Glutaraldehyde (**COO-1**) used as an aldehyde starting material due to known fast crosslinking behavior by the discussed literature. Both reactants will be provided in aqueous solutions.[28]

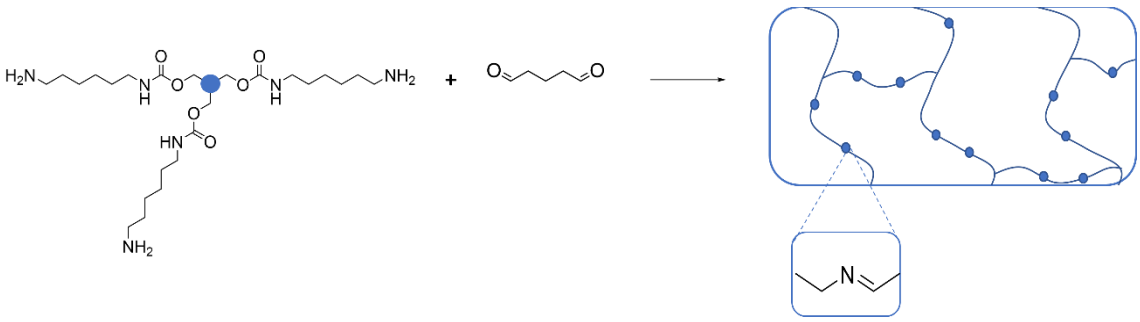

Figure 7 Illustration of a possible network obtained by imine formation as a result from the reaction of primary amines and aldehydes. The blue circles depict the crosslinking points.

If this crosslinking reaction can be carried out as illustrated, **COO-1** will be replaced with a macromolecular aldehyde in order to reduce potential toxicity. Regarding small molecule aldehydes, it is known that their cytotoxic behavior is relatively high. Suggestions regarding the mechanism behind their toxicity have been published.[29] Even if commercially available glutaraldehyde

(Bioglue®) is used, it is only stated to be non-toxic when bonded to the NH_2 groups of bovine serum album (BSA) which is used for crosslinking.[28] The incorporation of an aldehyde into a macromolecular compound would therefore represent a suitable method to decrease the toxic potential of such a curing agent.[30]

HYGEL-2: crosslinking via alkoxy silane condensation

Prepolymer-1 will be used as a starting material and will be modified with ethoxy silane as chain ends. Amine containing ethoxy silanes can be attached to isocyanates *via* urea formation, as demonstrated in Figure 8. **EtOSi-1** was chosen for the modification as it provided three alkoxy silanes in α position which are known for their enhanced reaction kinetics *via* condensation process.[31]

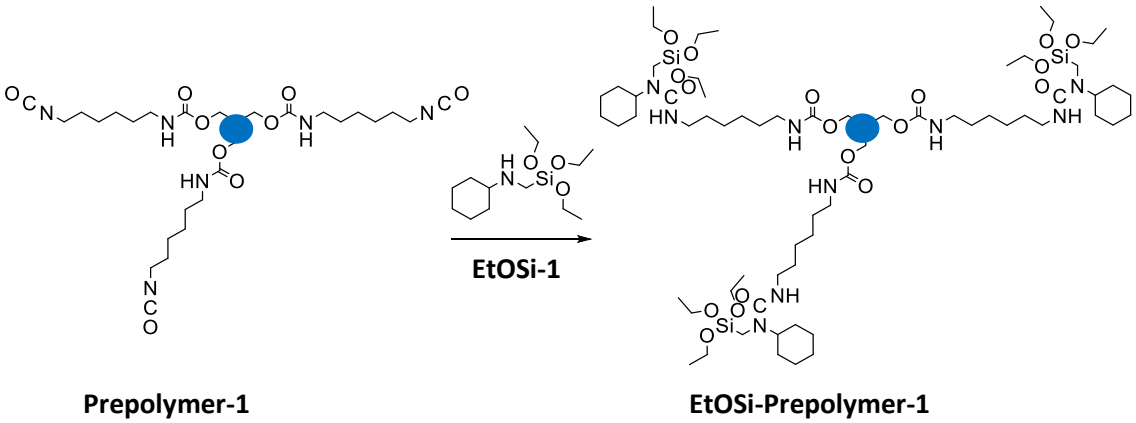

Figure 8 Reaction route for the implementation of an ethoxysilan group (*here*: **EtOSi-1**) to the chain ends of **prepolymer-1** to obtain an α-silane terminated prepolymer (α-STP) as **EtOSi-Prepolymer-1**.

After the functionalization with **EtOSi-1** the obtained substance is moisture sensitive. By adding a small amount of water, the condesation reaction starts immediately to form **network-2** as a resulting network, illustrated in Figure 9. Crosslinks are circled in blue. The condensation reactions of alkoxy silanes in the presence of water will be described in detail in chapter 3.4.

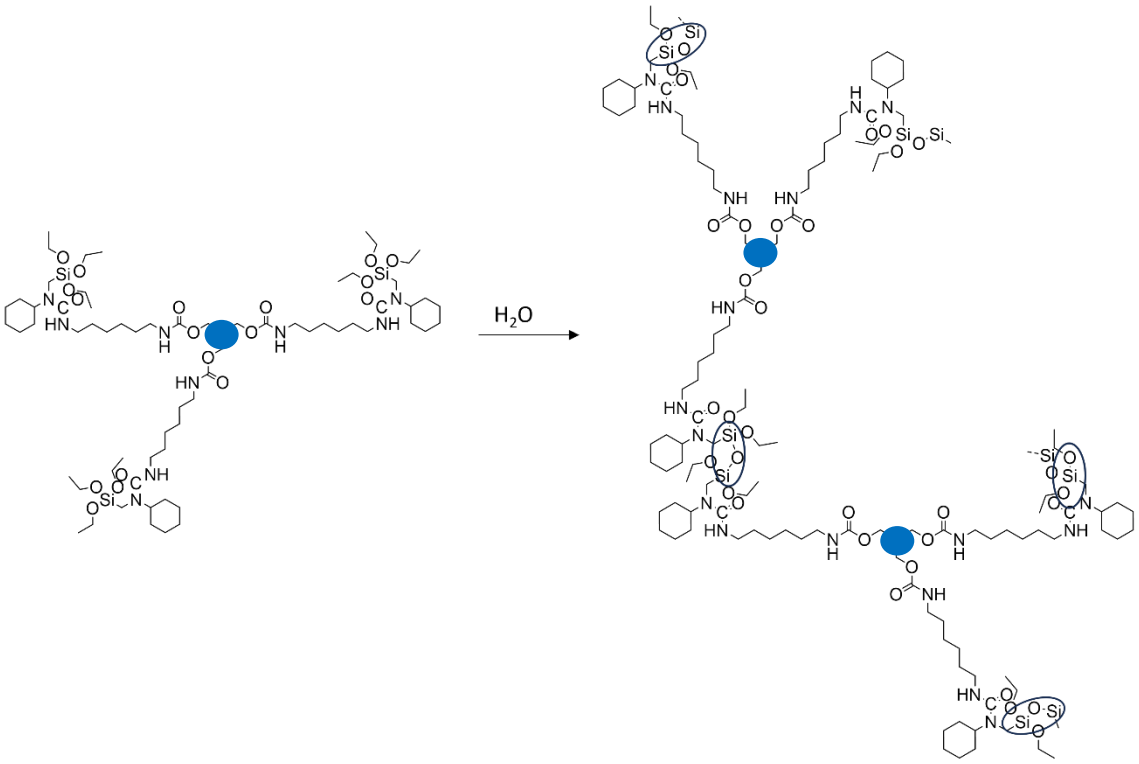

EtOSi-Prepolymer-1 **Network 2**

Figure 9 Water induced condensation reaction, yielding **network-2** as a hydrogel network. Crosslinks are circled in blue and schematically depicted as one crosslink per one **EtOSi-1** molecule. Probably there will be more than one crosslink on one **EtOSi-1** molecule as the silane carries three ethoxy groups. Since the reaction of **EtOSi-1** is directly induced by the presence of water no second curing agent is necessary. The application of such a system would therefore differ from the presented general concept in Figure 2.

HYGEL-3: crosslinking via polyaddition of NCO and NH_2

HYGEL-3 approach is based on a simple addition of a primary amine group to the NCO groups of **prepolymer-1**, as presented in Figure 10. For this reaction primary amines were chosen as reactants since they are described as the fastest reaction partner of NCO groups,[32] forming urea groups as crosslinks. A highly EO based diamine was used as crosslinker to provide water solubility (**Jeffamine ED2003**). For this crosslinking mechanism **prepolymer-1** will be used without further modification.

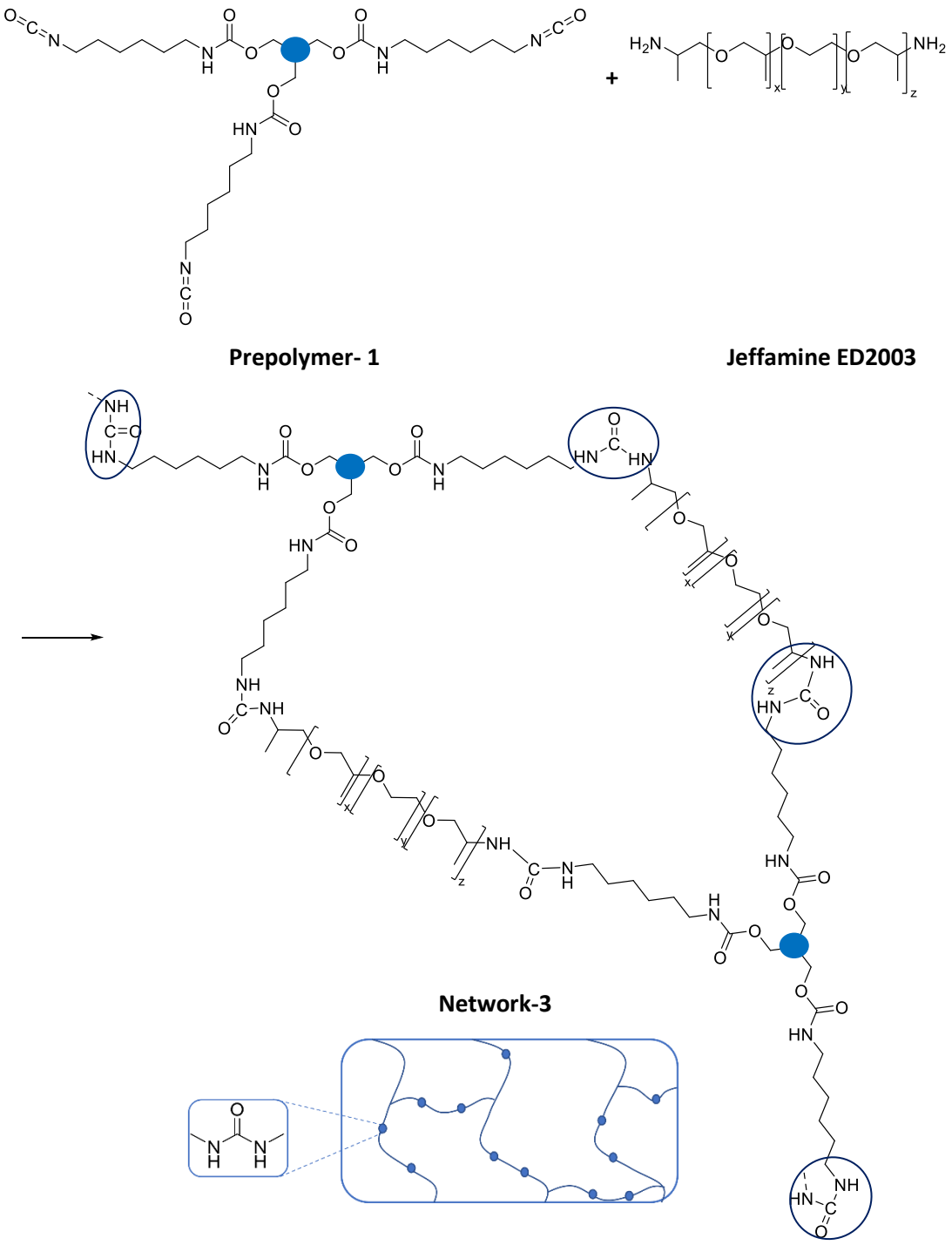

Figure 10 Reaction route to for the crosslinking mechanism of **prepolymer-1** with **Jeffamine ED2003** to obtain **network-3** as a resulting hydrogel network. Urea groups are formed as crosslinking groups and are circled in blue.

HYGEL-4: physical crosslinking via thermoresponsive curing

In contrast to all other approaches HYGEL-4 relies on a physical gelation mechanism and a conventional second component as crosslinking agent will not be used. The parameter which induces the gelation behavior is temperature.

Since fluctuating EO/PO blocks are known to behave in a thermoresponsive manner[33], it was decided to conduct the modification with an amine-capped polyol with *f*=1. Especially the amine polyether **Jeffamine M2005** is of interest, since the monofunctional polyether is described in

the literature to exhibit thermoresponsive behavior.[34] Moreover, a *f*=2 prepolymer with a high PO content will be synthesized and two more polyether types with *f*=1 (**polyether 25** and **34**) will be used as modification agents for both prepolymers, **prepolymer-1** and **prepolymer-thermo**. In sum, six different macromolecules will be obtained which will be analyzed with regard to a potential thermoresponsiveness. By introducing monofunctional amines, NCO groups were modified to urea groups, additionally further EO/PO groups are introduced at the chain ends to obtain large building blocks which can arrange as described in chapter 3.1.2. The reaction route to obtain **809** as a possible network precursor is presented in Figure 11.

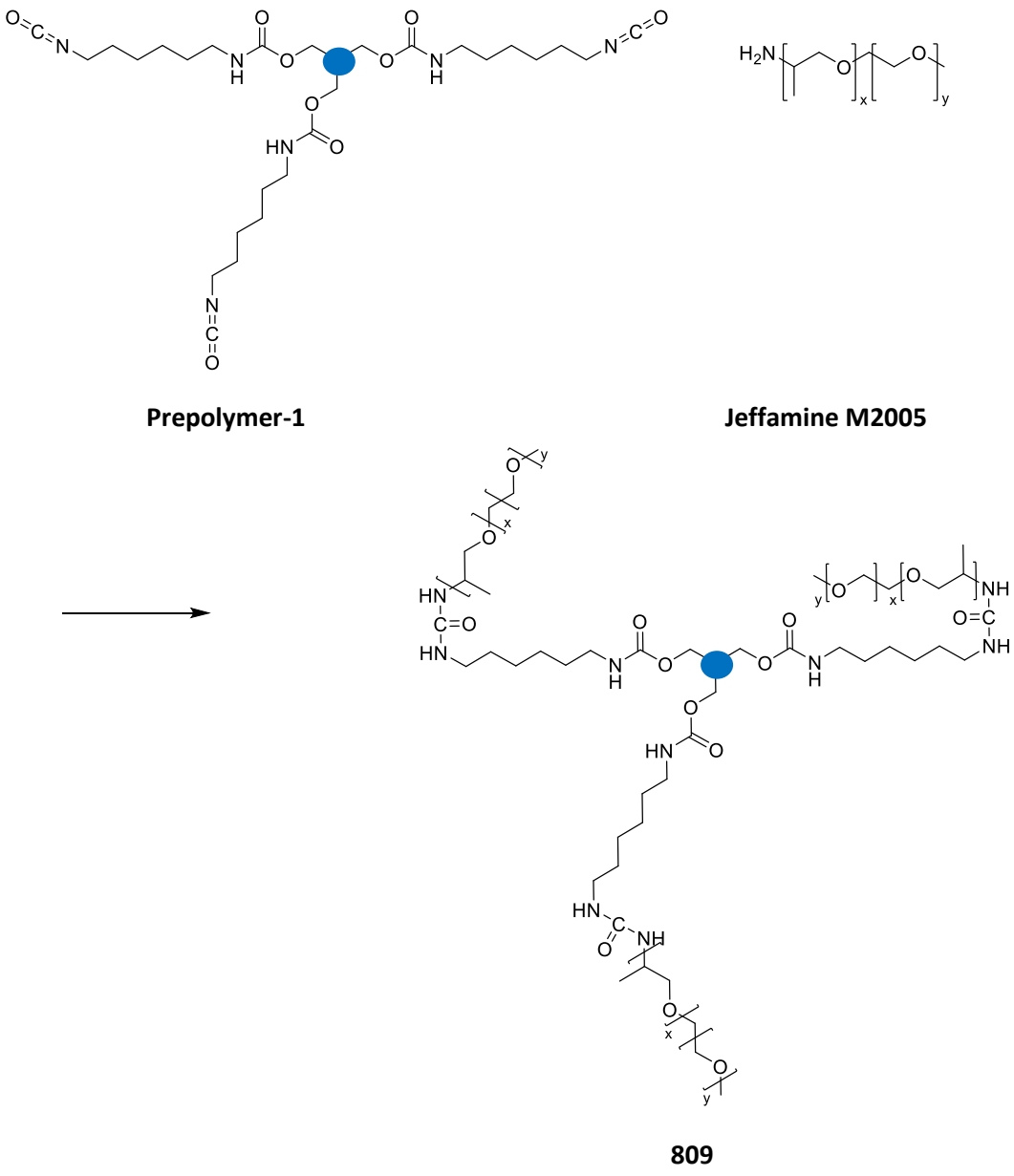

Prepolymer-1 **Jeffamine M2005**

809

Figure 11 Reaction route for the synthesis of a macromolecule containing probably thermoresponsive chain ends to allow a gelation in an environment of 37°C. **Prepolymer-1** as basic prepolymer is modified with **Jeffamine M2005**, a monofunctional EO and PO based Polyether which is known to behave in a thermoresponsive manner. While it is soluble in water at 4°C, it starts to precipitate at higher temperature and a dispersion is obtained. The mechanism for thermoresponsive gelation is described in chapter 3.1.2.

All four approaches (HYGEL1-4) will be initially tested in chapter 4.1 and the concept, which will be identified as most suitable will be addressed in chapter 4.2 considering the remaining requirements from Table 5.

Biodegradation

The hydrogel system needs to provide biodegradability, otherwise a second surgery would be necessary to remove the barrier material. Since all four screening approaches (HYGEL1-4) were started from **prepolymer-1**, the implementation of biodegradable sites is irrespective of the latter identified crosslinking reaction.

The incorporation of biodegradable sites is mostly achieved by the implementation of hydrolysable ester groups into the polymeric backbone. Ester units can later be hydrolyzed, either by pure water or by catalysis of enzymes.[35] Lactide[36], glycolide[37] and caprolactone[38] units are common building blocks for the implementation, but also copolymers[39–41] of them can be used. The incorporation of these units is often achieved by condensation methods.[42,43] Since the herein presented polyols are manufactured by a ring-opening polymerization process, only cyclic ester groups can be implemented to avoid a chain termination. The mechanism which is evaluated as suitable for the polyol synthesis is illustrated in Figure 12, where glycerol, which represents the starting material of **prepolymer-1**, as OH-containing substance attacks the carbonylic carbon which leads in the following reaction cascade to a ring opening of the cyclic dilactide unit. The terminated OH-group is able to further react with other electrophilic compounds. Methods for the manufacturing have already been described.[44] Starters with a larger molecular weight will also be used.

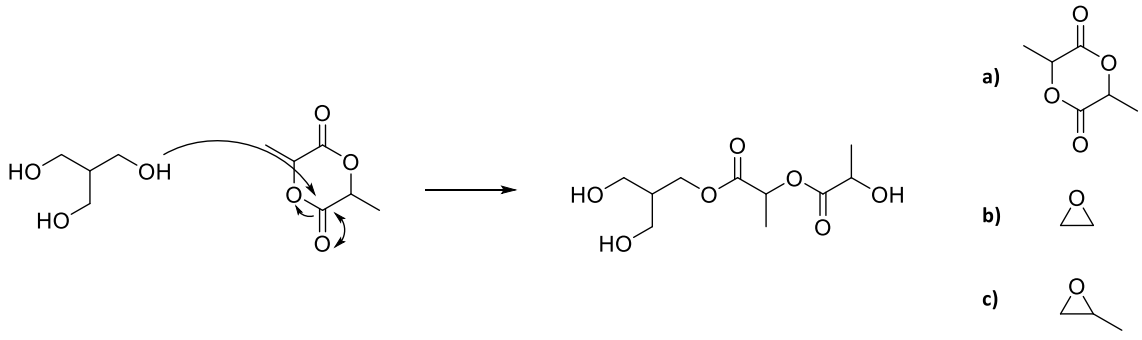

Figure 12 Reaction of glycerol as starter with a cyclic dilactide unit. The ring opening is obtained by a reaction of an OH-group of the glycerol with the carbonylic carbon. By the ring opening, an OH group is localized at the chain end which can further react with the different building blocks, present during the polyol synthesis a) dilactide b) ethylene oxide (EO) and c) propylene oxide (PO)

Dilactide units were chosen as a starting point for the investigation of biodegradability.

In addition, an intense investigation of structure-property relationships of the resulting hydrogels will be conducted to address the remaining requirements from Table 5 in a downstream process. Advanced biochemical tests will be conducted to investigate the adhesion preventing potential *in vitro* and moreover in *in vivo* studies.

3 State of the Art

Since advanced hydrogels for medical application, as well as polyurethane based materials are common topics, there is a huge input of research and development results into the addressed scientific community. A selection of relevant topics, regarding the chemistry and the application development addressed in this thesis, is presented in this chapter.

3.1 Hydrogels

Hydrogels are 3D networks capable of absorbing a large amount of water without getting into solution themselves.[4] The ability to absorb high amounts of water can be influenced by the implementation of hydrophilic groups into the hydrogel matrix like -OH, -COOH, -CONH, -SO_3H.[45] On a macromolecular scale the incorporation of polyethylene glycol (PEG) or natural polysaccharides provide a certain swelling.[2,25] Depending on the crosslinking mechanism, at least one of the network forming agents needs to exhibit *f* greater 2, to avoid dissolution of the matrix and obtain a 3D network. The network spans the entire gel which makes the molecular weight infinite. The crosslinks of a network can be derived from different mechanisms as will be presented in chapter 3.3. On a practical level gels can be described by rheological measurements. To describe the formation of a hydrogel network in a solvent, the sol-gel theory can be considered, as presented in Figure 13. Crosslinking agents are in solution at first steps (sol). By affinity of these agents to each other or an external trigger, like pH value or salt concentration, the agents start to react and to form oligomers as precursors of a network. At a certain degree of crosslinking the network already spans a large part of the solution, while oligomers and monomers are still present and the gelation process is still ongoing. This state of the gelation process represents the threshold at which the properties of the solution rapidly change. This point is defined as the critical gel point. The end of the gelation process is reached when reactants are fully converted into the gel network. Single monomers or oligomers can remain embedded in the network structure causing possible network defects.[45]

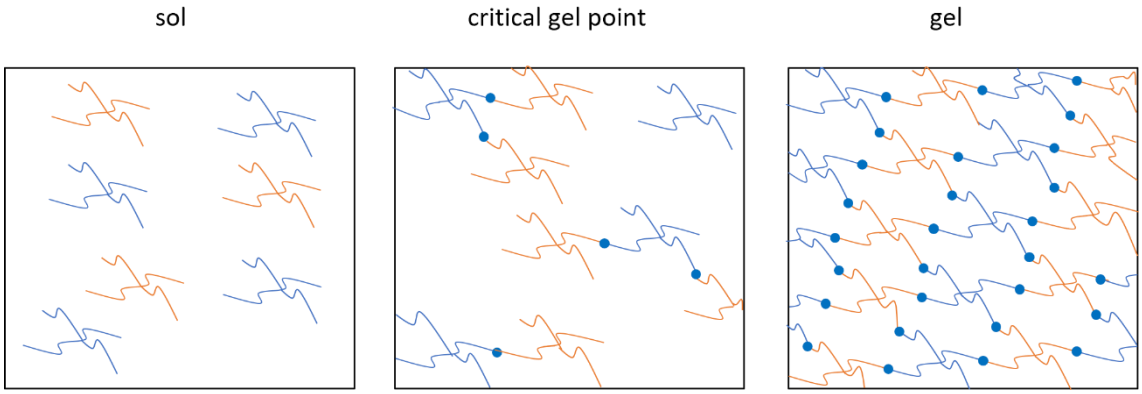

Figure 13 Illustration of the gel formation process in solution. In the sol exclusively monomers are present which start to react directly or by an external trigger leading to oligomers and smaller networks. At a certain point of gelation, properties of the solution rapidly change which is stated to be the critical gel point. Gelation is still ongoing, leading to a network which spans the entire sol and yields a gel.

There are two major types of network defects which can occur during the hydrogel formation as illustrated in Figure 14. A) the formation of inactive rings or loops occurs when a crosslinker is attached to the same crosslinking site. B) loose and dangling ends, attached only by one side to the network with an unreacted linker site. The presence of network defects is not critical in general but needs to be considered for estimation of crosslink density and mesh size, which is an important parameter for different applications like drug delivery or cell migration.

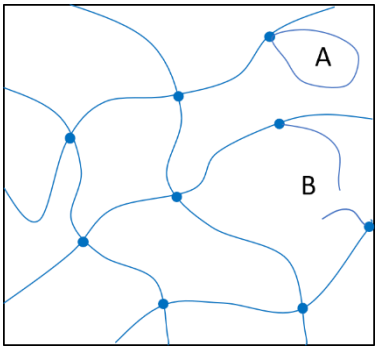

Figure 14 Depiction of two major network defects of a network with *f*=4 for each crosslink. A) Formation of inactive loops by attaching two reaction sites to one crosslinking site. B) Loose and dangling ends attached only by one site to the network leaving the other site unreacted. Illustration inspired by Ref. [45]

Hydrogels are often used in medical applications because they mimic the environment of the human body by high water retention and this leads to an increase in biocompatibility.[46] Common applications for medical hydrogels include contact lenses, wound dressings, tissue engineering and drug delivery.[3,5,7] To allow a high absorption of water into the hydrogel matrix the presence of hydrophilic groups is necessary. Common raw materials used for the manufacturing of hydrogels are listed in chapter 3.1.1.

3.1.1 Materials used for the Manufacturing of Hydrogels

The definition of a hydrogel already provides information about which important characteristics materials should have in order to be used as starting substances. They should be highly hydrophilic, showing significant swelling effects with *f*>2 in order to create a 3D network which enables the molecular weight to increase infinitely. Substances utilized for the manufacturing of hydrogels can be divided into natural and synthetic materials. Table 1 presents an overview on common materials.

Table 1 Overview on natural and synthetic derived polymers used for the manufacturing of hydrogels. Table adopted from Ref.[47]

Natural Polymers	Monomers for the Corresponding Synthetic Polymers
Alginate	Hydroxyethyl methacrylate (HEMA)
Chitosan	Hydroxyethoxyethyl methacrylate
Collagen	Hydroxydiethoxyethyl methacrylate
Cellulose	Methoxyethyl methacrylate
Chitin	Methoxyethoxyethyl methacrylate
Dextran	Methoxydiethoxyethyl methacrylate
Hyaluronic Acid	Ethylen glycol dimethacrylate
Gelatin	N-vinyl-2-pyrrolidone
Fibrin	Poly N-isopropyl acrylamide (PNIPAM)
DNA	Vinyl acetate
	Acrylic acid
	N-(2-hydroxypropyl) methacrylamide
	Ethylen glycol (EG)
	PEG
	PEG acrylate
	PEG methacrylate
	PEG diacrylate
	PEG dimethacrylate
	Methacrylic acid

Synthetic hydrogels were first described in 1960 by Wichterle *et al*. and publications rapidly increased over the last past years.[46,48] The most important representatives of the class of synthetic polymers as starting substances for hydrogels are HEMA, widely used in for contact lenses[49] and PNIPAM[50] or acrylamide-co-acrylonitrile[51,52] due to their thermoresponsive behavior of lower critical solution temperature (LCST) and upper critical solution temperature type, respectively.

The importance of polyurethanes as a substrate for the manufacturing of hydrogels also increased over the last years, which are reported to be useful in the manufacturing of wound dressings[53] or for drug delivery systems.[54] However, in comparison to the well-established acrylamides and acrylates from Table 1, polyurethane display a subordinate role in the preparation of hydrogels.

3.1.2 Gelation Mechanisms of Hydrogels

As well as the choice of raw materials for hydrogel preparation, the mechanism of the gelation behavior can be chosen. Gelation mechanisms can be divided into chemical and physical crosslinking. Figure 15 illustrates a selection of possible intermolecular interactions, leading to the formation of hydrogels. While Figure 15A represents the covalent crosslinking reaction, Figure 15B-D illustrates physical crosslinking mechanisms.

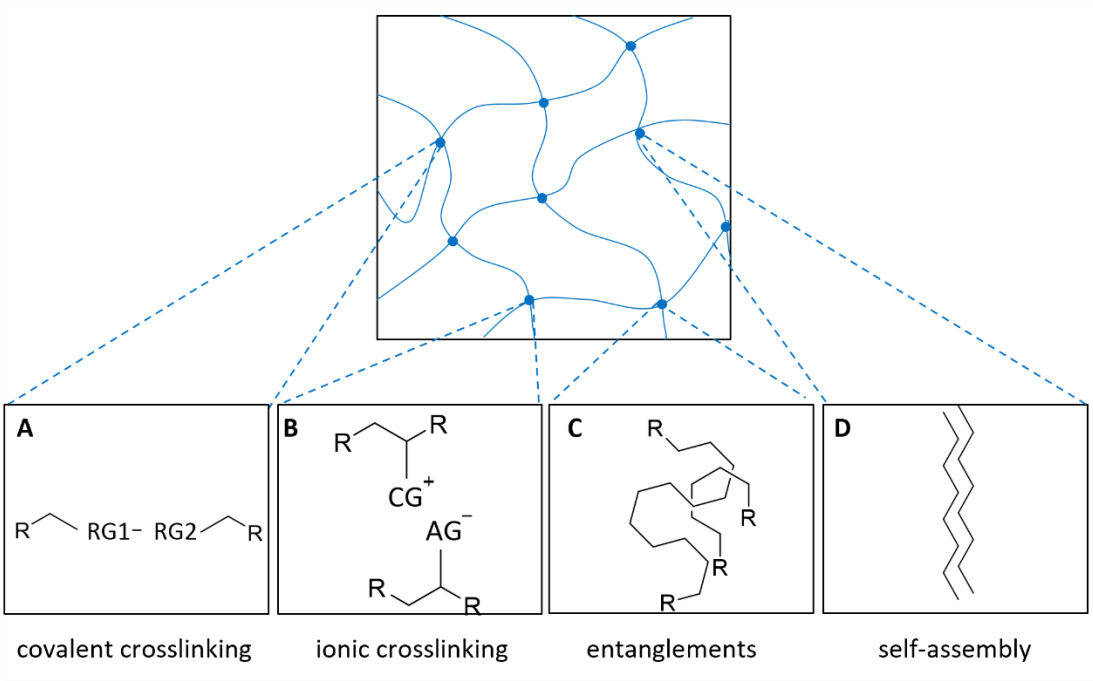

Figure 15 Overview of a selection of crosslinking mechanisms to obtain 3D networks. A) covalent crosslinking results in mechanical stable networks as the covalent bonds are relatively strong in comparison to physical crosslinking. B) ionic crosslinking as a physical crosslinking option, gelation can be triggered externally for example by pH value adjustment or salt concentration.[55] C) Entanglements are a special form of crosslinking and is often used additionally to e.g. increase mechanical properties as described for rotaxane.[56] D) Self-assembling is induced by the molecular structure and the corresponding interactions itself. One famous example is the secondary structure of amino acid based proteins which can take several formations like beta-sheet or alpha-helix. Our DNA is based on bases and sugars but also shows a self-assembling behavior.[57] This mechanism can be used to induce a gelation effect.[58]

Covalent crosslinking **A** requires a chemical reaction between reactive group (RG) 1 and RG 2 to form covalent bonds, responsible for the formation of a 3D network. Covalent crosslinked hydrogels are often synthesized using monomers or prepolymers that contain reactive functional groups, such as acrylates, methacrylates,[59] or vinyl groups.[59,60] These functional groups can undergo polymerization and crosslinking reactions in the presence of initiators, crosslinking agents, or other reactive species. They often consist of two components but can also be created from one component systems. Isocyanate prepolymers are examples for one component covalent crosslinked hydrogels. The hydrolysis of the NCO component leads to the formation of primary amines (NH_2) under elimination of carbon dioxide (CO_2). The resulting NH_2 groups react with not-yet hydrolyzed NCO groups to form urea linkages.

In comparison to covalently crosslinked hydrogels, physical crosslinking options are based on interactions between the two crosslinking species. Possible physical interactions leading to the formation of hydrogels can be ionic interactions as illustrated in **B** and are described in several publications, like for alginate based hydrogels.[61–63] The strength of the ionic interactions in combination with the special egg shape obtained by the alginate and Ca^{2+} reaction provides a certain mechanical stability.[64] Another physical crosslinking option is the implementation of entanglements into the hydrogel network as depicted in **C**. This type of crosslinking is frequently employed as a supplementary mechanism in dual-cured systems. Rotaxane-based hydrogels are examples of this type of crosslinking approach. These hydrogels based on linear polymers are interlocked by cyclic structures, that represent the 3D crosslinks since they can behave as flexible linkers due to their high mobility.[65,66] A common substance for rotaxanes are cyclodextrins which are cyclic oligosaccharides, able to imbed small molecules or short domains of linear molecule chains.[67,68] **D** illustrates the self-assembling process in general, which can also be used to create a 3D network. Self-assembling as an overarching concept encompasses different mechanisms which always assume a certain arrangement to each other, like organized structures or patterns due to a natural attraction. Until now, there is no uniform definition of this concept, so that also arrangements due to ionic interactions could be regarded as a form of self-assembly. A specific form of self-assembly which is exploited in this thesis is self-assembly of thermoresponsive polymers induced by a temperature change. Thermoresponsive polymers drastically change their physical properties due to a small temperature change. Although different physical properties may be affected, most research has focused on polymers that change their solubility in a solvent. These polymers exhibit a miscibility gap that either displays a lower or upper critical solution temperature (LCST or UCST). For this thesis polymers that exhibit this behavior in water as solvent are of interest.[69,70] Most common polymer classes with LCST-type miscibility gap are PNIPAM, hydroxypropyl cellulose (HPC), polypropylene glycol (PPG), poly vinyl methyl ether (PVME).[71,72] But also polymers based on PO and EO units, especially EO/PO block copolymers, are described to behave in a thermoresponsive manner.[33,73] Poloxamers are a class of EO/PO block copolymers, invented by BASF and known under trade names like Pluronic® or Kolliphor®. Since block copolymers consist of separated areas of EO and PO, the water solubility of the blocks differs. PO units are known to be less soluble in water and PPG blocks display a lower critical solution type miscibility gap in water while polymeric EO (PEO) blocks remain water-soluble between 0-100°C. To reduce the free energy at the interfaces of the system, PPG blocks aggregate when the LCST type demixing temperature is exceeded.[74] As a result PO units are located at the core of the micelle, while highly water soluble EO blocks are located at the outer shell. Additionally EO blocks tend to crystallize[75] and are reported to be at 60-80% crystallinity state present in pure PEO.[76] This effect also occurs between two outer shells of the micelles and can be used to induce a gelation behavior.[33,74] The energy input, provided by temperature increase, serves as activation energy to induce crystallization effect. The formation process is presented in Figure 16.

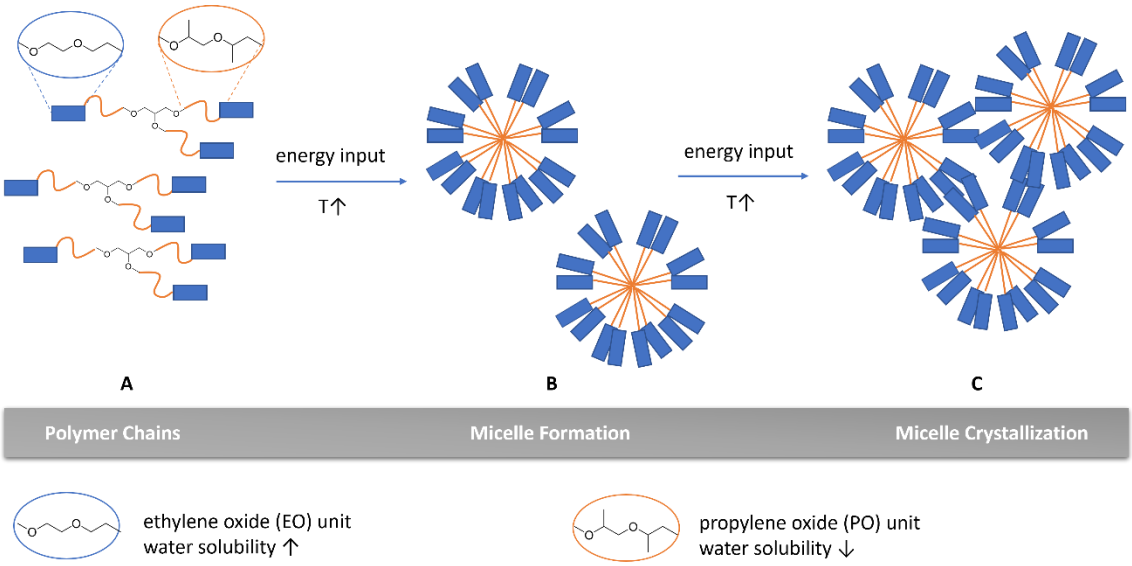

Figure 16 Illustration of the underlying concept of a thermoresponsive behavior of ethylenoxide (EO) and propylenoxide (PO) units within one polymer chain. **A**) The blue blocks depict the EO areas while the orange lines depict the PO areas. Both substances differ in their water solubility. **B**) By a temperature increase above the LCST-type demixing temperature, PPG-blocks aggregate to form PO areas and EO to EO areas in aqueous solutions. While the hydrophilic EO areas are located at the outer shell of the micelle, the hydrophobic PO areas are located to the core. **C**) Further energy input leads to a crystallization of the micelles at the outer EO regions which is responsible for the gelation effect. Figure illustrated in accordance with Ref.[33]

Since the introduction of EO and PO units into a polyol backbone, used for the manufacturing of polyurethane is a common technique, this class of LCST-type thermoresponsive substance is of special interest for the preparation of polyurethane hydrogels. The depicted mechanisms were described for EO-PO block copolymers, but are applicable for statistic polymers, as well.

3.1.3 Physico-chemical Properties of Hydrogels

Hydrogels are 3D networks allowing the uptake of high amounts of water without getting into solution themselves. Thus, hydrogels display large degrees of swelling, when being environed in aqueous solutions. The swelling degree of a hydrogel can be of interest for specific applications, such as drug delivery and is determined according to eq. 3.1.

$$Swelling\ degree = \frac{m_{swollen}}{m_{swollen} - m_{initial}} * 100\% \qquad (3.1)$$

Hydrogels in general are reported to be able to absorb amounts of 100% up to 1000% of water without getting into solution.[77] This render these types of materials into superabsorbers.

A hydrogel manufactured from a solvent (here: water) rapidly changes its properties when reaching the critical gel point. This can be traced by rheological measurements, like viscosity which displays a strong increase when reaching the critical gel point. The rapid change of a solution into a viscoelastic material leads to an infinite increase in viscosity.[78]

Moreover, the viscoelastic properties can be analyzed to investigate the gelation behavior of a system. According to the rheological definition the gelation process can be described by the relationship between the storage modulus (G') and loss modulus (G''). For a solvent, G'' is described to be above the value of G' as viscous properties are dominating, which means that more energy is dissipated as stored within the system. When reaching the critical gel point, values of G' and G'' approximate each other until G' overcomes G'' which displays the phase transition from viscous to viscoelastic properties and is described as the gel point. In the subsequent solid-state elastic properties are dominating as more energy is stored in the system as dissipated.[79] Thus, a possible definition for the gel point is described as the point at which G'=G''.[80] Figure 17 illustrates the gel point definition based on G'/G'' crossover.

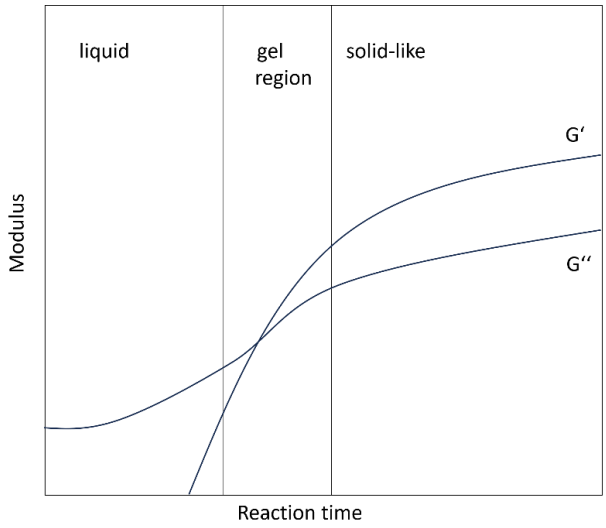

Figure 17 Schematic illustration of the dynamic mechanical behavior observed during a crosslinking reaction, described for the three present stages 'liquid', displayed by G''>>G', 'gel region', displayed by G''=G', 'solid-like', displayed by G'>>G''. Figure illustrated in accordance with Ref.[79]

Further characterization methods of hydrogels with focus on mechanical behavior are described in more detail in chapter 3.1.4.

With regard to biomedical applications, the concentration of hydrogen ions in the system, referred to as potential of hydrogen (pH), is a critical topic as acid/base balance is strictly required to enable biocompatibility.[81] In comparison to a solid matrix, diffusion of ions and molecules is enhanced in hydrogels as they consist of a large amount of water[56], leading to deviating pH values, displaying the acid-base character of substances used for manufacturing and of the resulting polymeric network. PH is an overarching parameter reflecting the acid base balance by taking the relation of concentration of H^+ and OH^- ions into account, as presented in equation 3.2.

Wherein $[H^+]$ is the concentration of the acid in pure H_2O.

$$\mathrm{pH} = -\log[\mathrm{H}^+] \tag{3.2}$$

The potential of hydroxide ions (pOH) values is in relation to the pH by maintaining the concept of auto-ionization of water, according to the chemical concept from equation 3.3.

$$H_2O \rightleftharpoons H_3O + OH^- \tag{3.3}$$

This relationship leads to equation 3.4 for the determination of the pOH and to equation 3.5 for the relationship of pOH and pH, displayed by the equilibrium constant of water K_w, from equation 3.6, presenting the dissociation of two molecules H_2O to H_3O^+ and OH^- which is 10^{-14}.

$$pOH = -\log[OH^-] \tag{3.4}$$

$$pH + pOH = 14 \tag{3.5}$$

(3.6)

$$K_w = \frac{[H_3O^+] * [OH^-]}{[H_2O]^2} = 10^{-14}$$

For the calculation of the pH or pOH, different cases can be categorized, depending on the strength of an acid or base. The most simple case is presented by a strong acid/base in pure water, wherein, the pH value is only dependent on the concentration of the acid since full dissociation of H^+ is assumed. Following this case, the pH can be calculated according to equation 3.2, the pOH subsequently *via* equation 3.5. In the case of weak acids, the pK_a value needs to be considered for the calculation of the pH, a logarithmic conversion of K_a reflecting the degree of protolysis of the analyte, which is defined in equation 3.7, wherein $[A^-]$ stands for the respective concentration of the deprotonated acid and [HA] for the concentration of protonated acid. The pK_a is utilized for the determination of pH of a weak acid in equation 3.8

$$pK_a = \log(K_a) = \log\left(\frac{[H_3O^+] * [A^-]}{[HA]}\right) \tag{3.7}$$

$$pH = \frac{1}{2}(pK_a - \log[HA]) \tag{3.8}$$

Moreover, buffer systems display an important role as they maintain pH values stable in the respective pH area for a certain amount of H^+ or OH^- ions, reflected by minor changes in pH over a certain concentration range. The pH value of a buffer can be calculated according to the *Henderson-Hasselbalch* equation, which is displayed by equation 3.9.[82]

$$pH = pK_a - log\left(\frac{[HA]}{[A^-]}\right) \tag{3.9}$$

In this thesis pH values of resulting hydrogels will be analyzed and adapted using buffer systems and diluted acid. Buffering systems will also be prepared *in situ via* CO_2 spray processes. Thus, the underlying concept is of interest.

In the former, parameters of interest have been analyzed valid for hydrogels in general. The following section focuses on the physico-chemical characterization of thermoresponsive hydrogels. Macromolecules which exhibit LCST behavior are favored for the targeted application and will be prepared based on different EO/PO contents, comparable to the underlying concept of poloxamer, wherein the gelation effect is based on aggregation of EO to EO and PO to PO blocks, as illustrated in Figure 16. Thus, the formation of aggregates as an indicator for gelation behavior can be traced. Typical measurements for identification are viscosity measurements as a function of temperature, whereby the temperature interval can be defined at which the phase transition occurs. LCST behavior would become visible by a rapid increase of viscosity.[33] Dynamic light scattering (DLS) can also be considered for the analyses of a thermoresponsive behavior induced by aggregation of macromolecules. Herein, an increase above the LCST would become visible by an increase in particle size. Both concepts are illustrated in Figure 18A (viscosity) and Figure 18B (particle size analysis) and represent measurements of sample 809 which will be investigated in chapter 4.1.5.

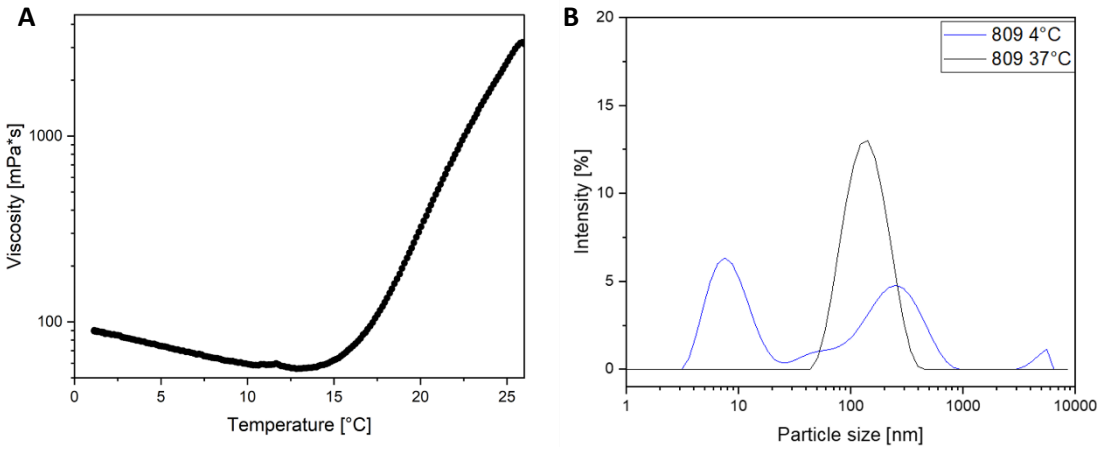

Figure 18 Methods useful for the investigation of a thermoresponsive bahavior. A) Viscosity as a function of temperature. Above the LCST the viscosity will increase caused by the gelation effect. B) Particle size analysis at different temperatures of an LCST behaving macromolecule. Particle size increases at 37°C indicating that aggregation of macromolecules is present.

Moreover, LCST behavior can be traced *via* transmittance as a solution becomes less soluble upon gelation leading to effects of turbidity.[83]

Since the macromolecules synthesized for their potential as LCST behaving substances were prepared for a defined application, analyzes of the haptic are essential to estimate their potential to serve as an adhesion prophylaxis. This includes heating of samples to 37°C and comparison to samples at room temperature.

3.1.4 Mechanical Characterization of Hydrogels

Due to their low solid content the mechanical properties of the majority of hydrogels are weak[56] in comparison to other elastomer networks, such as rubbers. This effect is usually a consequence of the solution like properties which are present in hydrogels, mainly caused by a low concentration of polymer chains and by inhomogeneity of the network.[84]

In order to be able to describe the mechanical properties of the hydrogels, methods were chosen for the characterization of the manufactured hydrogels, presented in this thesis and will be regarded in detail in this chapter.

Determination of Elongation, Tensile Strength and E-modulus

Tensile tests are a possible method for the determination of elongation at break, tensile strength at break and the E-modulus. Stress is described as σ, strain as ε, and the E-modulus or Young's modulus is described as E.[45] The tensile stress is described as the quotient of force F per area A_0, according to equation 3.10.

$$\sigma = \frac{F}{A_0} \tag{3.10}$$

The strain ε is determined as the quotient of the length of the sample in stretched state L minus the length L_0 of the initial sample, and the length of the sample in the initial state L_0 according to equation 3.11.

$$\varepsilon = \frac{L - L_0}{L_0} = \frac{\Delta L}{L_0} \tag{3.11}$$

According to Hook's law, the tensile stress σ is proportional to the strain ε as given in equation 3.12.

$$\sigma = E * \varepsilon \tag{3.12}$$

The E-modulus or Young's modulus depicted by E, is determined typically at low strains, in the region from 0.05% to 0.25%[85], since Hook's law is only valid in the linear region of the tensile curve. E indirectly represents a parameter for stiffness and correlates to the hardness of a material. The higher E, the higher stress σ needs to be applied to reach a defined strain.[86] Guide values which need to be reached with the manufactured hydrogel materials will be presented in the requirement profile in chapter 3.3, Table 5.

Determination of Loss and Storage Modulus

The viscoelastic nature of polymeric materials can be described studying G', G'' and loss factor (tanδ). These parameters are generally measured by dynamic mechanical analyses (DMA) which represents a non-destructive method for the measurement of mechanical parameters. Often temperature ramps are employed to study the temperature dependence of the moduli. A periodic low strain is applied to the sample and the resulting stress is measured. Measurement of the displacement at the peak and lag phase (δ) enables the quantification of modulus, viscosity and damping. The principle behind is presented for a stress-strain experiment in Figure 19.[87]

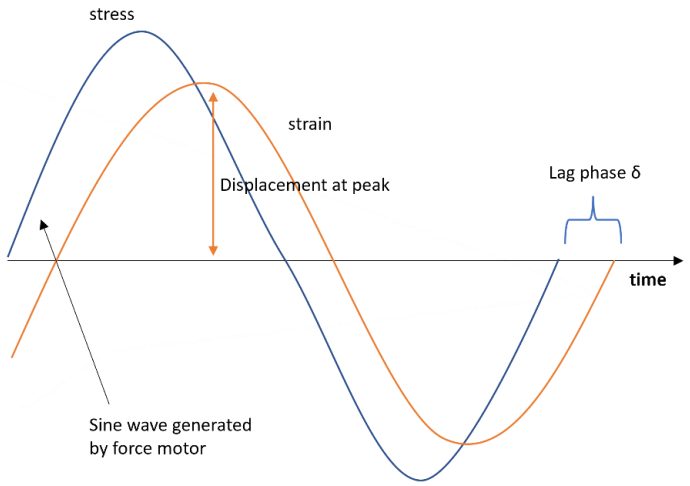

Figure 19 Simplified measurement principle of dynamic mechanical analysis (DMA) in a stress-strain experiment. A periodic stress is applied by the force motor to a sample (blue line) and the stress is measured (orange line). Measurements of the amplitude of deformation at peak of the sine wave and the lag phase (δ) enable quantification of modulus, viscosity and damping. Figure illustrated in accordance with Ref.[87]

For the characterization of hydrogels G'', G' and tanδ are parameters of interest and can be calculated *via* trigonometrical relationships from the displacement and lag phase δ. For detailed information the reader is referred to the extensive literature on this topic.[87] As described in chapter 3.1.3, G' represents the elastic moiety of a material and moreover the energy which is stored therein, while G'' represents the viscous moiety of the material and thus the energy which is lost due to inner friction. The gel point can be described at the point at which G'=G''.[80] By investigation of G' and G'' a characterization of elastic behavior of a sample is enabled, expressed by tanδ which equals 0 for ideal elastic materials and thus excludes viscous behavior, according to equation 3.13.

$$tan\delta = \frac{G''}{G'} \tag{3.13}$$

G', G'' and tanδ of materials will be analyzed *via* DMA measurements in different testing modes.

Determination of Molecular Weight between Crosslinks, Crosslink Density and Mesh Size of a Hydrogel Network

Crosslink density (v_e) is an important parameter concerning mechanical stability. Beyond that, crosslink density can be considered to influence the diffusion of smaller molecules or biologic macromolecules through a polymeric membrane like a hydrogel network.[88] The migration of larger biomolecules like cells can also be considered for estimations. V_e is determined according to equation 3.14.

$$v_e = -\frac{ln(1 - v_{2,s}) + v_{2,s} + \chi_1 v_{2,s}}{V_s\left(v_{2,s}^{1/3} - \frac{v_{2,s}}{2}\right)} \tag{3.14}$$

However, crosslink density v_e is a hardly comprehensible parameter on a practical level. A parameter closely bond to v_e is the molecular weight between two crosslinks (M_c) which allows further estimation on the resulting mesh size of the hydrogels.

Assuming an ideal network, M_c for the herein analyzed hydrogels can be described by equation 3.15.

$$M_c = \frac{1}{f}\left(MW_{prepolymer}\right) * 2 + MW_{crosslinker} \tag{3.15}$$

Wherein f is the functionality, $MW_{prepolymer}$ is the molecular weight of the component with f>2 and $MW_{crosslinker}$ represents the molecular weight of the difunctional component.

M_c can differ from the theoretical values, caused by network defects of loops or loose and dangling ends within the hydrogel network, as described in chapter 3.1. Moreover, M_c can be calculated from practical measurements. For a crosslinked polymer the storage modulus G' of the rubbery plateau is correlated with M_c. Equation 3.16 presents the correlation between G' and M_c.[89] Equation 3.16 is restricted to homogenous materials which excludes the use of a solvent, like in hydrogels in a wet stage, since this leads to varying G' values and subsequently to different M_c values.

$$M_c = \frac{RT\rho}{G'_{rubbery}} \tag{3.16}$$

Where M_c is the molecular weight between crosslinks, R is the universal gas constant, T is the absolute temperature and ρ is the density of the polymer.

It is also reported that the storage modulus of the tension mode E' in the rubbery plateau can be considered for the determination of M_c, by the assumption that E' is three times greater than G', as depicted in equation 3.17. This is valid when the poisson's ratio of the material is 0.5. For rubbery materials, like elastomers this is given.[90]

$$M_c = \frac{3RT\rho}{E'_{rubbery}} \tag{3.17}$$

A second approach for the determination of M_c is the equilibrium swelling theory according to the Flory-Rehner equation. A modification of the Flory-Rehner equation from Peppas and Merril, known as the Peppas-Merrill equation, valid for hydrogels prepared in solvents is described in equation 3.18.[91]

$$\frac{1}{M_c} = \frac{2}{M_n} - \left[\frac{v_{spec.}\left[\ln(1 - v_{2,s}) + v_{2,s} + \chi_1 v_{2,s}^2\right]}{V_1 v_{2,r}\left[\left(\frac{v_{2,s}}{v_{2,r}}\right)^{-1/3} - \left(\frac{v_{2,s}}{2v_{2,r}}\right)\right]} \right] \tag{3.18}$$

Where $v_{2,r}$ is polymer volume fraction at relaxed state, which means in the initial prepared concentration, $v_{2,s}$ is polymer volume fraction at swollen state, χ_1 is the polymer-solvent interaction parameter, V_1 is the molar volume of the solvent (for water 18 cm³/mol) M_n is the molecular weight of the monomer in the absence of a crosslinker.

Once determined the M_c of a network, the calculation of the crosslink density v_e is simplified as demonstrated in equation 3.19, wherein ρ is the density.[92]

$$v_e = \frac{\rho}{M_c} \tag{3.19}$$

In an additional step the mesh size can be calculated from the obtained M_c by the use of equation 3.20.[89]

$$\xi = v_{2,s}^{-1/3} * l \sqrt{\frac{2C_n M_c}{M_r}} \tag{3.20}$$

Where l is the bond length along the polymer backbone, C_n is the flory characteristic ratio and M_r is the molecular weight of the repeating units.

The mesh size is obtained as an average value, which complicates the estimation of its effect on network parameters, since the real size of each pore can differ from this value, as Figure 20 demonstrates. A difunctional component is cured with a trifunctional component leading either to a pore of a smaller size by forming a pore of 4+2 molecule arms or to a pore of bigger size by forming higher adducts, here 8+4 molecule arms. Thus, it is important to notice that calculated values for mesh size represent an average of all pores within the network. Local differences within the hydrogel network at different sites cannot be excluded, which makes it more complex to determine diffusion or migration behavior into or out of the network, even with known mesh size ξ. Practical application experiments are therefore necessary as a control tool for the determination of migration and diffusion behavior.

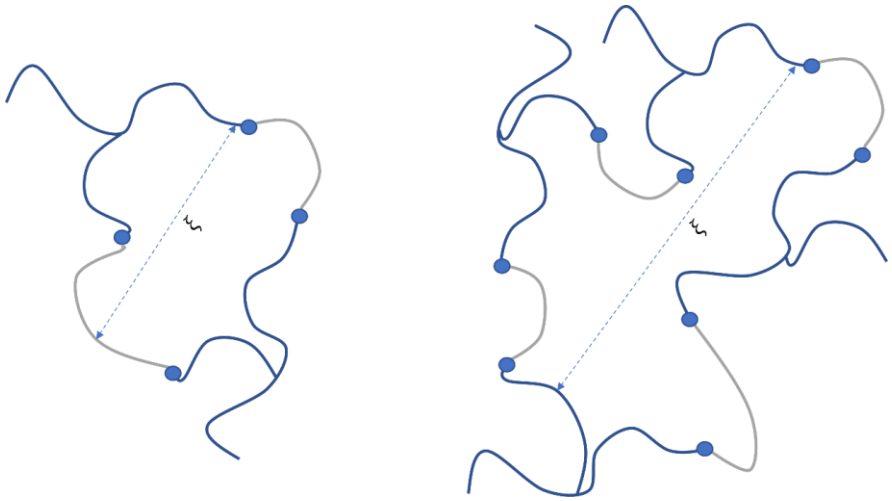

Figure 20 Illustration of the difference in the mesh size ξ of a pore of 2+2 molecules (left) in comparison to a mesh size of a pore of 4+4 molecules, both depicted as ξ.

X-Ray Diffraction Measurements

X-ray diffraction (XRD) is a common tool to determine crystallinity properties of a material. This applies for hydrogels, too. Since the M_c of a hydrogel network can be determined from G' and subsequently the crosslink density and the mesh size, as described previously, this is only valid for homogenous materials, like hydrogels in a dried state. Hydrogel networks contain a huge amount of water. It can be assumed that there may be differences in the properties of the network by removing up to 90% of mass, here: water, from the network.[93] Since the mesh size is a very sensitive parameter for a network, which should be able to avoid cell migration or will be later on used for drug delivery by diffusion of pharmaceutical active molecules through the hydrogel network, it is of great importance to gain precise values of mesh size and crosslink density. Potential post-crystallization of the hydrogel network after drying might interfere with the calculations of these parameters. Since especially EO blocks, due to their semi-crystallinity, tend to crystallize[76] , the drying process of the highly EO based hydrogels is a potential source of error applying for majority of hydrogels requiring analytical measurements. XRD measurements were found to be suitable, as illustrated in Figure 21, presenting a fully amorphous material (blue line) in comparison to semi-crystalline material (pink line). While the amorphous material exhibits a very broad single signal, the semi-crystalline sample shows defined and sharp x-ray reflexes in addition to the broad amorphous signal, representing signals from different crystal configurations. XRD measurements are carried out as qualitative measurements exclusively, comparing samples in the dried state to samples in the wet state, in order to evaluate possible post-crystallization effects.

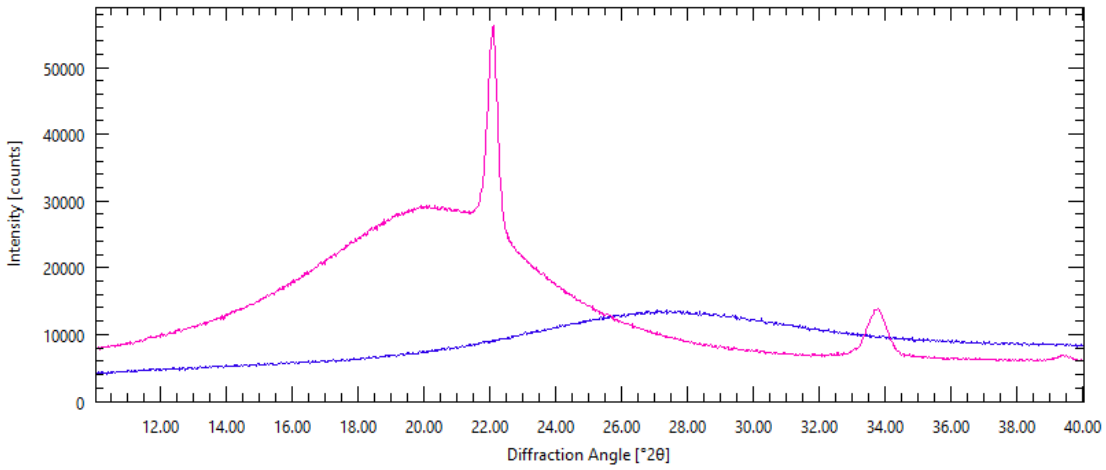

Figure 21 XRD diffractogram of a sample in purely amorphous state (blue line) in comparison to a sample in amorphous state with crystalline parts evidenced by sharp peaks (pink line).

3.2 Chemistry of Polyurethanes

Since their discovery in 1937, polyurethanes have formed an extensive class of artificial materials, which are used in a variety of fields. Polyurethanes can be found in building materials such as sealants or adhesives. They can also be found as coatings for textiles. As a consequence of their good biocompatibility, polyurethanes are also utilized for medical applications.[32]

Polyurethanes are synthesized in a polyaddition reaction starting from diisocyanate monomers and Polyols, as illustrated in Figure 22.

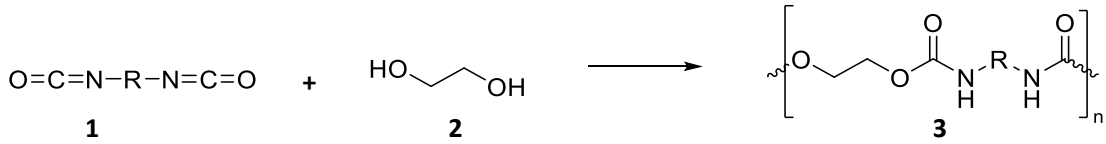

Figure 22 Polyaddition reaction of a representative diisocyanate **1** and a polyol **2** leading to urethane **3** .

Typical diisocyanates are presented in Figure 23 (idealized structure). To avoid a release of aromatic amines caused by the hydrolysis of a respective aromatic isocyanate, aliphatic diisocyanates were used exclusively in this thesis.

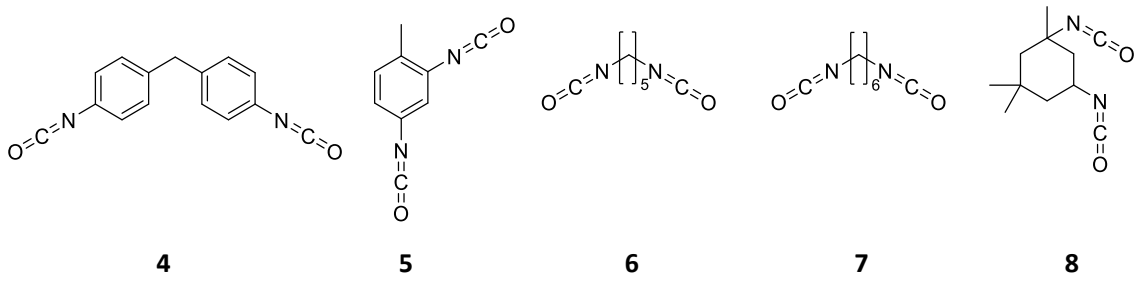

Figure 23 molecular structures of common diisocyanates: Diphenylmethan-4, 4'-diisocyanate (MDI) **4**, Toluen-2, 4-diisocyanate (TDI) **5**, Pentamethylen-1, 5- diisocyanate **6**, Hexamethylen-1, 6-diisocyanate (HDI) **7**, Isophorondiisocyanate (IPDI) **8**.

The reactions of isocyanates are versatile depending on the reaction mixture. Figure 24 presents an overview on possible reaction types of isocyanates starting all from R-N=C=O. Possible

reactants can be carboxylic acids (top left) leading to the formation of amides under elimination of CO_2, alcohols (bottom left) leading to the formation of urethanes which can react with a second isocyanate molecule under formation of allophanates, H_2O (bottom right) leading to the formation of primary amines which can react with a second isocyanate molecule under formation of urea. The urea group can therefore further react with another isocyanate molecule under formation of a biuret. The trimerization reaction of an isocyanate with other isocyanate groups leads to isocyanurates (top right).

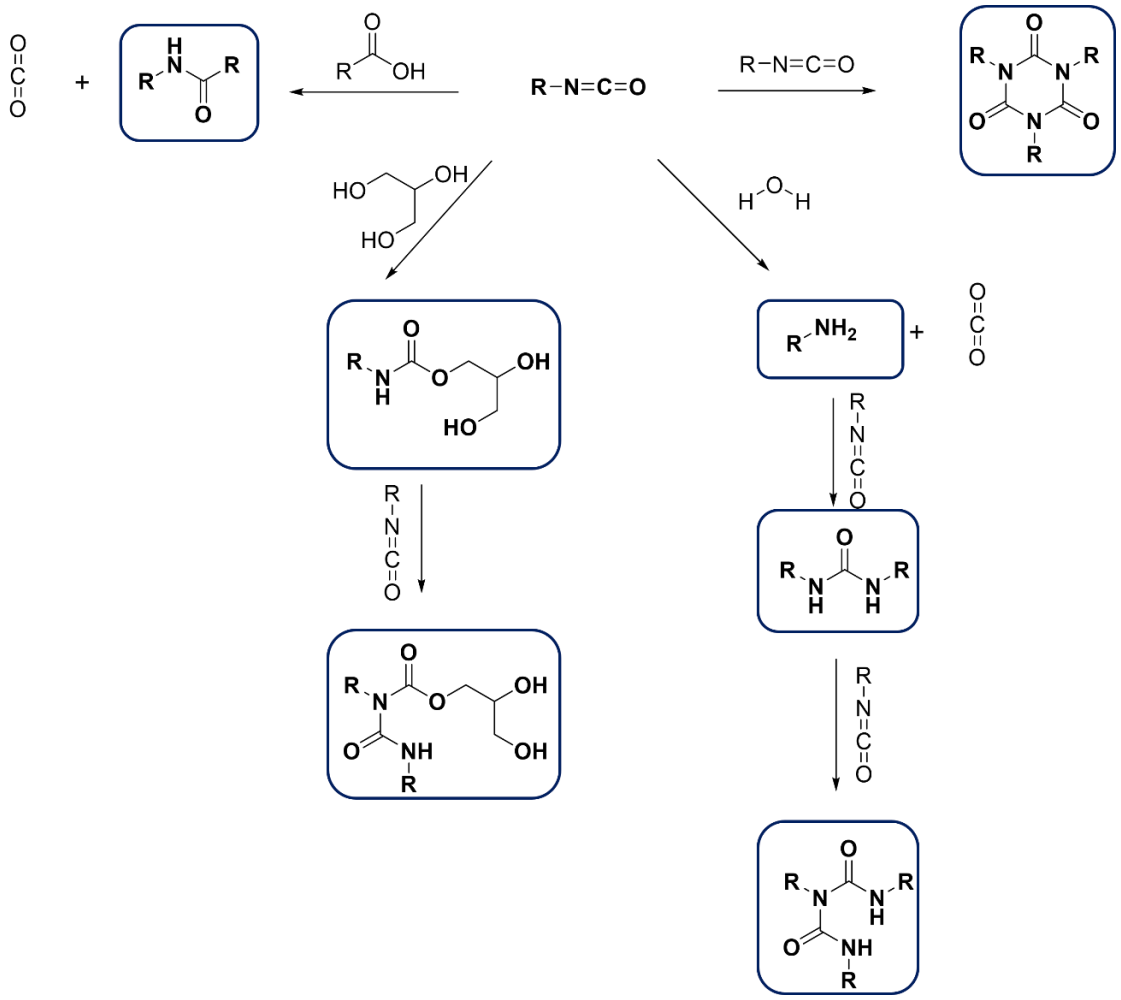

Figure 24 Possible reaction types of isocyanates with different substrates. Coupling reaction of isocyanate and a carboxylic acid lead to the formation of an amide under elimination of CO_2. The reaction of polyalcohols with isocyanates lead to the formation of urethane groups which can react in a second step with a second isocyanate to an allophanate. The reaction of isocyanate with water leads to the formation of a primary amine under elimination of CO_2. The reaction with a second isocyanate leads to urea which can react in a similar way as the urethane with a further isocyanate molecule to form biuret. The intermolecular reaction of isocyanates lead to the formation of isocyanurate.

The synthesis of the herein presented prepolymers have been conducted by the reaction of hydroxy groups (OH) and isocyanate groups (NCO). Thus, the bottom left route is the most important reaction pathway, meaning that especially the formation of allophanates as side products is of interest. Additionally, biuret formation cannot be excluded since a low amount of water

is sufficient for the conversion of R-N=C=O to R-NH_2 which induces the formation of biuret. Both side products, biuret and allophanate, can be analyzed *via* ^{1}H and ^{13}C NMR spectra.

The reaction of NCO and OH depicts the core of the prepolymer formation. However, the effect of the connecting reaction on the physico-chemical properties of the prepolymer is minor. More influence on the properties of the yielded prepolymers is given by the chosen backbone of the polyol type. Different classes of polyols can be considered for PU synthesis and are listed in Table 2. While polyether polyols are known to soften a material,[94] polycarbonate polyols are known to implement mechanical strength into the backbone.[95] Polyester types can be designed as both and also providing a certain biodegradability by implementing possible hydrolysis sites into the prepolymer backbone.[36,37] The choice of a suitable backbone is essential to design a (pre)polymer for its later use.

Table 2 presents an overview on the different structures of the three main classes of macromolecular polyol types.

Table 2 Overview on schematic molecular structures of common OH-capped polyol types used for the synthesis of PU.

Polyol type	Basic structure
Polyether polyol	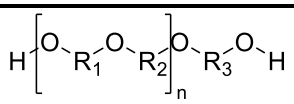
Polycarbonate polyol	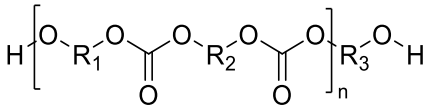
Polyester polyol	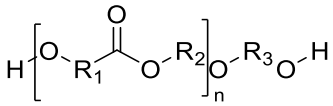

The three main types of polyol classes for PU synthesis, described in Table 2, are exclusively OH-capped for the illustrated examples. Additionally, products are available providing NH_2- or SH-capped reactants for PU synthesis. Changing the end group of a reactant leads to different reaction kinetics as presented in Table 3 and to different mechanical properties in the final material. Moreover, urea or thiourethane groups are yielded as products, instead of a PU group.

Table 3 Overview on relative reaction rates of active hydrogen compounds against isocyanate, non-catalyzed at 25°C. The isocyanate structure was not given. Data were normalized according to the water-isocyanate reaction rate. Table adopted from Ref.[32] with data from Ref.[94]

Hydrogen active compound	Formula	Relative reaction rate (non-catalyzed 25°C)
Primary aliphatic amine	R-NH_2	1000
Secondary aliphatic amine	R_2NH	200-500
Primary aromatic amine	Ar-NH_2	2-3
Water	H-O-H	1
Primary hydroxy	RCH_2-OH	1
Secondary hydroxy	R_2CH-OH	0.3
Urea	R-NH-CO-NH-R	0.15
Tertiary hydroxy	R_3C-OH	0.005
Phenolic hydroxy	Ar-OH	0.001-0.005
Urethane	R-NH-COOR	0.001

For polymers not only the primary structure is important, but also advanced structures are of interest since many of the material properties are dependent on them. The reaction of polyether with isocyanates leads in most cases to so called soft segments (SS). With the addition of smaller di-alcohol types like butane diol, hexane diol or dodecane diol hard segment (HS) domains are introduced into the polymer structure exhibiting a higher affinity to crystallize.[96] The hardness of a polymer can be adjusted by the degree of hard segments within the polymer chain obtained by the relative amount of HS, but also the choice of linker is a parameter thereof. Since polyethers are not limited to OH-capping, NH_2-capped polyethers can be applied as well. As listed in Table 3, the reaction of amines with isocyanates is much faster compared to other hydrogen active compounds, which can be beneficial, depending on the application. By using amines, the resulting linker group is urea instead of urethane as illustrated in Figure 25.

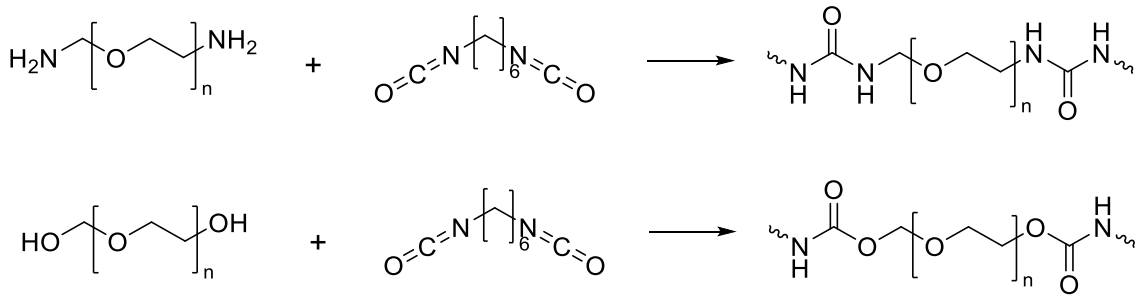

Figure 25 Illustration of the reaction of isocyanates with A) NH_2-capped polyether to obtain urea groups as linking groups. B) OH-capped polyether to obtain urethane groups as linking groups.

Not only the reaction kinetic is influenced by this, also the morphology and mechanical stability within the obtained polymeric structure. The molecular interactions differ between urea und urethane groups as only one hydrogen bond is present per urethane group, provided by the proton bond to the amide in the resulting CONH-group. The proton can form a hydrogen bond to the oxygen of a second carbonyl group. The urea group exhibits two NH groups bound to the carbonyl group, leading to the formation of two hydrogen bonds per one urea group to another carbonyl oxygen. The difference in interactions between urea und urethane hydrogen bonds is presented in Figure 26.

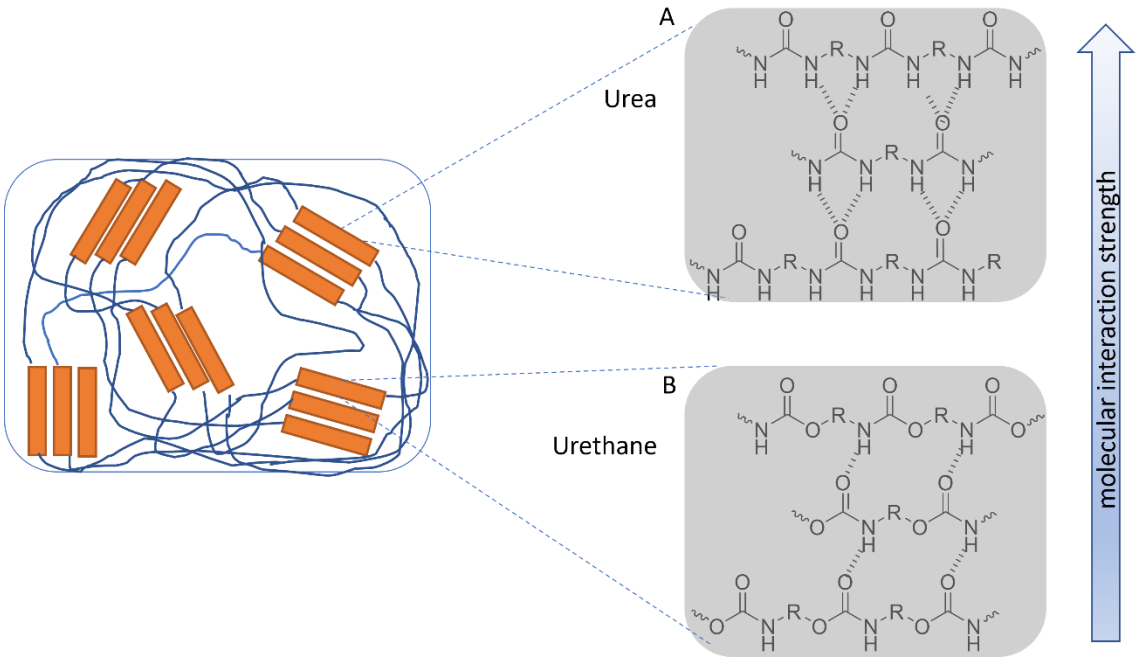

Figure 26 Molecular interactions of urea groups and urethane groups. A) Urea groups possess two NH moieties, enabling the formation of two hydrogen bonds between the NH groups and the oxygen atom of a second carboxyl group and resulting in an increased molecular interaction strength. B) In contrast, urethane groups contain only one NH group, facilitating the formation of a single hydrogen bond per urethane unit between the NH group and the oxygen atom of a second carboxyl group. Consequently, the molecular interaction strength is reduced compared to urea groups. Figure inspired by Ref.[97]

3.2.1 Material Classes of Polymers and their Mechanical Properties in General and of Elastomers in Detail

Depending on the mechanical-thermal behavior artificial materials can be divided in three different classes: Thermosets, Elastomers and Thermoplastics. Polyurethanes can be synthesized for all three different artificial material classes, depending on the design of their backbone. The difference between them are illustrated in Figure 27.[98]

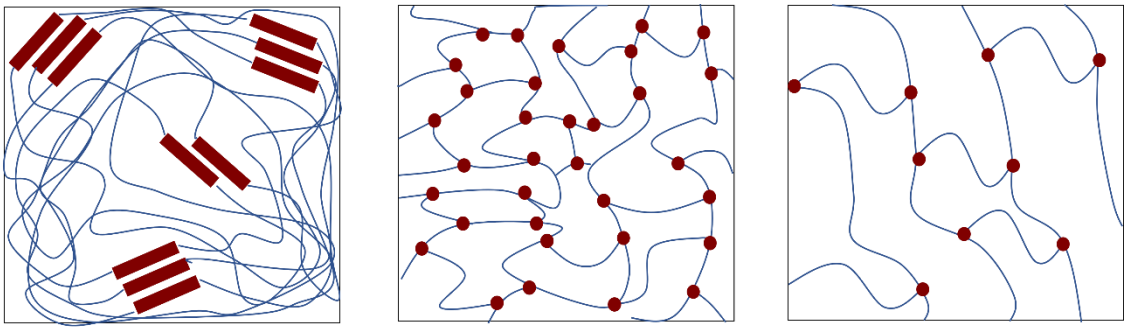

Figure 27 Schematic depiction of the three main classes of polymeric materials. A) Thermoplastics: this class is built up by linear macromolecular chains, exclusively. By introducing small molecules as chain extenders, hard segments (HS) are introduced into the network structure. HS tend to aggregate and therefore show a crystallinity effect. The molecular interactions within the crystalline part work similar to crosslinks but are reversible for example by heating whereby the structure melts but can be reformed in a different shape. B) Thermosets: highly crosslinked polymeric networks. The formation process is irreversible due to the covalent links. As a result, the network occurs as a hard and rigid material unable to dissolve. C) Elastomers: crosslinked systems but with a much lower crosslink density as in thermosets. Thus, the resulting material provides high elasticity and deformation potential, by long polymer chains in the backbone. The deformation process is reversible by the crosslinks of the network. Figure illustrated according to Ref.[98]

A) Thermoplastics represent a class of linear polymer chains with a macromolecular backbone that also includes a defined amount of smaller molecules known as chain extenders. Due to intermolecular interactions, the regions where the chain extenders are present tend to aggregate with each other, leading to crystallization as a result of the high degree of interactions within these chain extender regions.[96] As a result hard segments (HS) are obtained which introduce a certain mechanical stability into the polymer. The degree of chain extenders represents one parameter to design the thermoplastic material more soft (low degree of chain extenders) or more hard (high degree of chain extenders). B) depicts the class of thermosets, these are highly crosslinked systems, which aren't able to undergo a deformation of the completed curing process and are additionally insoluble. Once in shape, they can't be reformed. To obtain a crosslinked system f needs to be >2. The formation of a thermoset is an irreversible process since it is built up by covalent bonds. The high degree of crosslinks leads to a high strength and stiffness which makes it a hard and rigid material class.[99] C) depicts the class of elastomers. This class of polymers also exhibits covalent crosslinks but in a lower density as in the class of thermosets, which makes the material more elastic. The hydrogel networks investigated in the present thesis belong to the material class of elastomers. The mechanical properties of elastomers are therefore regarded in more detail.

Elastomers are able to undergo a very high deformation process, which needs to be complete recoverable. To meet this type of elasticity, three molecular features are required. 1) the material needs to consist of polymeric chains 2) The polymeric chains must exhibit a high degree of

flexibility and mobility 3) the chains must be introduced into a 3D network structure. While the first and second requirement lead to a high deformability of the network, the third requirement is responsible for the recoverability of it.[100] During a stress application the polymeric chains slide by one another as mentioned with requirement 1) and 2). To avoid an irreversible sliding of the macromolecular chains by each other, according to requirement 3) chains fixations points need to be available within the network structure that with the relaxation process the elastomer returns into its original shape. The fixation point, referred to as crosslinks, can be of chemical or physical nature and were regarded in more detail in chapter 3.1.2. Intermolecular interactions as van-der-Waals or hydrogen-bond interactions are present within the network and are responsible for the shape of the elastomer. They increase mechanical stability in addition to the crosslinks and make the system more stable. A higher degree of interactions within the network leads to an increase in the applied force strength to allow a deformation process. This renders the degree of intermolecular interactions, as well as the crosslink density a parameter for the mechanical stability of an elastomer network.[100]

3.2.2 Synthesis of Polyurethane based Prepolymers

As a basic substance for hydrogel formation, isocyanate capped prepolymers will be used. Since polyurethanes are synthesized by the reaction of isocyanates and polyols, as described in chapter 3.2, the molar ratio of the equivalents OH and NCO is an important parameter and is called *index*, described by equation 3.21.

$$Index = \frac{f_{NCO} * n_{NCO}}{f_{OH} * n_{OH}} \tag{3.21}$$

Wherein f_{NCO} is the functionality *f* of the isocyanate, n_{NCO} is the mole of isocyanate, f_{OH} is *f* of the polyol and n_{OH} is mole of polyol. If the index equals 1 a full polymer chain, or a network (depending on the functionalities used) is obtained, OH-capped at one end and NCO-capped on the other end. If the index is <1 both ends are OH capped and additionally the molecular weight decreases as the index deviates further from 1, and more chains are produced due to the excess hydroxy groups in the reaction mixture.

If the index is >1 the end of the polymer chains or networks are NCO capped and more chains/networks with decreased molecular weights are obtained. This effect is used to manufacture NCO-capped-prepolymers which are used in a broad range as basic substance for two-component crosslinker systems, to either reduce toxicity or improve handling properties.[101,102] Figure 28 illustrates the relation of index and the molecular weight of the resulting polymer chains/networks.[103]

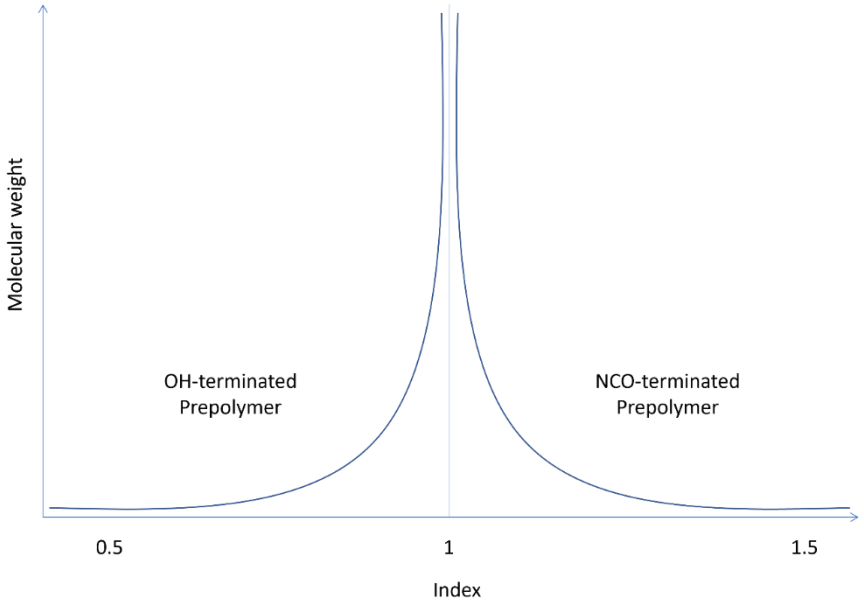

Figure 28 Illustration of the influence of the index on the molecular weight of resulting polymer chains/networks. The further away the index from 1 the more molecular weights of the obtained polymers decrease. Index <1 leads to OH-terminated prepolymers, while index >1 leads to NCO-terminated prepolymers. Illustrated in accordance with Ref.[103]

For the control of the molecular weights of the resulting prepolymers, Schulz and Flory discovered a molecular size distribution for linear condensation polymers in 1936. The distribution applies also for other polymer-synthesis-classes as they are derived from step-growth-synthesis and the reaction can be conducted in a controlled manner, but is limited to linear polymer chains and therefore only valid for reactants with *f=2*.[104] According to Schulz and Flory the distribution of different x-mers can be calculated according to equation 3.22 with $P_x(\mathrm{NCO})$ as the molecular amount of each x-mer within the prepolymer fraction, *x* as an odd natural number (1; 3; 5; ..) and r as the molar ratio of OH/molecular amount of NCO.

$$P_x(\mathrm{NCO}) = r^{\frac{(x-1)}{2}} * (1-r) \tag{3.22}$$

By applying equation 3.22, the resulting molecular weight distribution, expressed as different adducts, for a linear prepolymer example is presented in Figure 29, wherein the molar fraction of each adduct is reported in mol.%, before and after short path evaporation (SPE). Concentration *via* SPE is necessary to remove an excess of diisocyanate monomer which results from the increase of the index >1. Calculations were conducted for index=15 or $r = \frac{1}{15}$ (dark- and light-blue bars) and index=2 or $r = \frac{1}{2}$ (black and grey bars). The difference in adduct yields between index=15 and index=2 is evident. While the favored 2:1 adduct constitutes 27.5 mol% of the polymer when index=2, the value is more than three times higher when the index is set to 15. In the latter case, the 2:1 adduct accounts for 88.2 mol% of the polymer.

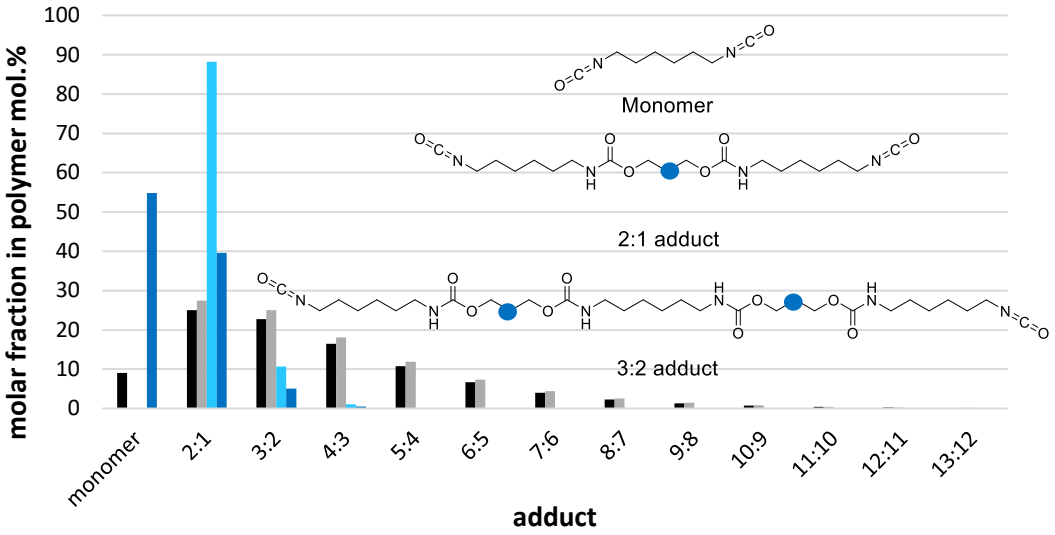

Figure 29 Molar fraction in mol.% of each formed adduct within a polymer, according to Schulz-Flory-distribution, given for the polymer before (black, dark-blue) and after short path evaporation (SPE) (grey, light blue). [40] The herein shown dark- and light-blue bars apply for a prepolymer example with index=15 or $r = \frac{1}{15}$. The black and grey bars apply for index=2 or $r = \frac{1}{2}$. Additionally, the molecular structure of a 2:1 and 3:2 adduct is shown, as well as the NCO monomer used for the reaction. The blue buttons within the molecular structures represent the polyols backbone.

As illustrated in Figure 29, an index=15 leads to 88.2mol.% of the 2:1 adduct within the polymer fraction, which is favored to keep the MW of the prepolymer as close to the assumed MW as possible, to avoid an increase in viscosity. 10.69mol.% consists of the 3:2 adduct which yields in higher MW than the 2:1 adduct.

However, results for the MW distribution of prepolymers with *f*=3 differ from the relations investigated by Schulz and Flory, since it is valid for linear polymers. The distribution still represents an important parameter for the estimation of the resulting MWs within the polymer. In systems where *f*>2 not only the MW within the different x-mers differs, also *f* increases in higher x-mers. 3:1 and 5:2 adducts are shown representative for the *f* increasing effect in Figure 30.

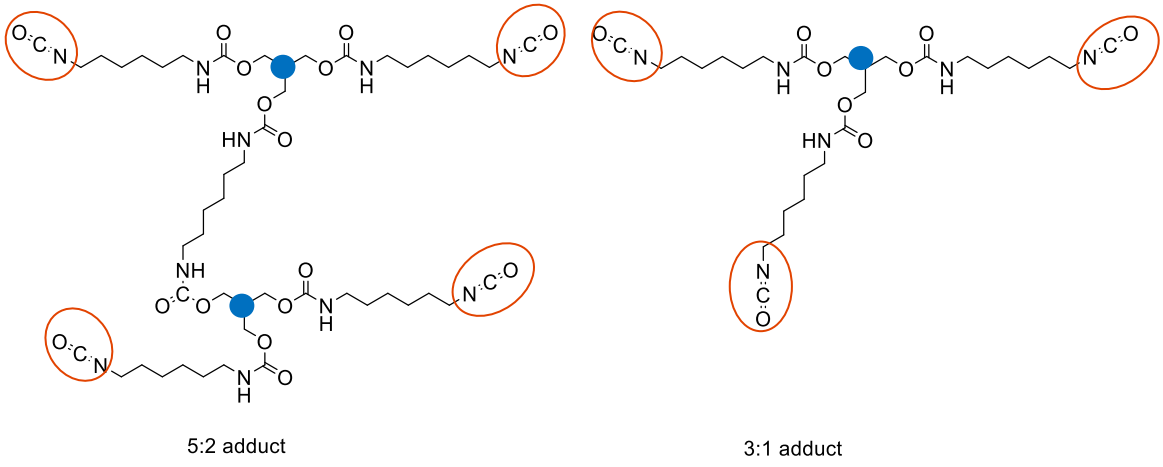

Figure 30 Molecular structures of an obtained 5:2 adduct with *f*=4 in comparison to the favored 3:1 adduct where *f*=3. Functional NCO groups are circled in orange.

Thus, the index represents a significant parameter for the adjustment of the molecular weight distribution of a prepolymer synthesis. It is a balance between yielding a high amount of the favored adduct on the one side, and the material input and effort for distilling off unreacted monomer after the reaction, on the other side. For prepolymers with $f>2$ it is even more important since f increases with an increased amount of higher x-mers. Higher mathematical models are described for polymers with $f>2$ which are more complex and the reader is referred to the extensive literature on this topic.[151, 152]

Within the scope of this thesis, unless stated otherwise, prepolymers were synthesized employing an index value of 15.

3.3 Adhesion Prophylaxis

The core objective of this thesis is the development of an *in situ* fast curing hydrogel formulation serving as an adhesion barrier, thereby enabling its utilization as an adhesion prophylaxis. The application of adhesion prophylaxis warrants further elaboration. The formation of postoperative adhesions has been described in more detail in chapter 1. An adhesion prophylaxis can be a barrier which is placed inside the body to separate affected organs and tissues from each other, thus preventing them from adhering together. Figure 31 briefly illustrates the principle behind membrane materials as adhesion prophylaxis. When considering the application process itself, it is important to comprehend the two main categories of surgical procedures: laparotomic and laparoscopic surgery. In laparotomic surgery, the entire abdomen is opened, affording the surgeon greater flexibility during the surgical process. Consequently, this approach inflicts greater harm on the patient, as it exerts a more substantial influence on the physiological system compared to a laparoscopic procedure. In the latter, only small incisions are made on the patient, therefore it is additionally described as a minimally invasive surgical process. Trocars are inserted as long and narrow channels through which surgical instruments can pass, enabling the surgical procedure. Unfortunately, not all surgeries can be conducted in a minimally invasive manner. Sometimes, laparotomic procedures are required.

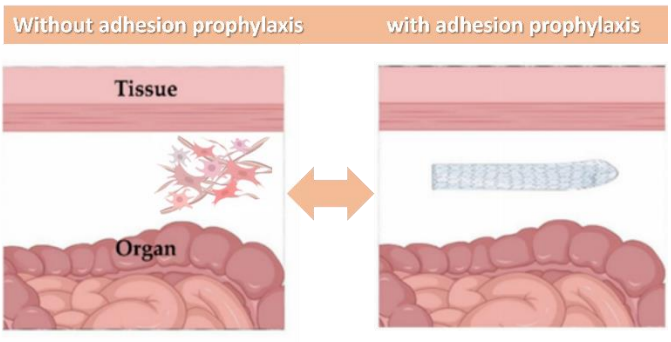

Figure 31 Schematic illustration of the intraabdominal room after a surgery process. Without an adhesion prophylaxis, postoperative adhesions, connecting tissues and organs, are present and can lead to long term side effects (left). By placing an adhesion prophylaxis (here illustrated as a membrane sheet) the formation of postoperative adhesions is prevented (right). Figure, modified and adapted, from Ref.[105] and [12] (CC BY license).

Current technologies are available to prevent postoperative adhesion. These can be divided into three main categories *solid membranes incl. powders, scavenging solutions,* and *sprayable solutions*. Table 4 presents a selection of available adhesion prophylaxis products, the material they are consisting of the crosslinking technology behind (if applicable) and the time of *in vivo* resorption of the material.

While solid membranes are provided as membrane sheets, their use is limited to open surgery processes. Even if a trial for Seprafilm described the use of this product in laparoscopic surgery processes and is described by the authors as 'simple technique', the average time for the placement took 4.0+1.47 min. 2 of 26 placements of the membrane failed which is equal to 7.7%.[17] A trial for the use of INTERCEED™ in laparoscopic procedures after colorectal section was discontinued in 2021 since the expected superiority in efficacy of INTERCEED™ compared to control (no prophylactic adhesion) could not be evidenced.[21] Major advances in the area of solid barrier placement in laparoscopic surgeries have not been reported yet.

In general, solid membranes are often provided as dried barriers which start to gel once in contact with the body fluid and stick to the area where they are applied on. This effect is beneficial but also makes it more cumbersome to handle these barriers since they can't be removed in a whole, once they start gelling. Thus, it is necessary that they are directly applied on the affected tissue without touching other areas. Seprafilm is stated to be the market leader for preventing postoperative adhesions. A special form of solid membranes are powders. The product 4DryField® is the only representative for this class. The powder is applied on the affected surface and starts to gel once in contact with the body fluid. The gelatinizing effect leads to the formation of a membrane.

Scavenging solutions have a different technology to prevent postoperative adhesions. The main volume from a scavenging solution is used for the scavenging process. After the last step a certain amount of the volume (up to 1 L) remains inside the body of a patient leading to an aerial separation of tissue and organs.[106] By the separation of the different body compartments postoperative adhesions are reduced. The solutions stay up to three days inside the body until they are fully resorbed. However, this time is not sufficient according to the requirement profile, which was established by interviews with doctors and a literature review. The critical healing period is reported to be 7 days on average[107], therefore adhesions may still occur after resorption of the scavenging solutions.

The class of sprayable solutions and hydrogels is more advanced as more features are required compared to solid membranes. A defined requirement profile for this class is described in Table 5. Beneficial here is the provision of a higher degree of freedom during the application process since they can also be used in minimally invasive surgery processes.

Table 4 Overview on different products available on the market for the use as adhesion prophylaxis divided into the main classes *solid membranes*, *scavenging solutions*, *powders* and *sprayable solutions*. If not stated other, information on the different parameters were taken from the reference listed in the column 'product'.

Class	Product	Material	Crosslinking reaction (if applicable)	Degradation time
Solid membranes	Seprafilm® [108]	HA/CMC	anionic complex	28 days
	INTERCEED™ [109]	Oxidized regenerated cellulose	Woven cellulose	28 days
	REPEL-CV® [108]	PLA/PEG	-	28 days
	Cova™ CARD [108]	Porcine type 1 collagen	Collagen crosslinked with polysaccharides	6 months
	Cardio Wrap®/ Surgi Wrap® [108]	PLA	-	8 weeks
	GORE PRECLUDE® [108]	ePTFE	-	Not resorbable (not biodegradable)
	Incert™ [110]	HA derivative	-	Bioresorbable, no time reported
Powders	4DryField® [111]	Starch	-	Bioresorbable, no time reported
Scavenging solutions	ADEPT® [112]	4% Icodextrin	-	3-4 days [106]
	Physiological NaCl solution	0.9% NaCl	-	
Sprayable solutions	Coseal® [113]	PEG	Thiol + N-Hydroxysuccinimd (NHS)- ester	6 days [114]
	Hyalobarrier® [115]	HA	-	Bioresorbable, no time given
	SprayShield ™ [116]	PEG, Trilysin	Amine+ NHS-ester	2-7 days
	Carbylan SX [117]	Thiol modified HA PEG diacrylate	Thiol-ene	Bioresorbable, no time given

From Table 4, the preference of manufacturers of adhesion prophylaxis products for materials which provide a huge swelling becomes visible. It is therefore not surprising that many of these materials are also used as raw materials for the general production of hydrogels. The strong swelling seems to be the preferred feature for all systems, irrespective of whether sprayable or solid barriers.

A defined approach for the requirements for such an application was missing. In order to determine which features are required from the chemical system for adhesion prophylaxis, an interview with a questionnaire for different surgeons was prepared. The interview was prepared and conducted by employees from *Covestro Deutschland AG* and *Erbe Elektromedizin GmbH*. Five different experts from the University Hospital of Tübingen, Department of Women's Health, were included in the interview. Additionally, a literature research was conducted. The results are summarized in Table 5. If no reference is provided, the guideline values either come from the interviews with the surgeons or are requirements from the project partners regarding the application with the spray applicator.

Table 5 Summary of the requirements profile drawn up. Obtained values either come from a literature research (source in brackets) or are based on the survey of five physicians at the *University Hospital* Tübingen, *Department for Women health*.

Parameter	Guide value	Affected part of the formulation
Biodegradability	Stable for 7 days, degraded within 28 days	Cured hydrogels
Curing time	Maximum 60 sec.	Single components, cured hydrogel
Design as a sprayable system:		
Low viscosity	Viscosity limit of 9 mPa*s	Single components
Water solubility		Single components
Mechanical properties:		
Elongation	Min. 32% [118]	Cured hydrogel
Compression/Tensile strength	1.6-21 kPa [119]	Cured hydrogel
Biocompatibility	Non-cytotoxic, non-genotoxic, suitable pH value (6.1-7.4) [120,121]	Single components, cured hydrogel, biodegradation product

The table presents an overview on the different key properties which will be discussed here in more detail. Biodegradability is a feature the system needs to provide for an application as adhesion prophylaxis. There are products on the market which are not biodegradable, such as GORE PRECLUDE® and need to be removed in a second surgery process.[16] By the necessity of a

second surgery, the use of such a product is at least questionable since postoperative adhesions are caused by the wound healing cascade, which is induced by the tissue injury. The time until the material needs to be removed from the body and thus represents the upper limit, is not clearly stated, but can be summarized as 28 days, as can be seen from the existing technologies (Table 4). This value also reflects the statement of the physicians interviewed. In comparison, the lower limit can be clearly described by the critical wound healing period for peritoneal wounds which is specified as 7 days on average.[122,123] Post-operative adhesions can also occur during this time, so it is important to bridge this period with a stable material. As a consequence, the material needs to provide a stable network for 7 days, so that no cells can migrate through the network and should be degraded fast afterwards.

Curing of the network should occur in max. 60 sec. as reported by the physicians.

Since the herein investigated materials should be provided as a sprayable system, the single components need to exhibit a water solubility. Low viscosities of max. 9 mPa*s are required, to provide sufficiently good sprayability. The water solubility of the single components should therefore be sufficiently high to be able to dilute to the required viscosities.

Mechanical properties were also addressed in the research. The intraabdominal pressure (IAP) is described in the literature as 1.6 kPa at standard conditions which means without applying mechanical stress on the body. [124] Under abdominal press by coughing the IAP can raise up to 8.7 kPa. The highest values were reported for *valsalva maneuver* with an IAP of 21 kPa. [119] Values of 1.6 kPa and 21 kPa were therefore chosen as upper and lower limit for tensile strength. For Elongation values there is no defined guide value which needs to be fulfilled. It is described that the varying IAP leads to a certain expansion of the abdominal wall. [125] Junge *et al*. reported on different elongation ratios of the abdominal wall when applying a force of 16 N on the whole samples, which were taken from human tissues postmortem. Mean distensions of 11% to 32% have been reported herein.[118] These experiments are barely comparable to distensions under living conditions but provide at least a hint of the expected distensions *in vivo*.

High biocompatibility is also an important requirement for the system. Since the safety of polyurethanes for their use in medical applications is confirmed by several applications, they gain large interest as substrate materials for different systems[126,127] and will be considered as basic materials as non-(geno-)toxic substances may be used, exclusively. The system should be designed in such a way that the solutions can be rinsed out aqueously in case of a user error. In addition, the pH value is important for good biocompatibility. An application in the body needs to exhibit a physiological pH value in the range of 7.4.[81]

3.4 Fast Curing Click-Chemistry

Click chemistry is a useful tool aiming for the fast integration of interest building blocks and was first described and summarized by Sharpless *et al*. in 2001. The aim behind was the implementation of a fast access to compounds which are characterized by their carbon-heteroatom-carbon (C-X-C) bonding. In their Review, Sharpless and coworkers characterized click chemistry to be 'modular, wide in scope, give very high yields, generate only inoffensive byproducts that can be removed by nonchromatographic methods, and be stereospecific (but not necessarily enantioselective)'.[128] The required process characteristics include simple reaction conditions (ideally, the process should be insensitive to oxygen and water), readily available starting materials and reagents, the use of no solvent or a solvent that is benign (such as water) or easily removed, and simple product isolation.[128]

In chapter 3.4.1 the requirements for an adhesion prophylaxis were presented (Table 5). A fast curing time (<60 sec.) was identified as an important parameter here. In order to make such a curing possible, a chemical reaction must be found which shows short reaction times and high yields, also proceeds quickly when diluted and does not use (toxic) catalysts. The use of a cross-linking rection derived from the platform of click chemistry will therefore be considered within this chapter.

Literature research was carried out to search for possible reaction pathways that fulfill the requirements. Table 6 provides an overview of the identified reaction types which are considered in more detail.

Table 6 Overview on different reaction routes identified by a literature research for fast curing reaction types. Reactants are described as reactive group (RG) 1 and 2. In case of a hydrogel formation, the product displayed the crosslinking group of the resulting 3D hydrogel network.

Reaction type	Reactive group 1		Reactive group 2	Product	Reaction time at RT
1.) Diels-Alder	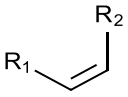			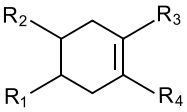	Overnight [129]
2.) Azide-Alkine			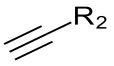	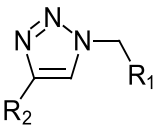	7 min.[130]
3.) Thiol-ene	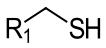		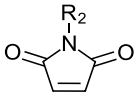	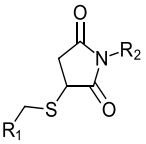	30 min. [131]
4.) Imine formation			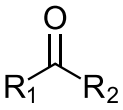	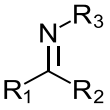	120 sec.[28]
5.) Condensation	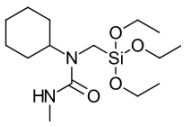		H_2O	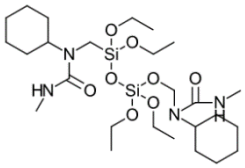	Range of min. for epoxy systems[132]
6.) Polyaddition	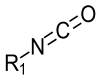	a)		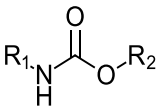	Range of min.-hours[32]
		b)		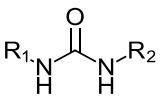	Range of sec.-min.[32]

Diels-Alder reaction is described to be fast and at high yields. [133] It represents a pericyclic reaction between a conjugated diene (diene) and an alkene (dienophile) leading to the formation of a monounsaturated cyclohexene and therefore belongs to the group of [4+2] cycloadditions. Two π-bonds are converted into two σ-bonds. In the intermediate state six delocalized π-electrons are present leading to an aromatic state and subsequently to an ortho-para coordination. Meta products can be achieved by steric hindrance. This makes the Diels-Alder reaction a

regioselective reaction. In this type of reaction, the highest occupied molecule orbital (HOMO) of the diene and the lowest unoccupied molecule orbital (LUMO) are reacting. Therefore Diels-Alder is also a stereoselective reaction. Both, stereo- and regioselectivity are neglectable for the crosslinking reaction of a hydrogel.[134] An example of a simple Diels-Alder reaction is presented in Figure 32.

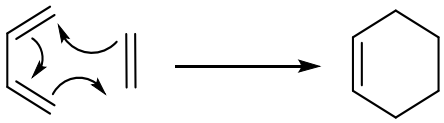

Figure 32 The reaction of a diene and a dienophile according to the described Diels-Alder reaction pathway leading to the formation of a monounsaturated cyclohexene.

Yu *et al.* reported on the formation of a 2K hydrogel *via* Diels-Alder reaction. The curing process occurred at 37°C and persisted overnight.[129] In the context of a requisite reaction rate under 60 seconds, no literature was identified demonstrating the necessary reaction speed facilitated *via* Diels-Alder reaction.

Azide-alkyne reactions also belong to the class of cycloaddition reactions, but in contrast to the Diels-Alder reaction, they are characterized by a [3+2] cycloaddition mechanism. Azide-alkyne reactions are classified as click chemistry reactions, but are frequently metal-catalyzed, primarily facilitated by the employment of copper-based catalysts.[135,136] The reaction route is discussed in detail elsewhere and is shortly summarized and presented in Figure 33.[137]

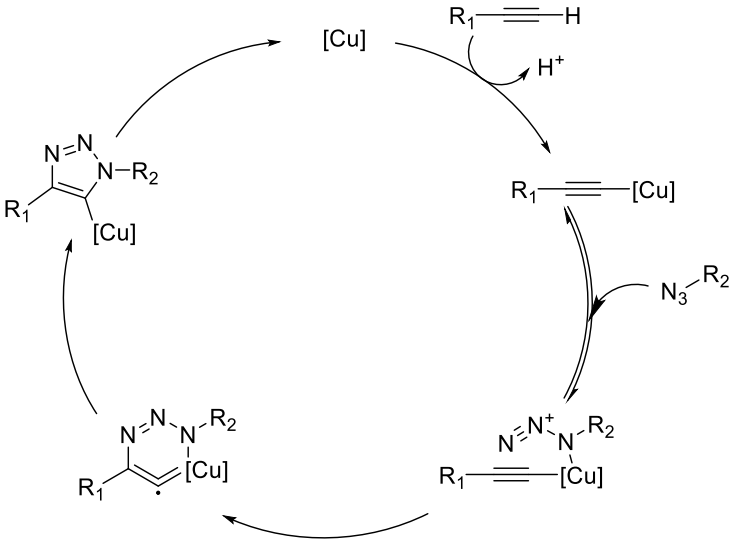

Figure 33 Proposed reaction cycle of the azide-alkyne [3+2] cycloaddition catalyzed by copper [Cu]. The alkyne coordinates to the copper molecule under elimination of H^+. The added azide component leads to an equilibrium state between bounded N atom to copper and the free copper bond alkyne. A ring closing by a reaction of the alkine-carbon to the azide nitrogen atom yields a cyclo-hexyl. A rearrangement at the carbon atom bounded to the copper atom yields a triazol as a product. Copper is removed by an exchange with H^+. Illustrated according to Ref.[137]

Additionally photocatalyzed azide-alkyne reactions are described in the literature.[138] Copper is stated to be cytotoxic and is related to Alzheimer's disease and hepatitis.[139–141] A photocatalyzed

reaction would enlarge the equipment needed for the preferred application of adhesion prophylaxis, thus a preferred curing mechanism avoids metal catalysts and catalysis by light. A reference was identified reporting on an azide-alkyne reaction which was conducted without the use of a catalyst. Different ratios where evaluated and the best in curing time (7 min.) was obtained at a 1:2.5 ratio of azide/alkyne and a weight concentration of 33% at a reaction temperature of 37°C.[130] This type of reaction therefore reaches the dimensions of the required curing time but still exceeded by 700%, so it is questionable to what extent the reaction speed can be accelerated without the addition of catalytic agents or sources.

Thiol-ene reaction is additionally stated as a fast reaction type belonging to the class of click chemistry.[142] This type of reaction can be mediated *via* two different ways. A) by the formation of a free radical and B) by the addition of a Michael addition agent. Both pathways yield the same product. These reactions are also described as 'fast'. Fastest thiol-ene reaction without catalytic agents or photocatalysis were reported to be at 30 min.[131] This time is evaluated as not suitable for a fast curing adhesion prevention material.

A further approach from the category of click chemistry is depicted by the imine formation of a primary amine and an aldehyde under elimination of H_2O. Reaction speed is reported to be in the range of hours to minutes.[143] Additionally there is one product on the market belonging the class of surgical glues and is called Bioglue®. It is available as a 2K system, consisting of BSA and glutaraldehyde. The primary amine groups in the BSA react with the dialdehyde directly under imine formation to yield a network. The crosslinking reaction occurs within 120 sec.[28] Although this is not yet fast enough for the intended application, it can be concluded that the reaction rate can be increased by adjustments within the system. Imine formation will be considered as possible curing mechanism for fast curing 2K hydrogels.

The condensation of silanes induced by H_2O represents a special condensation reaction yielding siloxanes as a product. This reaction is well established in the area of prepolymer design. Depending on the structure, silanes can easily be attached to a prepolymer. In the case of NCO capped prepolymers this is ideally done by the use if silane amines. Standard silane terminated polymers are relatively slow in their curing behavior which can be explained by the position of the silicium atom, which is in standard compounds at γ-position. By shortening the chain to a methylene group the reactivity of the silane increases, yielding faster crosslinking kinetics when curing with moisture.[31] Since α-STPs are reported to be much faster, this approach will be considered for the fast curing hydrogel concept.

Concerning polyurethane chemistry, a well-established approach is the curing of polyisocyanates with reactive compounds like polyamines or polyalcohols, which can be regarded as a poly-addition reaction. The reaction pathways have been discussed in detail in chapter 3.2. The fastest reactions were described for primary amines (relative reaction rate: 1000, Table 3) OH groups are reported to be less reactive (relative reaction rate: 1, Table 3). Both crosslinking

reactions can be considered. However, a non-catalyzed reaction is preferable to avoid unnecessarily broadening of the formulation for a possible future product.

The potential toxic behavior of possible monomers and the resulting cured products thereof, is barely foreseeable by the reaction route. In general, it can be assumed that macromolecules are less prone to induce cytotoxic behavior due to their larger molecular weight in comparison to smaller molecules.[30] Reaction 4.) uses small molecular aldehydes for the crosslinking which are also known for their cytotoxic potential and is still used for medical implants due to its fast reaction speed and the subsequent statement that no glutaraldehyde is present.[28] Depending on the curing time and the macromolecular backbone, which will be implemented, cytotoxic potential can primary be evaluated by regarding the reaction pathway but needs to be investigated for the resulting system in total. It can be assumed that there might be a difference between a small molecular weight aldehyde in comparison to a macromolecular aldehyde.

Physical gelation methods can additionally be considered for the formation of polyurethane based hydrogels. Physical crosslinking opportunities comprise a high reaction speed as an advantage. Most reactions derive by ionic interactions which are known to be fast.[144] Three different physical gelation methods are listed in Table 7.

Table 7 Selection of physical crosslinking routes to allow hydrogel formation. Approach 7.) and 8.) build on electrostatic interaction by using ionic substances as RG1 and their counterions as RG2 for the hydrogel formation. Approach 9) differs since it can be designed as a one component system using a thermoresponsive component. Thereby a formation change of the component in a solvent is induced by an external trigger like temperature as described in chapter 3.1.2.

	Gelation type	RG1	RG2	Product
7.)	Ionic Gelation	Anions	Counter Ions (e.g. Ca^{2+})	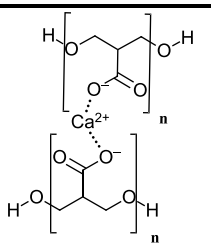
8.)	Polyelectrolyte complex	Polyanion	Polycation	Complex of polyanions and polycations
9.)	Thermoresponsive behaviour	Thermoresponsive substances	Curing by Temperature gradient	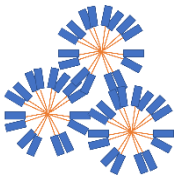

As described in chapter 2, approaches 4, 5 and 6 from Table 6 and approach 9 from Table 7 will be investigated as underlying crosslinking concept for the preparation of fast curing hydrogels.

3.5 Design of Experiments

A formulation often provides different parameters which need to be adjusted to get to the final product, featuring all requirements for a certain application. To optimize the formulation to fit to a certain requirement profile, experiments need to be conducted to investigate the influence of different parameters on the defined requirements. An often conducted method is the try and error method, wherein different parameters are changed at the same time to find a formulation fitting to the requirements and thus follows the principle of coincidence. This method lacks a systematic approach and makes it hard to understand the influences and impacts of each factor onto a certain response.

Within the most common standard procedure, one factor at a time is varied (OFAT) to measure the direct impact of the changing factor on the response. This leads to an increase in the number of conducted experiments dramatically with each additional factor. In comparison, a better design of experiments (DoE) can be chosen to investigate the impact of different factors at the same time by varying more than one factor in each experiment. Figure 50 presents the difference of the testing procedures OFAT vs. DoE. Assuming a testing series wherein the influence of two different catalysts (A and B) should be investigated, as well as the influence of reaction temperature at 20°C and 40°C. For sufficiently accurate results eight repetitions should be conducted, leading to 24 experiments in total for three different factor combinations (1. Catalyst A, 20°C; 2. Catalyst B 20°C, 3. Catalyst A 40°C). In comparison to the OFAT method, a DoE only requires four repetitions per combination since multiple factors at a time can be varied. The experiment can then be used for the determination of the influence of the different catalysts, as well as the influence of the temperature. Due to the multiple usage of each result, experiments can be reduced. In comparison to the OFAT which requires 24 experiments for 3 different factor combinations, the DoE requires 16 experiments for 4 different factor combination (+ 4. Catalyst B 40°C). Reducing the experiments while maintaining the same statistical power, as within the OFAT testing series, is only possible by varying more factors at a time. Additionally, synergistic or anti-synergistic interaction effects between factors can be detected. In the example given, the influence of a temperature can be investigated in dependency of the chosen catalyst by adding the 4. Factor combination. This information cannot be detected in the herein presented OFAT design.

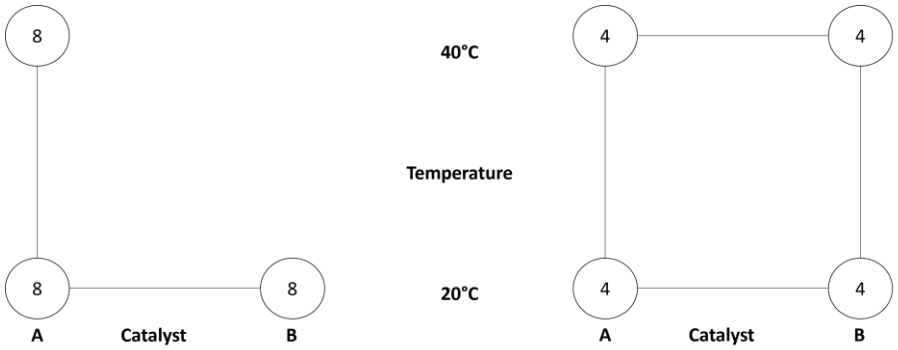

Figure 34 Example of an experimental study run for OFAT (left) in comparison to the systematic DoE (right). In the latter, the factor combination of catalyst and temperature can be investigated additionally, which is not covered by the presented OFAT design.

A section of the results presented within this thesis are generated by using design of experiments and additionally a software (Design Expert 13). As a result, an empirical model is created based on the results of the different analyzed experiments with given relations between the varied factors and the analyzed parameters. The obtained model is only valid within the investigated factor ranges. Extrapolation is not permitted.[145]

Within this thesis not only the components of the hydrogel composition itself are analyzed, but also different aspects dealing with the formulation parameters and therefore influencing the mixture. The DoE was conducted after useful factor ranges were deduced from initial screening experiments. The factors of interest were *solid content Isocyanate*, *amount of dilactide groups in the polyol backbone*, *buffering degree of amines* and *acid/buffer type*.

3.5.1 Design of Experiments with the use of a Software (Design Expert)

The use of a software for the preparation and evaluation of a DoE facilitates the process of planning and optimization. The DoE is prepared with a focus on balanced experiments. Limits can be set by the user of the Software to exclude impracticable formulations at the beginning.

For every response a model is calculated individually based on the results of the experimental part. As starting point linear models are predominantly used, but even models of higher polynomial orders can be achieved if a relationship is recognized differing from linear models. Often quadratic models are considered.

The study type used for DoE testing in the present thesis was *Response Surface*, which uses a second degree polynomial (quadratic design) due to simplification. The choice of the terms which are later included into the model is conducted with the use of an analysis of regression or variance where different types of algorithms can be applied. Assuming a backwards elimination, terms are first included into the model and eliminated in a successive manner. If terms are removed from a model, is determined concerning the significance level α, which is set to 0.05 in a standard procedure. Significance level α correlates (but is not equal to) the false positive risk that is accepted when deciding effects to be significant based on their p-value. Significance level of α =0.05 will judge only effects with p-values <0.05 (low false positive risk) to be significant. The significance level can be set by the user of the software individually but is kept to 0.05 for

the herein used evaluation of the DoE. Start of the evaluation is done by elimination of the factor with the highest p-value, all other p-values for the remaining factors are recalculated, the next highest p-value factor is eliminated and remaining factors are recalculated again. This procedure is repeated until all p-values are below 0.05 and therefore stated to be significant. The approach of reducing p-values represents a method for the choice of terms for the creation of a model. The pure focus on p-values is a discussed topic.[146] Other methods for the choice of terms are *akaike information criterion* valid for small sample sizes and *bayesian information criterion*. Effect terms are not limited to the linear effects of the factors but can also include higher order interaction terms between two or three factors such as AB or ABC or quadratic terms like A^2. If such higher order terms are included in the model, the corresponding lower order terms are recommended to remain in the model as well even if they were determined to be insignificant (keeping hierarchy).[145] The obtained model can deviate depending on the method used for the determination of included terms. For an evaluation of the model accuracy, an analysis of variance (ANOVA) is conducted to evaluate the model with its included terms as well as the residuals, consisting of the lack of fit and the error (pure error), wherein the residuals describe deviations of data which cannot be explained by the model itself. Herein the deviations from given means from the model function (lack of fit) and the error obtained by repetition of experiments (pure error) are already considered.[147] A normal plot of residuals is created to give an overview on the standard deviations and the mean response. Herein, high deviations from linear behavior indicating a power law relationship, which is a hint on necessary transformations to stabilize the residual variance, satisfying the assumptions for ANOVA. Investigations which transformation (Base 10 log, natural log, square root, inverse square root) is applicable, is evaluated by the software using a box-cox plot.[148] Evaluated lambda gives a hint on useful transformations, (λ=1 no transformation, λ=0.5 square root, λ=0 natural log, λ=-0.5 inverse square root, λ=-1 inverse).[149] Transformation is needed if the error (residuals) is a function of the magnitude of the response (predicted values).[150]

As a result of the DoE with the use of a software, an equation is created depicting the influence of each factor and/or factor combination of all terms which are included into the model as described above. The obtained equation can be used to determine the extent of influence for each term and predict the respective response for a given factor combination.

4 Results and Discussion

This chapter is divided in three main parts. The results of the preliminary screening phase of the four approaches HYGEL1-4, aiming for a fast curing hydrogel system, as presented in chapter 2, will be described and discussed in chapter 4.1. This chapter addresses the initial pretesting phase of the described HYGEL approaches to first identify the most favorable crosslinking technology regarding first application requirements, namely water solubility, viscosity and applicability in volume ratios 1:1 or 1:2. Downstream requirements such as biodegradability are not addressed in this chapter.

The most promising approach of the pretesting phase (HYGEL-3) was further developed and adjusted to the requirement profile for an adhesion prophylaxis and is described and discussed in detail in chapter 4.2. Additionally, an intense structure-property-relationship study was conducted to identify adjustable parameters within the limitations of the requirement profile. A final formulation was identified and was tested in advanced *in vivo* testing as a proof of concept, which will be described in chapter 4.3.

4.1 Four Approaches Preliminary Screening Phase

Four different curing approaches (HYGEL1-4) were considered for the underlying reaction types to yield fast curing hydrogels and were screened with a strong focus on the curing behavior by maintaining viscosity limitations and were summarized in Figure 5. The pretesting phase is limited to initial experiments and does not represent a full characterization of these systems.

The results of the pretesting phase will be anticipated at this point. All four approaches showed a fast curing, but except for HYGEL-3, all other comprised at least one major compatibility issue regarding the requirement profile from Table 5. HYGEL-3 was evaluated as most suitable featuring **prepolymer-1** in its initial structure, cured with a macromolecular diamine to yield a network *via* urea formation, serving as crosslinks. This concept was used as a basic reaction for further optimizations according to the requirement profile, as will be presented in detail in chapter 4.2.

4.1.1 Synthesis and Analyses of a Prepolymer as Starting Point for Hydrogel Manufacturing

Prepolymer-1, synthesized as described in chapter 6.3, featuring a high EO content (73wt.-%) polyol with *f*=3 in its macromolecular backbone, was utilized as initial starting point for the pretesting approaches HYGEL1-4. The general structure is presented in Figure 35.

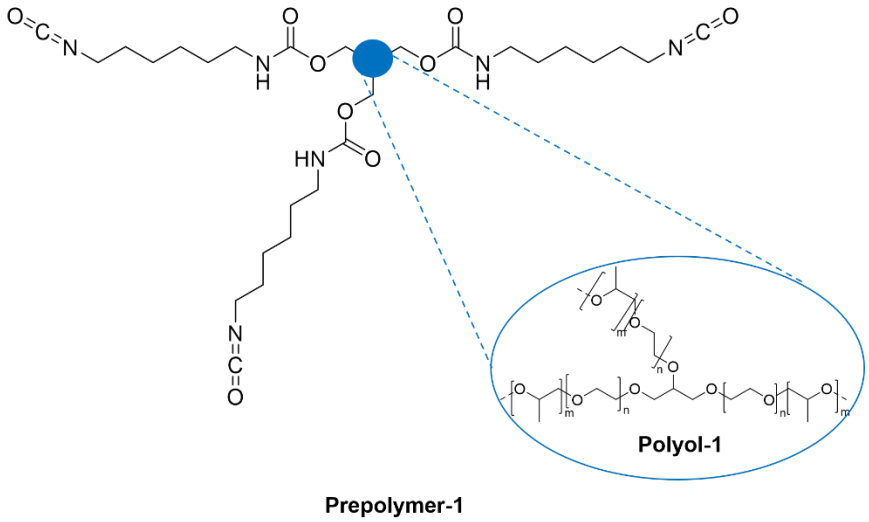

Figure 35 Illustration of the general structure of an aliphatic based **prepolymer-1** as initial starting point for further chemical modifications. The blue sphere depicts the polyol backbone of the prepolymer (**Polyol-1**) which consists of glycerol as starter, on which EO units (n), to obtain a high water solubility, and additionally a small amount of PO units (m), to avoid crystallization between the EO segments, were added during the polyol synthesis.

A reaction sequence whereby **prepolymer-1** was obtained is presented in Figure 36. As described in chapter 3.2.2, the index was set to 15 to obtain predominantly 3:1 adducts. Purification of **prepolymer-1** was conducted *via* short path evaporation (SPE) to remove the monomer excess of HDI.

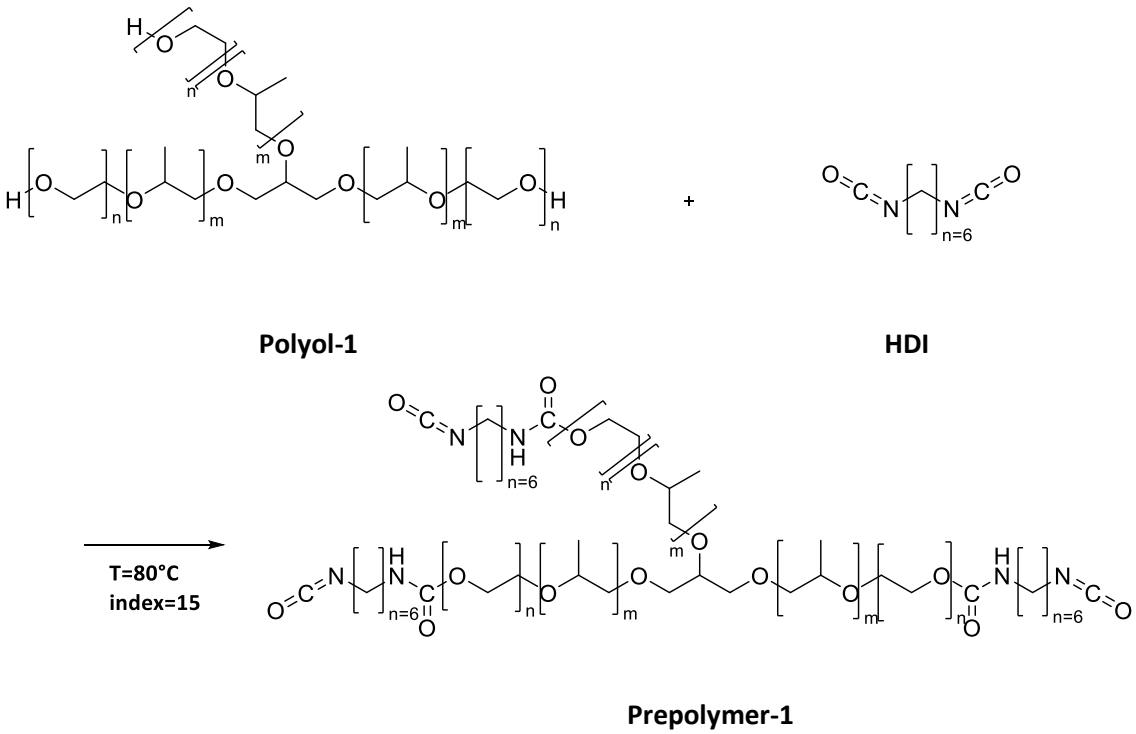

Figure 36 Synthesis sequence for the preparation of **prepolymer-1**. HDI (15 eq.) is heated to 80°C and **polyol-1** (1 eq.) is added dropwise. **Prepolymer-1** is obtained as raw material, diluted in remaining HDI monomers. Purification *via* short path evaporation or distillation is necessary.

^{1}H NMR spectra after purification presents the resulting EO/PO distribution (Figure 37). Integration of both peaks yields 85% urethane groups bond to EO, arising at a chemical shift of 7.16 ppm vs. 15% urethane groups bond to PO, arising at 7.06 ppm. These values approximately represent the concentration of EO and PO units in **prepolymer-1**, as it is based on 73wt.-% EO and 27wt.-% PO (weight of starter not included).

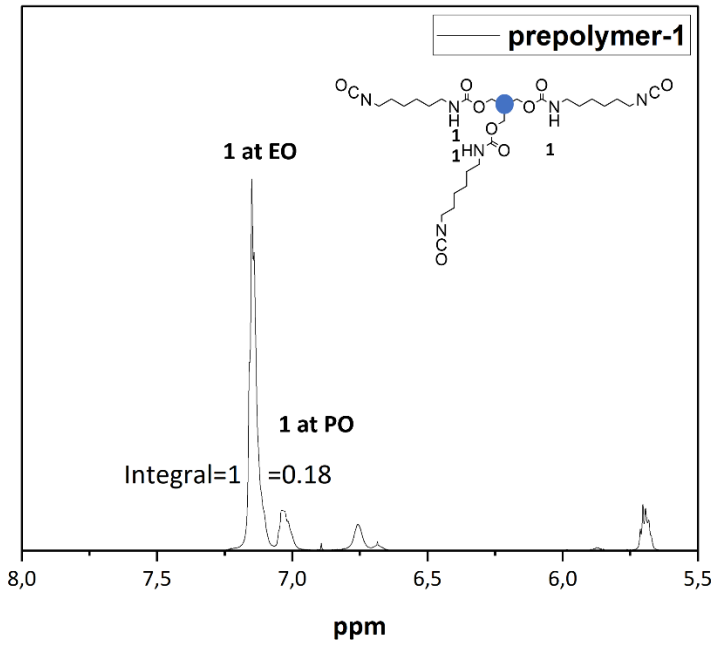

Figure 37 ^{1}H NMR of **prepolymer-1** in d_6-DMSO. Urethane bonds are marked as 1. Approximately 15% of urea groups are bound to PO units, while 85% of urea groups are bound to EO when comparing integrals of singlets at 7.16 ppm and 7.06 ppm.

Further characteristic values derived from measurements of **prepolymer-1**, namely FT-IR signal, NCO content, equivalent (eq.) weight, residual monomer content and viscosity at γ=50, T=23°C are presented in Table 8.

Table 8 Overview on characteristic values of **prepolymer-1** for charge CVAUJ001-3, measured as described in chapter 6.3. (s) denotes a sharp signal peak in FT-IR spectra

Parameter	value
FT-IR *v*(N=C=O)	2265 cm^{-1} (s)
NCO content	2.49%
Eq. weight	1686.75 g/eq.
Residual monomer content	0.02%
Viscosity (γ=50 sec.$^{-1}$,T=23°C)	3950 mPa*s

The eq. weight is used instead of the molecular weight as it is more meaningful in the case of prepolymers. It can be calculated from the molecular weight of a prepolymer ($MW_{prepolymer}$) *via* equation 4.1.1.

$$eq.weight = \frac{MW_{prepolymer}}{f} \quad (4.1.1)$$

The molecular masses of obtained **prepolymer-1** were analyzed *via* gel permeation chromatography (GPC) and are presented in Figure 38. Herein the different adducts given by Schulz-Flory distribution can be observed. Moreover, Table 9 presents an overview on the theoretical distribution according to equation 4.1.2 in comparison to observed distribution of x-mers by GPC measurements. Theoretical values differ from practical measurements, which might be caused by the comparison of practical measurements of a *f*=3 prepolymer to the theoretical calculations according to Schulz-Flory, valid for linear, *f*=2, polymers.[104] The prediction models for assessing the x-mers in linear polymers becomes much more complex in higher branched polymers and the reader is referred to the extensive literature on this topic.[151,152] Applying the model for *f*=2 polymers on *f*=3 may lead to failures.[151] However, the comparison of the experimental values with theoretically valid values for *f*=2 polymers allows a simpler and yet reliable estimation of the x-mer distribution. The results from Table 9 revealed that the increase of the index leads to the predominance of the smallest 3:1 adduct, which was obtained at 70.4wt.-% in the purified resin.

Theoretical values have been calculated according to eq. 4.1.2, wherein $P_x(\mathrm{NCO})$ as molecular amount of each x-mer within the prepolymer, x as an odd natural number (1; 3; 5; ..) and r as the molar ratio of OH/molecular amount of NCO.[104]

$$P_x(\mathrm{NCO}) = r^{\frac{(x-1)}{2}} * (1-r) \quad (4.1.2)$$

Table 9 Distribution of molar masses/adducts of **prepolymer-1** according to Schulz-Flory in comparison to obtained distribution by GPC measurements

Adduct	P_x(NCO)% according to Schulz-Flory	P_x(NCO)% obtained by GPC
3:1	93.3	70.4
5:2	6.22	17.9
7:3	0.41	11.1

The resulting molecular mass distribution of the synthesized **prepolymer-1** is presented in Figure 38. Adducts of 3:1, 5:2 and 7:3 could be detected herein, obtained at index=15.

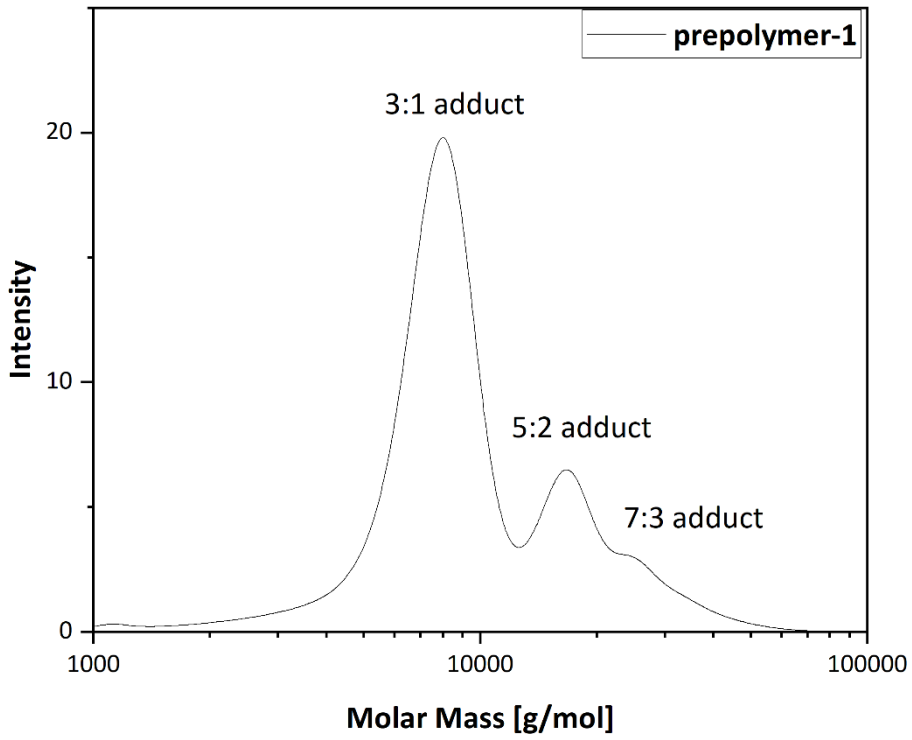

Figure 38 GPC chromatogram of **prepolymer-1**, displaying the 3:1 adduct at 7,998.7 g/mol, 5:2 adduct at 16,732.6 g/mol and 7:3 adduct at 21,195.26 g/mol.

Higher x-mers will probably influence the viscosity of aqueous solutions, as it leads to a higher molecular weight and moreover to an increase in urethane groups which is reported to correlate with an increase in viscosity.[153] The upper limit for viscosity is 9 mPa*s to provide a good spray-ability during the application. Viscosity measurements of **prepolymer-1** in different concentrations in water were conducted to identify the concentration limit at which the viscosity of the solution exceeds the viscosity limit (Figure 39). An exponential fit was applied on the data (blue line) with identified R^2 of 0.998.

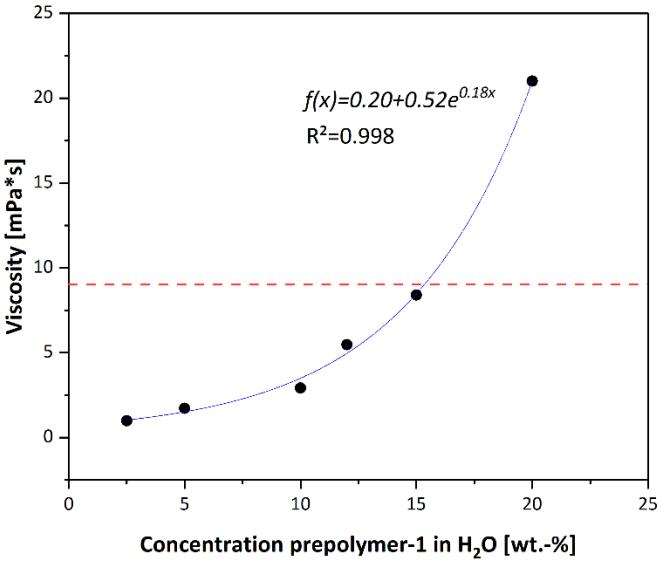

Figure 39 Measured viscosities of different concentrations of **prepolymer-1** in H_2O expressed by an exponential fit with R^2=0.998. The red line marks the viscosity limit of 9mPa*s. A 15wt.-% solution of **prepolymer-1** was identified as the upper limit of concentration.

A concentration of 15wt.-% of **prepolymer-1** in water exhibits a viscosity of 8.39 mPa*s and was identified as the maximum concentration for initial spray tests. According to Figure 39, the viscosity for a 15wt.-% solution of **prepolymer-1** in H_2O is calculated at 7.94 mPa*s. Further modification might also influence the viscosity regarding the approaches of HYGEL 1, 2 and 4. Conversion of NCO to urea or to urethane will likely lead to an increase in viscosity.

Further modifications of **prepolymer-1** were conducted as illustrated for the four approaches in Figure 5 and will be presented in chapters 4.1.2 to 4.1.5.

4.1.2 Preliminary Screening of Approach HYGEL-1

The amine-aldehyde curing mechanism is considered to be a fast reaction type[28] wherein **amine-1** converts with glutaraldehyde (**COO-1**) to obtain crosslinks and therefore an infinite network *via* imine formation, as illustrated in Figure 40.

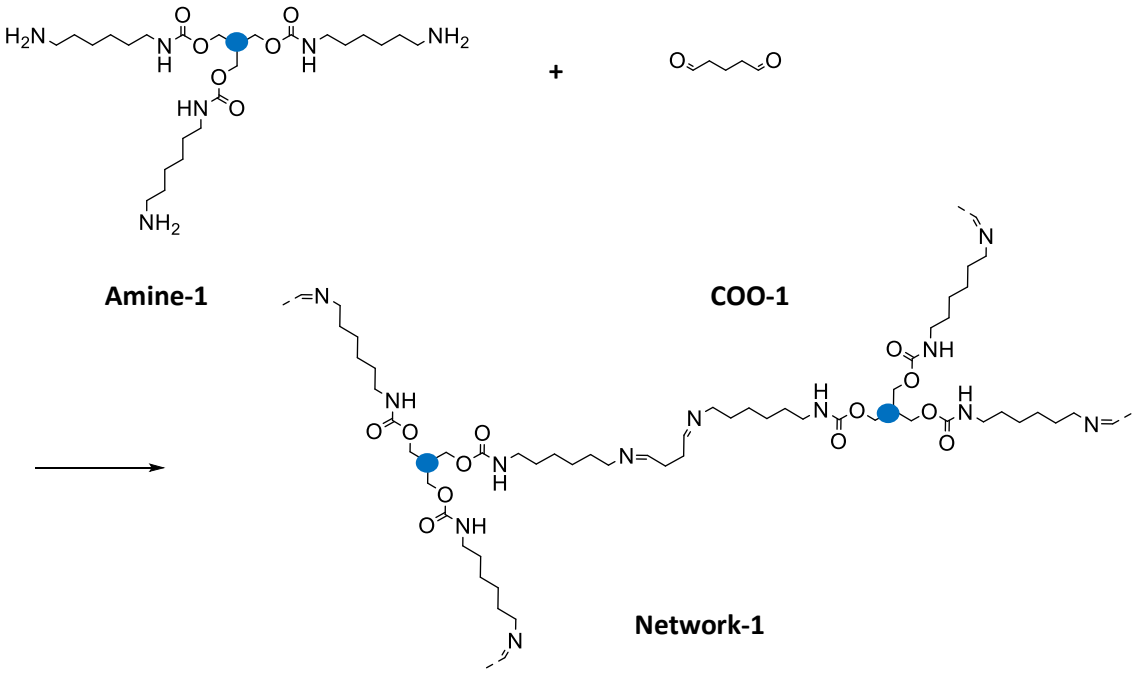

Figure 40 Reaction route of **amine-1** with aldehyde **COO-1** to obtain **network-1**.

Prepolymer-1 was hydrolyzed according to the mechanism illustrated in Figure 41.

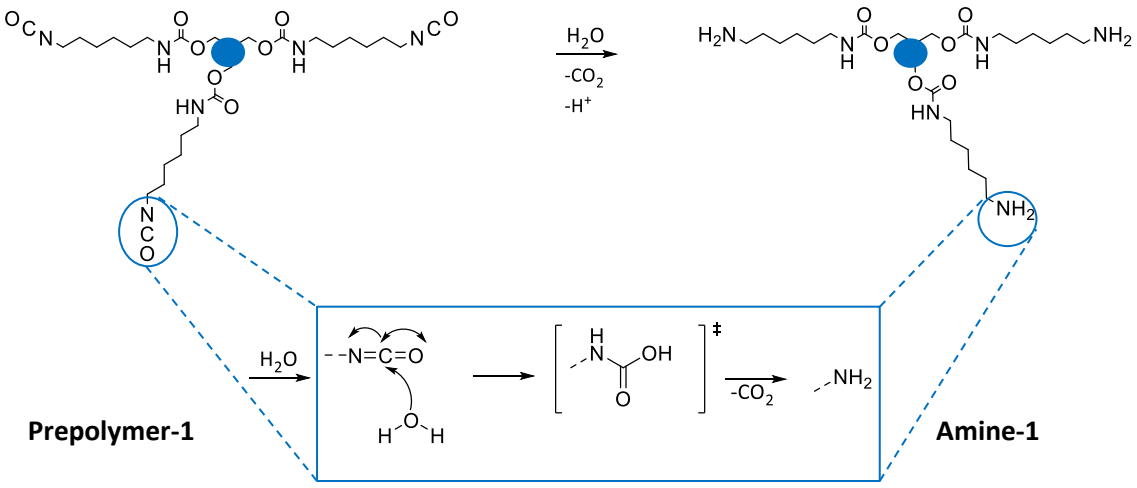

Figure 41 Reaction mechanism of the hydrolysis of NCO groups into primary amines. Basic **Prepolymer-1** is dissolved in a large amount of water. The hydrolysis process starts immediately to first form the carbamic acid which degrades under separation of CO_2 an H^+ to give primary **amine-1**.

As a side reaction, the formation of oligomers and smaller hydrogel networks can be observed. After hydrolysis of the first NCO groups into NH_2 groups, the obtained NH_2 groups can react with remaining NCO to also form a polymeric hydrogel or at least lead to oligomers of **prepolymer-1** (Figure 42). To reduce this side reaction, the hydrolysis was performed in high dilution of 2wt.-% of **prepolymer-1** in H_2O.

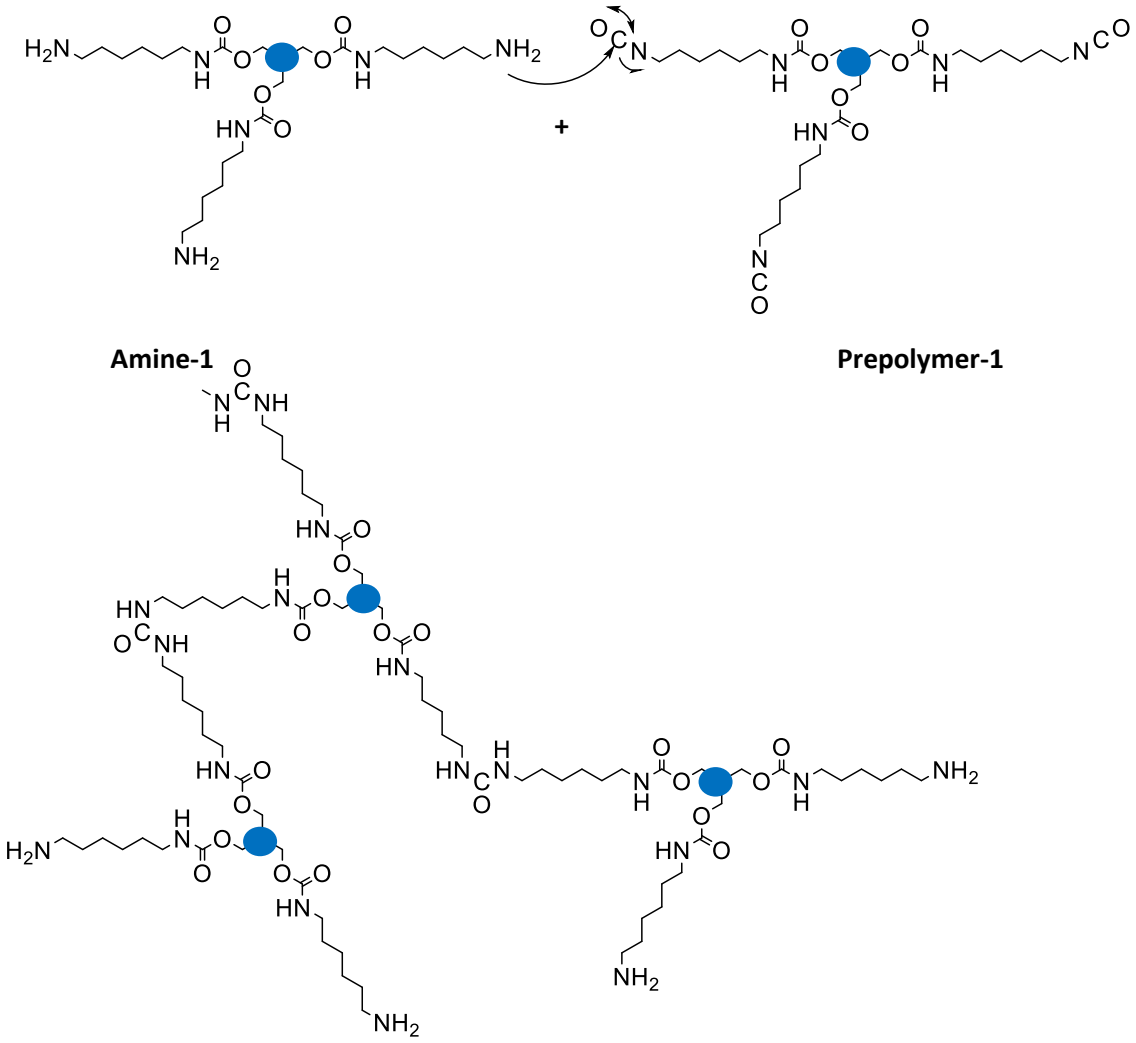

Figure 42 **Amine-1** in reaction with not yet hydrolyzed **prepolymer-1** by a polyaddition of primary amines to yet unreacted NCO groups to form urea groups as crosslinks and build **Oligomer-1** or higher adducts of it.

Oligomers or smaller hydrogel networks of **prepolymer-1** were probably detected as a gelling sediment in the reaction vessel after the completed reaction. The sediment was filtered off and the supernatant was transferred into 20 mL vessels for the freeze drying procedure. The amine value (AV) of **amine-1** was determined at 12.7 mg/kg eq. KOH. Equation 4.1.3 was used to determine the eq. weight of **amine-1**.

$$eq.weight\ R-NH_2 = \frac{56.1 * 1000}{AV} \tag{4.1.3}$$

The equivalent was calculated to be 4417.3 g/eq. In comparison to the eq. weight of 1647.1 g/eq. of **prepolymer-1** before hydrolysis, the eq. weight of **amine-1** increased, which indicates that freeze dried **amine-1** also contained **oligomer-1** or higher adducts of it, which were not filtered off before.

To avoid the formation of **oligomer-1** and higher adducts, the hydrolyses should be performed at higher dilutions. However, the absolute yield will decrease which leads to greater efforts during the concentration process *via* freeze drying.

FT-IR spectra showed also a difference between **prepolymer-1** and **amine-1** (Figure 43). Both characterization methods, AV determination and FT-IR, demonstrated that free NCO groups were either hydrolyzed to NH_2 groups or converted to urea groups in **oligomer-1** or higher adducts. Thus, **Amine-1** was used for further tests.

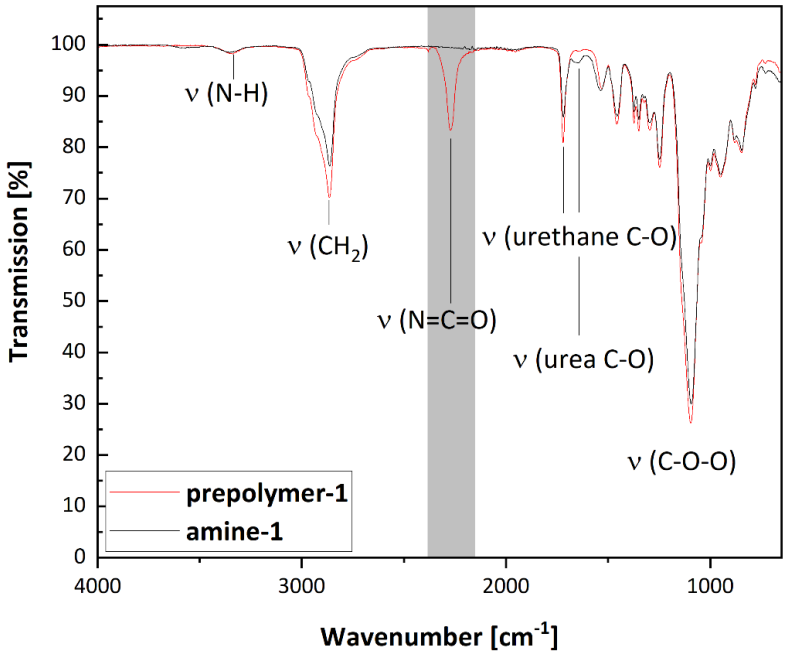

Figure 43 FT-IR spectra of **prepolymer-1** (red line) in comparison to **amine-1** (black line) showing a complete depletion of characteristic NCO band at 2265 cm^{-1}. Remarkable is the occurrence of the urea peak in **amine-1** at 1651 cm^{-1}, indicating that crosslinking of obtained NH_2 groups to remaining NCO groups was present.

First gelation tests were conducted by preparing a 10wt.-% solution of **amine-1** and dropwise addition of a 50wt.-% solution of aldehyde **COO-1**. A gel was obtained within seconds (<60 sec.), as illustrated in Figure 44. The pretesting of the gelation behavior of **amine-1** and aldehyde **COO-1** exhibited a fast curing as it was required. This initial experiment can be seen as proof of concept. The rapid reaction kinetics within <2 minutes, previously reported for the Bioglue system (bovine serum albumin crosslinked with glutaraldehyde **COO-1**) by Chao and Torchiana[28] are corroborated for the presently investigated system under the stated conditions.

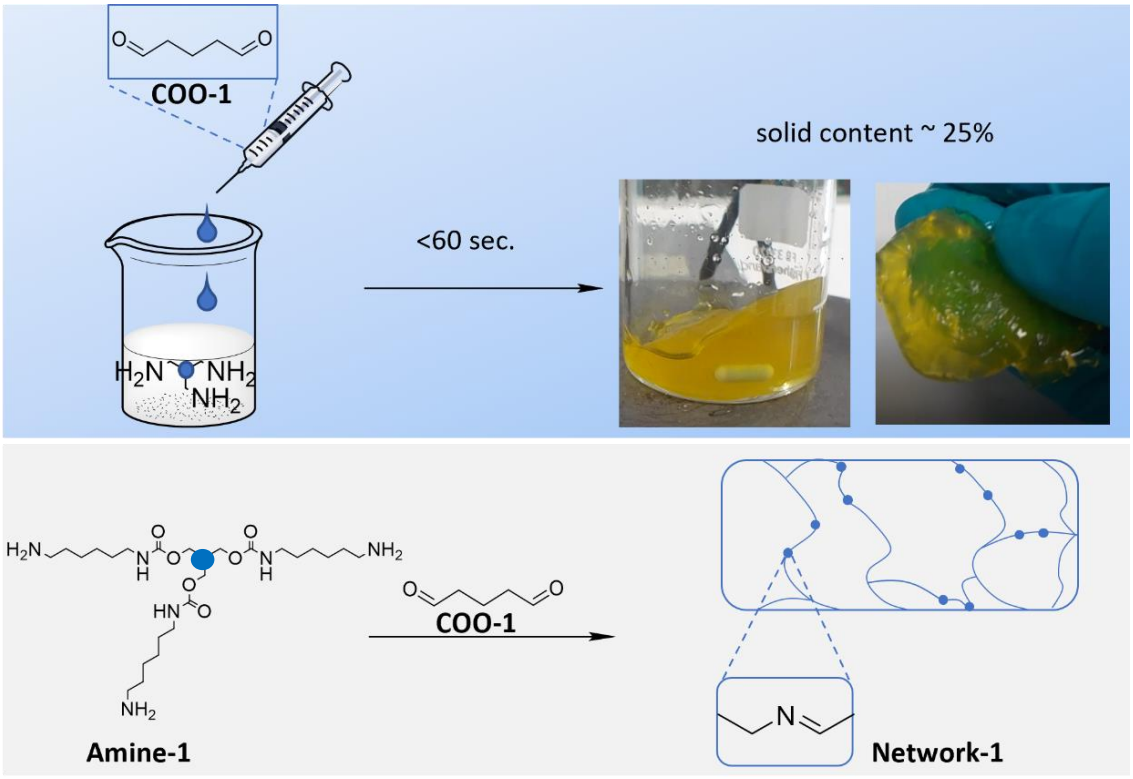

Figure 44 Illustration of the reaction route to yield networks *via* imine formation. This reaction is derived from **amine-1** and aldehyde **COO-1** to yield **network-1**. The resulting network was obtained in <60 sec. as a yellow hydrogel with mechanical strength to allow removement from the beaker as a whole. Imine bonds as crosslinkers are depicted in **network-1**.

For adjustment of the system to the viscosity limits required for the application, viscosity measurements of **amine-1** and aldehyde **COO-1** were conducted and summarized in Table 10.

Table 10 Overview on viscosity measurement results of aldehyde **COO-1** and **amine-1** to find a suitable concentration within the limitations of 9mPa*s. Highest possible concentration of **COO-1** is 25wt.-% in water while **amine-1** can be adjusted to the molar amount resulting from a 25% solution of **COO-1** in water.

Substance	Concentration of substance in H_2O [wt.-%]	**Resulting viscosity** (γ=50, T=23°C) [mPa*s]
Aldehyde **COO-1**	50	17.3
Aldehyde **COO-1**	25	8.3
Aldehyde **COO-1**	10	1.29
Amine-1	10	14.2

Since a 10wt.-% solution of **amine-1** displayed a viscosity of 14.2 mPa*s it was decided to work with a concentration of 9wt.-% **amine-1** in H_2O. A volume ratio of 2:1 (**amine-1**:**COO-1**) was used. The solution of **amine-1** was stirred while the solution of **COO-1** was added dropwise. The reaction mixture turned slightly yellow after a few seconds without yielding a gel. Since the addition of acidic components is described as catalyzing imine formation[154–156] a few drops of HCl (0.1M) were added. The reaction mixture turned red while a gelation behavior was observed which differs from the proof of concept experiments, from Figure 44. Regarding the solid content of

6.7wt.-% the resulting network is likely close to the sol-gel border and thus not able to span a network through the entire solution, as schematically illustrated in Figure 45.

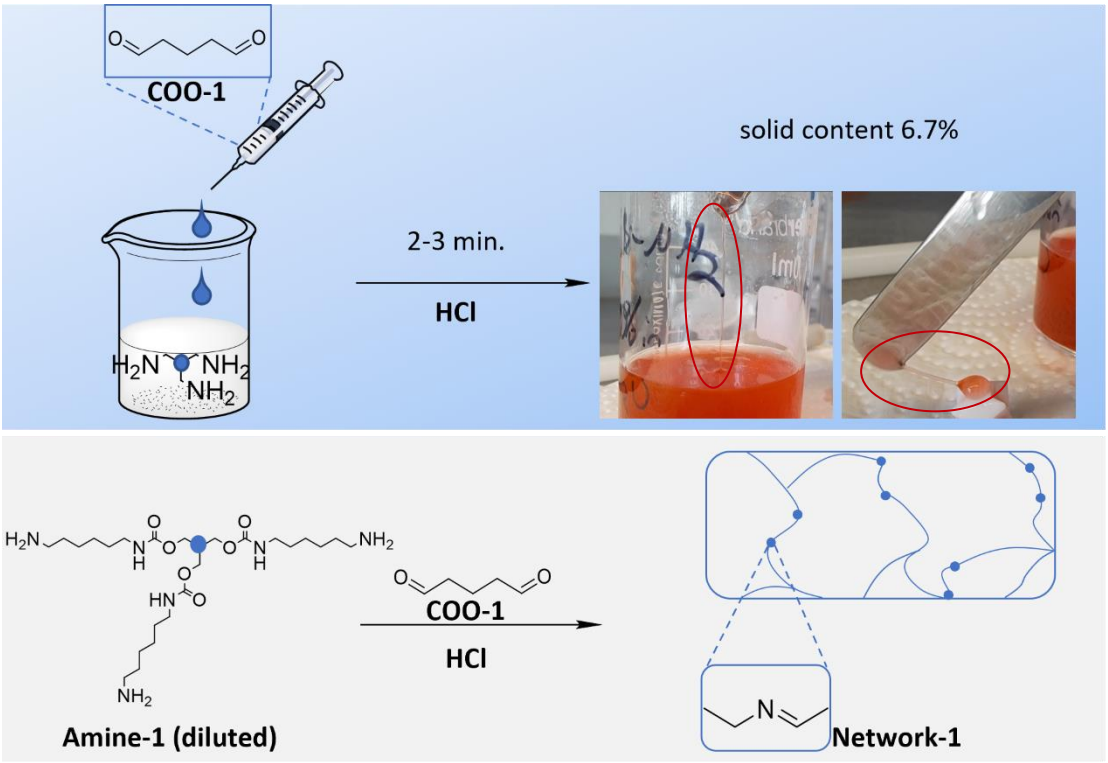

Figure 45 Illustration of the reaction route for diluted networks from the formation of imine as crosslinkers. This reaction is derived from **amine-1** and aldehyde **COO-1** to yield **network-1.** Since no rigid network formation could be observed after 2 minutes, a few drops of HCl were added. The color turned from slightly yellow to red. A gelation effect was observed but without the formation of a rigid network with advanced mechanical properties. **Network-1** might be close to the sol-gel border und thus not able to hold the huge amount of water inside as the solid content is 6.7wt.-%.

By the use of small dialdehydes as crosslinking agent, solid contents are limited when maintaining an equal molar ratio of amines/aldehydes. One option to increase the solid content is to implement the aldehyde function into a macromolecular backbone. By maintaining the molar equivalents of **amine-1**, the solid content increased since the eq. weight of the aldehyde increased.

One reaction route to implement aldehyde functions into a polyurethane backbone is illustrated in Figure 46.

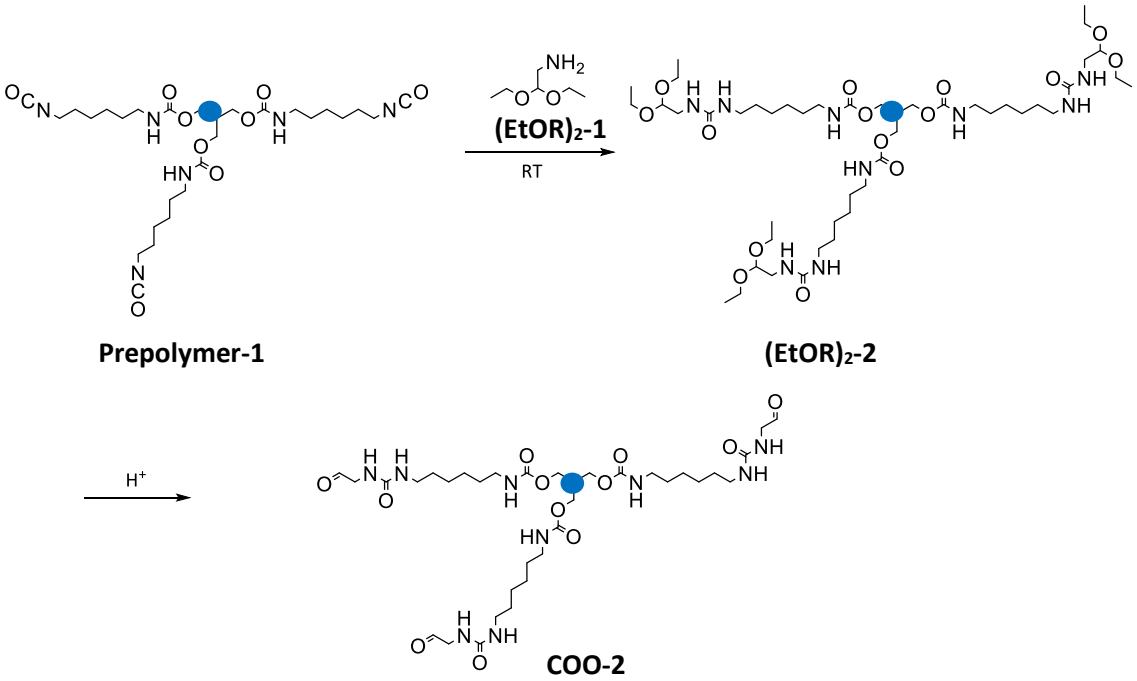

Figure 46 Sequence for the implementation of aldehyde functions to the chain ends of prepolymer-1 with the use of amino-diacetal. Addition of an acidic component leads to acetal splitting and **COO-2** might be obtained.

Acidic splitting of acetals to aldehydes, is described in the literature[157] **(EtOR)$_2$-2** was chosen as a reagent since the reaction of NH_2-groups and NCO groups are fast and can be conducted at RT. Conversion of **prepolymer-1** to **(EtOR)$_2$-2** was monitored using FT-IR. After the addition of **(EtOR)$_2$-1** was completed, the characteristic NCO absorption band depleted.

Figure 47 compares the ^{1}H-NMR spectra of **prepolymer-1** and obtained **(EtOR)$_2$-2**. Herein, two urea groups have been detected as triplets at 5.9 and 5.7 ppm. The latter also occurred in the spectra of **prepolymer-1**, where no urea groups should be present. This effect can be explained by the residual water content in d_6DMSO, which was used as a solvent for the measurements. The included water leads to hydrolysis of NCO to NH_2, yielding urea groups as crosslinks by an intermolecular reaction of **prepolymer-1**. Urea group at 5.9 ppm exclusively appears in **(EtOR)$_2$-2**. Further characteristic peaks are detected at 4.38 ppm, which arises from the proton at position 3, 3.08 ppm arising from protons of position 4. 4 is herein detected as triplet, which is deviating from expectations wherein it should appear as doublet. This effect could probably be explained by a coupling to urea proton. Additional tripletts at 1.12 ppm were detected, arising from protons at position 5. Other alkyl signals could not be detected as they are probably arising in the huge area depicting several alkyl-protons from 1.0 ppm to 1.6 ppm.

^{1}H-NMR spectra indicates that conversion of **prepolymer-1** to **(EtOR)$_2$-2** was successful.

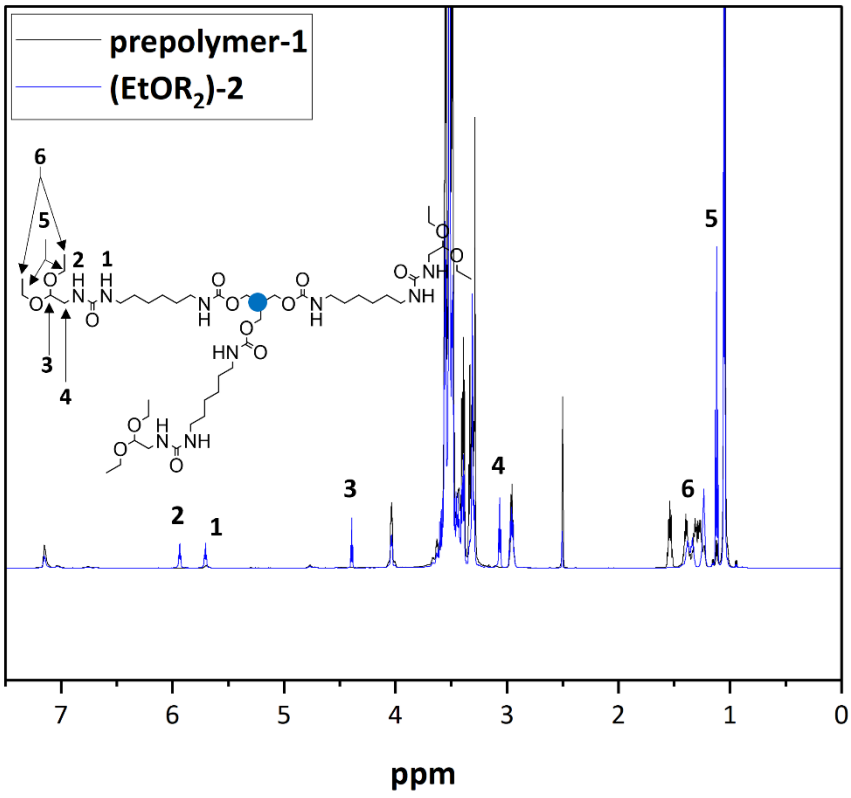

Figure 47 Comparison of ^{1}H-NMR spectra of **prepolymer-1** (above) to obtained **$(EtOR)_2$-2** (below).Urea peaks arise at 5.9 and 5.7 ppm, wherein the latter additionally occurred in **prepolymer-1** mainly caused by residual water content in d_6DMSO. Ethylene groups are probably below huge signals from alkyl peaks in the area of 1.0ppm-1.6 ppm and could not be detected, for this reason.

Acetal splitting of **$(EtOR)_2$-2** to **COO-2** was carried out under acidic conditions by the addition of HCl. The solution was stirred for 4 h at RT and was neutralized with NaOH afterwards. Freeze drying procedure was conducted to obtain **COO-2**. FT-IR spectra of **$(EtOR)_2$-2** in comparison to **COO-2** are presented in Figure 48, herein it becomes visible that a certain amount of water has not been removed from the reaction mixture. Additionally, it is unclear if the peak at 1712 cm^{-1} arises from the aldehyde, which are reported to occur at 1720-1730 cm^{-1}.

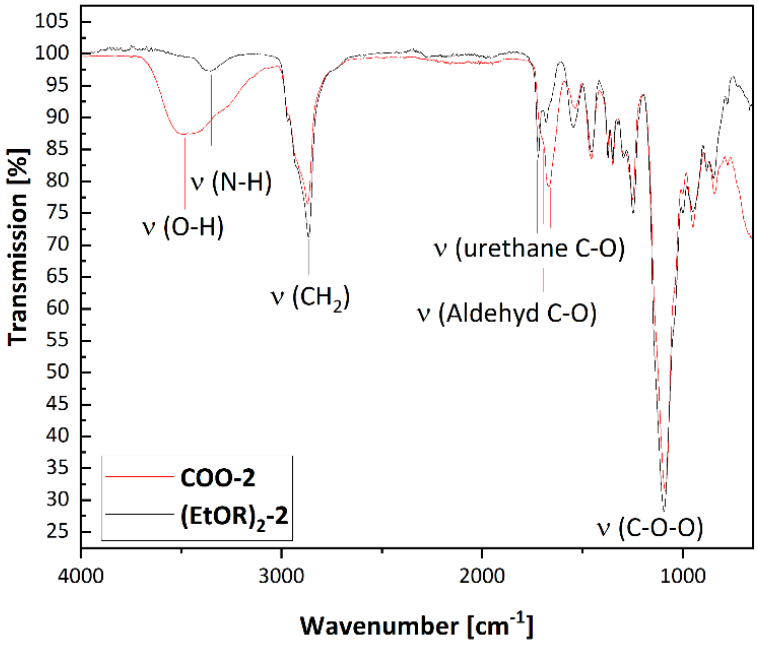

Figure 48 FT-IR spectra of **(EtOR2)-2** (black line) in comparison to **COO-2** (red line). The broad peak in **COO-2** at 3400 cm^{-1} indicates a certain amount of water after purification. An aldehyde peak could be likely appear at 1712 cm^{-1} but interferes with the C-O band from urea and urethane.

^{1}H NMR were conducted to identify a characteristic aldehyde peak (Figure 49).

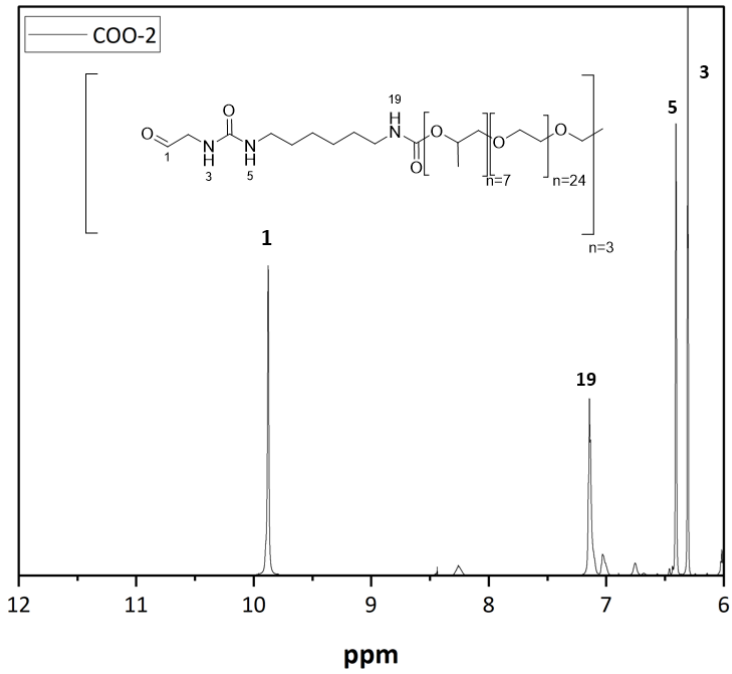

Figure 49 ^{1}H NMR spectra of **COO-2** in d_6DMSO. The occurrence of a sharp singlet at 9.88 ppm evidenced the introduction of an aldehyde to **prepolymer-1**.

Since **COO-2** features *f*>2 in its initial structure, the amine was changed from **amine-1** (*f*>2) to **Jeffamine ED2003** (*f*=2) for first gelation experiments. A 16.6wt.-% solution of **Jeffamine ED2003** in water was prepared and 10 mL of a 25wt.-% solution of **COO-2** were added dropwise. After

72 h no visual gelation reaction could be observed (Figure 50). It is questionable whether this effect occurred by a decrease of reaction kinetics, since functional groups of NH_2 and **COO-2** are provided as macromolecular substances.

As demonstrated via IR and ^1H NMR, the aldehyde **COO-2** was obtained from precursor prepolymer **$(EtOR)_2$**. The provision of the aldehyde as a macromolecule might decrease reaction kinetics, compared to small aldehydes like **COO-1** which indicates a decrease in reaction kinetics in the gelation reaction.

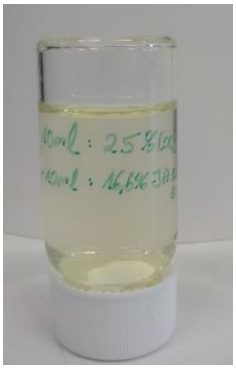

Figure 50 10 mL of 16.6wt.-% **Jeffamine ED2003** mixed with 10 mL of 25wt.-% of **COO-2** after 72 h. Gelation was not detected by visual analyses.

As this crosslinking approach needed further effort for the improvement of the crosslinking reaction, it was decided to continue with a crosslinking approach which showed sufficient properties in initial experiments, which was HYGEL-3. However, the concept of HYGEL-1 could still be of interest for fast crosslinking application.

4.1.3 Preliminary Screening of Approach HYGEL-2

The curing mechanism of HYGEL-2 is based on a polycondensation method using alpha-ethoxy-silane terminated prepolymers which start to crosslink rapidly once in contact with water, which excludes the use of water as a solvent for the spray application. Application of a system based on **EtOSi-prepolymer-1** would be possible A) as pure substance, or B) in organic solvents, unreactive to alkoxysilanes. Since the latter can be excluded due to cytotoxicity concerns regarding the use of solvents for an application in the body, an application of **EtOSi-prepolymer-1** as a pure substance is favored.

As illustrated in Figure 8, **prepolymer-1** was modified with **EtOSi-1** to functionalize NCO groups and yield a silane-terminated-prepolymer **EtOSi-prepolymer-1** which is able to crosslink *via* H_2O induced condensation reaction. IR measurements indicate a full conversion of NCO to EtOSi bearing urea groups (**EtOSi-prepolymer-1**) by complete depletion of NCO band at 2265 cm^{-1} (Figure 51).

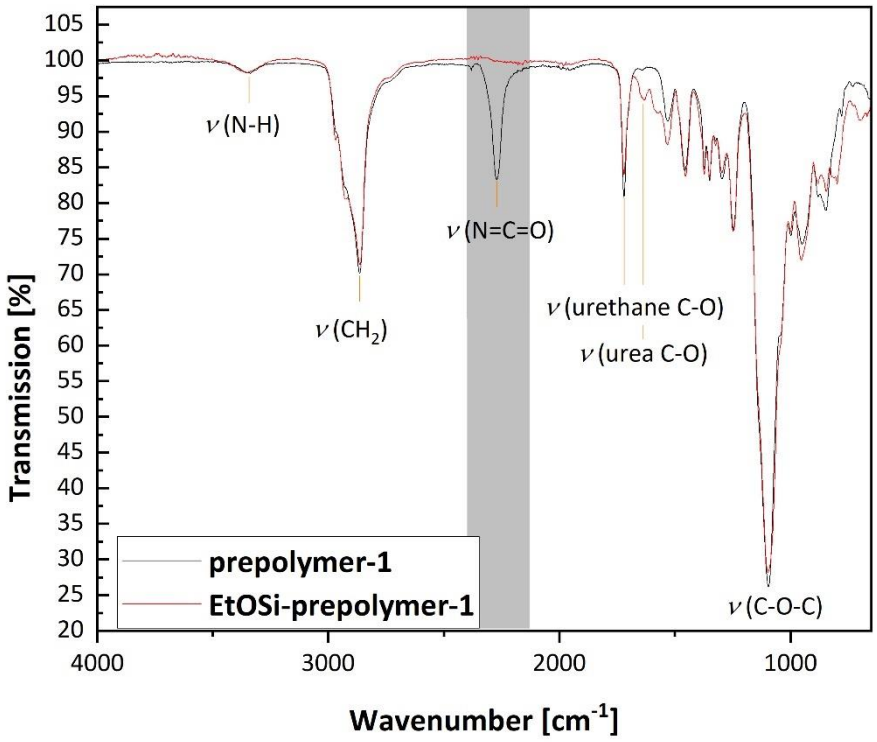

Figure 51 Comparison of FT-IR spectra of prepolymer-**1** (black) in comparison to **EtOSi-prepolymer-1** (red). The grey marked area depicts the characteristic NCO band at 2265 cm^{-1} which fully depleted in **EtOSi-prepolymer-1**.

The viscosity of **EtOSi-preolymer-1** was determined to be 28,900 mPa*s, which is a large increase in comparison to **prepolymer-1** with a viscosity of 3,950 mPa*s.

In this system an application of the pure substance was favored. For this reason, it was decided to apply a thin film of the pure **EtOSi-prepolymer-1** on a release paper at a film thickness of 240 µm to analyze the curing behavior. Three different curing approaches have been conducted:

a) addition of water after application b) applying on a moistened surface c) curing by humidity on the release paper. Figure 52 presents the visual appearance of the resulting material after curing and the respective curing time. For this experiment, the curing time is defined pragmatically as the time needed until no more material sticks to the glove upon touching the thin film. All samples were brittle after the curing process, probably caused by the resulting high crosslink density. However, the identified curing time reaches the dimensions of the required fast crosslinking of <60sec.

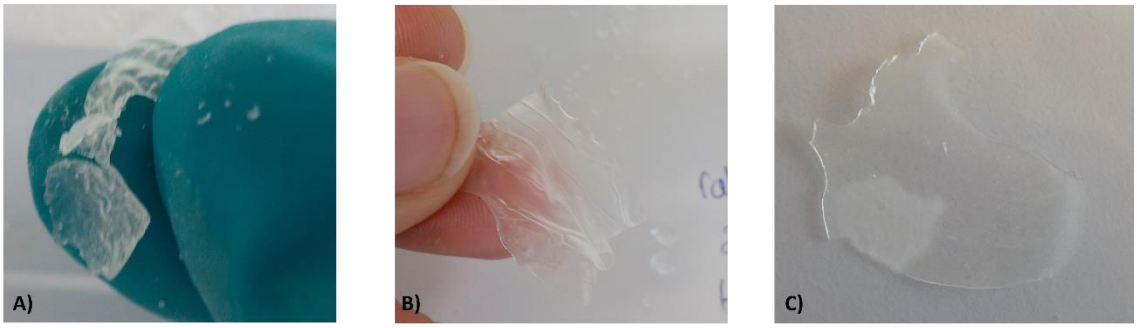

Addition of water after application Curing time: 80 sec.

Applied on moistened surface 72 sec.

Cured by humidity 749 sec.

Figure 52 Cured materials from **EtOSi-prepolymer-1** obtained by different curing approaches. A) Addition of water after the supplication B) applying EtOSi-prepolymer-1 on a moistened surface C) cured by humidity. Curing times are given for each approach defined here as the time taken until no more material sticks to the gloves when touching the film.

Additionally for this approach tensile tests of the pure substance **EtOSi-prepolymer-1** have been conducted. Tensile testing was carried out from samples of the cured **EtOSi-prepolymer-1**. Means of Elongation at break were detected at 8.5±4.5% and tensile strength at break at 0.41±0.27 N/mm² (=410±270 kPa) (Figure 53). Regarding the requirement profile tensile strength at break seems to be sufficient, which is reported in literature as 1.6 kPa to 21 kPa.[119] With regard to the elongation ratios which are obtained at 8.5%±4.5% it is difficult to estimate whether these values might negatively influence the normal abdominal wall mobility, when being applied on the surface of tissues. For elongation values there is no defined guide value which needs to be fulfilled. However, it is described that the varying intraabdominal pressure leads to a certain expansion of the abdominal wall.[125] It was reported on different elongation ratios of the abdominal wall when applying a force of 16 N on the whole samples, which were taken from human tissues post mortem. Mean distensions of 11% to 32% have been measured herein.[118] Assuming that these results are comparable to real life conditions, a coating of pure **EtOSi-prepolymer-1** would strongly influence the normal mobility of the abdominal wall, which should be avoided. Without further dilution strategies, this approach seems to be unsuitable for an application as adhesion prophylaxis product, when being applied as a pure compound. Currently, application techniques that can handle very high viscous materials under operational/medical conditions are missing which would require further efforts outside the scope of this thesis work. For these reasons, the HYGEL-2 approach was abandoned.

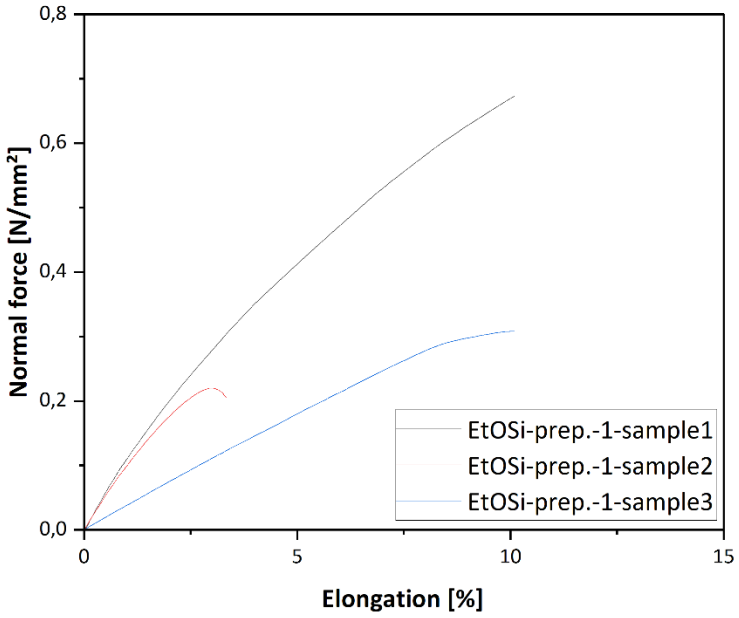

Figure 53 Tensile testing of a cured **EtOSi-prepolymer-1** in a threefold determination. Tensile strength at break at mean=0.41±0.27 N/mm² with elongation ratios of mean=8.5%±4.5%.

4.1.4 Preliminary Screening of Approach HYGEL 3

Since the HYGEL-3 approach was most successful in the screening and pretesting phase, initial experiments are limited to a brief summary as the investigation and adaption of this system according to the requirement profile will be presented in chapter 4.2.

In the HYGEL-3 approach, the reaction of NCO groups with primary amines was investigated as the basic crosslinking reaction to yield a network. This reaction type is reported in general to be fast at high yields. Reaction half times of primary aliphatic amines with aromatic diisocyanates (monomers) have been reported at ~0.002 s.[158] A decrease in reaction speed of primary aliphatic amines to isocyanates linked to a macromolecular backbone is expected. For this approach no further modifications were necessary, **prepolymer-1** was used as initial starting point. As a cross-linking agent many amines would be suitable, comprising at least two primary NH_2 functions. Due to its high eq. weight and large EO based backbone **Jeffamine ED2003** was chosen as starting substance, comprising *f*=2. Due to the large eq. weight of the herein used amine, a volume ratio of 1:1 was chosen for initial curing tests. 40 g of a 10wt.-% solution of **prepolymer-1** in water was chosen as a starting concentration. 40 g of an equimolar solution of **Jeffamine ED2003** in water was prepared (6.8wt.-%). This solution was mixed with the solution of **prepolymer-1** and stirred for 60 sec. in a speedmixer to yield a hydrogel network with a solid content of 8.4wt.-%. The underlying reaction concept and a thereby obtained hydrogel is depicted in Figure 54.

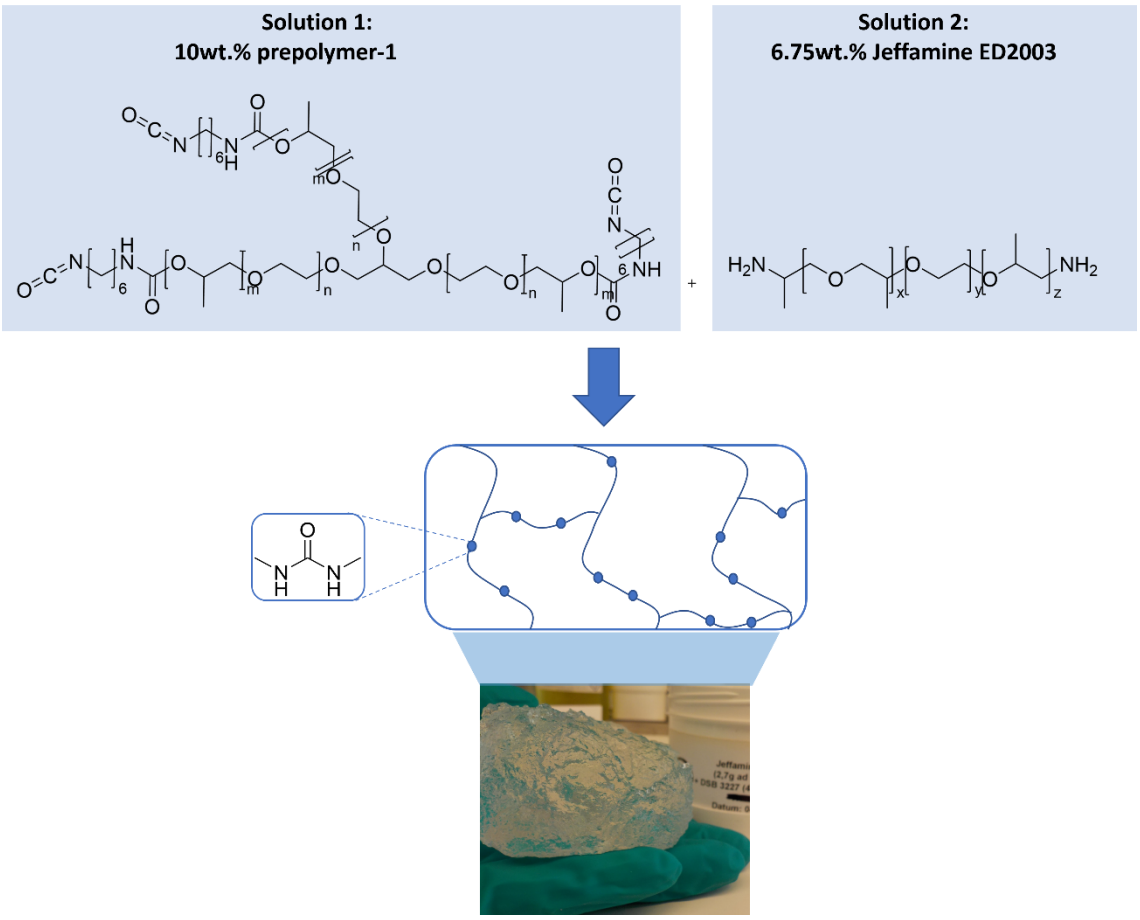

Figure 54 General reaction sequence to obtain hydrogels by NCO and NH_2 reaction. The obtained hydrogel after stirring a 10wt.-% solution of **prepolymer-1** with a 6.8wt.-% solution of **Jeffamine ED2003** for 60 sec in a speedmixer is depicted below. Solid content of the resulting hydrogel is 8.4%.

Visual assessment revealed rapid crosslinking of both components, resulting in a hydrogel as illustrated, within 60 seconds. From visual and haptic evaluation, this hydrogel also comprises a certain mechanical stability. Single solutions have been prepared while obeying the viscosity limitations. Further characterization of the features of this system will be investigated in detail in chapter 4.2.

Regarding the initial experiments HYGEL-3 seems to be a promising approach for an adhesion prophylaxis system. From this point in time the system is compatible with the required viscosity limit of 9 mPa*s. Solutions used herein have been measured below this value. Moreover, this approach allows a fast curing of ≤60 sec. and is water soluble in the required concentrations. Mechanical properties had not been analyzed in detail at this point, but haptic and visual assessment indicated sufficient mechanical strength.

4.1.5 Preliminary Screening of Approach HYGEL-4

The underlying concept of approach HYGEL-4 was addressed in detail in chapter 3.1.2. Macromolecules with different constitutions of EO/PO ratios will be analyzed for the investigation of a potential thermoresponsive behavior. Two different basic prepolymers were chosen (**prepolymer-1** and **prepolymer-thermo**) to investigate their thermoresponsive behavior after NCO-

inactivation with *f*=1 reactants, consisting of different EO/PO ratios. **Prepolymer-thermo** comprises a high PO based backbone with *f*=2 and was investigated since the gelation mechanism of the thermoresponsive approach differs and *f*=3 is not mandatory. According to Soliman *et al*.[33] the first step of the gelation process is the formation of micelles with a PO-based core and an EO based shell. With further energy input the EO shells of the micelles begin to adhere to each other, as described in chapter 3.1.2, pure polymeric EO (PEO) tends to crystallize.[76] However, crosslinking is not induced *via* single polymer strands, but by the arrangement of micellar strands consisting of individual polymer strands. **Prepolymer-1** contains a high amount of EO units (~75wt.-%), thus modifications with PO based reactants are useful for a potential integration of a thermoresponsive behavior. **Prepolymer-thermo** mainly consists of PO units so that the implementation of further EO based agents may be useful.

Table 11 Constitution of prepolymers used for the implementation of modifcations agnets, aiming for introducing of thermoresponsive behavior, including EO/PO amounts, molecular weights and *f*.

Prepolymer	Amount EO/Amount PO [%]	Molecular weight [g/mol]	*f*
-1	72.84/27.16	5060	3
-Thermo	13.78/86.72	4200	2

Prepolymer-1 and **prepolymer-thermo** have been prepared to conduct further modifications according to Figure 5. NCO inactivation was carried out by the use of polyether with *f*=1, either OH or NH_2 capped as modification agents. Thus, three different polyether types, differing in their EO/PO content or in their M_W, as reported in Table 12, were used as modification agents.

Table 12 Overview on three different reactants for the modification of prepolymers with *f*=1. Main differentiation parameter is depicted by "Amount EO/Amount PO". "Molecular weight", which is in this case equal to eq. weight, is comparable between the three reactants. Molecular weight is calculated from determined OH/NH_2 value.

Reactant	Amount EO/Amount PO (Starter and isocyanate excluded) [%]	Molecular weight [g/mol]	Reacting group to NCO prepolymer
Jeffamine M2005	13.56/86.44	2157.7	NH_2
Polyether 34	47.14/52.86	1607.4	OH
Polyether 25	84.36/15.64	2125.0	OH

One equivalent of the reactant was added to the prepolymer and stirred either at RT (NH_2 capped-reactant) or at 80°C (OH-capped-reactant) until depletion of the NCO peak at 2265 cm^{-1} was observed. NCO conversion was analyzed *via* FT-IR-measurements by tracking respective

NCO bands at 2265 cm^{-1}. Spectra are presented in Figure 55 A and B with identified significant IR signals for urethane and urea compounds.[159]

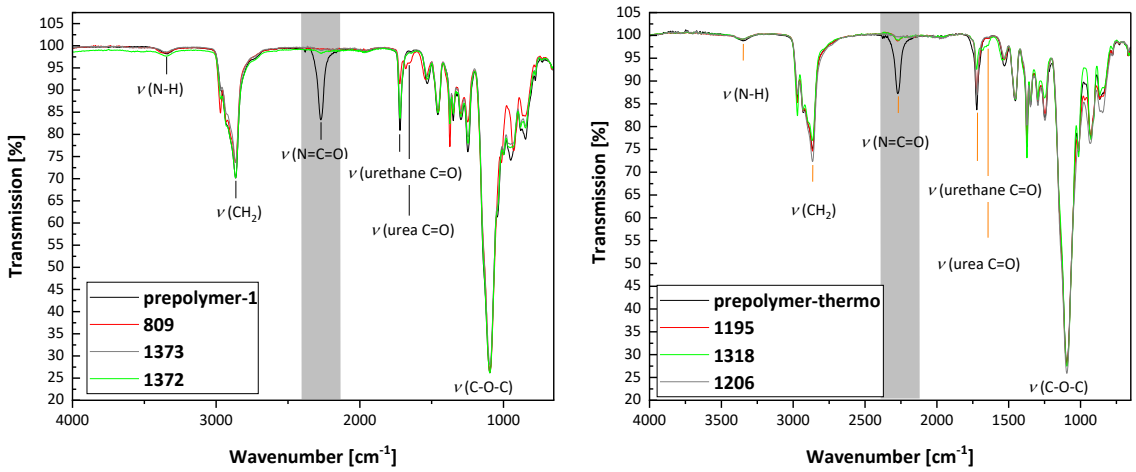

Figure 55 FT-IR spectra of A) **prepolymer-1** and synthesized macromolecules thereof *via* different modification agents. B) **prepolymer-thermo** and synthesized macromolecules thereof *via* different modification agents. Full depletion of characteristic NCO band was observed during the synthesis of all six macromolecules.

Additionally, a C=O stretching vibration was observed in the spectra of **809** (1682 cm^{-1}) and **1318** (1674 cm^{-1}) originating from the respective urea groups which had formed *via* modification with NH_2 capped reactants.

Table 13 presents an overview on the reaction times until 100% NCO conversion was reached for each prepolymer and the respective reactant.

Table 13 Overview of the reaction times of different prepolymers with different reactants at RT (**Jeffamine M2005**) or 80°C (Polyether 24, Polyether 25). Time is given for 100% NCO conversion.

Prepolymer	Reactant	Name of resulting macromolecule	Time until 100% NCO conversion [h]
Prepolymer-1	Jeffamine M2005	809	2.5
	Polyether 34	1373	23
	Polyether 25	1372	24.5
Prepolymer-Thermo	Jeffamine M2005	1318	1.67
	Polyether 34	1206	42
	Polyether 25	1195	16

As expected, the reaction speed of the **Jeffamine M2005** is the highest, since it is NH_2-capped and as described by Delebecq *et al*. by factor 1000 faster than OH-capped reactants.[32] The remarkably low reaction kinetics of prepolymer-thermo with **Polyether 25** can be attributed to a slight excess of the **prepolymer-thermo** component. After an initial reaction period of 30 h, an

additional 0.5 mL of **Polyether 25** were added to the reaction vessel. Consequently, complete depletion of NCO groups was achieved within a further 11-hour period.

Since according to Table 5, chapter 3 the viscosity is a limiting factor, three different concentrations of each product were prepared (10wt.-%, 20wt.-% and 50wt.-%) and stirred in an ice bath to get a clear solution. 50wt.-% did not result in a solution, indicating that saturation is reached <50wt.-%. Figure 56 and 57 present the appearance of the different samples at 4°C in comparison to their appearance at 37°C. It is clearly visible that **1206**, **1372** and **1373** did not display visual changes with varied temperature. Sample **1195** shows a phase separation at 37°C, as visible from Figure 56, indicating a thermoresponsive behavior. However, the sediment of sample **1195** still exhibits flow properties. Sample **809** shows gelating behavior, especially in the 20wt.-% solution as it sticks to the bottom of the glas vial when being flipped without a separation of the aqueous phase. The prepolymer-thermo analogue of **809** is **1318**, which appears turbid at 4°C and at 37°C, indicating that this sample is insoluble at the tested concentrations of 10 and 20wt.-%, leading to a dispersion instead of a solution. This effect could be caused by the high amount of PO units in the macromolecule. Of all tested samples, **1318** comprises the highest PO content.

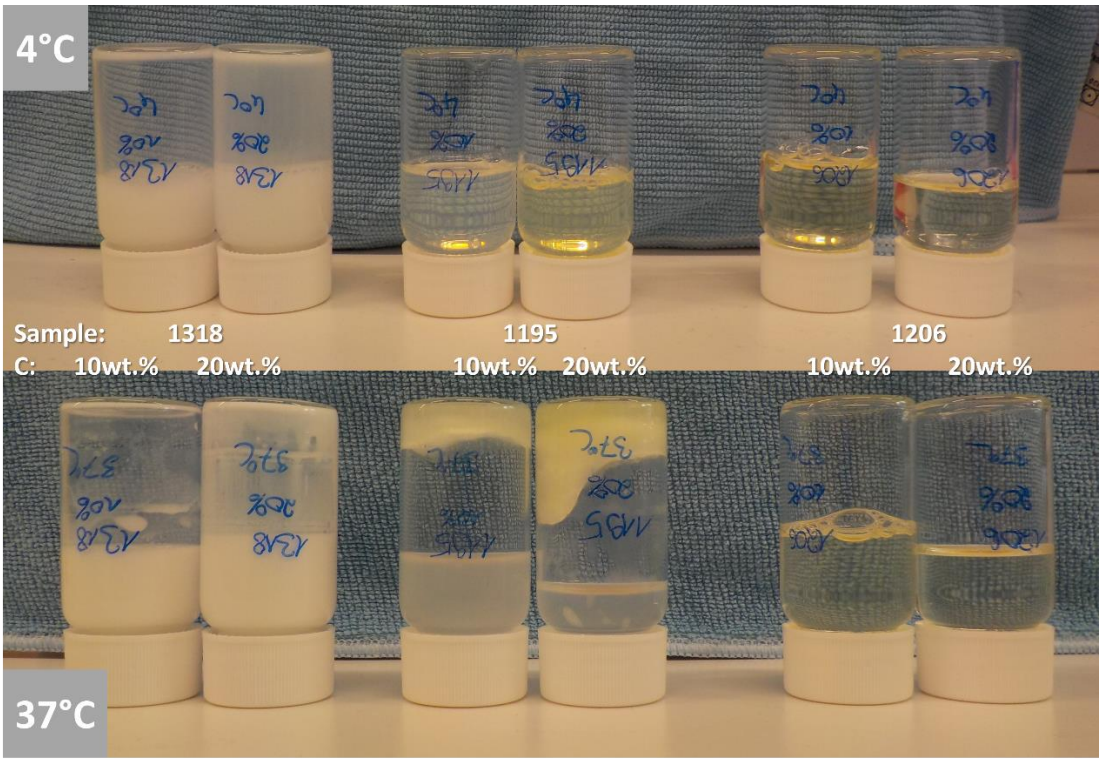

Figure 56 10wt.-% and 20wt.-% solutions of samples **1318**, **1195** and **1206** at 4°C (above) vs. 37°C (below). Increased turbidity indicates a thermoresponsive behavior in **1318** and **1195**. Additionally, samples of 1195 showed gelation behavior *via* visual analyses.

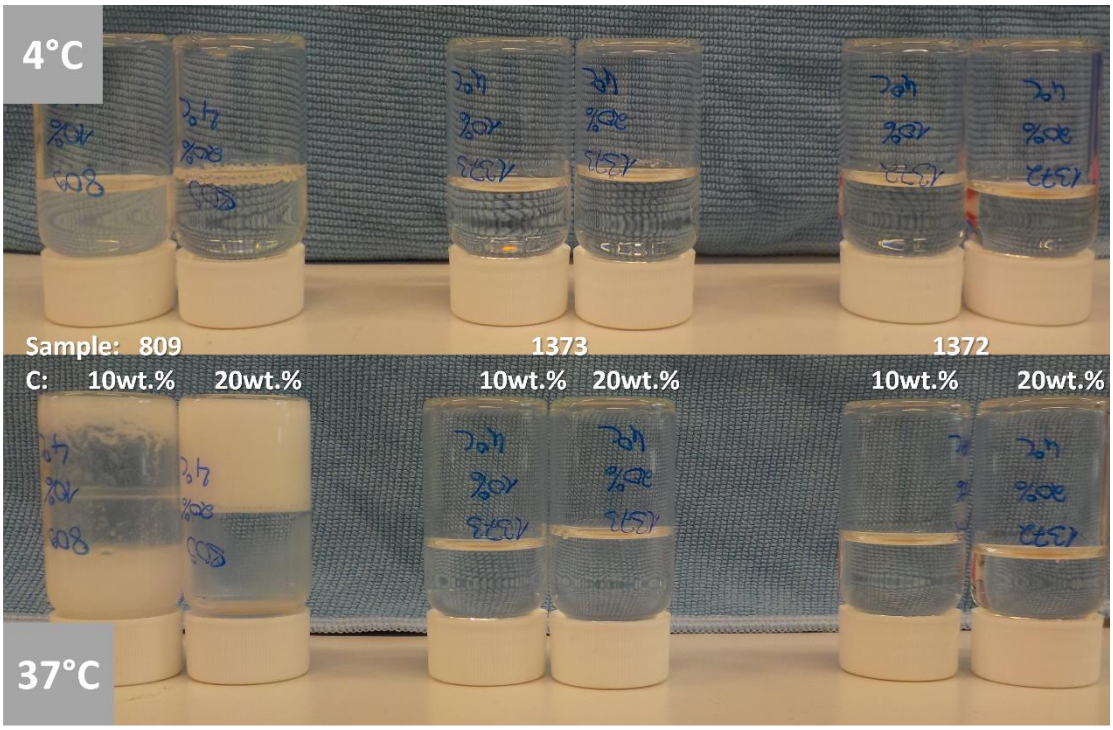

Figure 57 10wt.-% and 20wt.-% solutions of samples **809**, **1373** and **1372** at 4°C (above) vs. 37°C (below). Increased turbidity indicates a thermoresponsive behavior in **809**. Additionally, both samples of **809** showed gelation behavior analyzed by visual analyses.

The occurred turbidity indicates a temperature influenced solubility, showing that a thermoresponsive behavior was introduced on sample **809** and **1195**.

For further investigation of a potentially thermoresponsive behavior of the modified prepolymers in a concentration of 10wt.-% and 20wt.-%, each, rheological measurements were conducted with a temperature profile from 0°C to either 26 or 37°C at a shear rate (γ) of 250 sec.$^{-1}$ and a heating rate=1°C/min. Table 14 summarizes crucial results from the rheological measurements, namely the highest measured viscosity, the lowest measured viscosity and the temperature at which each was detected.

Table 14 Overview of the measured viscosity parameters as a function of the temperature of the two **prepolymers -1** and **-thermo** each modified with one of three different monofunctional polyether. The measurements were carried out in the temperature range 0-26°C/37°C, τ =250/s, heating rate=1°C/min.

Prepoly-mer	Modification agent	Name	C in H_2O [wt.-%]	Highest viscosity [mPa*s]	Tem-pera-ture at highest viscosity [°C]	Lowest viscosity [mPa*s]	Temepra-ture at lowest vis-cosity [°C]
-1	Jeffamine M2005	809	10%	133	24.79	1.20	5.82
			20%	3193	25.9	55.98	20.39
	Polyether 34	1373	10%	15.34	-0.08	5.30	30.28
			20%	71.47	-0.07	23.61	29.78
	Polyether 25	1372	10%	21.44	-0.25	8.01	25.52
			20%	94.26	-0.25	34.86	25.52
-thermo	Jeffamine M2005	1318	10%	9.56	-0.12	1.04	30.02
			20%	49.09	-0.15	1.71	31.77
	Polyether 34	1206	10%	11.47	-0.03	2.72	31.77
			20%	16.19	15.77	54.57	36.78
	Polyether 25	1195	10%	11.46	-0.03	2.72	31.52
			20%	54.57	31.28	16.19	15.77

Additionally rheological measurements are presented in Figure 58, displaying the viscosity of each modified prepolymer in comparison to 10wt.-% and 20wt.-% aqueous solutions thereof as a function of temperature. Herein it is clearly visible that samples of **1372** and **1373** showed no thermoresponsive behavior in the measured temperature profile as they feature higher viscosity values at lower temperatures and lower viscosities at higher temperatures, which is expected for viscosities of solutions.[160] The highest influence of temperature on viscosities is reached in sample **809**, using **Jeffamine ED2005** as modification agent, which has been described previously to display a thermoresponsive behavior.[161,162] 20wt.-% solutions of **1318** and **1195** showed a slightly increase in viscosities which might be thermo-induced. Sample **1206** also showed a slight peak from 28°C to 37°C.

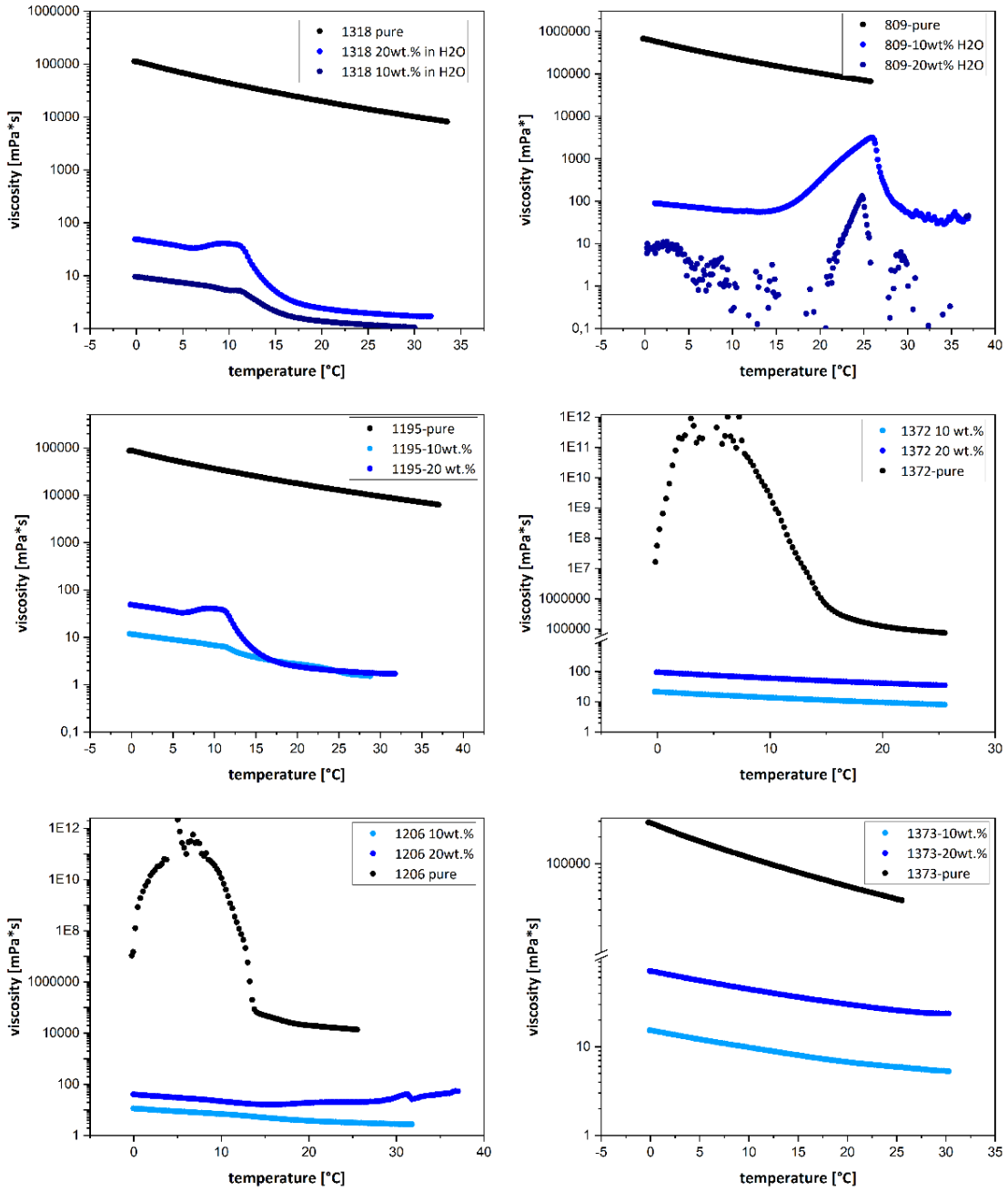

Figure 58 Rheological measurements of the six synthesized macromolecules. Viscosity is presented as a function of temperature for the pure macromolecule (black), a 10wt.-% solution (light blue) and a 20wt.-% solution (blue).

As demonstrated by rheological measurements, differences in viscosity at different temperatures are present in samples **1318**, **809**, **1195** and **1206**.

For further investigation of the themoresponsive behavior of the six synthesized macromolecules, DLS was performed to analyze the particle size distribution at T=4°C and at T=37°C. Results are presented in Figure 59, wherein both in a row show the different prepolymers with the same modification agent, depicting the difference between both prepolymer reactants (left:

prepolymer-thermo + modification reactant, right: **prepolymer-1** + modification reactant). Additionally, Table 15 summarizes the measured particle sizes.

Table 15 Overview on obtained particle size distributions at 4°C and 37°C. Measurements were carried out for 80 sec.

Sample	Particle size average at 4°C [nm]	Particle size average at 37°C [nm]
1318	145.2	385.2
809	18.97	113.7
1195	22.68	89.29
1372	16.36	24.51
1206	115.2	38.26
1373	13.09	7.16

Sample of **1318** comprises the highest particle size average at both temperatures. This effect might be explained by the high PO content of the included macromolecules, as it appears as a turbid solution indicating that particles are already undissolved, containing aggregated particles. However, a gelation effect has not been observed *via* visual assessment of the solutions of **1318** (Figure 56). Samples of **1318**, **809** and **1195** exhibit an increased particle size at higher temperatures, indicating a thermoresponsive behavior *via* aggregation at higher temperatures. These samples also showed an increase in viscosities at higher temperatures, which support the proposal of introduced thermoresponsive behavior.

A slight increase in **1372** and **1373** can be explained by measurement fluctuations. Interestingly **1206** exhibits a decrease in particle size.

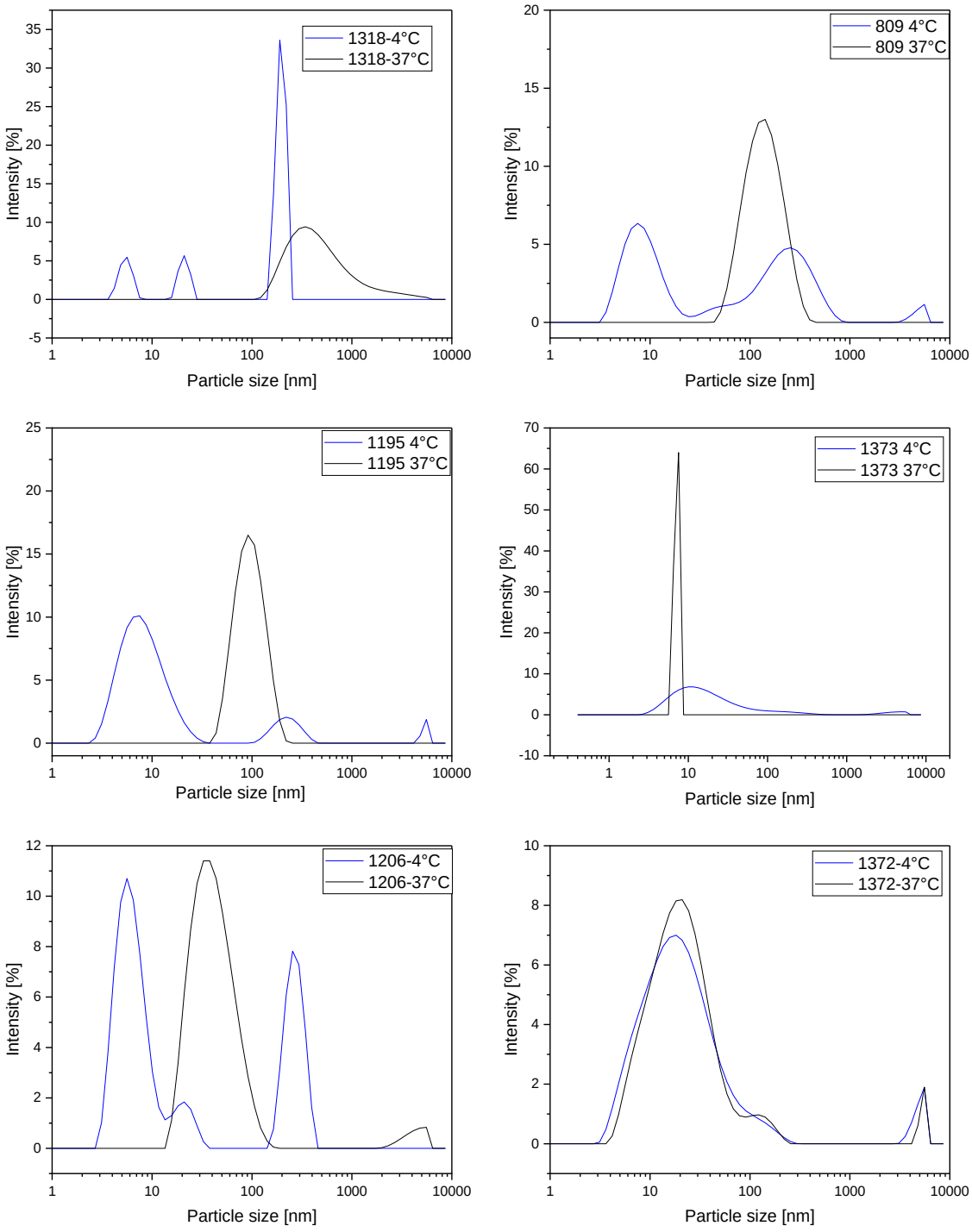

Figure 59 Particle size distribution at 4°C in comparison to 37°C of synthesized macromolecules with the aim to introduce a thermoresponsive lower critical solution temperature (LCST) behavior.

Table 16 presents a summary of the tested samples with regard to viscosity increase from lowest to highest viscosity in %, ratio of particle size at 4°C to 37°C and gives the whole EO/PO ratio of each sample.

Table 16 Overview on crucial parameters of analyzed macromolecule, giving the EO/PO ratios as indicator for thermoresponsive behavior, the ratio of highest/lowest viscosity measured in a temperature profile and the ratio of particle size at 4°C and 37°C. The (-) denotes that the highest viscosity was obtained at lower temperature as the lowest viscosity. The (+) denotes that the highest viscosity was obtained at higher temperatures as the lowest viscosity.

Sample	EO/PO ratio	Ratio highest viscosity/lowest viscosity [10wt.-% solution/20wt.-% solution]	Ratio particle size average 4°C/particle size average 37°C
1318	13.7/86.3	(-)9.2/(-)28.7	2.65
809	55.1/44.9	(+)110.8/(+)57.0	5.99
1195	37.5/62.5	(-)4.2/(+)3.4	3.94
1372	76.2/23.8	(-)2.7/(-)2.7	1.50
1206	23.0/77.0	(-)4.2/(-)0.3	0.33
1373	66.6/33.3	(-)2.9/(-)3.0	0.55

Results of viscosity measurements as a function of temperature (Figure 58), visual analyses (Figure 56, 57) and DLS measurement (Figure 59) indicate that sample **1318**, **809** and **1195** exhibit a thermoresponsive behavior. The obtained values for average particle size ratio and ratios of highest/lowest viscosity are the highest for these three samples. Average particle size ratio and effects detected by visual analyses from 4°C to 37°C is more pronounced in **1195** in comparison to **1318**. **809** shows the strongest temperature indicated effect with a ratio in particle size of 4°C to 37°C of 5.99 and a ratio of highest to lowest viscosity of 110.8 (10wt.-% solution) and 57.0 (20wt.-% solution). Additionally, a 20wt.-% solution of **809** shows no fluid character at 37°C when being flipped (Figure 57).

The requirement of a fast curing system is of special interest in order to avoid a fluid like character, which bears the risk to not adhere to the surface and therefore affecting the barrier properties. Since this type of hydrogel does not form a covalent network contrary to HYGEL-1-3, it is questionable whether mechanical stability will be sufficient to prevent cells from migrating through the network. All samples, instead of a 20wt.-% solution of **809** exhibits fluid properties at 37°C. A potential cytotoxic effect of the herein used modification reactant **Jeffamine M2005** is unclear.[34] Due to these uncertainties this approach was abandoned as it needs further advanced biochemical measurements to investigate a principal barrier function and a cytotoxic effect of imbedded **Jeffamine M2005**.

4.1.6 Summary of Preliminary Screening of Approaches HYGEL1-4

The approaches HYGEL1-4 exhibited fast curing, which was a focus during the pretesting and screening phase. HYGEL 1, 2 and 4 comprised at least one feature which was unsuitable for the targeted application and thus have been excluded from further optimization.

HYGEL-1: aldehyde-amine crosslinking approach

The conversion of NCO groups to predominantly NH_2 groups by incubation of 2wt.-% **prepolymer-1** in distilled H_2O (dH_2O) for 24 h and followed by freeze drying, was successful as shown *via* AV determination and FT-IR measurements. Results of AV determination moreover indicated that a reaction of obtained NH_2 groups and remaining NCO groups was present, yielding oligomers of **prepolymer-1** and **amine-1**, as evidenced by an increase in molecular weight and characteristic urea band at 1640 cm^{-1} FT-IR spectra.

The crosslinking mechanism of obtained **amine-1** with glutaraldehyde (**COO-1**), yielding a ~25wt.-% hydrogel was fast enough for the requirements of the targeted application which is <60 sec. When adjusting the system to the available volume ratios for a sprayable system (1:1; 1:2) and obeying the viscosity limit of 9 mPa*s, the maximum achievable solid content of the hydrogels was 6.7wt.-%. A solid content of 6.7wt.-% seems to be insufficient to obtain a solid-like hydrogel, as preliminary analyzed by haptic behavior. The comparison of both obtained hydrogels indicates that the latter is unable to form a gel network spanning the entire solution. This effect has not been analyzed in more detail. The combination of low eq. weight of aldehydes and viscosity limitation led to the exclusion of this approach.

Introduction of aldehyde functions at the chain ends of **prepolymer-1** has been conducted successfully, as proved *via* ^1H NMR and IR measurements. Curing of **COO-2** with **Jeffamine ED2003** was not achieved within the set limitations of viscosity and volume ratios. Since NMR analytics showed a clear introduction of aldehyde functions onto the macromolecular backbone, a possible explanation might be the decrease in reaction speed as a result of the larger macromolecular backbone.

HYGEL-2: α-STPs condensation approach

The implementation of **EtOSi-1** to the chain ends of **prepolymer-1** was conducted successfully as shown *via* FT-IR measurements. Viscosity of resulting **EtOSi-1-prepolymer** was determined at 28,900 mPa*s. Since the condensation reaction is induced by the addition of H_2O, the system cannot be diluted using this solvent. Organic solvents are not suitable with regard to the targeted application. Coating experiments with the pure substance have been conducted on a release paper and curing was carried out *via* A) humidity curing (749 sec.), B) curing on a moistened surface (72 sec.) and C) addition of water after coating (80 sec.). Films were obtained fast. However, it remains unclear how such a viscous substance can be applied during laparoscopic surgery.

Tensile testing was conducted of the pure, moisture cured system showing elongation at break of 8.5%±4.5 and tensile strength at break of 407 kPa±266. An ideal system for adhesion prevention would avoid effects on organ or tissue mobility and expansion. It is questionable whether this system would still allow normal movement of compartments in the intraabdominal room when being coated with pure **EtOSi-prepolymer-1**.

As the system cannot be diluted in organic solvents, no option was found how to apply the viscous polymer without abandoning the convenient spray application concept. Therefore, this approach was dismissed.

HYGEL-4: Thermoresponsive approach

The introduction of thermoresponsive **Jeffamine M2005** at the chain ends of **prepolymer-1** and **prepolymer-thermo** was conducted successfully, as shown *via* FT-IR measurements. Further macromolecules using different modification agents have been synthesized with **prepolymer-1** and **prepolymer-thermo** as starting points and the conversion was also analyzed *via* FT-IR.

A potential thermoresponsive behavior of the resulting six macromolecules was investigated *via* DLS and rheology temperature profiles, showing that thermosensitivity could be implemented in three different macromolecules, namely **1318**, **809** and **1195**. However, the resulting gels at 37°C (Figure 56, Figure 57) behave more like dispersions with partially flow properties, except the 20wt.-% solution of **809**. Even if sufficient mechanical properties were achieved it is questionable whether this merely physically crosslinked material could prevent cell invasion followed by postoperative adhesion. Additionally, the cytotoxic effect of the herein used modification agent **Jeffamine M2005** is unclear and strongly depends on the formulation.[34]

HYGEL3 was evaluated as the most suitable approach in initial screening experiments. A hydrogel could be obtained fast (≤60 sec.) by maintaining the viscosity limitations for a sprayable system with certain mechanical strength. The development process and characterization of HYGEL3 represents the core of this thesis and is discussed in more detail in chapter 4.2.

Table 17 presents a brief summary of approaches HYGEL1-4 addressing the underlying crosslinking technologies and the reason for dismissal of approaches 1, 2 and 4.

Table 17 Overview on the approaches of the pretesting and screening phase with reported critical parameter. HYGEL3 was most suitable and will be regarded and optimized in detail.

Approach	Crosslinking Technology	Critical parameter
HYGEL1	Imine formation	Solid content, curing time
HYGEL2	Silane Condensation	Water compatibility, high viscosity, mechanical properties
HYGEL3	Urea formation	None
HYGEL4	Thermoresponsiveness	Mechanical properties, cytotoxicity

4.2 Hydrogels obtained from covalent Crosslinking of Isocyanates and Primary Amines

All four approaches developed for a fast curing hydrogel forming approach (HYGEL1-4) have been initially screened and pretested in chapter 4.1. The approach with the highest compatibility to the demands of the requirement profile (HYGEL-3) was identified herein and will be presented in more detail. Figure 60 briefly summarizes the crosslinking concept of HYGEL-3.

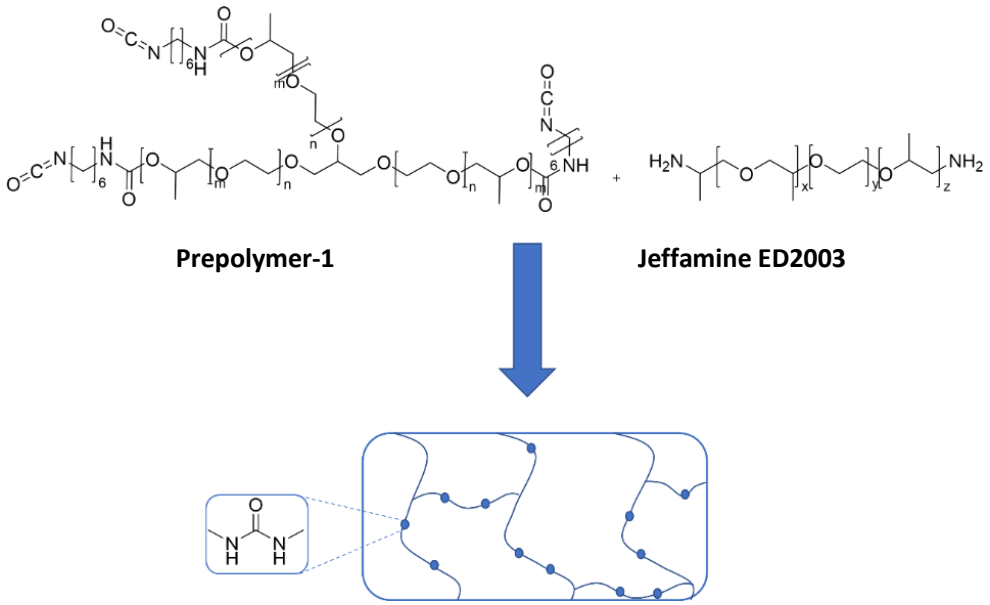

Figure 60 Brief summary of the crosslinking concept of HYGEL-3. An NCO capped prepolymer (here: **prepolymer-1**) is provided in an aqueous solution and is mixed with an aqueous solution of **Jeffamine ED2003** to obtain a hydrogel network with urea groups as crosslinks.

In chapters 4.2.1 and 4.2.2 the choice for raw materials (crosslinkers) and the prepolymer design, with the aim of an implementation of biodegradable groups, will be presented, which is fundamental for the hydrogel system. In chapter 4.2.3 the hydrogel system will be adapted to the requirement profile from Table 5 in chapter 3, which addresses viscosity of single solutions, pH values of resulting hydrogels, adhesion behavior of resulting hydrogels to organic surfaces, degradation behavior.

In chapter 4.2.4 the structure activity relationship of the developed hydrogel formulations will be analyzed using design of experiments with DesignExpert13 as a Software for the evaluation. As a result of this chapter influences of factors in the hydrogel formulation have been identified for every specific response, by which the formulation is adaptable on the respective requirement. This is especially of interest since in chapter 4.3 adaptions of the system where necessary as shown *via* the proof of concept *in vivo* study. A final formulation was developed matching the requirements profile which will be analyzed in more detail in chapter 4.2.5 regarding the physico- and biochemical properties.

Results presented up to chapter 4.2.5 have been developed on hydrogels prepared *via* mixing or spraying with inert gases (compressed air, N_2). Significant changes in hydrogel properties have been detected when preparing hydrogels *via* CO_2 spray application. Since the use of CO_2 is common laparoscopic praxis, sprayable hydrogel formulations need to be compatible with CO_2 as a carrier gas. The adjustment of the hydrogel formulation to the use with CO_2 as carrier gas will be presented in chapter 4.2.6

4.2.1 Synthesis and Characterization of Polyols and Prepolymers for covalent crosslinked Hydrogels

As described earlier, biodegradability is required for the targeted application of adhesion prophylaxes. For the implementation of such into the prepolymer backbone, cyclic dilactide units have been introduced into the polyol during polyaddition reaction *via* EO and PO dosing. The implementation is carried out *via* a ring opening reaction during the polyaddition reaction, leading to a linear chain containing two lactide units in vicinity bond to the macromolecular strand. During the polyaddition cycle EO, PO and dilactide are present at the same time. The resulting macromolecule has a statistical randomized constitution. Positions of dilactide in the polymer strand are hardly foreseeable. The synthesis sequence is illustrated in Figure 61.

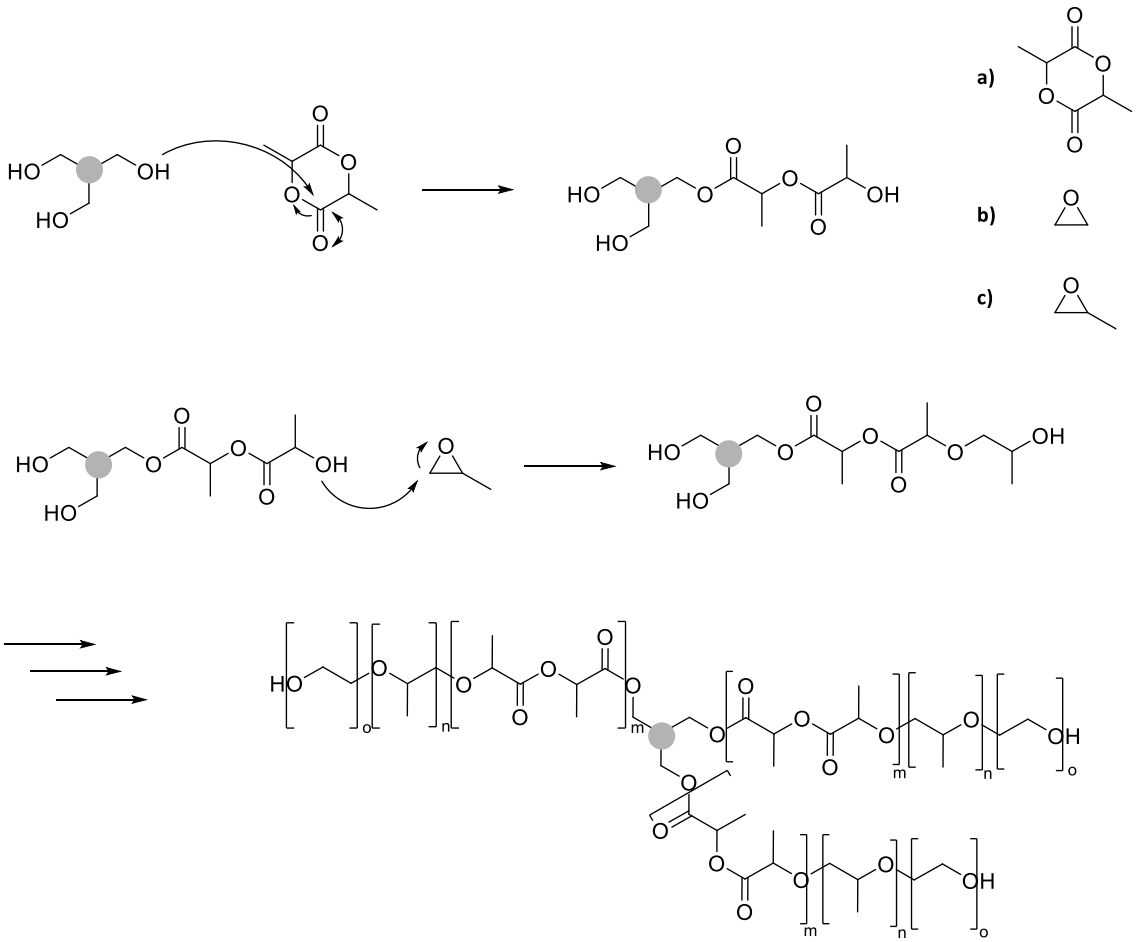

Figure 61 Synthesis sequence for dilactide containing polyols used for the herein presented experiments. A starter based on glycerol and added up with EO and PO (depicted by the grey circle) is added to a catalyst and dilactide, EO and PO monomers are additionally added for further polyaddition reaction and increase. Polyols are obtained as statistical constituted macromolecules.

The synthesis sequence starts with glycerol as the initiator, where already EO and PO have been added, as illustrated by the grey button (M_W=722 g/mol). Four polyols with different dilactide contents have been synthesized according to this reaction sequence and are reported in Table 18, addressing the EO/PO/dilactide ratio (weight of starter not included) and the statistical amounts of units dilactide per eq. ($i_{dilactide}$) which was calculated according to equation 4.2.1. Herein $MW_{starter}$ is the molecular weight of the starter which is 722 g/mol respectively and $MW_{dilactide}$ is the molecular weight of the dilactide monomer, which is 144 g/mol and wt.-% dilactide is the respective amount of dilactide in the polyol.

$$i_{dilactide} = \frac{(eq.weight - \left(\frac{1}{3} * MW_{starter}\right)) * \frac{\text{wt.}-\%_{dilactide}}{100}}{MW_{dilactide}} \quad (4.2.1)$$

The general structure of the resulting polyols is illustrated in Figure 61.

Table 18 Overview on synthesized dilactide containing polyols useful for the synthesis of degradable prepolymers. **Polyol-2** to **polyol-5** comprise *f*=3. EO/PO/dilactide ratios are calculated for the polyol synthesis, the weight of the starter is not included.

Polyol	EO/PO/Dilactide ratio	Statistical dilactide units/eq.
-2	72.5%/26.5%/1%	0.1
-3	72.5%/25.0%/2.5%	0.25
-4	72.5%/22.5%/5%	0.5
-5	72.5%/17.5%/10%	1

To investigate whether the polyols are already degradable, a 25wt.-% solution of each polyol was prepared in water and the pH was monitored over 7 days. Results are presented in Figure 62.

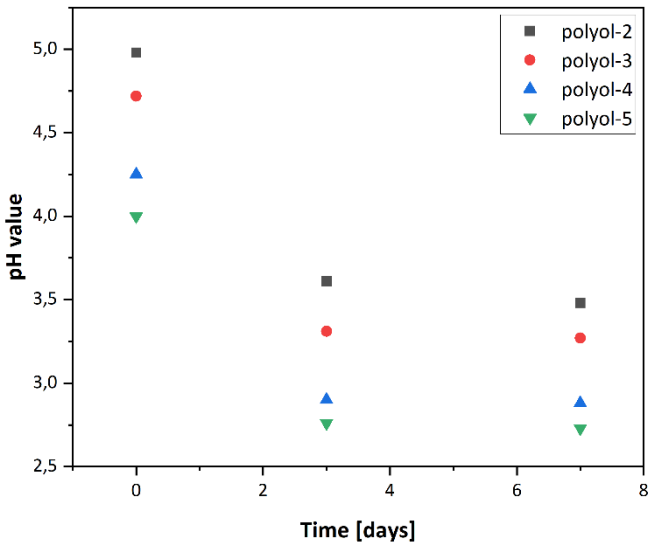

Figure 62 PH values of 25wt.-% solutions of **polyol-2-5** in H_2O as a function of time. A constant decrease in pH values indicates a hydrolysis of ester groups to carbonic acids and alcohols as degradation products.

A constant decrease of pH was detected, which indicates that hydrolysable sites have been implemented into the polyol backbone. By a degradation process carbonic acids are released, leading to a decrease in pH values.[163] Prepolymers synthesized out of each polyol should therefore allow degradability of the resulting hydrogels which will be analyzed in detail in chapter 4.2.3, chapter 4.2.4 and chapter 4.2.5.

Prepolymer-2 -5 have been synthesized out of each polyol by the reaction of **polyol-2** to **polyol-5** with an excess of HDI as already been described in chapter 4.1.1. The different characteristic values of the obtained prepolymers are listed in Table 19. Molecular weights were determined *via* NCO-titration, residual monomer content was determined using GC-MS.

Table 19 Overview on crucial values of **prepolmer-2-5**, namely characteristic FT-IR band, NCO content, residual monomer content, viscosity at γ=50,T=23°C. (s) denotes a sharp signal peak in FT-IR spectra.

Parameter	Prepolymer-2	Prepolymer-3	Prepolymer-4	Prepolymer-5
Characteristic FT-IR band (νN=C=O)	2265 cm^{-1} (s)	2265 cm^{-1} (s)	2265 cm^{-1} (s)	2265 cm^{-1} (s)
NCO content	2.63%	2.67%	2.53%	2.59%
Eq. weight	1597.0	1573.0	1647.0	1621.6
Residual monomer content	0.03wt.-%	0.02wt.-%	>0.01wt.-%	0.03wt.-%
Viscosity (γ=50,T=23°C)	3967 mPa*s	4451 mPa*s	3990 mPa*s	9451 mPa*s

The viscosity of **prepolymer-5** was measured a few weeks after the synthesis. Until this point NCO could have been already partly hydrolyzed by humidity and oligomers of **prepolymer-5**

could have formed. This effect lead to an increase of urea groups which is reported to increase viscosity values[164], leading probably to a deviating viscosity in **prepolymer-5**.

4.2.2 Development of a Crosslinking Concept

Primary amines are used exclusively for this crosslinking approach. They should ideally comprise a macromolecular backbone, otherwise the solid content will decrease since volume ratios are fixed by the targeted application. HYGEL-1 presents an example which was canceled due to too little solid content and lacking opportunities if implementation of a larger macromolecular backbone to the respective crosslinking technology. During the experiments from chapter 4.1.3 **Jeffamine ED2003** was used exclusively. Further primary amines with an EO rich macromolecular backbone and $f \geq 2$ are commercially available. Table 20 presents an overview on the analyzed primary amines for the crosslinking of a 15wt.-% concentration of **prepolymer-1** in H_2O and on the resulting concentrations of crosslinker in H_2O and resulting solid content in hydrogels assuming a volume ratio of 1:2, wherein 2 applies for the prepolymer solution. AV was measured and eq. weight calculated as described in chapter 6.2.

Table 20 Crucial values from commercially available jeffamine types, namely amine value, eq. weight, resulting concentration in an aqueous solution calculated for a volume ratio 2:1, wherein 2 is represented by a 15wt.-% prepolymer solution with NCO content=2.55%, and the resulting solid content in a hydrogel thereof.

Jeffamine	Amine Value [mg KOH/g]	Eq. Weight [g/eq.]	C in 1:2 Volume ratio [wt.-%]	Resulting solid content in hydrogel
EDR148	741.0	75.7	1.4	10.5
T403	353.0	158.9	2.9	11.0
ED600	187.0	300.0	5.5	11.8
ED900	120.4	465.9	8.5	12.8
ED2003	54.5	1021	18.6	16.2

It has been shown in chapter 4.1.4 that a hydrogel with a solid content of ~8.4wt.-% comprises a certain mechanical strength. However, reductions in solid content *via* adaptions of the sprayable system cannot be excluded from this point in time. Thus, it is useful to work with raw materials with an eq. weight ratio of NCO/NH_2 as close to 1 as possible by maintaining viscosity limitations. The highest possible solid content in a hydrogel formulation can be achieved when using **Jeffamine ED2003** as crosslinking agent, comprising a ratio of eq. weights of NCO/NH_2=1.6. It will be used as a curing agent for further optimization of the hydrogel system.

4.2.3 Adjustment of the Hydrogel System to the Requirement Profile for an Adhesion Prophylaxis

The requirement profile for an adhesion prophylaxis product is described in detail in chapter 3.3, Table 5. The herein listed requirements are used as guidance for the development process of

the hydrogels in this chapter, addressing *viscosity of single solutions used for hydrogel manufacturing*, *pH values of the resulting hydrogels*, *adhesion behavior to organ substrate*, *degradation behavior of resulting hydrogels*. Suitable formulations for hydrogel manufacturing will be developed and limitations of the system will be investigated.

Viscosity of the Single Solutions used for the Preparation of Hydrogels

Viscosity of **prepolymer-1** was investigated during the screening phase. A concentration of 15wt.-% of **prepolymer-1** in water was identified as the highest possible concentration regarding the viscosity limit of 9 mPa*s. **Prepolymer-2 -5** are strongly comparable to **prepolymer-1**, in order to exclude a viscosity increase due to increasing dilactide concentrations in the backbone, the viscosities of each prepolymer in an aqueous 15wt.-% solution was measured and are listed in Table 21.

Table 21 Overview on measured viscosities of a 15wt.-% solution of **prepolymer-2 -5** in water, at γ=50 sec.$^{-1}$ and T=23°C.

Prepolymer	Viscosity of a 15wt.-% solution in water [mPa*s]
-2	7.21
-3	8.77
-4	9.08
-5	4.35

All solutions were within the specified upper limit for viscosities of 9 mPa*s. 15wt.-% was therefore chosen as the upper concentration limit for further investigations and slightly deviations in **prepolymer-4** were accepted. Solid content of the NCO component depicts a parameter for further investigations. Therefore, experiments will be conducted in the range of 10-15wt.-% solid content NCO.

Regarding the prepolymers in water, these can also form a hydrogel network by the hydrolysis of NCO in water to primary amines. This reaction has already been used and discussed in chapter 4.1.2 and was probably observed to occur even in a low concentrated solution of 2wt.-%, indicating that the self-crosslinking of the prepolymers is a competing reaction to the NCO NH_2 reaction. Regarding the reaction kinetics, the NCO NH_2 reaction is much faster, therefore self-crosslinking can be avoided, but needs to be considered when preparing aqueous solutions of the different prepolymers. To determine the time which remains for processing with NH_2 groups, viscosity measurements have been conducted. To illustrate the gelation behavior of the pure prepolymers in water, the gelation behavior of **prepolymer-1** was selected as representative example, as shown in Figure 63. Major deviations between the synthesized **prepolymer-1-5** are not expected.

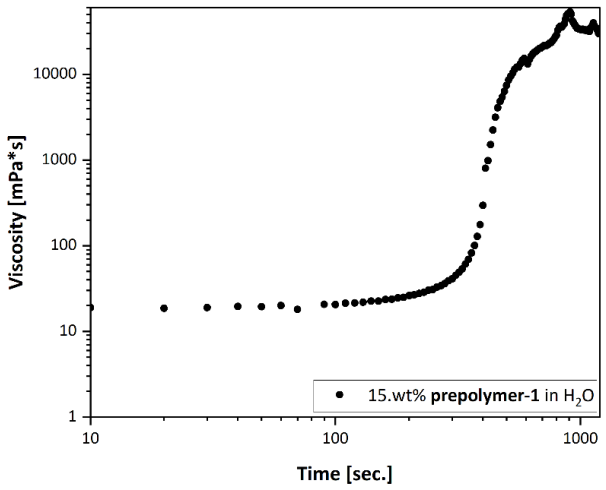

Figure 63 Rheological behavior of a 15wt.-% solution of **prepolymer-1** in H_2O. A rapid increase in viscosity is detected at t=320sec. A time delay between the preparation of the solution of **prepolymer-1** until measurements were started was 3 min, indicating a limitation of pot life to 8.33 min. γ =50 $sec.^{-1}$, T=23°C.

A strong increase in viscosity is detected at t=320 sec. A time delay between mixing and starting of the measurement took 3 min, leading to a maximum pot life of 8.33 min for a 15wt.-% prepolymer in water, which marks the upper limit of the required timeframe for application. Deviations of latter viscosity values are visible in Figure 63 and might be caused by slipping of the surface of the hydrogels which had cured and thus is less flexible.

The solution of the curing agent is also limited to 9 mPa*s. Regarding possible volume ratios of 1:2 or 1:1 the viscosities of the curing agents were analyzed for four different concentrations (5; 10; 17 and 25wt.-%). Results are presented in Figure 64.

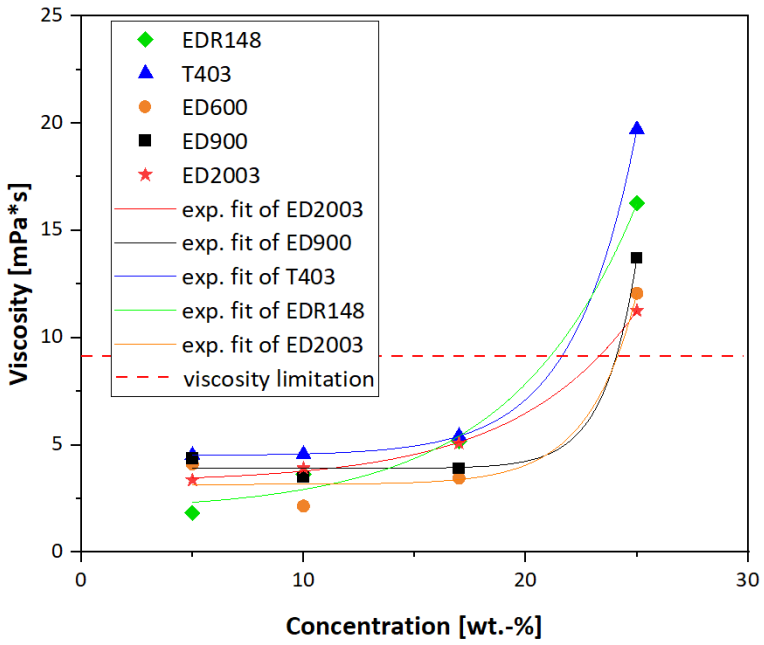

Figure 64 Measured viscosities for different concentration of different Jeffamine types. Measured at tau= 50 1/s and T=23°C.

The equation for the exponential fit and respective R^2 are reported in Table 22.

Table 22 Identified equations for the exponential fit and respective R^2 for viscosities of different Jeffamine types, measured in a concentration range of 5 to 25wt.-%. The corresponding curves are presented in Figure 64.

Jeffamine	Equation of the exponential fit	R^2
EDR148	$f(x) = 1.90 * 0.18 * e^{0.18x}$	0.993
T403	$f(x) = 4.51 * 0.002 * e^{0.35x}$	1
ED600	$f(x) = 3.16 * 0.0001 * e^{0.46x}$	0.968
ED900	$f(x) = 3.92 * 0.0000042 * e^{0.68x}$	0.995
ED2003	$f(x) = 3.26 * 0.087 * e^{0.18x}$	0.999

Until 17wt.-%, all measured solutions of Jeffamine types are within the viscosity limitation of 9 mPa*s. By maintaining 17wt.-% as an upper concentration for amines, the requirement for viscosity is fulfilled.

pH values of Resulting Hydrogels

The synthesized hydrogels are considered for an application in the body which comprises a pH value of 7.4.[81] The pH value of resulting hydrogels is a critical topic, since it should ideally be maintained at neutral to slightly acidic pH values in order not to interfere with sensitive processes during wound healing.[165] PH measurements of the curing reaction were conducted and the resulting curve as a function of time is depicted in Figure 65. For the pH measurements, a 10.0wt.-% solution of **prepolymer-1** was mixed with a 11.7wt.-% solution of **Jeffamine ED2003** (Table 53, formulation 1), as being described in chapter 6.2. The highest pH value was recorded at 10.37 after 4 sec. and decreased to 9.86 after 52 sec., remaining to be stable over the next 29 min. Such an alkaline pH value is not suitable for applications in the human body. Modifications of the system were necessary to obtain hydrogels that exhibit physiological pH values.

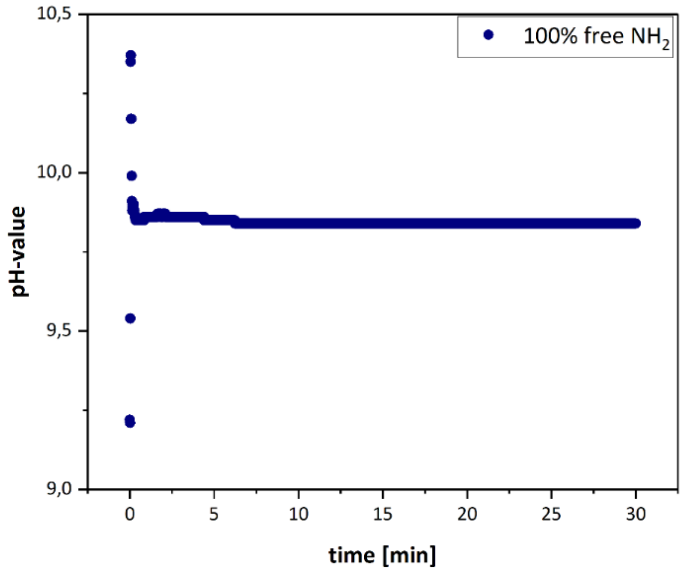

Figure 65 PH value as a function of time of the resulting hydrogel with a solid content=11% derived from mixing a 10wt.-% solution of **prepolymer-1** with a 11.7wt.-% solution of **Jeffamine ED2003,** both provided as purely H_2O system without the addition of buffering agents.

An increase of pH to alkaline pH values after curing of the hydrogel in pure water was not expected, since in theory all NCO and NH_2 groups should be fully converted to urea groups, which are reported to be at neutral or slightly alkaline state.[166] A possible explanation for the alkaline pH value of 9.86 could be that after the network is mostly cured, unreacted groups are embedded into this rigid state. Dangling NH_2 and NCO groups are sterically hindered in their crosslinking und would stay left unreacted. At a certain point in time, NCO groups will be hydrolyzed by the included water to yield primary NH_2 groups, inducing a protonation with H^+ to form NH_3^+ as a result of the autoprotolysis of water. The increase of OH^- concentration leads to an increase of pH values of the hydrogel. Thus, irrespective of the reaction speed, the NCO hydrolysis is a competing reaction at a certain point in network formation. The proposed mechanism is presented in Figure 66.

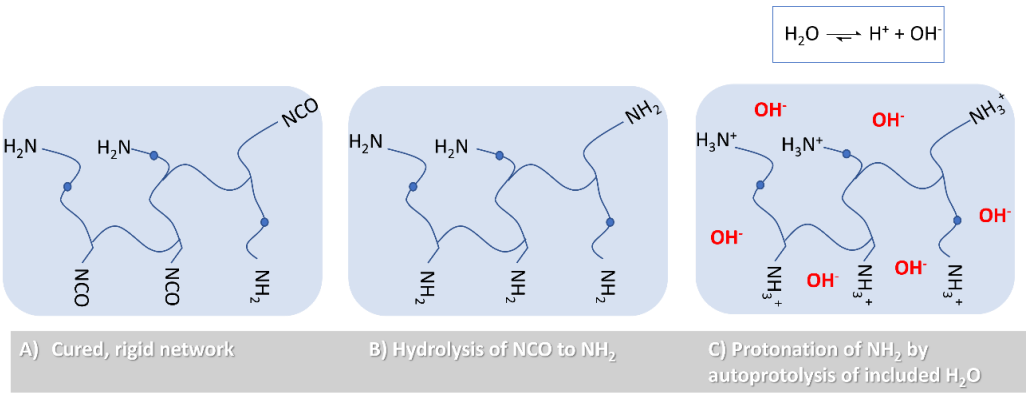

Figure 66 Illustration of a protonation process after the hydrogel is cured. A) A rigid network is obtained after the initial crosslinking reaction with remaining unreacted NH_2 and NCO groups. B) NCO groups were already hydrolyzed by included H_2O to primary NH_2 groups. C) Included water protolyzed to H^+ and OH^- leading to a protonation of unreacted amines. As a result, OH^- concentration increases leading to an increase of pH values to alkaline values, subsequently.

Karakyriazis *et al.* reported on a hydrogel system using imine formation as crosslinking reaction, wherein NH_2 groups have been used for the gelation. The resulting hydrogel was also reported to be at alkaline state.[167] Therein, buffering substances have been used to reduce resulting pH values of the gels. Under acidic pH values of the NH_2 based curing agent no crosslinking could be observed due to dominating conversion of NH_2 to NH_3^+ groups, which are unable to crosslink.

By the use of buffers or diluted acid for the hydrogel preparation, a defined amount of NH_2 groups will be converted by protonation to NH_3^+ groups. A pre-buffering of the NH_2 groups which would stay left unreacted after the initial curing process and therefore obtain neutral to slightly acidic pH values in the resulting hydrogels, is desired. Thus, protonation of NH_2 groups by auto-protolysis of included water and therefore OH^- formation is reduced, leading to lower pH values. The proposed mechanism for the pre-buffering concept is presented in Figure 67.

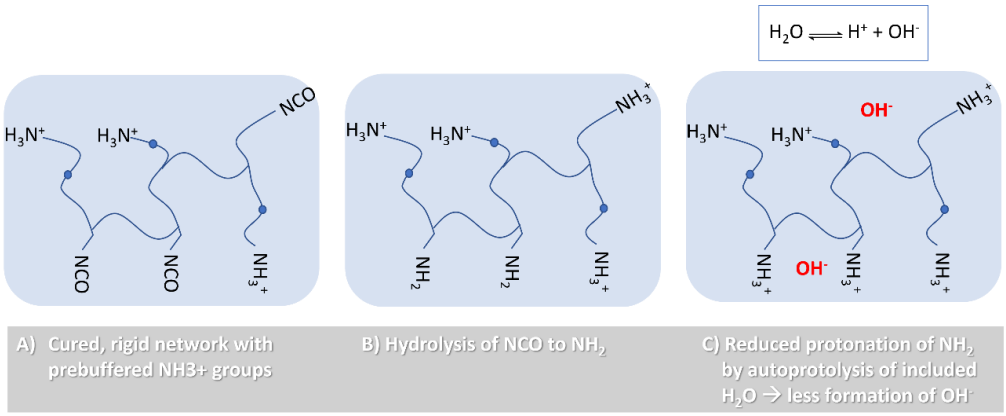

Figure 67 Illustration of protonation processes of a pre-buffered hydrogel system. A) A rigid network is obtained after the initial crosslinking reaction with groups of NCO left unreacted, as well as pre-buffered NH_3^+ groups, unable to crosslink. B) NCO groups have already been hydrolyzed by included H_2O to primary NH_2 groups. C) Included water protolyzed to H^+ and OH^- leading to a protonation of hydrolyzed NH_2 groups. OH^- concentration is reduced due to lower concentration of NH_2 groups. As a result, pH shift to alkaline values is reduced/avoided.

Adjustments of the hydrogel system were carried out by the use of buffers or diluted acid. Three different buffer systems were analyzed: phosphate buffer (monobasic/dibasic), acetic acid/acetate buffer and diluted hydrochloride acid (HCl). Different molarities were analyzed for each buffering agent and are listed for phosphate buffer (monobasic/dibasic) and acetic acid/acetate buffer in Table 23, for diluted HCl in Table 24. Additionally, the last measured pH value of each formulation is reported.

Table 23 Different buffering degrees of amine of the curing formulation and the resulting molarities of the buffering agents (here: phosphate buffer (monobasic/dibasic) and acetic acid/acetate buffer). Molarity of acidic and alkaline components is summed to give the whole molarity. Detailed formulations are listed in chapter 6.2, Table 53, 2a-g (phosphate buffer) and 3a-g (acetate buffer).

Molarity of buffering agents in a 11.71% Jeffamine ED2003 solution	Remaining unprotonated NH_2 groups in buffer solution [mol.%]	Last measured pH value in phosphate buffer (monobasic/dibasic)	Last measured pH value in acetic acid/acetate buffer
0.012M	95%	8.72	-
0.023M	90%	9.48	-
0.035M	85%	8.72	8.61
0.058M	75%	8.14	8.90
0.081M	65%	7.84	6.65
0.092M	60%	7.78	-
0.104M	55%	7.58	-
0.116M	50%	7.51	-
0.134M	42%	-	6.46
0.150M	35%	-	6.33
0.173M	25%	-	6.29
0.200M	13.4%	-	6.25

Figure 68A presents an overview on the resulting pH curves of hydrogel formulations using phosphate buffer in comparison to Figure 68B wherein formulations are presented using acetic acid/acetate buffer.

With phosphate buffer in an amount that 90mol.% to 50mol.% of all amines are left unprotonated (protonation degree 10mol.%-50mol.%), the lowest pH value was observed at 50mol.% free NH_2 groups which was determined at 7.51 which appeared to be slightly high since neutral up to slightly acidic values are required for the targeted application.[121] Phosphate buffer (monobasic/dibasic) was chosen first, as it mimics the *in vivo* present environment[168] and should therefore comprise a certain biocompatibility. Regarding the pK_a value of the monobasic/dibasic ion pair, which is reported at 7.2[169] the buffering effect to slightly acidic values might be restricted when buffering alkaline substances. The alkaline ionic counterpart of the buffering system will lead to a shift to more alkalic pH values. The use of phosphate buffer seems to be unsuitable. It was decided to try a buffer with a reduced pK_a value which should additionally comprise a certain biocompatibility. Another buffer system often used for pharmaceutical and medical issues is acetic acid/acetate buffer with a pK_a=4.76.[170] Molarity of the acetic acid/acetate buffer, buffering degree and last measured pH value are reported in Table 23. Molarity of acetic acid and acetate is summed up to give the whole molarity.

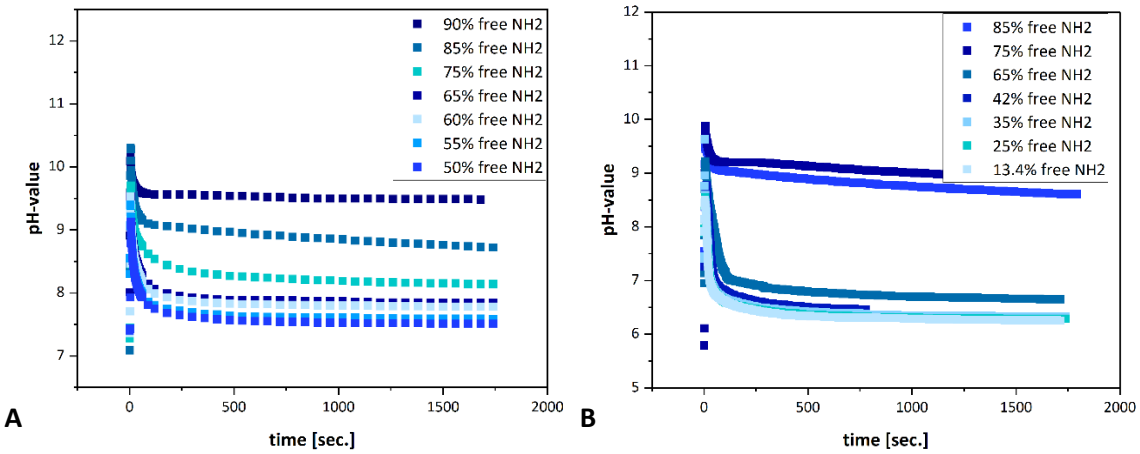

Figure 68 Overview on different pH values as a function of time of formulations using A) phosphate buffer (monobasic/dibasic) as buffering agent in a defined amount each. B) acetic acid/acetate buffer as buffering agent in a defined amount each.

As evident from Table 23 and Figure 68B, a significant decrease in pH values was observed, ranging from 75mol.% to 65mol.% free NH_2, when using acetic acid/acetate derived formulations. This reveals that the protonation degree is sufficient to protonate the remaining unreacted amines at the end of the hydrogel formation process. A molarity of 0.081M, protonating 35mol.% of NH_2 and leaving 65mol.% free NH_2, was identified as a suitable concentration for the acetic acid/acetate buffer. Formulations with 42mol.% or less free NH_2 did not result in solid-like hydrogels, as observed in the initial formulation. It appears that these hydrogels did not form stable networks. This instability is likely caused by the reduced number of resulting crosslinks due to the higher protonation degree of NH_2. In summary, the protonation degree of amines plays a crucial role in the formation and stability of hydrogels. The balance between protonated and free NH_2 groups significantly impacts the crosslink density and, consequently, the structural integrity of the hydrogel network.

The testing series was repeated using diluted HCl to investigate whether a pure acidic component might be sufficient. A summary of the last measured pH value for different molarities of buffer and the respective remaining molar amount of NH_2 groups unprotonated, is presented in Table 24.

Table 24 Overview on different buffering degrees of amine of the curing formulation and the resulting molarities of the buffering agents (here: diluted HCl). Molarity of acidic components is equal to the whole molarity. Detailed formulations are listed in chapter 6.2, Table 53, 4a-d.

Molarity of HCl in a 11.71% Jeffamine ED2003 solution	Remaining unprotonated NH_2 groups in buffer solution [%]	Last measured pH value
0.0115M	95%	9.44
0.0346M	85%	6.76
0.0577M	75%	6.78
0.0808M	65%	6.71

PH curves of the measurements in diluted HCl are presented in Figure 69 revealing that hydrogels with a pH value of ≤7.4 were obtained at molarities leading to 85mol.% and less free NH_2 groups.

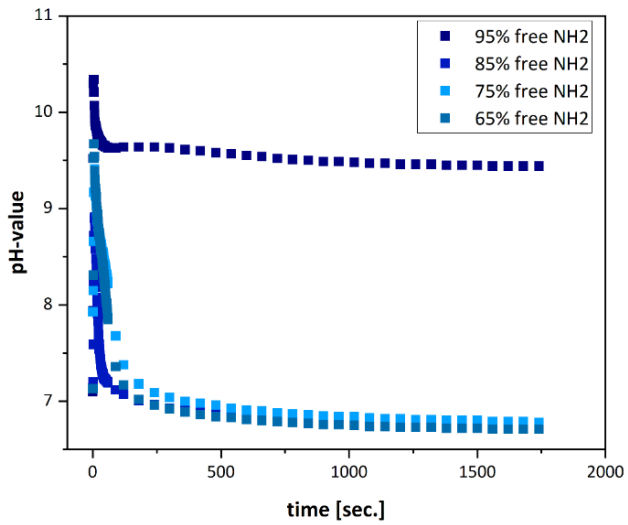

Figure 69 Overview on different pH values as a function of time of hydrogel formulations using diluted HCl as buffering agent in a defined amount each.

The concept of NH_2 pre-buffering was confirmed by the obtained pH values as a function of time. When using acetic acid/acetate buffer or diluted HCl as buffering system, 65 -75mol.% (acetic acid/acetate buffer)/85mol.% (HCl) of free NH_2 groups are considered to be a suitable ratio to obtain solid networks which comprise neutral to slightly acidic pH values. The range of buffering degrees was therefore predefined from 65mol.%-85mol.% of free NH_2 groups.

Adhesion Behavior of Resulting Hydrogels to Organic Surfaces

The hydrogels are considered as an application as adhesion prophylaxis, which represents a kind of coating for organs or the abdominal wall. To provide the barrier effect, one aspect features the adhesion to the surface where the hydrogel is applied on.

To evaluate the adhesion to an organic surface, porcine derived kidneys have been used as a substrate for spray experiments.

Initial spray tests have been conducted using a formulation listed in Table 25. This formulation was identified in pH measurements to comprise a suitable pH value, as demonstrated previously.

Table 25 Overview on main parameters of a formulation used for initial evaluation of adhesion behavior of resulting hydrogels to organic surfaces (here: porcine derived kidney).

Concentration (C)$_{Prepolymer}$ (single solution 1)	$C_{Jeffamine\ ED2003}$ (single solution 2)	Solid content of resulting hydrogel	Molar ratio NCO:NH_2	Mol.% free NH_2	Buffering system
10wt.-%	11.71wt.-%	10.6%	1:1	65	Acetic acid/acetate buffer

The described formulation was applied to a porcine derived kidney, using a 2K applicator. Unexpectedly, no hydrogel was obtained on the organic surface, revealing the presence of effects which influence the crosslinking reaction.

Since pH measurements have been identified as a useful tool for obtaining information on the curing reaction, measurements of the hydrogel curing reaction were conducted with small pieces of the porcine derived kidney. Herein the 100% free NH_2 formulation was used, to exclude interaction by pre-buffered systems. Figure 70 presents the resulting pH curves in comparison to the 100% free NH_2 system without the addition of pieces of kidney, showing significant differences between the two measurements. To avoid interactions between buffering agents and possible effects of the organic substrate, both measurements were conducted without any buffering agent to comprise 100% free NH_2 groups. Differences between both measurements were detected regarding the obtained curve and the resulting pH value after 30 min, which was at 9.86 for the 100% free NH_2 groups, in comparison to a resulting pH value of 7.77 for 100% free NH_2 + pieces of kidney. The difference of nearly two units in pH is tremendous and was not expected before the conducted measurements. The results indicate that the organic substrate (here: porcine kidney) comprise a protonation/buffering effect which was not considered when adjusting the system to 65mol.% free NH_2. The additional buffering effect led to a decreased amount of free NH_2 which do not form a stable network below a certain limit.

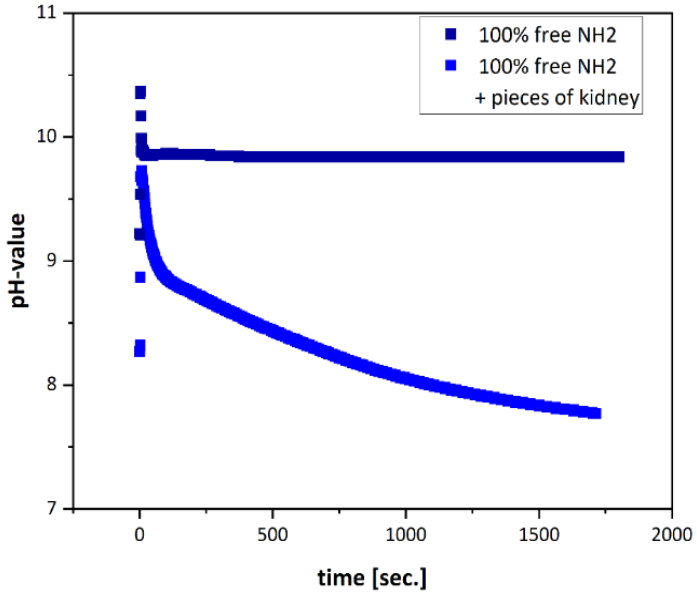

Figure 70 Comparison of different pH value curves over the time of a formulation with 100% free NH_2 in pure water to a formulation with 100% free NH_2 in pure water plus pieces of a porcine kidney. PH values after 30 min were detected at 9.86 vs. 7.77.

However, a pH of 7.77 is slightly alkalic and not suitable for the targeted application. Thus, the molar ratio of NCO to NH_2 groups was set to 1.2:1, which represents a 20mol.% excess of NCO groups. This concept has been reported to be applied in prepolymer curing formulations, which also utilize amines, to obtain reduced pH values in hydrogel dressings. Therein, a 30mol.% excess of NCO was applied to achieve dressings with pH values of 7.30-7.51 in comparison to dressing without molar NCO excess, which were obtained at pH=8.99.[171] The pH measurements were repeated for a 100% free NH_2 formulation in a molar ratio of 1.2:1 (NCO/NH_2). The resulting hydrogel sticks to the kidney, upon application but comprised a pH value of 8.72 when measured as a pure system without the addition of pieces of kidney. A combination of both, pieces of kidney plus 20mol.% excess NCO, was not tested in pH measurements. Further adjustments with buffering agents seem to be still necessary with consideration of the buffering effect provided by the organ surface. Therefore, the amount of free NH_2 was set to 85mol.% and the experiment was repeated on a porcine kidney with the adapted formulation as described in Table 26.

Table 26 Adapted formualtion of the hydrogel comprising a 20mol.% excess of the NCO component. A buffer was added to the formulation in a molaritiy that 15mol.% NH_2 groups are buffered and 85% will stay left unprotonated.

$C_{prepolymer}$ (single solution 1)	$C_{Jeffamine\ ED2003}$ (single solution 2)	Solid content of resulting hydrogel	Molar ratio NCO:NH_2	Mol.% free NH_2	Buffering system
12.0wt.-%	11.7wt.-%	11.9%	1.2:1	85	Acetic acid/acetate buffer

This formulation exhibits sufficient curing and adhesion behavior to the kidney upon application. When measuring the resulting pH of the formulation of Table 26 in the presence of pieces of porcine kidney, the pH after 30 min. was detected at 6.76, 32 sec. after the application, the pH is <7.4 which is marked as the physiological upper limit. The highest measured pH value was detected after 8 sec. at 8.91. If the alkaline peak at 8 sec. of 8.91 is critical, needs to be regarded in more advanced biochemical testing. From this point in time the pH as a function of time and the curing and adhesion behavior on organ surfaces is sufficient.

However, it needs to be evaluated whether the 20mol.% NCO excess could lead to an influence of biocompatibility. IR measurements have been conducted to investigate how long free NCO is available and would therefore remain in the body after the application. The hydrogel system was applied on the IR surface and measurements started immediately, with a focus on NCO band at 2265 cm^{-1}. Figure 71 compares the system of a molar ratio of NH_2/NCO 1:1 to a molar ratio of NH_2/NCO 1:1.2. Monitoring of the curing reactions was limited to a 10 min time interval, which appears to be too short to detect the timepoint of 100% NCO conversion. However, it is visible that 81% of NCO already reacted at the beginning of the measurement in a 1:1 molar ratio, mainly caused by a time delay between mixing and measurement's start, which was ~20 sec. and appears to be stable over the remaining 10 min.

In comparison, the 1:1.2 molar ratio formulation starts with 69% NCO conversion, reaching 76% after 10 min.

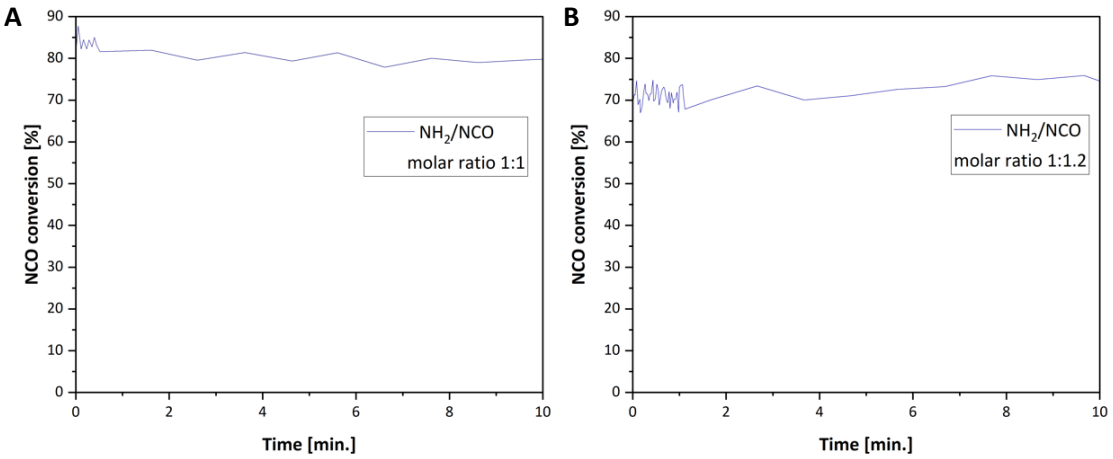

Figure 71 Comparison of NCO conversion of a formulation using a NH_2/NCO molar ratio of 1:1 (A) with a formulation using a molar ratio of 1:1.2 (20mol.% NCO excess) (B). Measurements were carried out *via* FTIR focusing on decreasing of NCO peak at 2265 cm^{-1}.

Both analyzed formulations behave similarly concerning the NCO conversion. After 10 min. the difference in NCO conversion is at 5% (81% in 1:1 vs. 76% in 1:1.2).

In this subchapter it was shown that the hydrogel formulation, developed on the bench and sufficient for adhesion on inert surfaces, is not suitable for the application on organic surfaces, since they comprise a buffering effect by the tissue itself. The effect is probably caused by the constant exchange of the peripheric fluid and blood, hence surrounding fluid of tissues comprise

comparable buffering effects as present within the blood.[172] The extent of this buffering effect was underestimated. It was identified that the buffer capacity of a few pieces of a porcine kidney is high enough to reduce resulting pH values of cured hydrogels for more than 2 units (9.86 vs. 7.77). Moreover, it was demonstrated that a combination of a 20mol.% NCO excess in combination with a reduced buffering degree to 85mol.% free NH_2 is suitable to allow the formation of a mechanical stable hydrogel on the surface of organic tissues, which comprise a buffering effect and adhered to it.

Degradation Behavior of Resulting Hydrogels

The implementation of (bio-)degradable sites into one component of the hydrogel formulation is necessary to allow removement of an applied hydrogel in the body without the necessity of a second surgery, which would cause another source for the formation of postoperative adhesion.

The implementation of degradable sites was carried out *via* implementation of dilactide units for co-polymerization during the polyol synthesis. The synthesis of polyols and prepolymers thereof was described in detail in chapter 4.2.1. Herein it was additionally shown that polyols are degradable, as visible from pH measurements of incubated polyols in H_2O (25wt.-%).

However, the degradation behavior of the resulting hydrogels needs to be investigated to evaluate whether the hydrogels are sufficiently degradable to fit to the requirement profile for the intended application. This provides that gels should be stable for 7 days and during this time prevent the migration of fibroblasts through the network. Afterwards, they should be degraded as soon as possible, ideally within 28 days.

In a hydrogel formulation, using **prepolymer-5** (10wt.-% dilactide, weight of starter not included) and **Jeffamine ED2003** in a molar ratio of 1:1, without the addition of any buffering agent, a fast degradation was observed (Table 53, formulation 6b). Within a few hours the solid-like hydrogel collapsed and exhibits a certain flowability. It was unclear whether this effect appeared by hydrolysis of implemented ester units or if the covalent crosslinking of the hydrogel is unstable and therefore results in fast collapse. To investigate whereby this effect is caused, pH measurements were conducted as shown in Figure 72. Herein a rapid decrease in pH of the cured hydrogel was visible, starting from 10.42 and yielding a pH of 8.71 after 1444 min/24.1 h.

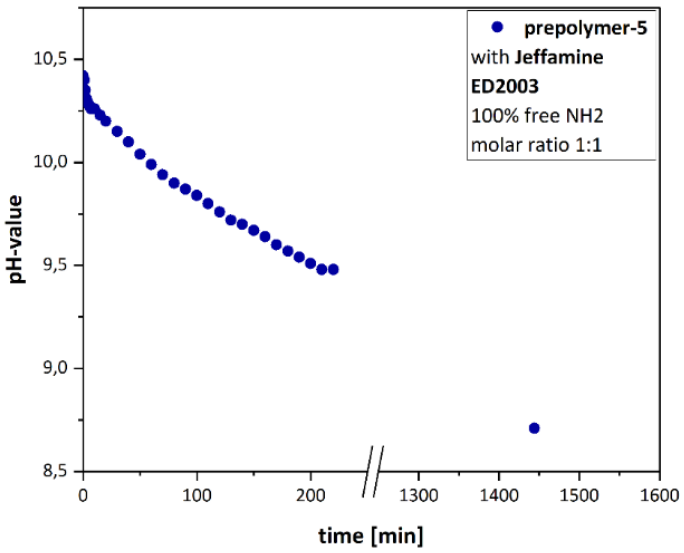

Figure 72 pH values of a prepared hydrogel based on **prepolymer-5** (10wt.-% dilactide content in polyol, starter not included) and **Jeffamine ED2003** without any buffering agent in a molar ratio of 1:1, measured for 24 h.

The hydrogel exhibited partial degradation after a time period of 2 h. The constant decrease in pH values indicates that the fast degradation is caused by the implemented ester groups which lead to release of primary alcohols and carboxylic acids, which are responsible for decrease in pH values as illustrated in Figure 73.

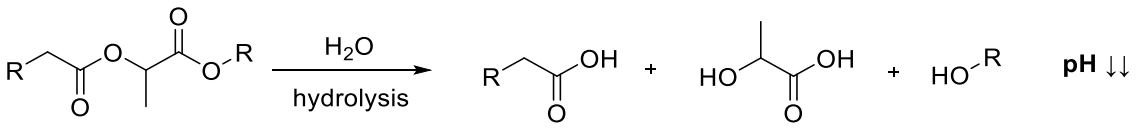

Figure 73 Hydrolysis sequence of an embedded dilactide unit resulting in two molecules carboxylic acid and alcohol. The release of carboxylic acid during the hydrolysis can be monitored by a decrease in pH values.

To identify functional groups of the degraded hydrogels, the hydrogel formulation was prepared in deuterium oxide (D_2O) and ^{13}C NMR of the degraded sample was recorded. Spectra of the polyol used for the prepolymer synthesis was additionally recorded for a better comparability. ^{13}C NMR spectra are presented in Figure 74.

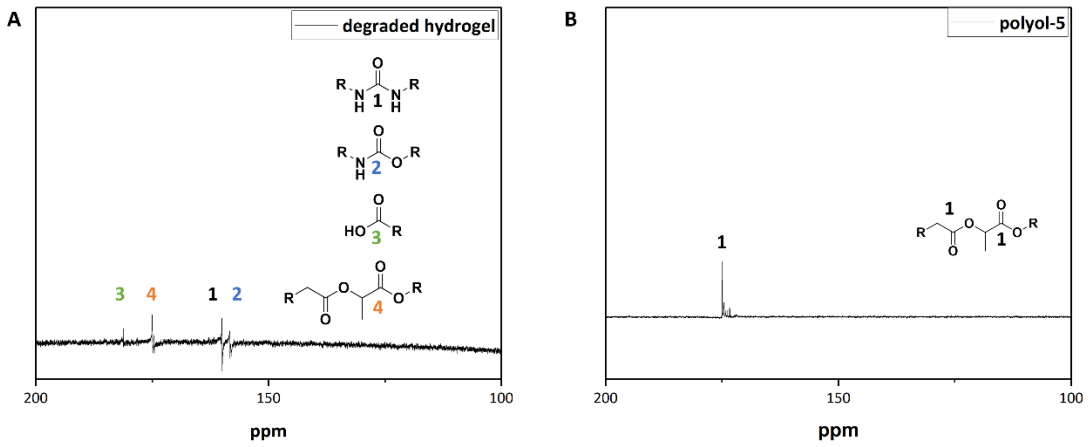

Figure 74 Comparison of ^{13}C NMR spectra in D_2O of A) degraded hydrogel based on **prepolymer-5** and **Jeffamine ED2003** prepared in D_2O with colored peaks of urea (**1**), urethane (**2**), carboxylic acid (**3**) and remaining dilactide (**4**) to B) **polyol-5**, a 10wt.-% dilactide containing polyol (weight of starter not included) with identified carbonyl group (**1**) at chemical shift of 174.7ppm.

In comparison to the spectra of **polyol-5**, the spectra of the D_2O degraded hydrogel displayed additional peaks of urea (160.2ppm), urethane (158.4ppm) and probably carboxylic acid (181.1ppm). The detection of urea and urethane groups provides the information that these remained inside the degraded hydrogel and thus are most likely not responsive for the dissolving of the network. The occurrence of a carboxylic acid peak at 181.1ppm indicates that the hydrogel indeed degraded by hydrolysis of dilactide units to carboxylic acids and alcohols, as presented in Figure 74. This effect is additionally responsible for the decrease in pH values after the curing process. Interestingly the peak of dilactide units at 174.7ppm is still present, indicating that dilactide units have not been hydrolyzed in their entirety. However, the partially hydrolyzed units are sufficient to dissolve the hydrogel network.

Concerning the targeted application, a hydrogel which degraded after 2 h is insufficient. The herein used hydrogel formulation comprised a high pH value of 10.4 at the beginning of the hydrolysis. The high starting pH could have catalytic effects on the degradation of dilactide units since ester hydrolysis is reported to be pH dependent[173] and moreover, hydrogel formulations with buffers haven't shown the effect of fast degradation. Additionally, **prepolymer-5** features the highest dilactide content which might lead to further increase in degradation kinetics.

Defined degradation studies will be conducted in chapter 4.2.4 and 4.2.5 to identify formulations with a suitable degradation profile.

Summary of the Adjustments to the Requirement Profile

In the previous chapter the identified fast crosslinking reaction HYGEL-3 from chapter 4.1 has been adapted to main parts of the requirements profile for a system useful for adhesion prophylaxis, from Table 5.

Jeffamine ED2003 was selected as the amine-based curing agent, enabling the formation of hydrogels with high solid content. This careful selection of components facilitates the manufacturing of hydrogels with elevated solid contents. Concentration limitations have been investigated *via* viscosity measurements. These studies revealed an upper threshold of 15wt.-% for the prepolymer concentration of **prepolymer-2-5**. Consequently, the maximum attainable concentration of the **Jeffamine ED2003** solution was constrained to 17wt.-%. This maximum concentration falls within the predefined viscosity threshold of 9 mPa*s.

The hydrogels obtained *via* NCO-NH_2 reaction, conducted according to previously established protocols, exhibited alkaline pH values which are unsuitable for the intended applications. The addition of buffers to the NH_2 providing solution has been investigated in detail *via* protonating a defined amount of NH_2 groups each, with three different buffer types and tracking of the pH during the hydrogel formation. Acetic acid/acetate buffers and HCl were identified as suitable buffering concepts in a range of 75-85mol.% free NH_2 fraction.

The adhesive properties of the hydrogel formulations were evaluated on organ tissue substrates. The experimental findings indicate that the curing process on the organ surface is potentially attributable to the buffering capacity of the tissue itself. This buffering effect was not accounted during the initial adjustment of the free NH_2 fraction using buffer solutions. To overcome this challenge, two modifications were implemented: 1) a reduction in the free NH_2 fraction, and 2) the incorporation of a 20mol.% excess of the NCO component. These adjustments effectively resolved the adhesion issue, enabling the hydrogel formulations to achieve adequate adhesion to the organ tissue substrate. Notably, the resulting pH values of the adapted hydrogel system were within the suitable range for the intended application.

Furthermore, hydrogel formulations prepared with degradable prepolymers exhibited rapid degradation, potentially caused by the alkaline pH conditions in interaction with a high amount of dilactide groups in the backbone. Analytical investigations *via* ^{13}C NMR revealed that the dissolved hydrogel network consisted of cleaved dilactide units, indicating that the degradation mechanism proceeded *via* ester hydrolysis. Consequently, the observed degradation is not a stability issue arising from the urea or urethane moieties within the hydrogel network.

4.2.4 Determination of the Influence of Different Factors of a Formulation on the Properties of Resulting Hydrogels Using Design of Experiments

Numerous parameters of the hydrogel system were optimized by employing sequential approach driven by scientific hypotheses as shown in previous chapters. Hereby, factor ranges of the formulation had been investigated in order set useful constraints. For the investigation of factor effects within the formulation on different properties, an I-optimal quadratic DoE was used with Design-Expert13 as software for the evaluation. The initial experimental design contained only two levels of wt.-% dilactide in the NCO-terminated prepolymers (5 and 10%) which was later augmented with an additional 12 experimental runs also including 1 and 2.5wt.-% dilactide. Factors and constraints, already identified by previous experiments, are summarized in Table 27.

Table 27 Overview on parameters and their set upper and lower limitations adjusted in accordance with the design of experiments.

Factor	Lower limit	Upper limit	Numeric/categoric
Dilactide content	1%	10%	Discrete numeric
Solid content NCO	10%	15%	Numeric
Buffering degree of NH_2	75%	85%	Numeric
Buffer/diluted acid	-	-	Categoric

In total, 31 different formulations have been tested and are listed in detail in chapter 6.4, Table 55. The following responses were evaluated: *curing time*, *swelling behavior*, *degradation speed*, *tensile strength at break*, *elongation at break*, *pH value after 30 min.* and *adhesion to organ substrate*. These responses cover the main part of the requirement profile, giving a reason why the structure-property relationship is especially of interest for possible later adjustments. Run 21 was excluded for the entire evaluation as it led to exceedingly large errors to the models for multiple responses (in some cases more than 30 standard deviations) and therefore regarded as an outlier.

Curing Behavior

The curing behavior analyzed by rheological measurements of a final formulation will be investigated in chapter 4.2.5. The herein used method for the determination of the curing behavior was carried out by a vertical set up, wherein the formulation was applied on a release paper in 90°. The time which was required until no more fluid ran off the paper was measured. Upon gelation gelled droplets were observed, which are still connected to the release paper. This point in time was defined as the curing time. Requirement for curing time in the targeted application was defined at <60 sec.

The identified terms of significance which are recommended for inclusion into the model and fit statistics are summarized in Table 28 with identified statistical parameters. The R^2 and predicted R^2 of 0.80 and 0.74, respectively, indicate a good fit and predictive power of the model. The lack of fit is also stated as significant with p-value 0.026 which indicates that a more complex model with additional higher order terms would likely further improve the model fit. However, safe determination of additional model terms would require a significant higher number of experimental runs.

A Log10 transformation was suggested for the evaluation and has been applied for the analyses, ʎ was detected at 0 in a box-cox-plot. A reduced linear model was suggested, with included terms: dilactide content (**A**), solid content NCO (**B**) and free base fraction (**C**).

Table 28 Overview of included parameters for the proposed model to describe influences on the curing time of the hydrogel system with respective p-values. Terms with p-values <0.05 have been included in the model.

Source	R^2	Predicted R^2	p-value		Coefficient of coded factors
Model	0.80	0.74	<0.0001	significant	
A: dilactide content			<0.0001	significant	+0.14
B:solid content NCO			<0.0001	significant	-0.23
C: free base fraction			0.0490	significant	-0.05
Lack of Fit			0.0263	significant	

The factor with the strongest effect was identified as solid content **B** of the hydrogel with a respective coded coefficient of -0.23, which indicates a decrease in curing time for increasing solid contents. A possible explanation for curing time is the increase of concentrations of reactants (here: NCO and NH_2) forming the urea groups as crosslinks. By an increase of reactants the reaction kinetic of hydrogel formation might be enhanced to form urea groups faster which is also displayed by reaction kinetics of first and second order.[174] This might not influence the full conversion of NH_2 and NCO to urea, but reaching the gel point might be accelerated. From Figure 75B a decrease in curing time can be observed for hydrogel formulations with increasing solid content NCO, which is equal to a higher reactants concentration. The p-value of the linear factor effect was identified to be highly significant with a p-value of <0.0001.

Interestingly dilactide content **A** was identified at a coded coefficient of +0.14, indicating a decrease in curing time for increasing dilactide content. Indeed, this effect becomes visible from the scatter plot in Figure 75A. An explanation for the influence of dilactide content on the curing time is missing. Lactide groups, for example as in PLA, are reported for their hydrophobicity.[175]

An increase in dilactide concentration might lead to a capsulation effect of the reacting NCO group, but with regard to the amount of dilactide in comparison to the whole formulation this explanation seems to be insufficient. However, the term **A** was identified as highly significant with a p-value of the linear factor effect of <0.0001.

Free base fraction was also included in the model leading to a coefficient of -0.05 indicating that a higher free base fraction leads to a decrease in curing time. Differences in free base fraction leads to different degrees of freely available NH_2 groups, which are able to crosslink and thus reduce the amount of available NH_2 groups, comparable to a decrease in concentrations of reactants. In the DoE, the free base fraction differs from 75-85mol.% causing less influence on curing time, being compared to solid content NCO which differs in a broader range, explaining the lower coded effect coefficients. The term C was identified as significant with a p-value of 0.049.

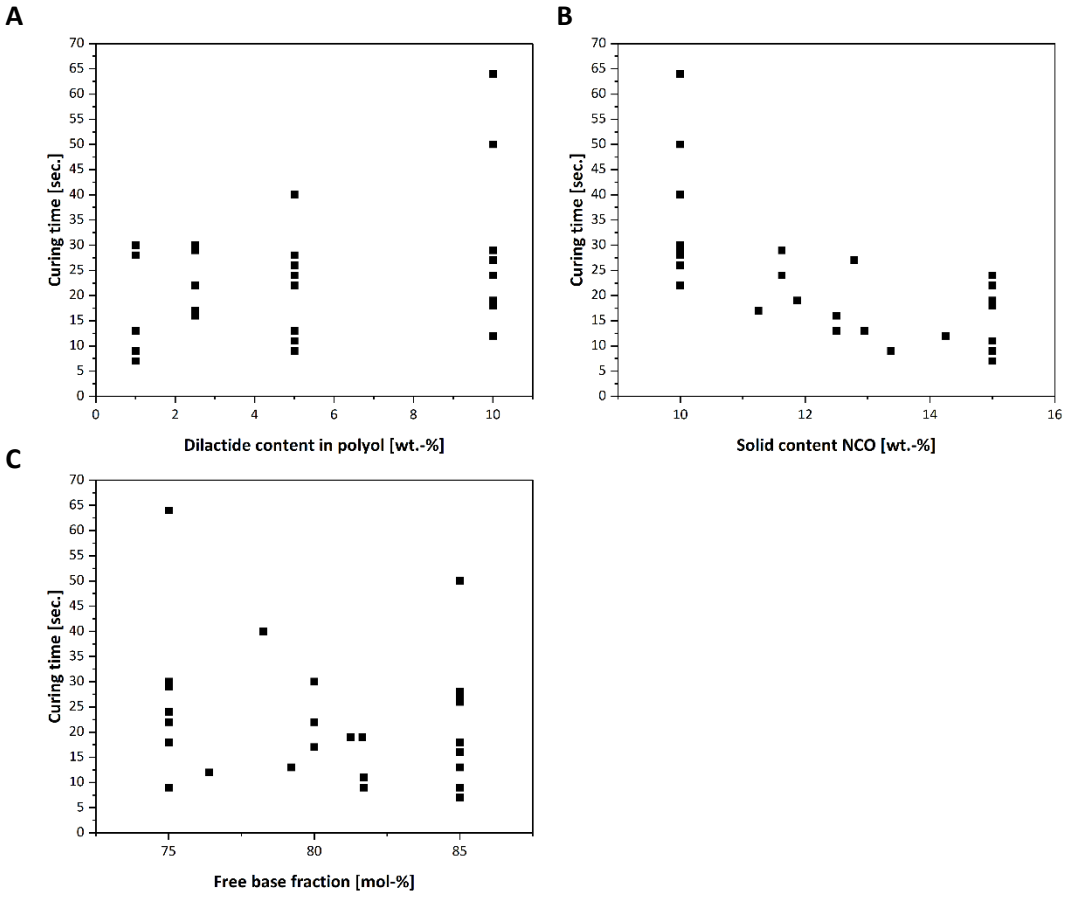

Figure 75 Curing time of 30 different hydrogel formulations gel as a function of the identified factor of impact A) dilactide content [wt.-%] B) solid content NCO [wt.-%]. C) free base fraction [mol.%].

The coded equation 4.2.2, obtained from the software for the applied model, allows an estimation on the relative impact on the analyzed parameter. Herein, A is the dilactide content, B the solid content NCO and C the free base fraction.

$$Log_{10} Curing\ time = 1.29 + 0.140A - 0.229B\ - 0.052\mathrm{C} \qquad (4.2.2)$$

All experiments comprised curing times in the range of 7 sec. to 64 sec. showing that nearly all analyzed formulations fit the requirements for the *curing time*.

Swelling Behavior

Swelling behavior was investigated to gain information on the possible expansion of the hydrogel formulation and swelling degrees were determined by incubating hydrogel samples in PBS and weighing them after 24 h and after 48 h. Equation 4.2.3 was applied for the determination of swelling degrees.

The manufacturing process of the hydrogels results in the incorporation of a high amount of water molecules within the polymeric structure of the hydrogel. Consequently, the hydrogel's polymeric matrix inherently contains a significant amount of water from the outset, prior to any subsequent hydration or swelling processes. Dry samples exhibit much higher swelling degrees.

$$Swelling\ degree\ (\%) = \frac{M_{swollen} - M_{initial}}{M_{initial}} * 100 \qquad (4.2.3)$$

The identified terms of significance which are recommended for inclusion into the model and fit statistics are summarized in Table 29 with identified statistical parameters. The R^2 and predicted R^2 of 0.55 and 0.41, respectively, indicate a moderate fit and predictive power of the model. The lack of fit is stated as not-significant with a p-value of 0.170.

ʎ was detected at 1 in a box-cox-plot, no transformation was recommended. A reduced quadratic model was suggested, with included terms: dilactide content (**A**), free base fraction (**C**) and dilactide content squared (**A^2**).

Table 29 Overview of included parameters for the proposed model to describe influences on the swelling degree after 24 h of the hydrogel system with respective p-values. Terms with p-values <0.05 have been included in the model.

Source	R^2	Predicted R^2	p-value		Coefficient of coded factors
Model	0.55	0.41	<0.0001	significant	
A-Lactide Content			0.4197	not significant	+1.69
C-Free base fraction			0.0007	significant	-7.22
A^2			0.0014	significant	+12.88
Lack of Fit			0.1702	not significant	

The factor with the strongest effect was identified as the dilactide content squared (**A^2**) with a coefficient of +12.88. Dilactide content A as such, was identified at a coefficient of +1.69, which

is statistically insignificant. However, for statistical reasons it is recommended to keep the lower order linear term in the model (if quadratic terms are significant, corresponding linear terms should be kept in the model). The inclusion of $\mathbf{A^2}$ indicates that the quadratic relationship between the factor and the response is statistically confirmed. A possible explanation for a minimum swelling around 5% lactide could be that the introduction of hydrophobic lactide groups decreased swelling but at higher dilactide content faster degradation could lead to a higher swelling due to bigger mesh size obtained by partially hydrolysis of the network. However, $\mathbf{A^2}$ was identified as significant as the p-value of the quadratic factor effect was detected at 0.0014, while **A** was not detected as significant supporting the assumption of a quadratic relationship of factor and swelling degree after 24 h.

Interestingly, after 48 h of swelling the term of dilactide content A turns significant as its p-value decreased to 0.0109, as visible from Table 30. $\mathbf{A^2}$ increases in p-value from 0.0014 to 0.0044, being still significant.

Free base fraction was identified to have an impact on the swelling after 24 h with an identified coefficient of -7.22, displaying that an increase in free base fraction leads to a decreased swelling. A possible explanation could be the inclusion of higher salt concentration which might enhance hydrophilicity of the hydrogels and lead subsequently to higher swelling degrees. A lower free base fraction is equal to a higher amount of buffer agent/acidic concentration and therefore of salt concentration. In general, swelling is reported to be at higher degrees when hydrogel samples are incubated in PBS in comparison to incubation at H_2O.[176] It is also reported in the literature on increased swelling as a result of higher ion concentrations within the polymeric network of a hydrogel.[177] The findings could potentially serve as an indication that this concept is applicable to the hydrogel formulations analyzed in the present study. No significant variations were observed between the different buffer/acid types suggesting that if this explanation is applicable, both buffer and acid, influence swelling of the hydrogels to the same extent. Free base fraction is determined as significant with a p-value of 0.0007.

The swelling degree within a timeframe of 24 h is illustrated as a function of the identified significant parameters for all experiments in Figure 76.

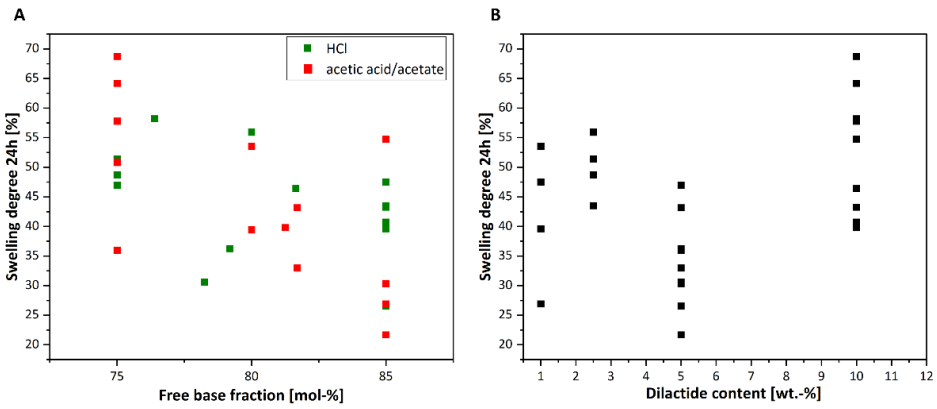

Figure 76 Swelling degree after 24 h of 30 different hydrogel formulations gel as a function of the identified factor of impact A) free base fraction [mol.%] B) Dilactide content squared [wt.-%].

The coded equation of the included terms for the relative impact is expressed by equation 4.2.4, wherein A is the dilactide content and C is the free base fraction.

$$Swelling\ after\ 24h = 37.55 + 1.69A - 7.22C + 12.88A^2 \quad (4.2.4)$$

Moreover, swelling after 48 h was investigated. For the analysis, run 14 was excluded for reasons equal to run 1. The identified terms of significance which are recommended for inclusion into the model and fit statistics are summarized in Table 30 with identified statistical parameters. The R^2 and predicted R^2 of 0.66 and 0.55, respectively, are acceptable for indication of a good fit and predictive power of the model. The lack of fit is stated as not-significant with p-value 0.229.

A reduced quadratic model was suggested, with included terms: dilactide content (**A**), free base fraction (**C**) and dilactide content squared (**A^2**).

The same terms as already been included in *Swelling after 24 h* have been included into the model for *Swelling after 48 h* with deviating coefficients and p-values. ʎ was again detected at 1 so no transformation was recommended.

Table 30 Overview of included parameters for the proposed model to describe influences on the swelling degree after 48 h of the hydrogel system with respective p-values. Terms with p-values <0.05 have been included in the model.

Source	R^2	Predicted R^2	p-value		Coefficient of coded factors
Model	0.66	0.55	<0.0001	significant	
A-Lactide Content			0.0109	significant	+7.90
C-Free base fraction			<0.0001	significant	-13.45
A^2			0.0044	significant	+15.51
Lack of Fit			0.2289	not significant	

Possible reasons for influences of terms were already discussed in *Swelling after 24 h.* The explanation of degraded ester units which could lead to higher degrees of inclusion of water is supported by the increase of coefficient for **A** to +7.90. At the same time **A^2** decreased to +15.51 which is also reflected by p-values for dilactide content of 0.0109 and for **A^2** of 0.0044. The results might indicate deviations from a quadratic relationship. However, **A^2** still comprises the highest influence on swelling after 48 h, followed by **C**, followed by **A**.

The swelling degree after 48 h is illustrated as a function of the identified significant parameters for all experiments in Figure 77.

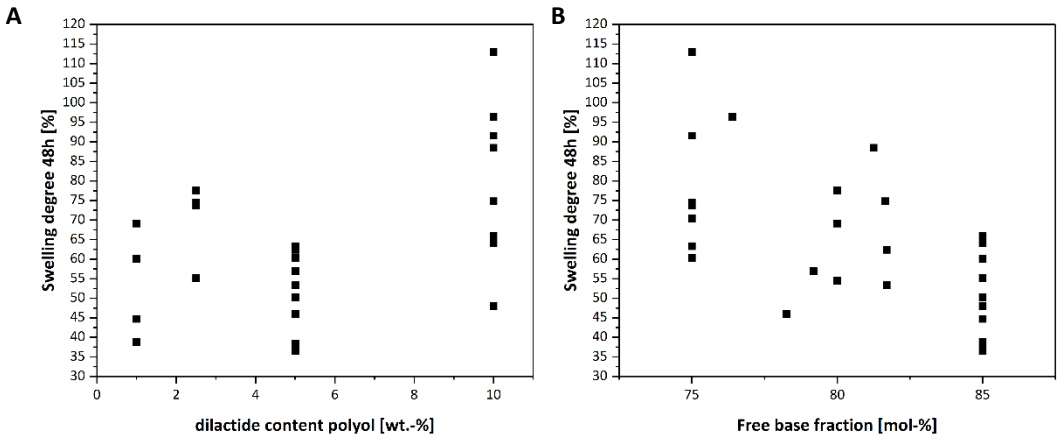

Figure 77 Swelling degree after 48 h of 30 different hydrogel formulations as a function of the identified factor of impact A) dilactide content polyol [wt.-%], B) Dilactide content squared [wt.-%], C) free base fraction [mol.%].

The coded equation of the included terms for the relative impact is given by equation 4.2.5. Herein, **A** is the dilactide content and **C** is the free base fraction.

$$Swelling\ after\ 48\ h = 57.76 + 7.9A - 13.45C + 15.51A^2 \qquad (4.2.5)$$

For swelling degrees no target values have been defined. However, the uptake of water is of interest regarding the amount of fluid available in the intraabdominal body compartment. Values of swelling differ between 21.7-68.7wt.-% for 24 h and between 36.6wt.-% to 113wt.-% for 48 h. Assuming a total amount of 10 g hydrogel per application, a maximum of 11.3 g of water will be absorbed after 48 h into the network.

Degradation Behavior

The degradation behavior of the hydrogels for formulations with different dilactide contents has been qualitatively analyzed in chapter 4.2.3, revealing that degradation behavior is indeed induced *via* ester hydrolysis as demonstrated *via* pH and NMR measurements.

In the DoE, this investigation is continued but extended to a quantitative analysis to characterize degradation times of hydrogels and moreover detect, or exclude possible influences of solid content NCO, free base fraction and/or acid/buffer type. It is important to notice that the point of degradation was determined as the point of loss of mechanical properties, when the material starts to show flow properties, as it is expected that in this state a barrier effect is reduced or nonexistent. The determination was carried out *via* analyses of the haptic, rheological measurements have not been conducted.

The identified terms of significance which are recommended for inclusion into the model and fit statistics are summarized in Table 31 with identified statistical parameters. The R^2 and predicted R^2 of 0.75 and 0.68, respectively, indicate a good fit and predictive power of the model. The lack of fit is also stated as significant with p-value <0.0001 which indicates that a more complex model with additional higher order terms would likely further improve the model fit. However, safe determination of additional model terms would require a significant higher number of experimental runs.

A Log10 transformation was suggested for the evaluation and has been applied for the analyses, as λ was detected at 0 in a box-cox-plot. A reduced linear model was suggested, with included terms: dilactide content (**A**) and solid content NCO (**B**), as described in Table 31.

Table 31 Overview of included parameters for the proposed model to describe influences on the degradation of the hydrogel system with respective p-values. Terms with p-values <0.05 have been included in the model.

Source	R^2	Predicted R^2	p-value		Coefficient of coded factors
Model	0.75	0.68	<0.0001	significant	
A-Lactide Content			<0.0001	significant	-0.61
B-solid content NCO			0.0115	significant	+0.18
Lack of Fit			<0.0001	significant	

The strongest effect is observed for the dilactide content **A** with an identified coefficient of -0.61, displaying that an increase in dilactide content leads to a decrease of the degradation time, which is reflected from the scatter plot of Figure 78A. A decrease of the degradation time with an increase of lactide units have already been reported in the literature.[178] For the presented hydrogel system dilactide units are responsible for the degradation behavior of the hydrogels as already has been demonstrated in chapter 4.2.3. An increase of dilactide groups leads to an increase of concentration of hydrolysable groups, and in terms of reaction kinetics to an increase of reaction speed, assuming a first or second order reaction kinetic.[174] Ester hydrolyses is reported to follow (pseudo) first order kinetics.[179,180]

The effect of solid content on the degradation time is less pronounced but still identified at a coefficient of +0.18, displaying an increase in degradation time for an increase of solid content. This effect also becomes visible from Figure 78B. Different dilactide contents are marked by different colors, presenting a slight decrease in degradation time for an increasing solid content in each dilactide row. Both terms, **A** and **B** have been identified as significant as the p-values of the factors were detected at <0.001 and 0.0115, respectively.

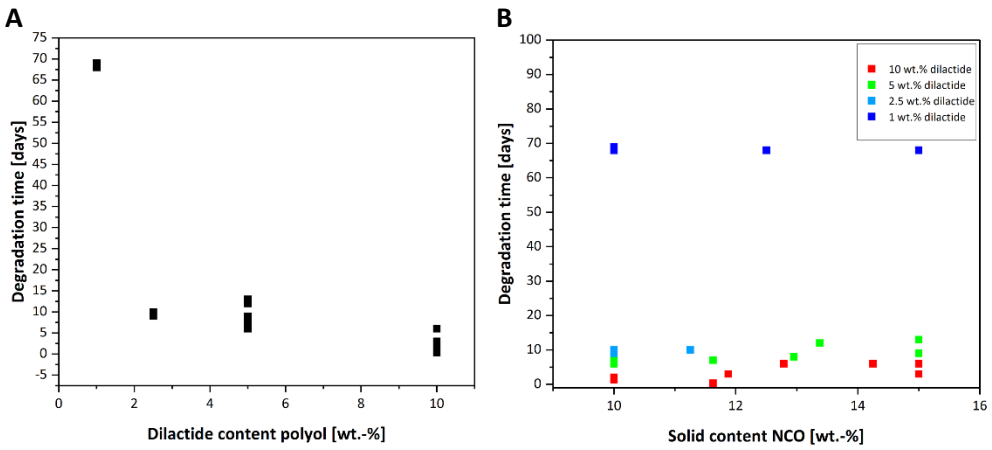

Figure 78 degradation time of 30 different hydrogel formulations as a function of the identified factor of impact A) dilactide content polyol [wt.-%], B) solid content NCO [wt.-%].

The coded equation of the included terms for the relative impact is given by equation 4.2.6, wherein A represents the dilactide content, whilst B being the solid content NCO.

$$Log_{10} Degradation\ time = 0.944 - 0.612A + 0.180B \qquad (4.2.6)$$

The effect of lactide groups on the degradation kinetics was known beforehand but with the use of the DoE a smaller positive effect of the solid content was additionally determined as significant. A decrease of degradation time by an increase in solid content has already been reported for the degradation of sewage sludge by Liao, Li *et al*.[181] but have not been discussed in more detail therein. A possible reason, applicable for the hydrogel system, might be the higher number of crosslinks in the network. At lower solid contents the likelihood that isocyanate groups hydrolyze before finding an amine-reaction partner increases, leading to less crosslinks and more dangling chains. To dissolve a less crosslinked network, a smaller amount of dilactide units need to be hydrolyzed.

Elongation and Tensile Strength at Break

Apart from common body movements larger mechanical forces within the abdominal area might arise from coughing or sneezing or physiological movement.[119] To investigate whether herein presented hydrogels are able to withstand such forces and which parameters might influence force resistance, tensile tests have been conducted to determine the elongation at break and tensile strength at break.

Elongation at break

The identified terms of significance which are recommended for inclusion into the model and fit statistics are summarized in Table 32 with identified statistical parameters. The R^2 and predicted R^2 of 0.63 and 0.41, respectively, display high deviation which indicate a good fit of the model but with limited predictive power regarding predicted R^2. The lack of fit is stated as not significant with p-value <0.2964.

A Log10 transformation was suggested for the evaluation and has been applied for the analyses, as λ was detected at 0 in a box-cox-plot. A reduced quadratic model was suggested, with included terms: dilactide content (**A**), solid content NCO (**B**), Acid Type (**D**), interaction of dilactide content and solid content (**AB**) and dilactide content squared (**A^2**).

Table 32 Overview of included parameters for the proposed model to describe influences on the elongation at break of the hydrogel system with respective p-values. Terms with p-values <0.05 have been included in the model.

Source	R^2	Predicted R^2	p-value		Coefficient of coded factors
Model	0.63	0.41	<0.0001	significant	
A-dilactide Content			0.0027	significant	-0.104
B-solid content NCO			0.2733	not significant	-0.032
D-Acid type			0.0137	significant	-0.063
AB			0.0243	significant	-0.087
A^2			0.0079	significant	-0.160
Lack of Fit			0.2964	not significant	

The strongest influence was detected for dilactide content squared (**A^2**) displaying a coefficient of -0.160, whereby an increase in dilactide content is related to a decrease in elongation, followed by dilactide content **A** with a coefficient of -0.104. The identification of **A^2** indicates a quadratic relationship. It is questionable whether this is a direct effect of dilactide content or might be an indirect effect by delayed measurements of samples in tensile testing. As shown in chapters 4.2.3 and previously in 4.2.4, hydrolysis of ester groups, depending on the initial pH

value, starts immediately and leads to fast dissolving of the hydrogel network, partially within 2 h. The delay between hydrogel manufacturing and tensile testing was between 2 and 24 h and some ester units might already be hydrolyzed which decreased the elongation at break. Explanations how dilactide content as such could influence elongation for such detectable extent, might be given by possible interactions of ester groups in dilactide units. Pure poly lactic acid (PLA) is reported to exhibit brittleness.[182,183] Due to its glass transition temperature (T_g) of ~ 60°C, polymer chains in PLA probably are less flexible in comparison to pure PEG/PPG which is reported to exhibit a T_g of -60°C.[184] An increase in dilactide could thus lead to a decrease of elongation at break. It is questionable whether the described effect of semicrystalline PLA can be transferred on dilactide containing elastomers but might be an explanation for the strong effect of dilactide content in the polymer backbone on elongation ratios. It is unclear where this effect arises from and wrong identification of **A** as a result of a delay between manufacturing of hydrogels and measurement cannot be excluded. However, $\mathbf{A^2}$ and **A** were identified as significant with a p-value of 0.0079 and 0.0027, respectively. The scatter plot of elongation at break as a function of **A** is presented in Figure 79A.

Following the coefficients, the third highest impact is given by the interaction of dilactide content **A** and solid content **B**, displayed by the coefficient of -0.087 indicating that the effect of lactide content depends on the solid content. At low solid content, elongation shows a maximum at 5% dilactide content whereas the curve at high solid content shows a more continuous downward trend with dilactide content. Higher solid content has been reported to decrease elongation at break by Zhang, Huang *et al*.[185] wherein this effect was explained by a higher crosslink density caused by an increase of crosslinker and therefore increased solid content. This effect does not apply to the hydrogels presented herein as the index is continuously kept at 1.2. By an increase in solid content NCO, the concentration of the crosslinking agent is increased to the same molar extent to keep the index constant. However, higher solid content in combination with higher dilactide contents might influence elongation at break in the analyzed design space as it was identified as significant with a p-value of 0.0243. The interaction plot is presented in Figure 79C.

Next, the acid/buffer type **D** has been identified to influence elongation at break, displayed by the coefficient of -0.063. Salt concentrations differ between buffer and acid, since the latter only comprises one component, whilst acidic buffers in general consist of a weak acid and the salt of its corresponding base.[170] The molar concentration of the buffer type is therefore increased by factor 2 in comparison to pure acids as buffering agents. The total amount of salt increases in buffer containing formulations, additionally. A correlation between salt concentration and mechanical elongation has already been described in the literature[186] and might be a reason for detection as significant term for influencing elongation at break. Herein chloride salts and sulfate salts have been reported to influence the primary structure of tested starch and therefore affecting elongation at break. This effect was mainly explained by the fact that salts might contribute to the viscous characteristics of the therein analyzed semi-solid starch films by interfering

with intermolecular hydrogen bonds at low concentration resulting in an increase in the elongation-at-break.[186] As visible from Figure 79B, acetic acid/acetate buffer in general leads to lower elongation ratios indicating that higher salt concentrations might decrease elongation ratios. Whether this hypothesis is applicable needs to be analyzed in more detail. With the obtained data, statements are limited to assumptions. However, term **D** was identified as significant with a p-value of 0.0137.

The term solid content NCO **B**, was also identified to influence elongation at break, displayed by the coefficient of -0.032. However, term **B** was not identified as significant with a p-value of 0.273.

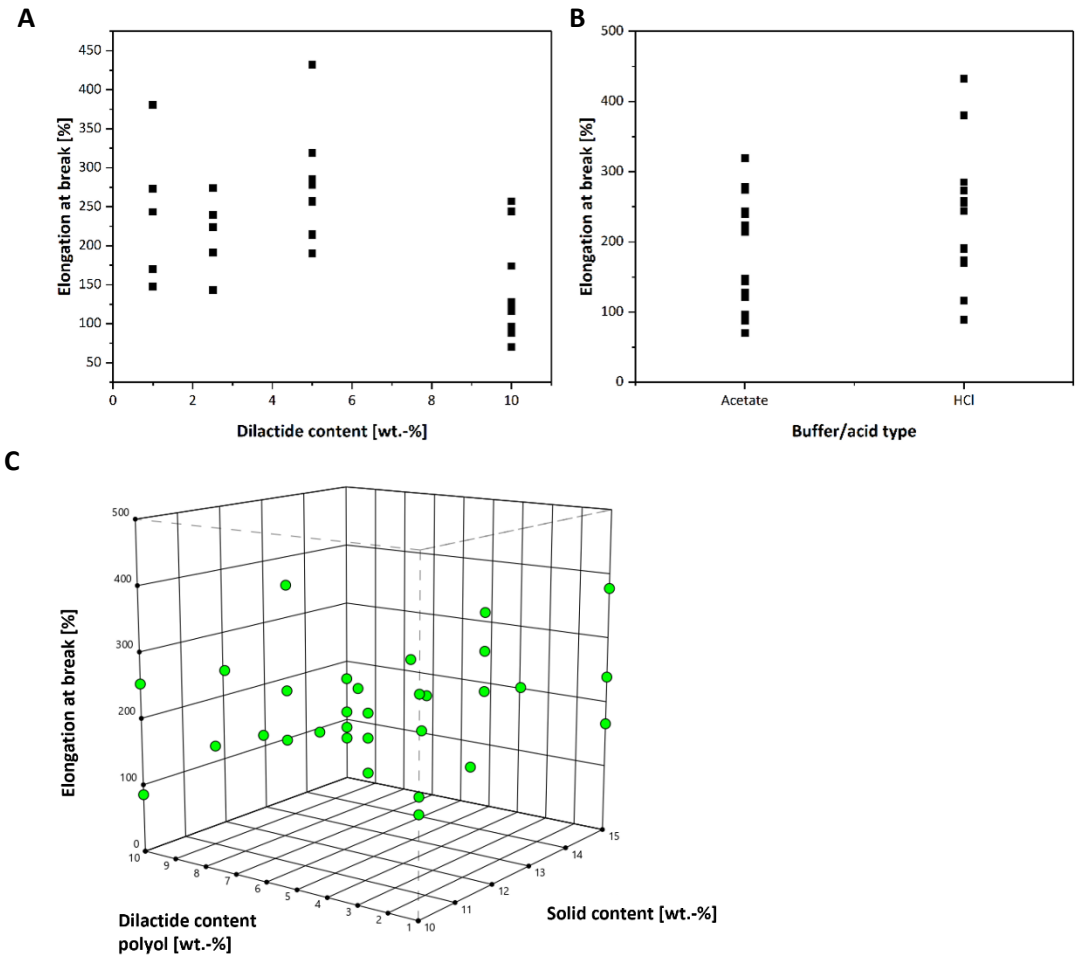

Figure 79 Elongation at break of 30 different hydrogel formulations as a function of the identified factor of impact A) dilactide content polyol [wt.-%], B) buffer/acid type, C) interaction of dilactide content and solid content.

The coded equation 4.2.7 for elongation at break includes the discussed terms, wherein **A** is the dilactide content, **B** is the solid content NCO and **D** is the buffer/acid type, **AB** is the interaction of dilactide content and solid content.

$$Log_{10}(Elongation) = 2.39 - 0{,}1041A - 0{,}0323B - 0.0629D - 0.0869AB - 0.01598\mathrm{A}^2 \quad (4.2.7)$$

Tensile strength at break

The identified terms of significance which are recommended for inclusion into the model and fit statistics are summarized in Table 33 with identified statistical parameters. The R^2 and predicted R^2 of 0.44 and 0.14, respectively, display a limited fit of the model with minor predictive power of the model. The lack of fit is stated as not significant with p-value <0.5824.

A Log10 transformation was suggested for the evaluation and has been applied for the analyses, as λ was detected at 0 in a box-cox-plot. A reduced quadratic model was suggested, with included terms: dilactide content (A), solid content NCO (B), interaction of dilactide content and solid content (AB) and dilactide content squared (A^2).

Table 33 Overview of included parameters for the proposed model to describe influences on the tensile strength at break of the hydrogel system with respective p-values. Terms with p-values <0.05 have been included in the model.

Source	R^2	Predicted R^2	p-value		Coefficient of coded factors
Model	0.44	0.14	0.0035	significant	
A-dilactide Content			0.1090	not significant	-0.093
B-solid content NCO			0.0125	significant	+0.139
AB			0.0482	significant	-0.134
A^2			0.0384	significant	-0.217
Lack of Fit			0.5824	not significant	

The strongest influence was detected for dilactide content squared (**A^2**) displaying a coefficient of -0.217, revealing that an increase in dilactide content leads to a decrease of tensile strength. The identification of dilactide content as squared term **A^2** indicates a quadratic relationship. The given explanation for a decrease in elongation at break by increasing **A^2** was based on the brittleness of pure PLA. If this explanation is applicable this should be visible by an increase of tensile strength at break. The detection of a negative influence of the dilactide content **A^2** on both, elongation and tensile strength at break, raises the question whether this effect might appear by partly hydrolyzed samples and thus, indicates that ester hydrolysis was here detected as major influence. However, term **A^2** was identified as significant with a p-value of 0.0384.

Solid content NCO **B** was identified to influence elongation at break, displayed by the coefficient of +0.139. This effect seems to be applicable since an increase in solids correlates with an increase in elastic links, responsible for the increase in tensile strength at break. Moreover, an increased solid content results in higher amount of physical interaction by a higher amount of urea. Both concepts might interfere in the present study. The effect of solid content **B** was identified as significant with a p-value of 0.0125.

The interaction term **AB** of dilactide content **A** and solid content NCO **B** was identified to have the next major influence, displayed by the identified coefficient of -0.134, revealing that an increase of **AB** leads to a decrease of tensile strength. This effect might be comparable to the results presented for elongation at break, and explanations given in this section, for the decrease in elongation ratios by increasing amounts of dilactide content, might be applicable. But for tensile strength at break the increase of **A** as single term is hardly explicable by the higher dilactide content, since pure PLA is reported to be brittle but a blend of PLA/PEG is reported for increase tensile strength with a higher amount of PLA by Li, Liang *et al*..[187] Results for negative influences of **AB** on both, tensile strength and elongation at break, support the hypothesis that testing delay and ester hydrolysis are detected here as major influence. However, the term **AB** is stated to be significant with a p-value of 0.0482. Interestingly, the single term **B** was identified to increase tensile strength at break, as visible from Figure 80B.

Overall, effects have been detected but due to R^2 of 0.44 of the model, the model fit to describe the obtained results for tensile strength at break is limited.

Figure 80 demonstrates the scatter plots for tensile strength at break as a function of each significant detected term.

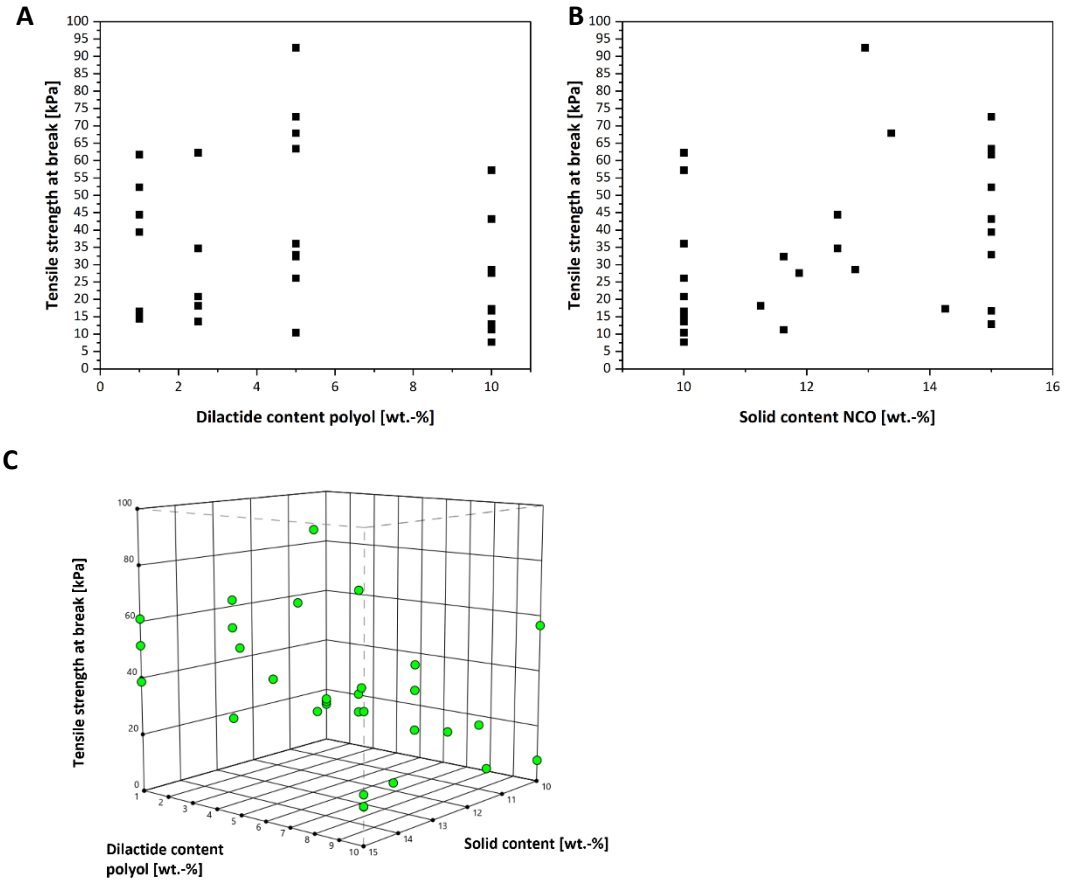

Figure 80 Tensile strength at break of 30 different hydrogel formulations as a function of the identified factor of impact A) dilactide content polyol [wt.-%], B) solid content NCO [wt.-%], C) interaction of dilactide content and solid content.

The coded equation 4.2.8 for tensile strength at break is useful for comparing the factor coefficients, wherein **A** is the dilactide content, **B** is the solid content NCO and **AB** is the interaction of dilactide content and solid content.

$$Log_{10}Tensile\ Strength = 1.60 - 0.093A + 0.139B\ - 0.134AB - 0.217\mathrm{A}^2 \qquad (4.2.8)$$

PH value after 30 Minutes

The identified terms of significance which are recommended for inclusion into the model and fit statistics are summarized in Table 34 with identified statistical parameters. The R^2 and predicted R^2 of 0.25 and 0.10, respectively, indicate a minor fit and predictive power of the model. The lack of fit is stated as not significant with p-value of 0.8394.

ʎ was detected at 1 in a box-cox-plot, no transformation was recommended. A reduced linear model was suggested, with included terms: dilactide content (**A**) and free base fraction (**C**).

Table 34 Overview of included parameters for the proposed model to describe influences on the pH values after 30 min. of the hydrogel system with respective p-values. Terms with p-values <0.05 have been included in the model.

Source	R^2	Predicted R^2	p-value		Coefficient of coded factors
Model	0.25	0.10	0.0178	significant	
A-dilactide Content			0.0419	significant	+0.182
C-Free base fraction			0.0214	significant	+0.195
Lack of Fit			0.8394	not significant	

The strongest influence was identified for the term free base fraction C, displayed by an obtained coefficient of +0.139, which reveals an increase in pH for an increase of free base fraction, which has already been identified in chapter 4.2.3, wherein it was demonstrated that a higher degree of free NH_2 leads to higher pH values in resulting hydrogels. PH values of obtained hydrogels were detected at 6.52 to 8.15. 26 out of 31 formulation comprised pH values in hydrogels in physiological ranges 6.5≥ to ≤7.4. Initial buffering testing series from chapter 4.2.3 were used as preselection for suitable buffering ranges. The amount of free NH_2 groups in the different formulations differed between 75mol.%-85mol.%. Figure 81 illustrates scatter plots for the identified significant terms from which is visible, that especially testing series of 5wt.-% dilactide content differs strongly in obtained pH value, but also does the 10wt.-% dilactide testing series. Dilactide testing series of 1 and 2.5wt.-% differ quite less. It is questionable whether this effect occurred by coincidence or by errors during the experimental phase. The correlation of

pH values after 30 min as a function of free base fraction becomes visible from Figure 81B. The term **C** was identified as significant with a p-value of 0.0214.

Next, the single term of dilactide content **A** was identified at a coefficient of +0.1823 revealing that an increase in **A** leads to an increase in resulting pH values. This effect is in contrast to the assumption of fast hydrolysis of ester groups which had likely been identified for elongation and tensile strength at break. Hydrolysis of the ester unit results in alcohols and carboxylic acids and thus leading to a decrease in pH values as already been identified in chapter 4.2.3. Higher deviations in resulting pH values for 5 and 10wt.-% formulations, as visible from Figure 81A, are barely understandable, assuming an ideal reaction. Miscibility problems may lead to higher deviations but might be restricted by maintaining the application method identical for all conducted experiments. However, term **A** was identified as significant with a p-value of 0.0419.

The obtained R^2 of the model of 0.25 indicate a limited fit of the model. This might be caused by the outliers of resulting pH values in 5 and 10wt.-% dilactide formulations.

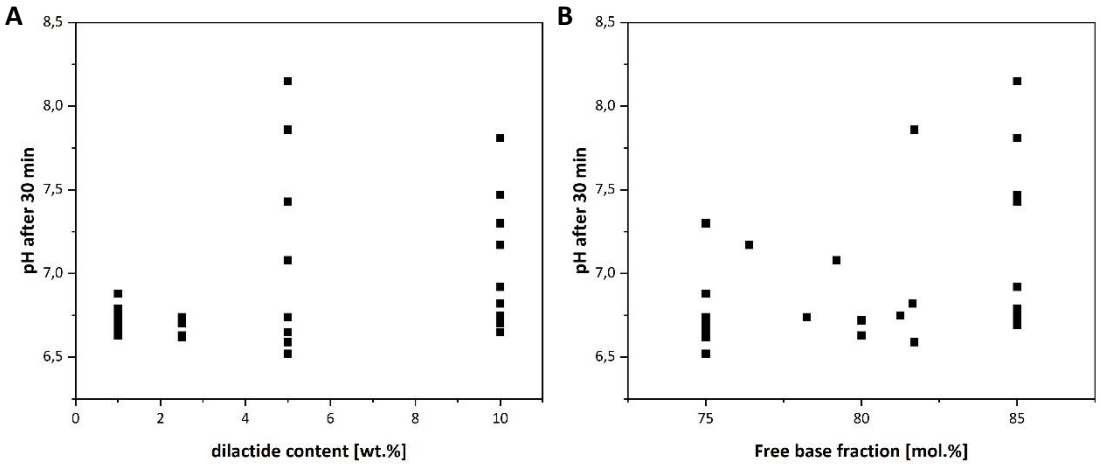

Figure 81 PH after 30 min of 30 different hydrogel formulations as a function of the identified factor of impact A) dilactide content polyol [wt.-%], B) free base fraction [mol.%].

The coded equation 4.2.9 for pH value after 30 min. is useful for comparing the factor coefficients, wherein A is the dilactide content and C is the free base fraction.

$$pH_{t=30min} = 6.92 + 0.182A + 0.195\mathrm{C} \qquad (4.2.9)$$

Adhesion Behavior to Organ Substrate

The determination of adhesion of hydrogels to organ substrate was measured by applying the hydrogel formulation on a 37°C preheated porcine kidney. After a short time of curing the kidney was removed from the incubator and the adhesion of the hydrogel to the surface of the kidney was evaluated according to Table 35. This parameter therefore bears the risk of a bias as it is

assessed subjectively. However, due to missing measurement set ups how to evaluate surface interaction between the hydrogel and the kidney, this system was used for the determination.

Table 35 Rating score for the evaluation of adhesion properties of a hydrogel formulation to the surface of organ substrate (here: porcine kidney).

Rating Score	Adhesion Properties
1	No adhesion
2	Very poor adhesion (hydrogel can be removed without applying mechanical force, e.g., by movement of the kidney)
3	Poor adhesion (hydrogel can be removed by applying light mechanical force, like wiping over the surface with moistened gloves)
4	Good adhesion (hydrogel can be removed by applying stronger mechanical force, like pulling or rubbing)
5	Very good adhesion (hydrogel cannot be removed as a whole by applying strong mechanical force, like pulling or rubbing)

The identified terms of significance which are recommended for inclusion into the model and fit statistics are summarized in Table 36 with identified statistical parameters. The R^2 and predicted R^2 of 0.70 and 0.67, respectively, indicate a good fit and predictive power of the model. The lack of fit is stated as not significant with p-value of 0.0532.

λ was detected at 0.5 in a box-cox-plot, square root transformation was recommended. A reduced linear model was suggested, with included terms: solid content NCO (**B**).

Table 36 Overview of included parameters for the proposed model to describe influences on the adhesion behavior to organ substrate of the hydrogel system with respective p-values. Terms with p-values <0.05 have been included in the model.

Source	R^2	Predicted R^2	p-value		Coefficient of coded factors
Model	0.70	0.67	<0.0001	significant	
B-Solid Content NCO			<0.0001	significant	+0.463
Lack of Fit			0.0532	not significant	

The term solid content NCO **B** is exclusively used for this model and thus the factor with the strongest influence on the organ adhesion, displayed by a coefficient of +0.463, revealing that an increase in **B** leads to an increase in the organ adhesion rating, wherein a higher value stands for a stronger adhesion of the hydrogel to the organ substrate, as described in Table 36. Figure 82 presents the organ adhesion rating as a function of the solid content NCO. Herein, the effect becomes visible.

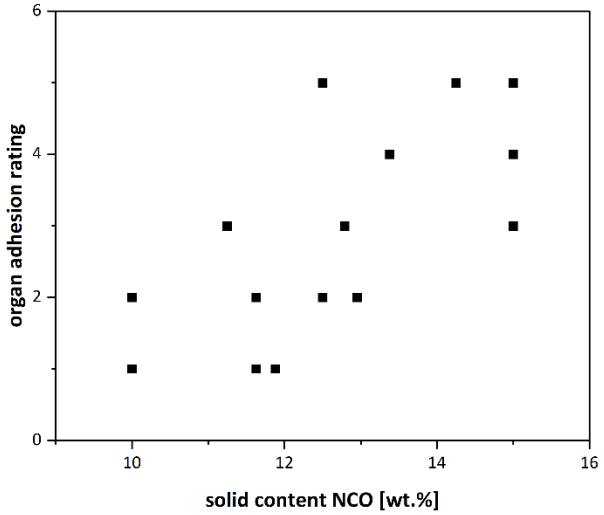

Figure 82 Organ adhesion rating of 30 different hydrogel formulations as a function of the identified factor of impact solid content NCO [wt.-%].

A possible explanation could be the higher degree of interactions, mainly caused by H-bondings, which could occur between urea groups and surface proteins.

The coded equation is expressed by equation 4.2.10. Significant influence on the adhesion on organs is limited to the term solid content NCO B, wherein a higher solid content leads to a higher adhesion on organ rating which is equal to an improved adhesion.

$$\sqrt{Adhesion\ on\ Organs} = 1.61 + 0.463B \tag{4.2.10}$$

Adhesion behavior to surfaces is associated with a high degree of chemical or physical interaction.[188] The chemical groups being most described for interaction in the macromolecular backbone might be urea groups. An increase in solid content correlates with an increase in urea groups per hydrogel mass and, hence, also on the hydrogel surface. Assuming a 100% conversion of NCO to urea groups, neglecting remaining NCO groups by an excess of NCO, eq. 4.2.11 can be used to determine the amount of urea in mol/kg. This value is equal to the amount of urea bonds per kg of hydrogel.

$$amount\ urea\ \left[\frac{mol}{kg}\right] = \frac{(f_{Prep.} * n_{prep.})}{m_{hydrogel}} \tag{4.2.11}$$

Equation 4.2.11 has been applied on the different formulations from the DoE and the adhesion rating score as a function of amount of urea is presented in Figure 83. As expected, an increase

in urea groups leads to a higher adhesion rating score, as already been assumed by the correlation of higher solids content with higher adhesion rating, presented in Figure 83.

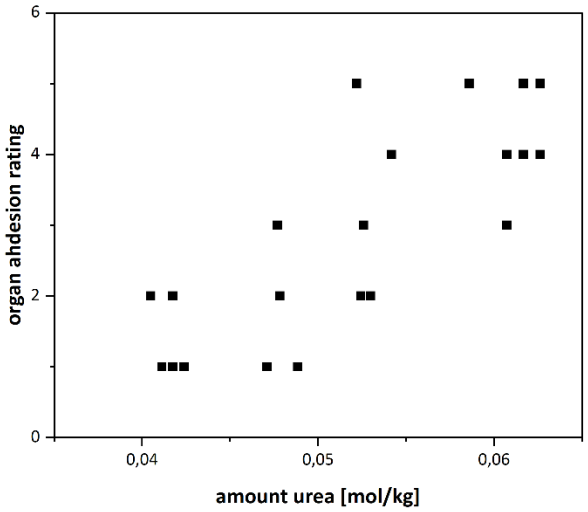

Figure 83 Organ adhesion rating as a function of amount urea in mol/kg. An increase in urea correlates with an increase in organ adhesion rating score.

However, covalent bondings between remaining NCO groups and NH_2 group containing amino-acids, potentially present on the surface of the organ samples, might also be a possible explanation for the improved adhesion properties.

Summary of Results of the DoE analyses

The DoE study was conducted to investigate structure-property relationships in the hydrogel system. Analyzed responses were: Curing time, Swelling behavior, Degradation behavior, Elongation at break, Tensile strength at break, pH value after 30 min and adhesion behavior to organ substrate. Factors which were adjusted during the hydrogel formulation were: dilactide content [wt.-%], solids content NCO [wt.-%], free base fraction NH_2 [mol.%] and acid/buffer type.

Overall, the term solid content **B** was identified to exhibit a significant impact on numerous analyzed responses. An improved behavior of a certain response often correlates with an increased solid content. Moreover, dilactide content (**A**) was identified in numerous responses as a major influence. In the responses elongation at break, tensile strength at break, curing time and pH value after 30 min. dilactide content was identified as significant term but was hardly explicable. Table 37 summarizes the analyzed responses with identified coefficient for significant terms, each.

Table 37 Summary of the DoE analyses with identified significant terms for each response and the corresponding coefficient of the coded factors.

Response	Significant Terms	Coefficient of coded factors
Swelling after 24 h (48 h)	A Dilactide content	+1.69 (+7.90)
	C Free base fraction	-7.22 (-13.45)
	A^2	+12.88 (+15.51)
Curing Time	A Dilactide content	+0.14
	B Solid content NCO	-0.23
	C Free base fraction	-0.05
Degradation behavior	A Dilactide content	-0.612
	B Solid content NCO	+0.180
Elongation at break	A Dilactide content	-0.104
	B Solid content NCO	-0.032
	D-Acid type	-0.063
	AB	-0.087
	A^2	-0.160
Tensile strength at break	A Dilactide content	-0.093
	B Solid content NCO	+0.139
	AB	-0.134
	A^2	-0.217
pH value after 30 min.	A Dilactide content	+0.182
	C Free base fraction	+0.195
Adhesion behavior to organ substrate	B Solid content NCO	+0.463

Parameters with an influence on certain responses have already been identified in former investigations. The structured DoE approach, however, was able to quantify and rank the relative influences of different factors and in some instances was even able to recognize new effects that were otherwise hard to separate from noise. For example, the increased adhesion to the surface correlates with a higher solid content and has not been identified before. Interestingly an NCO excess was used here to improve adhesion behavior. The NCO excess indirectly impacts the solid content, which could be an explanation why the NCO excess was successful in former investigations. This effect can be attributed either to the covalent binding of NCO- and NH_2-containing surface proteins of the organ samples, or to an increased physical interaction due to the higher amount of urea groups.

Moreover, a formulation, which fulfills the requirements required for the targeted application of adhesion prophylaxis was identified with the help of DoE. Significant parameters are

presented in Table 38 and the herein listed formulation will be referred to as PU-U-hydrogel in the following chapters.

Table 38 Main parameters of the identified optimized formulation for the use in an adhesion prophylaxis application.

	Dilactide content polyol backbone [wt.-%]	Solid content NCO [wt.-%]	Free base fraction [mol.%]	Acid/buffer type
	5	15	81.7	HCl

The obtained response values are reported in Table 39 as mean values (n=2).

Table 39 Obtained values for the analyzed responses of the identified optimal formulation, reported in Table 38. Values are summarized as mean values (n=2) since the formulation was repeated in a replicate.

Curing time	Swelling after 24 h (48 h)	Degradation time	Elongation at break (tensile strength at break)	pH value after 30 min.	Adhesion on organ substrate
10 sec.	38.1% (57.9%)	13 days	223 (48.15 kPa)	7.23	3.5

The dilactide content of 5wt.-% was chosen, as a suitable degradation behavior was observed in the resulting hydrogels. Higher solid content was identified to improve numerous performance parameters but is limited to a maximum of 15wt.-% as otherwise a viscosity increase above the limitation of 9 mPa*s consequently, as already demonstrated in chapter 4.2.3. The free base fraction of 81mol.% was identified to yield hydrogels exhibiting physiological pH values why enabling good adhesion properties to the surface. HCl was chosen as it is the easiest form of protonation agent and no significant deviations have been detected between the two buffering agents (HCl vs. acetic acid/acetate).

Since it has been demonstrated earlier that a 85mol.% free base fraction is sufficient to yield neutral pH values on organ substrate, the free base fraction was adapted to 85mol.% as buffering effects of organ tissue were not included in the pH measurements of the DoE.

4.2.5 Physico- and Biochemical Characterization of the Selected Hydrogel Formulation

Using a DoE concept, a formulation, matching the requirements of Table 5 in chapter 3.3, was identified by detailed investigation of the curing time, swelling behavior, mechanical properties (tensile strength at break, elongation at break), pH values of the resulting hydrogels, adhesion behavior to organic surface and degradation behavior. The best formulation, listed in Table 38 was adapted to 85mol.% free base fraction and is in the following chapter referred to as PU-U-hydrogel. This formulation was further studied concerning its physicochemical and biochemical properties, addressing NCO conversion, viscoelastic properties, pH value as a function of time,

tensile and compression testing, hydrolytic degradation, determination of molecular weight between two crosslinks (M_c) and resulting mesh size and biochemical characterization focusing on cytotoxicity and cell migration behavior and will be presented in this chapter. Parts of this characterization were conducted by scientists from NMI, Reutlingen and thus, cannot be attributed to the author of this thesis (Tobias Hokamp, PhD: viscoelastic properties, hydrolytic degradation as a function of time; Johanna Heider, M. Sc.: biochemical characterization). However, the results are listed here, as they are highly relevant for evaluating the safety and effectiveness of the herein presented hydrogels as adhesion prophylaxis *in vitro*. A publication has been submitted focusing on the physico- and biochemical characterization of the hydrogel, wherein the majority of this chapter has been reported.[189]

NCO Conversion During the Curing Reaction

The formation of the presented 2K hydrogel system is based on the well-established curing technology of the reaction of NCO and NH_2, yielding urea groups as crosslinks. The molar ratio of the identified best formulation was 1:1.2 NH_2/NCO. The excess of 20mol.% NCO was identified as suitable to obtain good adhesion to the surface of organ substrates, as described in chapter 4.2.3. According to Stockmayer, primary crosslinking occurs for such systems with indices (NCO/NH_2 ratios) below 2.0 according to equation 4.2.12 and 4.2.13.[190]

$$p_{NCO}p_{NH_2} = (f_a - 1)^{-1} * (f_{NH_2} - 1)^{-1} \quad (4.2.12)$$

$$\frac{p_{NCO}}{p_{NH_2}} = \frac{(f_{NCO} - 1)}{(f_{NH_2} - 1)} \quad (4.2.13)$$

Wherein p_{NCO} is the fraction of NCO groups, p_{NH2} being the fraction of NH_2 groups. Consequently, primary gelation was well ensured by setting the index to 1.2. Postcuring of the residual NCO groups yields eventually the completely crosslinked hydrogel.

The curing reaction was monitored for 120 min. and investigated *via* IR measurement. The NCO conversion as a function of time is presented in Figure 84, showing clearly an initial NCO conversion of 75% at t=0, which is probably caused by the reaction of NCO and NH_2 during the initial mixing step and a time lag of ~20 sec. until data were recorded. NCO conversion at 127 sec. is still at 75% and increases after this time interval. Full NCO conversion is reached at approximately 92 min.

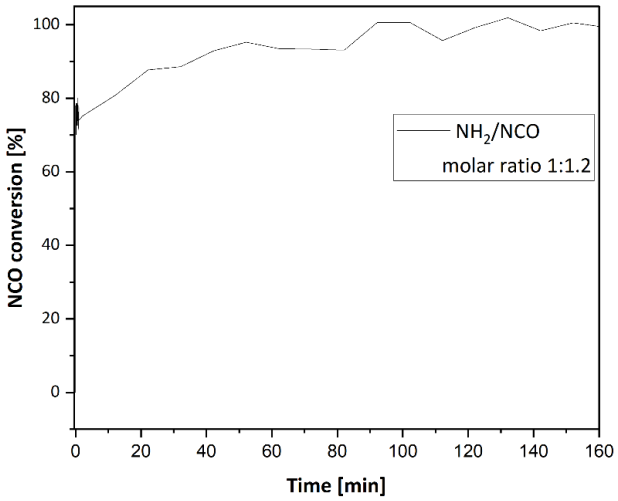

Figure 84 NCO conversion during the hydrogel curing reaction as a function of time. Reaction of NH_2 and NCO during initial mixing step and time lag between mixing and data recording causes 75% NCO conversion at t=0. 100% NCO conversion is reached after 92 min. NCO conversion was determined *via* IR-measurements during the curing reaction, by integration of NCO band at 2235 cm^{-1}.

NCO component represents 10wt.-% of the whole hydrogel system, leading subsequently to a concentration of 0.255wt.-% of pure NCO groups. Assuming a conversion of 75% NCO during the first seconds, as visible from Figure 84, 0.064wt.-% NCO in the hydrogel system would remain for an additional 92 min, being equal to 0.024 g of NCO groups. This amount might not strongly influence biocompatibility, as it is bound to a macromolecular backbone which is reported to reduce toxicity effects in comparison to isocyanate monomers.[101]

Rheological Determination of Viscoelastic Properties

Rheological measurements have been conducted as they represent a sensitive method for the detection of changes in the polymer structure or in the hydrogel formulation. A dynamic oscillation test was conducted to identify the linear viscoelastic region (LVER) of the hydrogel and is depicted in Figure 85B. Herein it is clearly visible that a decrease in G' and G'' occurs at a shear strain of approximately γ=10% deformation indicating the end of the LVER at this point. Frequency sweep experiments were conducted for investigation of a potential frequency dependance of the PU-U-hydrogel material in the range of 0.1-10 Hz at a constant shear strain (γ=1%) and is depicted in Figure 85A. As visible herein, G' and G'' are remaining parallel in the analyzed frequency range with G'>G''. Thus, a change from solid to liquid behavior of the hydrogel in the abdomen caused by deformation *via* organ movement in different frequencies can be excluded.

Additionally, a time sweep experiment was conducted for investigation of the gelation behavior of the PU-U-hydrogel. The targeted application of an adhesion prophylaxis requires a curing time of <60 sec. (Table 5). The time-dependent behaviour of the hydrogel starting with the initial mixing of both components can be observed in Figure 85C. It clearly demonstrates that the gelation point (G'=G'') was reached before the first measuring point was recorded, confirming that the transition from liquid-like to solid-like behaviour during the gelation process is reached

rapidly (<8 sec.). As identified in previous experiments the curing time falls within the limitations of <60 sec. Relative standard deviations (RSDs) of up to 53% were observed during the first minute of gelation for both moduli, which might be caused by a non-reproducible mixing of both components before the measurements or by slightly varying time lags between mixing and start of the measurements which was approximately 20 sec. However, high RSDs during rheological characterisations are commonly observed.[191] After approximately 20 minutes the gelation process is finished, which was defined by a plateau of G', G'', and loss factor tanδ (G' ~4900 Pa; G'' ~140 Pa; tanδ ~ 0.03). The low tanδ reveals an almost ideally elastic behaviour of the hydrogel reflected by a domination of G' over G''. Based on the results of the time sweep, the gelation process can be divided into two main phases, primary crosslinking and post-crosslinking. Primary crosslinking is defined by the rapid crosslinking of NCO and NH_2 groups, resulting in a stable 3D network. This is demonstrated by a rapid increase of G' and a decrease of tanδ, respectively. This phase is complete after approximately three minutes and subsequently followed by the post-crosslinking process, determined at a much slower gelation rate, which terminates after ~20 minutes. Post-crosslinking is defined as the phase after the majority of NCO and NH_2 groups have reacted so that a stable 3D network has already been established. Herein, the gelation is still proceeding, but the reaction rate has slowed down, as visible by less rapidly changing values for G', G'' and tanδ. The transition between these two phases was defined as the point at which the slope of tanδ is flattening, which is approximately after 180 sec.[189]

The process of primary crosslinking can be attributed to the NCO NH_2 curing reaction. Post-crosslinking might be a result of sterically hindered NCO NH_2 reaction and competes with the NCO hydrolysis, which will be present at a certain point in time, caused by the NCO excess of 20mol.%.

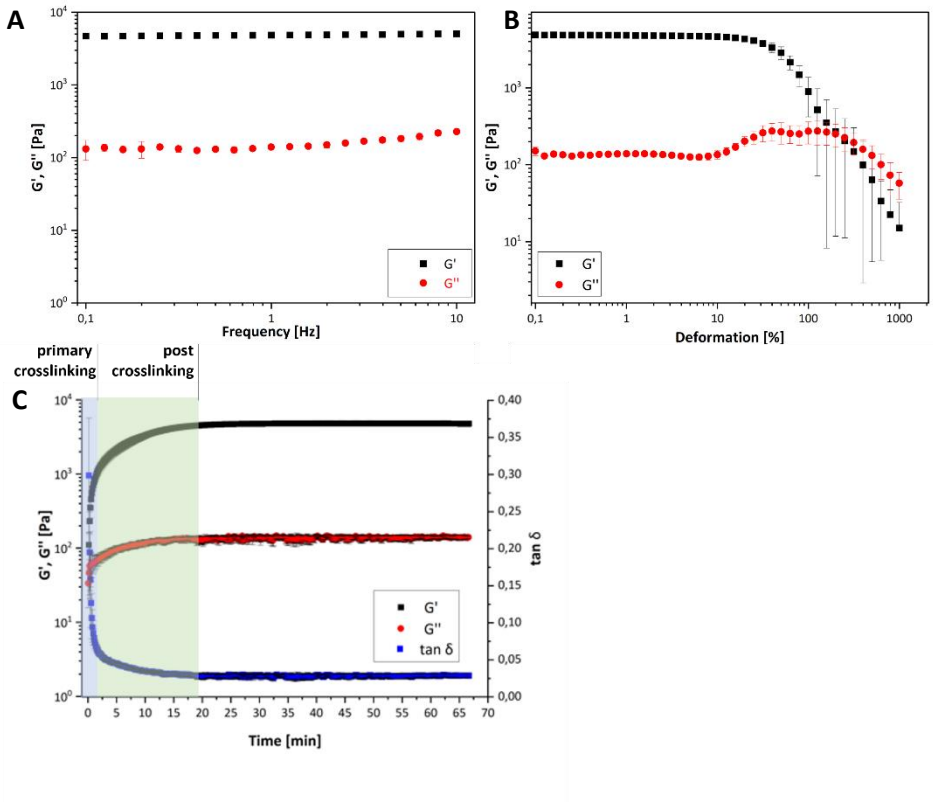

Figure 85 **.** Rheological measurements of the PU-U-hydrogel. (A) Frequency sweeps of the cured hydrogel at a constant shear strain (γ = 1%) and decreasing frequencies from 10 Hz to 0.1 Hz. G' and G'' are presented as a function of frequency. (C) Time sweep using parameters within the linear viscoelastic region determined in previous tests (f = 1 Hz, γ = 1%). Data are presented as G', G'' and loss factor tanδ as a function of time. (B) Amplitude sweeps of the cured hydrogel at a constant frequency (1 Hz) with increasing shear strains (0.1% to 1000%) were conducted to determine the viscoelastic properties of the PU-U-hydrogel, in particular the storage modulus G' and loss modulus G'' as a function of time. All analyses were performed in triplicates. Error bars: SD.

The theory of a crosslinking process *via* two different steps is supported by measurements in pH values, which will be described in the next chapter.

pH values of Resulting Hydrogels

According to what has been described in previous chapters, pH value of resulting hydrogels is a critical topic caused by the use of primary amines as crosslinking agent. The formulation of the PU-U-hydrogel has already been adapted to obtain physiological pH values after 30 min. PH values measured as a function of time of the hydrogel curing process are presented in Figure 86. Moreover, crucial values are summarized in Table 40. The alkaline peak of pH is reached after 9±5 sec. at 8.31±0.22 leading to physiological pH values (≤7.4) after 76±36 s.

Table 40 Summary of resulting pH values of the PU-U-hydrogel giving the highest measured pH value, the time when it is measured, time at which pH is equal or decreased 7.4 as indicator for biocompatibility and the resulting pH value after 30 minutes.

	Highest measured pH value (n=3)	t (highest measured pH value) [s] (n=3)	t (pH ≤7.4) [sec.] (n=3)	Resulting pH after 30 min. (n=3)
PU-U-hydrogel	8.31±0.22	9±5	76±36	6.50±0.02

The initial maximum pH was 8.31 and physiological values (<7.4) were reached after 76 sec. Although alkaline conditions above pH 7.4 are known to support bacterial growth and pH values in chronic wounds were described to range from 7.42-8.90 it is unlikely that short term exposition for 76 sec. pose comparable risks. While deviations to higher values can support the presence of chronic wounds, deviations to lower pH -values are described to support the wound healing process by their slightly acidic milieu, as the pH value strongly influences relevant enzyme activities.[120,121] Clinical indicators of lower pH milieu in wounds comprise pus, necrotic tissue, and serum crusts. Such wounds had a mean pH value of 6.1 (±0.6SD).[121] The pH range observed for the PU-U hydrogels from 6.1 to 7.4 is not expected to interfere with the sensitive wound healing processes. The herein presented hydrogel fulfills this requirement.

The resulting pH curve can be divided into three different stages: application, primary crosslinking, post crosslinking as marked by different color areas in Figure 86. Application is defined as the initial mixing step, where single reactants are mixed with each other. Concerning pH measurements, this stage is characterized by rapid increase in pH values, caused by the diffusion of the amine-containing reaction mixtures into the pH electrode. The second stage, primary crosslinking, is defined as rapid crosslinking of NCO and NH_2 groups, which can be traced by a strong decrease in pH that corresponds to the conversion of NH_2 to urea crosslinks. The onset of the final stage of post-crosslinking can be defined as the point after which the majority of NH_2 and NCO groups had crosslinked, but gelation is still ongoing and pH still decreases, but less rapidly. Considering the fast reaction kinetics of primary amines with isocyanates fast and complete conversion is expected.[158] Post crosslinking could probably be a result of delayed curing due to a rigidification of the network. However, with increasing network density the mobility of functional groups decreases and, additionally, at some point the isocyanate-amine reaction might compete with the isocyanate hydrolysis to amines that in turn react with residual isocyanate groups, that are in the immediate vicinity. Further decrease in pH values could be a result of eliminated CO_2 by the reaction of NCO and H_2O. Post-curing of the residual NCO groups yields eventually the completely crosslinked hydrogel.

During the stage of application, the pH rises to the highest value of 8.31±0.22 after 9s±5s caused by the increased concentration of amine on the surface of the electrode, induced by applying single solutions of NCO and NH_2 into the beaker. PH of 7.4 is reached after 76±36s. After 20 min. (1200 s) only minor deviations were detected, as from 20 to 30 minutes pH changed 6.52 to 6.49 (mean, n=3). Thus, from 30 min the pH value of the hydrogel appears to be stable.

Rheological measurements are intended to support the theory of the three subsequent stages during hydrogel formation (application, primary crosslinking and post crosslinking). In contrast, the stage of application is not detectable in rheological measurements caused by a time lag between mixing and start of the measurements. Detected time of transitions of both measurements (pH and rheology) are comparable. The transition from application to primary crosslinking was defined after the alkaline pH peak at 9 sec. The transition from primary to post crosslinking was defined at the point where the slope of pH is flattening, which is approximately after 110

sec., assuming that both measurements depict the same process. After 20 minutes (1200 sec.) no major alterations have been detected in both measurements.

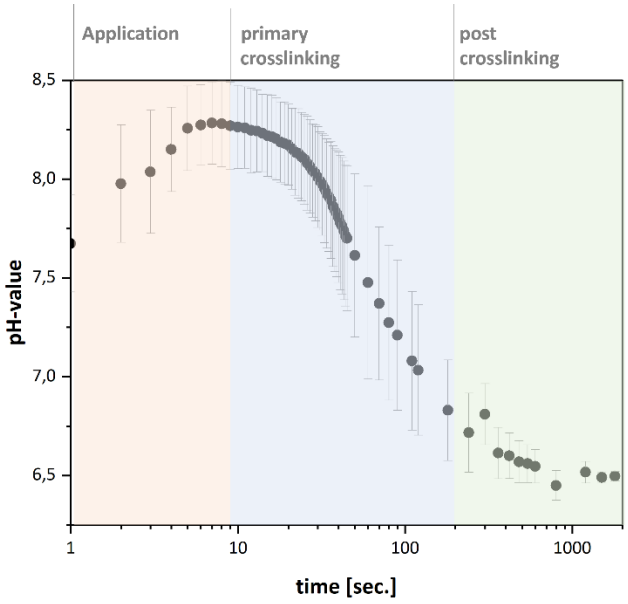

Figure 86 pH curve of the crosslinking reaction of the PU-U hydrogel as mean values (n=3) with SD as error bars. The alkalic peak of the pH value was reached within 9 seconds with an average of 8.31±0.22. The time at which the pH falls below 7.4 was 76±36s. After 30 minutes the pH reached a value of 6.5±0.02. A proposed three stage process of crosslinking reaction is marked in different colors. 1.) application, herein the total amount of both single solutions is applied visible in an increase of pH due to increased NH_2 concentration. 2.) primary crosslinking, initial crosslinking process of NH_2 and NCO groups, visible in a rapid decrease in pH values. 3.) post crosslinking: pH decrease is still present but less rapidly than in primary crosslinking indicating that crosslinking process is still ongoing.

Mechanical Properties

Apart from common body movements, larger mechanical forces within the abdominal area might arise from coughing, sneezing or physiological movement.[119] To investigate whether the herein presented hydrogels are able to withstand such forces, tensile tests have been conducted on four samples, prepared as S-2 test specimen (dog-bone), to determine the elongation at break and tensile strength at break. Results of average values (n=4) of the PU-U-hydrogel are presented in Figure 87. All samples prepared for tensile tests exhibit elongations ranging from 99%-237% with an average of 174.3±65.1%. Deviations are likely caused by small defects such as gas bubbles during sample preparation. The tensile strength at break was measured between 23-69 kPa, with an average of 48.2±21.6 kPa.

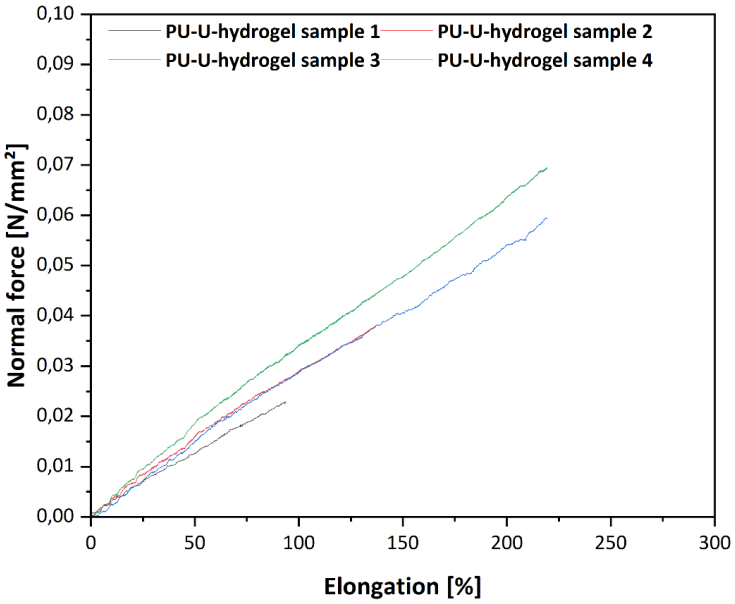

Figure 87 Fourfold tensile testing of PU-U-hydrogel sample 1-4 with reached elongations of 99%-237 % and reached tensile strength of 23 kPa-69 kPa.

All samples of the four-fold measurements showed at least an elongation of 99% (mean=174.3%±65.1%) which fulfills the requirement from Table 5 concerning at least 32% elongation at break, derived from Junge *et al.*[118] Tensile strength at break of single samples, varied between 23 kPa to 69 kPa (mean=48.2 kPa±21.6 kPa) in the fourfold measurements conducted. Additionally, compression forces will arise under *in vivo* conditions. The PU-U hydrogel was analyzed in a compression experiment with an applied force sweep, which is presented in Figure 88. Herein an increase of G' and G'' is detected for an increase of force. G' is constantly at higher levels at G'' indicating that solid-like behavior is present for the applied forces. The force of max. 13.6 N was applied on a surface of 24 mm in diameter, which is equal to an area of 4.52 cm² according to equation 4.2.14, leading to a compression pressure of 3.0 N/cm².

$$A = \left(\frac{d}{2}\right)^2 * \pi \qquad (4.2.14)$$

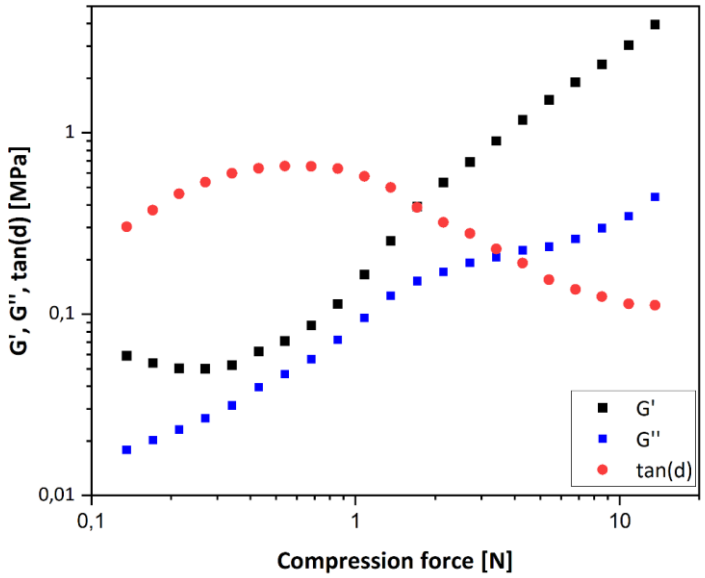

Figure 88 Compression experiment of PU-U-hydrogel with G‘, G‘‘ and tan(d) at different compression forces.

The results from the compression experiment demonstrated that the hydrogel would be stable under appeared pressure of 3 N/cm² equal to 30 kPa without losing its solid like properties. As a result, G’ increases to withstand the compression forces.

The limit for a normal intraabdominal pressure (IAP) is described in the literature at 1.6 kPa at standard conditions, without applying mechanical stress on the body.[124] Under abdominal press by coughing the IAP can raise up to 8.7 kPa. The highest values were reported for *valsalva maneuver* with an IAP of 21 kPa.[119] 21 kPa was therefore chosen as the lower limit of to withstand pressures for the hydrogel system. The results of the analyzed samples confirmed that the PU-U-hydrogel would withstand the applied forces by IAP on the intraabdominal wall without significant change in its properties.

Hydrolytic Degradation

Regarding the targeted application of adhesion prevention, a degradable system is required. As already discussed in previous chapters, the hydrogel needs to provide a barrier for at least 7 days[107] and should be fully degraded within 28 days, as an application as short-term-implant is aimed. It is well-known that the degradation process *via* hydrolysis starts immediately after hydrogel preparation, the target being to maintain the barrier effect for at least 7 days. The degradation behavior was already pre-analyzed in chapter 4.2.3 and 4.2.4. In this chapter, the degradation behavior of the final PU-U-hydrogel will be analyzed *via* weight loss experiments and the molecular weight distribution of resulting degradation products will be investigated.

Hydrolytic degradation is based on the hydrolysis of the implemented dilactide units and has been analyzed in degradation experiments by tracking the loss of weight as a function of time. Moreover, the concentrations of the degradation products, the resulting molecular weight M_W

thereof and the dispersity $Đ_M$ *were* analyzed *via* GPC. Two main fractions of degradation products were identified, as visible from Figure 89. In Figure 89D it becomes visible, that the minor fraction (fraction 1) was identified at low concentration levels ranging from 0.14±0.08 (0 days) to 1.0±0.4 mg/mL (21 days), while concentration levels for the major fraction (fraction 2) ranges from 1.9±0.9 mg/mL (0 days) to 10.8±1.5 mg/mL (14 days). The findings illustrate that the gravimetric analysis and GPC were well-aligned, as the total concentration of the two fractions matched the gravimetrically measured weight loss of the hydrogels.

In Figure 89A it becomes visible, that the M_w in fraction 1 increased from 717,000±74,000 g/mol (0 days) to 1,462,000±370,000 g/mol (21 days), while fraction 2 contained significantly smaller molecules, with molecular weights increasing from 29,000±4,800 g/mol (0 days) to 48,000±7,400 g/mol (21 days). The increasing M_w in the fractions over time might be attributed to the initial occurrence of superficial degradation by terminal polymer chain cleavage. As time progressed, larger oligomers located deeper within the hydrogel were cleaved off and detected, leading to an increase in molecular weight. Furthermore, as the large oligomers of fraction 1 underwent further cleavage, they contributed to an increased molecular weight of fraction 2.

Additionally, the degradation products displayed dispersities within 1.9±0.7 - 2.6±0.5 (fraction 1) and 2.2±0.1 - 3.4±0.3 (fraction 2), respectively, as visible from Figure 89C. An interesting observation was the opposite trend in dispersities between the two fractions. Fraction 1 exhibited an increase in dispersity values, whereas fraction 2 showed a decreasing dispersity over time. The broadening of the molecular weight distribution in fraction 1 can be attributed to the release of larger molecules into the supernatant, as previously explained. On the other hand, the

narrowing of the molecular weight distribution in fraction 2 was a consequence of the proceeding cleavage reactions of smaller fragments resulting in smaller sized degradation products.

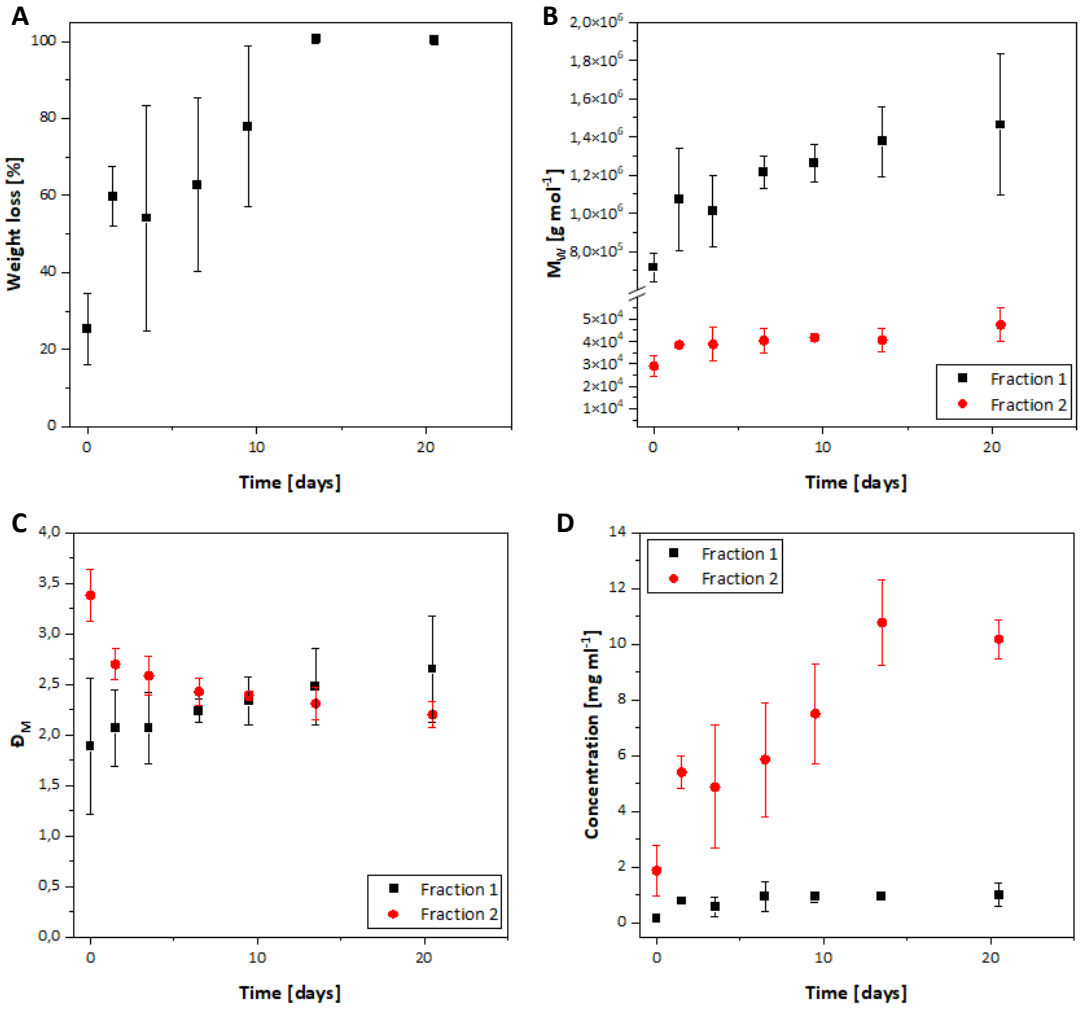

Figure 89 Hydrolytic degradation studies of PU-U-hydrogel in DPBS. A) Weight loss of hydrogels in DPBS buffer (1x) at 37 °C. B) Molecular weight M_w of degradation products in supernatant. C) Dispersity ÐM of degradation products in supernatant. D) Concentration of degradation products in supernatant. Data were obtained from three independent experiments. Error bars: SD

The results presented up to here indicated a full degradation of the hydrogel network after 14 days which is sufficient to prevent the formation of postoperative adhesions. Moreover, the size of degradation products is of interest since molar masses of up to 50,000 g/mol are reported to be suitable for renal elimination, while molecules with higher molar masses, such as albumin (67,000 g/mol) might negatively influence the glomerular filtration barrier.[192,193] The maximum M_w of fraction 2 was identified at 48,000 g/mol, which enables a renal elimination. The molecular weights of fraction 1 have been identified at high M_w levels of 74,000 to 1,462,00 g/mol, which is at much higher levels as the molecular weight limit of a renal elimination.

A follow up study on the M_w of the degradation product of the hydrogel network was conducted to investigate potential changes in M_w after 11 months. Degradation products were again

analyzed *via* GPC identifying a M_w of 13,158±817 g/mol, while M_n was determined at 4,923.7±57.2 g/mol. The results are presented in Figure 90.

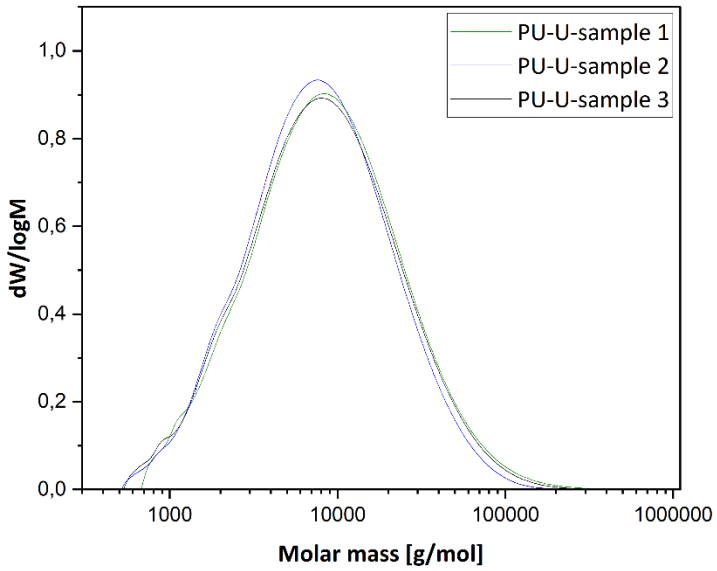

Figure 90 Obtained molar masses from the degradation products of the PU-U-hydrogel, measured as triplicates. The M_w was determined at 13,158±817 g/mol, M_n was determined at .4923.7±57.2 g/mol

The identified M_n and M_w revealed, that after a period of ≤11 months, degradation products fall below the renal elimination limit of 50,000 g/mol and become renally eliminable.

Determination of Molecular Weight between Two Crosslinks and Mesh Size Determination

The hydrolytic degradation was analyzed in the previous chapter, showing a fully dissolved hydrogel network after 13.5 days. The molecular weight between two crosslinks (M_c) might therefore change and thus the resulting mesh size in the hydrogel, which is an important parameter for cell migration.

To investigate this effect, degradation experiments were carried out, as described in chapter 6.2. Samples were taken on day 0, 1, 3 and 7. Hydrogel samples were freeze dried to remove imbedded water for improvement of measurement handling and X-ray diffraction (XRD) measurements were carried out of a wet PU-U-hydrogel in comparison to a dried PU-U-hydrogel to analyze potential post-crystallization effects. Results are presented in Figure 91, wherein both samples display predominantly amorphous behavior. Only minor variations have been observed between the two gels, and the absence of sharp peaks indicates a lack of post-crystallization, which facilitates the determination of M_c *via* storage modulus (G').

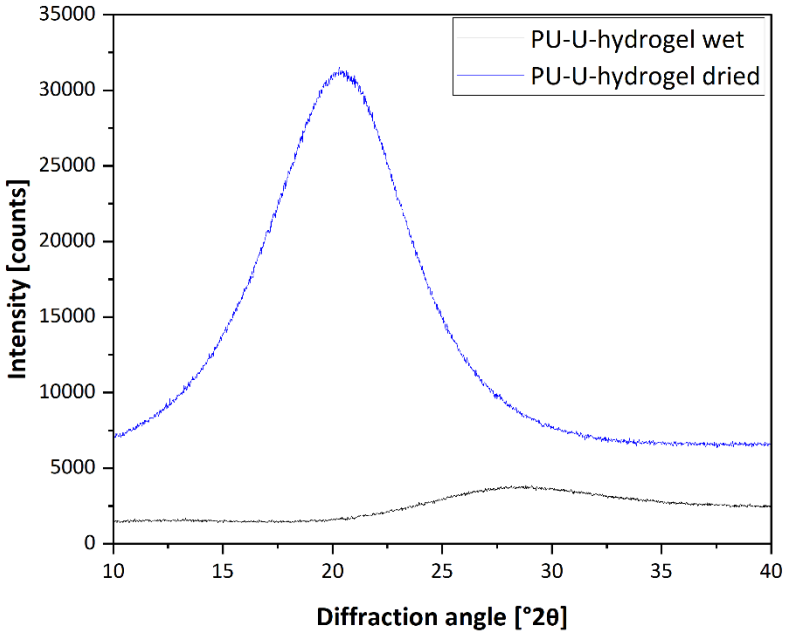

Figure 91 Wide angle XRD chromatogram of a wet PU-U-hydrogel (black line) in comparison to the dried PU-U-hydrogel (blue line). Sharp peaks are missing, indicating a lack of post-crystallization effects.

DMA was conducted for the determination G' used for calculations of M_c as an indicator for network cleavage progress. Figure 92 represents G' as a function of strain of the measured hydrogel samples for each day. For the calculation of M_c, the storage modulus from 4.7-4.9% strain was used and are marked in grey. This region was chosen since values seem to appear stable from 3-6% strain. Moreover, the mesh size will be determined based on the results of M_c *via* G' measurements.

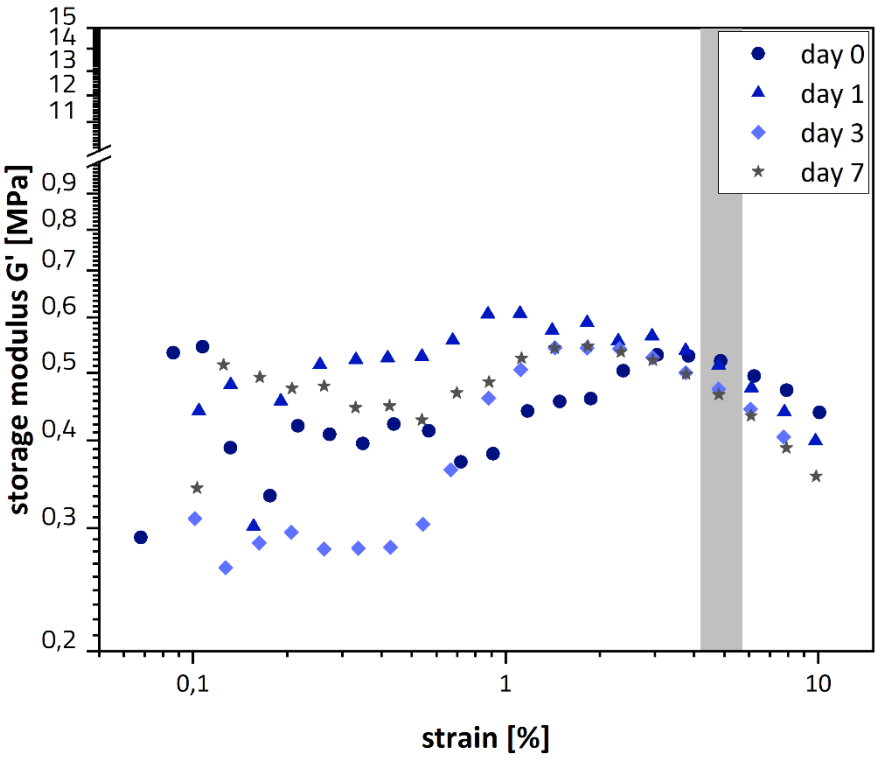

Figure 92 Storage modulus G' as a function of strain from incubated and partly cleaved hydrogels measured *via* DMA in strain experiments. Samples have been freeze dried before measurements to allow determination of M_c based on G' values from grey marked area.

M_c can be calculated according to equation 4.2.15, wherein *R* is the universal gas constant 8.314 Pa/mol*K*m³, *T* is the temperature taken from the respective measurement in degree K, *d* is the density, which was set to 1100 kg/m³ and *G'* as storage modulus deriving from the respective DMA measurement. M_c is obtained in kg/mol and resulting values are presented in Table 41.

$$M_c = \frac{RTd}{G'} \tag{4.2.15}$$

For the calculation of the mesh size from M_c values, the swelling ratio *Q* is required and was calculated according to eq. 4.2.14, wherein ρ is the density of the polymer (1.1 g/mL), $V_{swollen}$ is the volume of the swollen network, V_{dry} and m_{dry} are the volume and mass of the dry network. $m_{hydrated}$ represents the mass of the hydrated hydrogel samples after preparation and 0.15 represents the factor of the included solid content of 15wt.-%. $V_{swollen}$ was approximated from $m_{swollen}$ determined by weighing of the swollen samples assuming a density of 1.0 g/cm³. According to equation 4.2.16 the reciprocal value of Q_s depicts the polymer volume fraction $v_{2,s}$ which is used in eq. 4.2.20 for the determination of the mesh size.

$$Q_s = \frac{V_{swollen}}{V_{dry}} = \frac{\rho * V_{swollen}}{m_{dry}} = \frac{\rho * V_{swollen}}{m_{relaxed} * 0.15} \quad (4.2.16)$$

$$v_{2,s} = \frac{1}{Q_s} \quad (4.2.17)$$

Additionally, M_c determination can be carried out *via* swelling experiments using equation 4.2.20, which was published by Peppas *et al*.[194] and is a modification of the swelling theory according to Flory-Rehner but is applicable for determination of M_c for hydrogels which are prepared in the presence of water. Herein $v_{2,r}$ is the polymer volume fraction in the relaxed state, which is defined by Peppas *et al*. as the state of the polymer network immediately after crosslinking, but before swelling. $v_{2,r}$ is determined *via* equation 4.2.19 with Q_r occurring from equation 4.2.18.

$$Q_r = \frac{V_{swollen}}{V_{relaxed}} = \frac{\rho * V_{swollen}}{m_{relaxed}} \quad (4.2.18)$$

$$v_{2,r} = \frac{1}{Q_r} \quad (4.2.19)$$

$$\frac{1}{M_c} = \frac{2}{M_n} - \left[\frac{v_{spec.}\left[\ln\left(1 - v_{2,s}\right) + v_{2,s} + \chi_1 v_{2,s}^2\right]}{V_1 v_{2,r}\left[\left(\frac{v_{2,s}}{v_{2,r}}\right)^{-1/3} - \left(\frac{v_{2,s}}{2v_{2,r}}\right)\right]} \right] \quad (4.2.20)$$

M_n is the average molecular weight of the polymer but in the absence of a crosslinker, which is 4941 g/mol for **prepolymer-4**, $v_{spec.}$ is the specific volume of the polymer, which is again reduced to PEG, being 0.93 mL/g, V_1 is the molar volume of water (18 mL/mol), and χ_1 being the solvent interaction parameter which was set to 0.426, valid for PEG in water. The reduction of the hydrogel system to a PEG/water based system was again adopted by Rehman *et al*..[89] Obtained $v_{2,r}$ and $v_{2,s}$ values are presented in Table 42, obtained M_c values are reported in Table 41.

The degradation experiments are comparable to swelling experiments. Results of this experimental series were used for the determination of both, M_c *via* calculations based on G' (eq. 4.4) and M_c determination according to calculation *via* adapted Flory-Rehner-equation from Peppas *et al*. (eq. 4.2.20) by weighing of degraded samples before lyophilization. Table 41 presents an overview on calculated M_c derived from the different calculation approaches for each analyzed time point.

Table 41 Overview on obtained G' values measured at different strains *via* DMA. M_c values are calculated based on G' and on swelling experiments.

Degradation time [days]	G' [MPa]	Strain at G' for M_c determination [%]	M_c based on G' [kg/mol]	M_c based on swelling [kg/mol]
0	0.52977	4.88	5.2	2.2
1	0.51224	4.797	5.3	2.2
3	0.47374	4.807	5.7	2.3
7	0.46529	4.806	5.8	2.6

Herein it becomes visible that M_c values obtained *via* calculations based on G' are by factor ~2.3 higher than M_c values obtained *via* swelling. Assuming an ideal network M_c can be calculated according to eq. 4.2.21, wherein $MW_{higher\ functional\ component}$ is the **M_W** of **prepolymer-4** which is 4941 g/mol and $MW_{difunctional\ component}$ is the M_W of **Jeffamine ED2003** which is 2042 g/mol.

$$M_c = \frac{1}{f}\left(MW_{higher\ functional\ component}\right) * 2 + MW_{difunctional\ component} \quad (4.2.21)$$

Applying equation 4.2.21, M_c is obtained as 5336 g/mol, which is comparable to values obtained from M_c determination *via* G'. M_c values obtained *via* swelling are hardly comprehensible since there is no possibility for M_c for further decrease to such low values. The results indicate that simplifications of the system to pure PEG/water system might strongly influence obtained M_c values. With regard to the hydrogel network as a whole, mass concentration of EO decreased to ~70wt.-%, residual ~30wt.-% consist of aliphatic urethanes/ureas, PO and dilactide. Interaction parameters for PO in H_2O are not reported since it is reported to be insoluble at room temperature. The sum of simplifications in M_c calculation based on swelling experiments might lead to higher errors in calculation, leading to less comprehensible values. Thus, obtained M_c values based on swelling are reported but restricted in reliability.

The resulting mesh size ξ can be calculated according to eq. 4.2.20, wherein *l* is the bond length along the polymer backbone, which is herein reduced to sp^3-sp^3 hybridization-bonds with *l*=0.154 nm[195], C_n is the flory characteristic ratio (set to 4 for highly PEG based systems, as reported by Brandl *et al*.[196] and Rehmann *et al*.[89,196]) and M_r is the molecular weight of the repeating units, which can be reduced to the EO group in highly EO based systems with a molecular weight of 44 g/mol. For the calculation for more complex structures it was also reported by Rehmann *et al*. to neglect the chemical groups depicting only a low relative content within the polymeric network and focus on the main component which is PEG.[89] This procedure was adopted knowing that such a simplification can lead to errors in the calculation. $\upsilon_{2,s}$ is the polymer volume fraction, obtained by eq. 4.6. Calculated M_c values obtained *via* adapted Flory

Rehner equation (eq. 4.7) and from G' determination derived from the same experiments. Thus, $v_{2,s}$ is for each time interval identically irrespective of the determination method for M_c. $v_{2,s}$ day 0 sample was adopted from day $v_{2,s}$ day 1 since swelling could not be determined for day 0.

$$\xi = v_{2,s}^{-1/3} * l \sqrt{\frac{2C_n M_c}{M_r}} \tag{4.2.22}$$

Table 42 presents an overview on resulting mesh size ξ based on M_c values from Table 41. Herein the increase in mesh size from 10.5 nm (day 0) to 12.59 nm (day 7) becomes visible for M_c based on G'. By hydrolysis of dilactide groups in the polymer backbone an increase in M_c is visible leading to an increase in mesh size. The same trend is visible in mesh size based on M_c obtained by swelling. These values are less trustful since M_c values do not fit to M_W of reactants used for the hydrogel preparation.

Table 42 Overview on calculated mesh size ξ based on determined M_c values from Table 41. $v_{2,s}$ was obtained from swelling experiments *via* eq. 4.5 and 4.6 and was used for both ξ determination. $v_{2,s}$ of day 0 was not obtained and replaced by $v_{2,s}$ of day 1.

Sample day	$v_{2,s}$	$v_{2,r}$	Mesh size ξ based on M_c from G' [nm]	Mesh size ξ based on M_c from swelling [nm]
0	(0.092)	(0.618)	10.50	6.86
1	0.092	0.618	10.58	6.86
3	0.088	0.584	11.16	7.00
7	0.063	0.422	12.59	8.48

However, from both methods derived M_c and subsequent mesh sizes are presented in Figure 93.

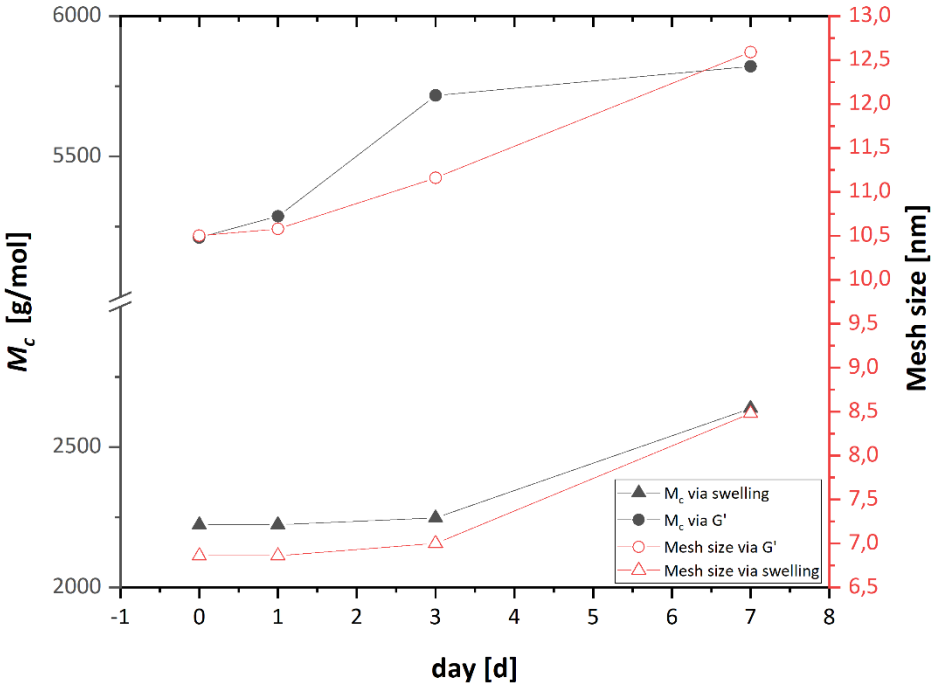

Figure 93 Calculated M_c (black lines) in g/mol determined *via* G‘ measurement and *via* swelling experiments and resulting mesh size (red lines) in nm based on M_c calculations as a function of time.

Both measurements showing the same trend visible in an increase in M_c and in mesh size caused by the degradation of the hydrogel network.

Regarding the targeted application as an adhesion prophylaxis, it is of great importance to prevent cells from migrating through the polymeric network, otherwise a barrier effect is not given.

Volumes of different human cell types are reported to vary across more than five orders of magnitude.[197] Absolute volumes are difficult to compare for the estimation on cell migration but might correlate with the diameters of cells as represented by eq. 4.2.23.

$$V = \frac{4\pi r^3}{3} \tag{4.2.23}$$

Most human cell types are reported to vary in a size range of 2-120 µm.[198] The most relevant cell types for consideration of adhesion prophylaxis are fibroblasts, which are present in the intraadominal room and are responsible for wound sealing. Fibroblasts are reported at a size of 10-15 µm[199] which is by factor 10^3 higher as the determined mesh size during the time interval 0-7 days for ξ based on M_c from G’.

The results indicate that invasion and migration of cells in general and fibroblasts in particular can be prevented by the resulting mesh size of the hydrogel and is maintained for at least 7 days.

Several assumptions have been applied to the equation for determining the mesh size based on M_c values. The resulting M_c and subsequently the mesh size *via* swelling experiments occurred at low levels which are not explicable under realistic conditions. However, M_c calculations *via* G' determination led to values which indicate the presence of an ideal network in average.

For initial estimations to assess the reliability of these values, the mesh size was calculated by considering the number of bonds in a pore consisting of two molecules of **Jeffamine ED2003** and 4 equivalents of **prepolymer-4**. **Prepolymer-4** has an eq. weight of 1647 g/eq., wherein 168 g/mol is contributed by the **HDI** molecule. Subtracting the molecular weight of **HDI** (168 g/mol) leaves the polyol backbone contribution of 1479 g/eq. The amount of a pure PO-based starter needs to be subtracted, which is 1/3 * 722 g/mol, leading to 1238.3 g/eq of which 72.5wt.-% is represented by EO units, which is equal to 897.8 g of EO content. Dividing by the molecular weight of EO, this amount corresponds to 20.4 EO units. 22.5wt.-% is represented by PO, which is equal to 278.6 g and corresponds to 4.8 PO units by dividing by the M_W of PO (58 g/mol). Dilactide with 5wt.-% was identified to be 61.9 g, which is equal to 0.42 units of dilactide.

The respective units have been reduced to the number of bonds responsible for chain elongation, which is 3 for EO and PO (excluding methyl groups) and 6 for dilactide (excluding methyl groups). Multiplying by the respective number of units, the bonds in one polymer arm are 78.18. Additionally, 9 bonds are present within the **HDI** unit, and 4.46 PO units are provided by 1/3 of the starter (722 g/mol) equivalent to 13.38 additional bonds. This results in a total of 100.56 bonds, of which approximately 2/3 is represented by sp^3 C-C bonding, reported to be 0.154 nm, and approximately 1/3 is represented by C-O bonding, with a length of 0.143 nm. According to equation 4.2.24, this leads to a chain length of 15.11 nm per one arm of the prepolymer. Herein, l_{chain} represents the chain length, $n_{C\text{-}O}$ represents the amount of bonds between carbon and oxygen, which is 1/3 of the whole amount of bonds and $n_{C\text{-}C}$ represents the amount of bonds between carbon and carbon, which is 2/3 of the whole amount of bonds, $l_{C\text{-}O}$ is the length of the C-O bond, which is reported to be 0.143 nm and $l_{C\text{-}C}$ is length of the C-C bond which is reported be 0.154 nm.[200]

$$l_{chain} = (n_{C-O} * l_{C-O}) + (n_{C-C} * l_{C-C}) \quad (4.2.24)$$

The same procedure was applied for the **Jeffamine ED2003** consisting of 39 units EO and 6 units PO in the backbone.[201] Assuming 3 bonds per EO and PO unit 135 bonds are present in the backbone. According to equation. 4.2.24 the chain length of one molecule **Jeffamine ED2003** is 20.3 nm. The smallest possible pore is depicted by 4 arms of the prepolymer and 2 molecules of **Jeffamine ED2003**. By the addition of the respective chain length the perimeter *P* of the pore can be calculated. Assuming a circle consisting of fully stretched atom bonds, one can calculate the resulting diameter *d via* equation 4.2.25.

$$d = \frac{P}{\pi} \tag{4.2.25}$$

The diameter *d* of the smallest pore at a fully stretched mode is 32 nm. This concept was applied on different possible pore constitutions. Results are presented in Table 43.

Table 43 Overview on estimated pore sizes for different pore types of the hydrogel network at fully swollen state assuming a circle.

Pore type	Arms of prepolymer	Molecules of Jeffamine ED2003	Resulting mesh size at fully stretched mode [nm]
[4+2]	4	2	32
[6+3]	6	3	48
[8+4]	8	4	64
[10+5]	10	5	80
[12+6]	12	6	96

The values obtained from the estimation concept are of the same order of magnitude as the calculated mesh size but are by factor 3-10 higher than the calculated values, depending on the pore type. The deviations can be explained by an increase in values when assuming a fully stretched system, as the calculations were based on the formation of circles. In theory these bonds will be more stretched at swollen state but might not reach a full circle *via* bond stretching. However, this approximation demonstrated that the mesh size is still far below the sizes of cells in general and fibroblasts in particular, allowing the assumption that cell migration through the polymeric network might be restricted by small mesh size.

Biochemical Characterization: Cytotoxicity and Cell Migration Behavior

In this chapter results will be presented addressing the cytotoxicity, the cell adhesion and migration and invasion behavior of cells through the polymeric hydrogel network to estimate the safety and the efficacy of the PU-U hydrogel as an adhesion prophylaxis *in vitro*.

Cytotoxicity

Adhesion prevention requires the hydrogel to serve as a barrier for migrating cells, whilst not negatively affecting the surrounding tissue. To exclude potential toxicological harm by the use of the PU-U-hydrogel *in vivo*, cytotoxicity tests have been conducted. The cytotoxicity of the degradation products was assessed using an assay for metabolic activity (MTT assay), which was conducted testing varying concentrations of PU-U gel extracts (undiluted, 1:2, 1:5, 1:10). Two different incubation time periods to obtain gel extracts were chosen to investigate cytotoxicity during the critical period of wound healing and at the end of the degradation process to exclude the cytotoxicity of smaller molecules that were formed during degradation (14 days). According to ISO 10993-5, the cytotoxicity threshold was set to <70 % viability of the negative control condition. Relative to cell viability in culture medium, which was defined as 100 %, no cytotoxic effects of any PU-U gel extracts on A549 cells were observed as visible from Figure 94. The

results indicate a presence of biocompatibility of hydrogel extracts and the resulting degradation products obtained until 7 days after application.

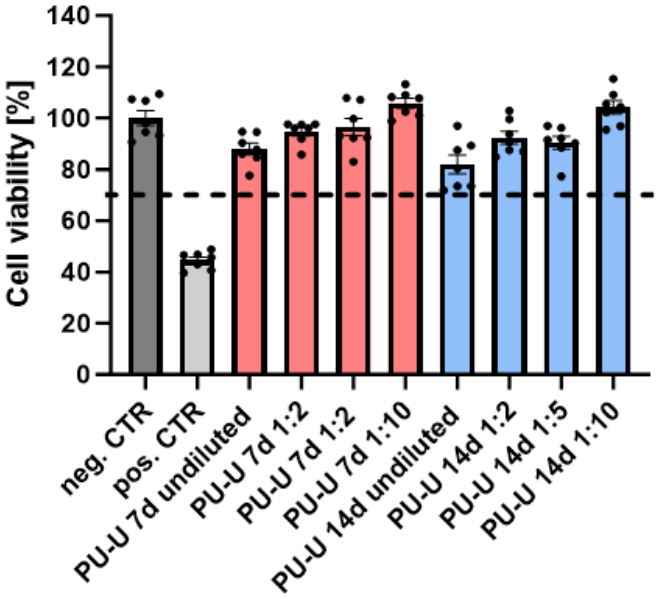

Figure 94 Cytotoxicity testing of PU hydrogel extracts. The cytotoxicity of PU-U-hydrogel extracts was assessed using an MTT assay. A cytotoxic effect was defined as <70% viability of the negative control (neg. CTR, i.e. culture medium). pos. CTR = Staurosporine (10 µM). Data points represent values obtained from individual wells. Error bars: S.E.M.

Cell Adhesion and Invasion into the PU-U-hydrogel

Since the hydrogel system needs to provide a barrier effect for at least 7 days, it is of great importance to yield a network with a mesh size smaller than diameters of cells in general and of fibroblasts in particular. The mesh size of the prepared hydrogels was analyzed and discussed in comparison to sizes of different cell types, previously. In the calculation for the determination few simplifications have been applied, like reducing the bond length to sp^3-sp^3 hybridization-bonds. Thus, application tests of the barrier function are necessary to confirm the barrier effect *in vitro*. To address this question, A549 cells have been seeded on the cured PU-U-hydrogel to study how well cells can adhere to the gel surface. Images of adherent cells are presented in Figure 95A and B, showing significantly fewer adherent cells on the PU-U-hydrogel in comparison to Matrigel, 48 h after seeding.

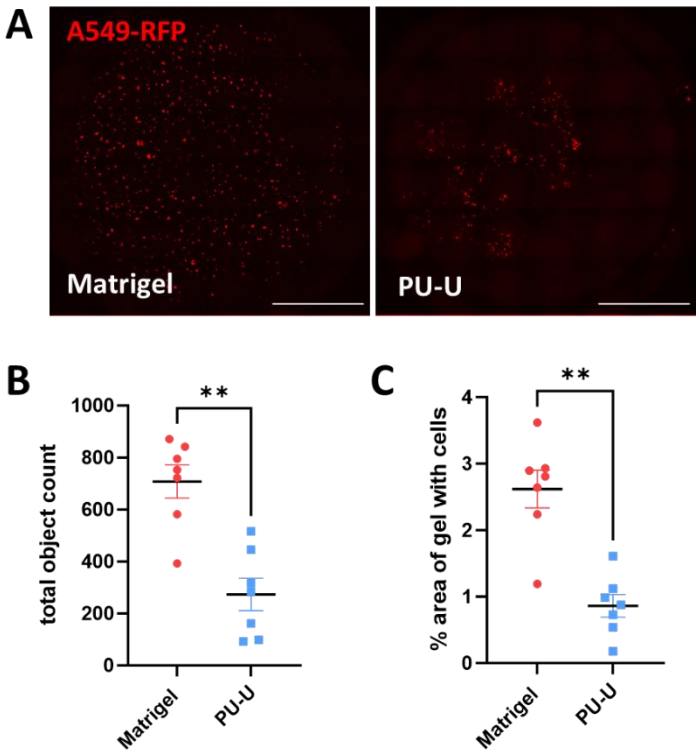

Figure 95 Cell adhesion on the hydrogel surface after 48 h. (A) Representative images of RFP-positive adherent A549 cells, 48 h after seeding, on the surface of Matrigel and PU-U hydrogels. Scale bars: 1 mm. (B) Total count of adherent cells (Mann-Whitney test, p=0.0041**). (C) Percentage of gel surface covered with cells (Mann-Whitney test, p= 0.0012**). Error bars: S.E.M.

Adhesion properties of cells on the surface of the PU-U-hydrogel are observed at low levels. To investigate the barrier function for adherent cells, experiments for cell invading and migration have been conducted. Herein A549 cells were cultured on the gel surface and cell invasion was stimulated using a serum gradient. The number of invasive cells which transversed the gel and the underlying porous membrane after 7 days were then finally quantified. Matrigel was tested as a positive control since it is reported to promote cell invasion.[202] After 7 days, a significantly larger number of invasive cells was observed in Matrigel compared to PU-U hydrogels, as visible from Figure 96A and B, which was reflected in a statistically significant reduction of the percentage of the PU-U hydrogel surface covered with cells from Figure 96C.

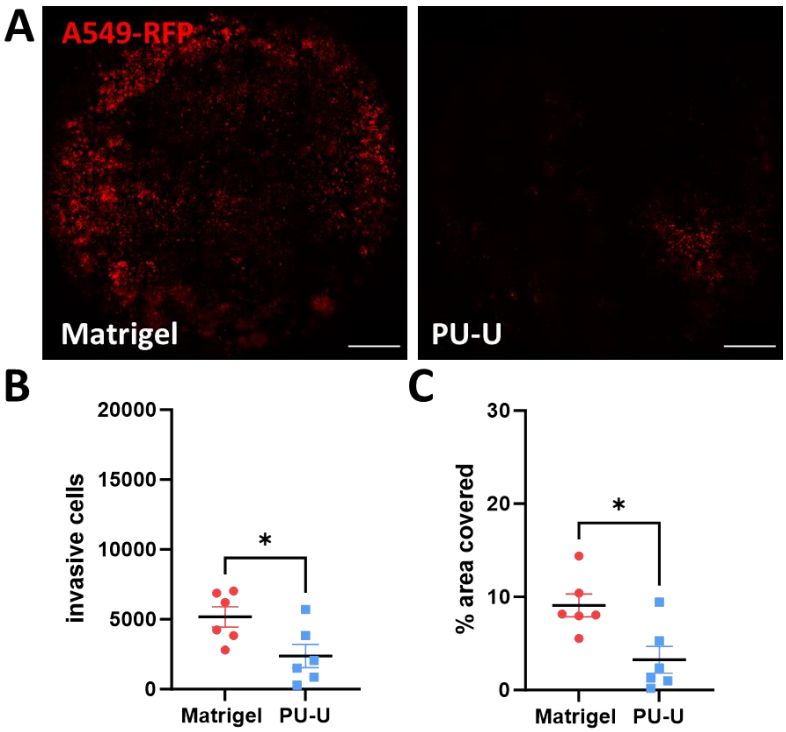

Figure 96 Cell invasion into hydrogels. (A) Representative images of RFP-positive A549 cells adherent to the Thincert membrane after transversion of Matrigel and PU-U-hydrogels for 7 days. Scale bars: 1 mm. (B) Quantification of invasive cells after 7 days (Mann-Whitney test, p= 0.026*). (C) Percentages of the Thincert membrane covered with cells after 7 days (Mann-Whitney test, p= 0.026*). Error bars: S.E.M.

The results indicate suitable properties for the function of the PU-U-hydrogel as an adhesion barrier for the time period of 7 days which is equal to the critical wound healing period after surgery. Cell surface adhesion to hydrogels is mostly mediated by absorption of proteins by the gel surface, which enables cell binding *via* e.g. integrin receptors.[203] A possible explanation for the anti-adhesive properties of the PU-U hydrogels could be a surface layer of water molecules binding to the hydrogel PEG units *via* hydrogen bonds.[204] This layer of water molecules might reduce the absorption of proteins and therefore cell attachment, as it has been proposed by other studies using polyurethane-based and natural polysaccharide-based hydrogels.[205,206]

In line with low cell adhesion, it was also observed that PU-U hydrogels prevented excess cell invasion. Previously, a similar assay, using a serum gradient to stimulate cell invasion in a Transwell-system, was employed by Chou *et al*. to study cell invasion in PNIPAM-based hydrogels.[207] Besides the initially low attachment of cells, which reduces the number of possible invading cells, there are several factors which can influence cell penetration. These include gel stiffness, network structure of the hydrogels and crosslink density (mesh size).[208] As confirmed by degradation analysis, cleavage of dilactide units in the macromolecular backbone was already in progress at this time point. However, PU-U gels maintained their barrier function until this critical point in time, suggesting that they present a suitable material for adhesion prevention. Thus, the cell adhesion and migrating experiments support the assumption that cells are

not able to migrate through the network based on calculation of M_c and subsequently of mesh size *via* DMA measurements.

Summary of the Physico- and Biochemical Characterization of the Identified Hydrogel Formulation

The analyses of the previous chapters demonstrated anti-adhesive and anti-invasive properties of PU-U hydrogels, confirming that the hydrogels provide a suitable barrier to prevent or minimize the formation of post-operative adhesions. Determination of the molecular weight between two crosslinks (M_c) of the hydrogels *via* dynamic mechanical analysis (DMA) experiments over the degradation interval of 0-7 days confirmed a small mesh size, ranging from 10.5-12.6 nm. The mesh size obtained from the DMA experiments was compared to the dimensions of various cell types. It was observed that the dimensions of cell types are reported to be approximately three orders of magnitude (10^3) higher than the mesh size of the hydrogels under investigation.

Additionally, it was demonstrated that the degradation products of the hydrogels are non-cytotoxic and do not exhibit mutagenic effects, which is critically paramount for prospective utilization of the hydrogels for in *in vivo* utilization. Moreover, the hydrogels exhibit favorable mechanical properties, sufficient to withstand damages and ruptures *via* elongation of the abdominal wall and by compression caused by differing IAP. PH values during the curing reaction of the hydrogel demonstrated that the utilization of NH_2-terminated crosslinker leads to an increase in pH values. However, the hydrogels exhibit physiological pH values after 76 seconds post application. Whether the initial alkaline pH stage during the onset of the crosslinking process is critical, necessitates further investigation through advanced biocompatibility assessments.

4.2.6 Sprayable Hydrogel Formulations with CO_2 as a Carrier Gas

All hydrogels presented up to here have been used either without a carrier gas or with N_2 or compressed air as carrier gas. In surgery rooms CO_2 is most common praxis for laparoscopic processes. The sprayable hydrogel solutions will therefore be applied during the application by a surgeon using CO_2.

The spray applicator, whereby the hydrogel system will be provided was designed and manufactured by *Erbe Elektromedizin* and was schematically presented in Figure 4. Single component 1 (blue) and single component 2 (green) will be provided in aqueous solutions, wherein the NCO component needs to be prepared freshly, due to the NCO hydrolysis in H_2O reaction and the presence of degradable sites in the backbone. Both solutions will be forwarded to the spray nozzles and are then dispersed into fine droplets facilitated by a carrier gas, which will predominantly be CO_2. The spray nozzles are arranged in a way that ensures both spray nebulas are overlapping. This process represents the mixing step of the two components. As a result, the crosslinking of both single components takes place on the surface, where it is applied on. Thus,

blockages by precuring of the gel within the channels are avoided. It is important to notice that the system is an outer mixing system and that there will be a direct contact between the single components and the carrier gas during the spray process. The carrier gas flow rate is fixed to a volume flow of 6 norm liters (NL)/min.

When the carrier gas was changed from N_2 to CO_2 a change in the gelation behavior comparable to first application to organic tissue (kidney), as described in chapter 4.2.3, was observed and thus giving a hint on a possible protonation effect.

To quantify this effect, a pure amine solution was sprayed by the applicator, without the corresponding NCO solution. No buffer was added and a 15.3wt.-% solution of **Jeffamine ED2003** in pure water was prepared. The pH value was measured before and after the spray process. Before it was sprayed *via* the applicator, the pH value was determined at 11.63, after the spray process it was determined at 9.77 leading to a difference of 1.86 units. The amine component for the optimized formulation comprises a pH value of 10.47. The results of the pH measurements of pure sprayed amine solutions also indicate that the utilization of the amine solution without any buffering agent, thereby relying exclusively on the buffering effect provided by the introduced CO_2, will not be sufficient since the pH value of the sprayed solution is still 0.7 units below the pH value of the ideally adjusted amine solution. The buffering effect of the introduced CO_2 is higher than the adjusted buffering capacity of the preferred formulation.

Two reactions are possible considering the application of primary amines in direct contact with CO_2, being A) reaction of 2 R-NH_2 and CO_2 yielding carbamic acid or carbamates and ammonia (R-NH_3^+) which are unable to crosslink. This mechanism is reported for mono ethanol amine, being used as CO_2 absorber, used in different industrial applications to reduce CO_2 pollution.[209] Another possibility is depicted by option B) CO_2 gets dissolved in the aqueous medium and provides a buffering effect to convert R-NH_2 to R-NH_3^+ by formation of carbonic acid. Both mechanisms are presented in Figure 97.

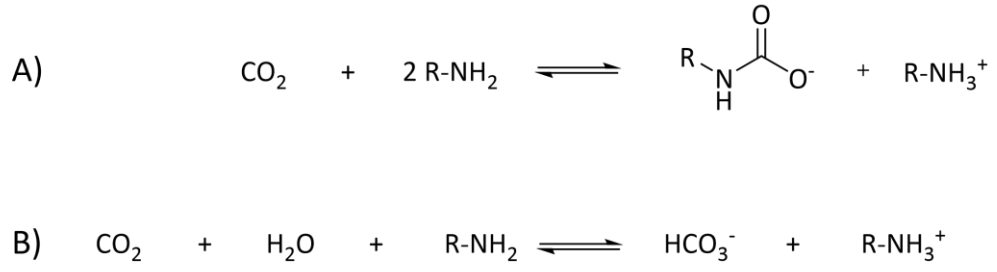

Figure 97 Illustration of possible reaction pathways of primary amines in aqueous solutions with CO_2 present. Reactions are reported for (A) by Ref.[210] and for (B) by Ref.[209]

Both mechanisms are reported to occur in a contact of CO_2 and NH_2 in aqueous media.[209,210] For this purpose a solution of 25wt.-% **Jeffamine ED2003** in D_2O was sprayed for 40 sec. with the spray applicator. ^{13}C NMR spectra was recorded and compared to ^{13}C NMR spectra of a native solution of 25wt.-% **Jeffamine ED2003** in D_2O. Both spectra are presented in Figure 98. Two identified peaks occurred after the spray process *via* CO_2. The peak at 163.9 ppm can be

attributed to the formed carbamate, while the identified peak at 161.2 ppm arises from the HCO_3^- and, if present, CO_3^{2-}. In comparable experiments from Lv *et al*., wherein monoethanolamine was captured with CO_2, a peak in ^{13}C NMR arised from the carbamate species of monoethanolamine was identified at 164.5 ppm, HCO_3^-(CO_3^{2-}) species was identified at 160.2 ppm.[209] In general HCO_3^- is reported to occur at 160.3 to 161.5 ppm, CO_3^{2-} is reported for 168.1 to 169.5 ppm.[211]

Chemical shifts of the two species carbamate and HCO_3^- reported by Lv *et al*. are comparable to the identified peaks of Figure 98 which indicates that both substances are present in the analyzed sample. ^1H NMR displayed no corresponding proton peaks, likely caused by a deuterium hydrogen exchange of labile protons in D_2O.[212]

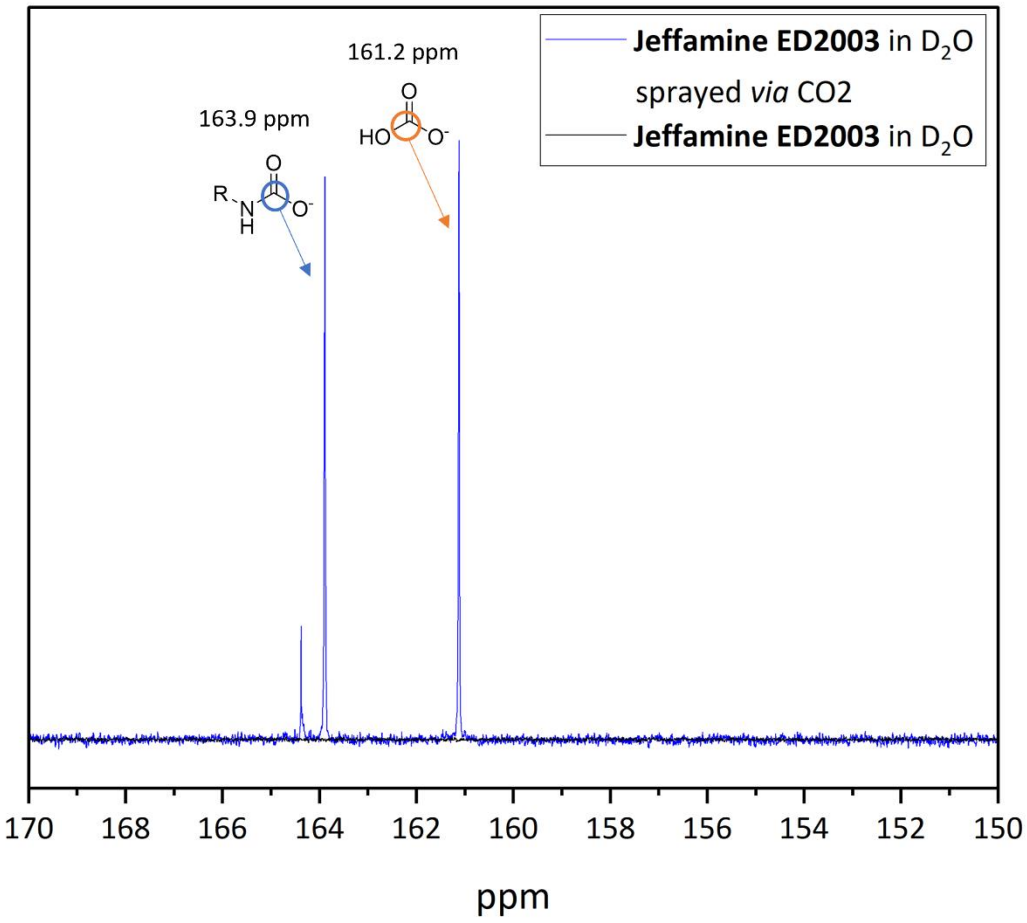

Figure 98 ^{13}C NMR of a 25wt.-% **Jeffamine ED2003** solution in D_2O. Comparison of a native solution (blue line) to a solution sprayed *via* CO_2 at 6NL/min for 40 sec (black line). Peak at 163.9 ppm is attributable to formed carbamate, peak at 161.2 is attributable to formed HCO_3^-. Identified chemical shifts are in accordance with reported literature for carbamate and HCO_3^-.

To investigate which effect is dominant, the system was reduced to the spraying of pure water *via* CO_2. Herein the reaction pathway of A) is avoided, while a potential buffering effect as in B) will be detected by a decrease in pH values. The amount of CO_2 is fixed to a volume flow of 6 NL/min, while the time for spraying was set to 20 sec, 40 sec. and 60 sec. 10 mL have been applied in each spray experiment. Table 44 presents an overview of resulting pH values after the

spraying process utilizing CO_2 as carrier gas. The initial pH value prior to the spray process was determined to be 6.22.

Table 44 Overview on pH values of samples of 10 mL pure water applied with the spray applicator from Figure 4. The volume flow is set to 6 NL/min leading to a time dependance of contact of CO_2 and H_2O. Time of spraying was set to 20 sec, 40 sec. and 60 sec., each carried out as triplicates. The pH value of pure water before it was sprayed *via* CO_2 was determined at 6.22.

Sample	Time of spraying [sec.]	Resulting pH value
A	20	4.52
B	20	4.40
C	20	4.28
Mean		4.40
A	40	4.35
B	40	4.31
C	40	4.30
Mean		4.32
A	60	4.35
B	60	4.29
C	60	4.32
Mean		4.32

Results indicate that the resulting pH value, and therefore the buffering degree, is independent from the time of spraying in the range of 20 sec.-60 sec. The amount of used CO_2 for the spray process is 2 L for 20 sec. time of spraying, 4 L for 40 sec. time of spraying, and 6 L for 60 sec. Resulting mass of CO_2 is calculated according to equation 4.2.26, wherein V_m is the molar volume describing the volume of 1 mol gas under normal conditions, which is 22.41 L/mol is the volume of 1 mol gas under normal conditions, V_{CO2} is the volume of CO_2 used for the spray application and MW_{CO2} representing the molecular mass of CO_2 which is 44.01 g/mol.

$$m_{CO2} = \frac{V_{Co2}}{V_m} * MW_{CO2} \tag{4.2.26}$$

Amounts of used CO_2 for the spray application are 3.9 g for 20 sec. spraying, 7.9 g for 40 sec. spraying and 11.8 g for 60 sec. spraying. Each calculated amount got in contact with 10 mL of pure water. The solubility of CO_2 in water is reported to be 1.003 g/L at a pressure of 1.013 bar.[213] All calculated values are far above the solubility limitations of CO_2, which is also visible from the resulting pH values from Table 44, which are comparable to each other, independent of the time of spraying. Saturation concentration of CO_2 in water seems to appear in all samples. Results indicate that buffering effect is independent from the time of spraying since the saturation

concentration is already reached after 20 sec. of spraying which is relatively fast. As reducing the adjusted buffering degrees by buffers or diluted acid and using instead the buffering effect of CO_2 will not maintain initial buffering degrees, other options will be considered to optimize the system for the use with CO_2 as a carrier gas.

Possibilities are given by an increase in amine concentration. Hereby more molecules of primary amines will be left unprotonated and therefore be able to form crosslinks to build up the hydrogel network. However, it may also leave a portion of ammonia- or carbamate-converted amines unreacted, which may raise potential safety issues that need to be addressed.

A second option is the addition of alkaline substances, like sodium hydroxide (NaOH), to the amine solution. The challenge herein is to find a concentration at which a hydrogel is obtained but still comprise physiological pH values between 6.1 to 7.4.

To identify this spot, a 15.32wt.-% formulation of **Jeffamine ED2003** was prepared in each NaOH concentration and sprayed with the spray applicator *via* CO_2 as carrier gas. The pH values of the solution were measured before and after the spray process. After the spraying of the amine component the corresponding amount for index=1.2 of NCO (15wt.-%) represented by **prepolymer-1** in H_2O was added slowly to the amine solution, observing if hydrogel formation was present. Table 45 presents an overview of prepared solutions, their pH values before and after spray application, if gelation could be observed and the time until gelation takes place.

Table 45 Overview on the different amine solutions which have been prepared in NaOH, their pH values before and after spraying, if gelation was observed after the addition of the NCO component, and if applicable at which time it could be observed.

Concentration of NaOH in a 15.32wt.-% Jeffamine ED2003 solution [mol/L]	pH value before spraying	pH value after spraying for 20 sec.	Gelation observed after addition of 15wt.-% NCO solution	Time until gelation [sec.]
1	13.08	12.91	No	-
0.5	13.02	12.82	No	-
0.1	12.9	12.46	Yes	<60 sec.
0.09	12.76	9.78	Yes	34 sec
0.08	12.75	9.74	Yes	37 sec
0.07	12.66	10.05	Yes	28 sec
0.05	12.55	9.83	Yes	<60 sec.
0.01	12.04	9.16	Slightly gel formation	<60 sec.

The formulations prepared with NaOH concentrations ranging from 0.09M to 0.05M NaOH concentration appear to be suitable candidates for further optimization concerning the properties

of the resulting hydrogel. Interestingly the pH measurements of these formulations do not significantly deviate from those of pure **Jeffamine ED2003** dissolved in H_2O and sprayed *via* CO_2.

pH values have been measured during the hydrogel formation, when applying both formulations, NH_2 and NCO with the spray applicator *via* CO_2 as carrier gas into a beaker. A pH electrode inside measured resulting pH values as a function of time. PH values have been recorded for 15 min. and are presented in Figure 99.

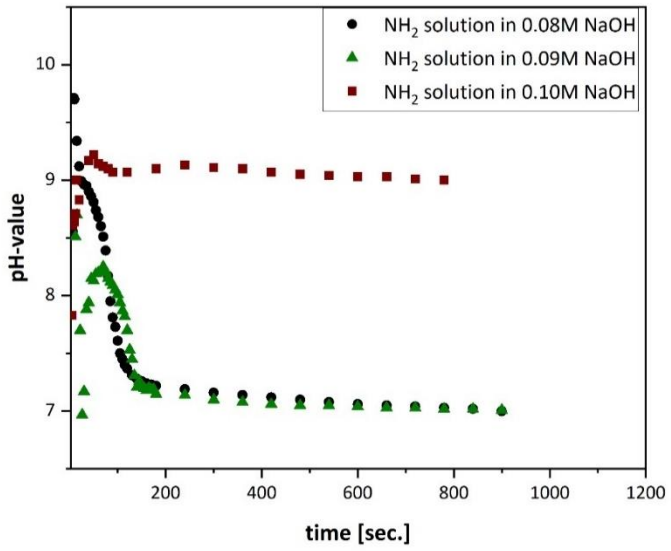

Figure 99 PH values as a function of time measured for formulations using 0.08M, 0.09M and 0.1M NaOH for the preparation of the amine component.

Interestingly pH curves of 0.08M and 0.09M NaOH are comparable after ~120 sec. PH values of <8 are observed after 105 sec. in 0.09M NaOH and after 85 sec. in 0.08M NaOH. Both formulations comprise pH values of 7.31 after 135 sec. and end in a pH value of 7.0 after 15 min, while 0.1M NaOH strongly deviates from these values, ending in a pH of 9.0 after 13 min.

Assuming a saturation concentration of CO_2 in water, 0.0255 g CO_2 would be solved in the total applied volume of 15 mL.

It is important to notice that the adjusted gas flow has a direct impact on the amount of CO_2 being introduced into the aqueous system. Formulations consisting of 0.09M or 0.08M NaOH which have been previously described to be suitable for the application, are exclusively tested at a CO_2 gas flow of 6 NL/min.

A reduction of the gas flow to 2.0 NL/min, tested for a different type of spray applicator, as will be described in chapter 4.3, requires an adjustment of the formulation.

4.3 Proof of Concept of a Sprayable Hydrogel Formulation in *in vivo* Testing and Further Optimization of the Sprayable System

The *in vivo* studies presented in this chapter were conducted by FREYTOX GmbH. The results obtained from the studies are reported and cited herein.

As proof of concept an animal study was conducted to identify the effectiveness of the presented hydrogel formulation as an adhesion prophylaxis. Since the use of CO_2 as carrier gas is a common set up employed in surgery rooms, a formulation adjusted to a gas flow of 6 NL/min CO_2 was chosen for the *in vivo* testing. For the study 24 rabbits were randomly divided into three groups which were treated with a) Seprafilm, as a negative control due to its well-established adhesion prevention properties b) NaCl rinsing, serving as a positive control without the addition of any adhesion-reducing agent c) the sprayable hydrogel formulation optimized for the use with CO_2 as carrier gas. The formulation which was used for the *in vivo* proof of concept is listed in Table 46.

Table 46 Tested hydrogel formulation of the *in vivo* proof of concept study.

	Applied Volume	Substance	Concentration	Concentration in resulting hydrogel
Component A	10 mL	Prepolymer-4	15.0wt.-%	10.0wt.-%
		dH_2O	85.0wt.-%	56.7wt.-%
Component B	5 mL	Jeffamine ED2003	15.3wt.-%	5.1wt.-%
		NaOH 0.06M	84.7wt.-%	28.2wt.-%

The study was designed for the investigation of efficacy for the prevention of postoperative peritoneal adhesions of the hydrogel. A traumatization of an approximately size of 3.0 x 4.0 cm was set to each animal before being treated according to the test group. This procedure was chosen to trigger the formation of postoperative peritoneal adhesions for the investigation of efficacy of the test item. A second *in vivo* study was conducted, with a different study set up. Herein the focus was laid on biocompatibility and degradation speed. Formulations adapted to the use of CO_2 have been investigated as well as formulations with inert carrier gases (herein: compressed air), to exclude a lack of biocompatibility caused by time lag between hydrogel application and reaching physiological pH values, which is prolonged in CO_2 compatible formulations. Furthermore, externally hardened hydrogels have been implanted to exclude effects by spraying of the reactive system, consisting of NH_2 and NCO. Especially the latter is often associated with skin irritation and cytotoxicity.[214]

The results presented in the subsequent chapters were derived from the respective study report and the histopathological examination report.

4.3.1 Results of the Proof of Concept *in vivo* Study

To investigate the hydrogel in question for its potential as adhesion prophylaxis a proof of concept *in vivo* study was conducted. The aim of this study was the evaluation of efficacy as an adhesion barrier. Animals were divided into three different groups as listed in Table 47. All animals underwent a laparotomic surgery procedure wherein a traumatization on the intraabdominal wall and on the intestinal tract was applied.

Table 47 Arrangements of animals for the proof of concept study for the investigation of efficacy for the test item HYGEL.

Groups	Number of animals	Implantation item	Time of Implantation
Test group	8	Test item (HYGEL)	21 days post operative
Reference groups	8	Reference item (Seprafilm)	21 days post operative
Positive control	8	Untreated control (NaCl rinsing)	21 days post operative

The tested hydrogel formulation is listed previously in chapter 4.3, Table 46 and is in the latter referred to as HYGEL. The spray applicator concept from Figure 4 was used for the *in vivo* study.

After 21 days *post operationem*, animals were euthanized and reopened to analyze the occurrence and the extent of postoperative peritoneal adhesions in the pre-traumatized area. Evaluations were conducted according to the modified Diamond score by Bigatti *et al*..[215] regarding the extent, tenacity and the type of the formation. Moreover, occurring adhesions between caecum and the muscle suture were also scored by the adhesion score by Zühlke *et al*..[216] Rating scores are described in detail in chapter 6.5, Table 56 and 57.

All animals survived the scheduled period. Macroscopically, in half of the animals of the test item group, the abdominal wall defect displayed adhesions to the caecum or other intestinal tissues. Additionally in two animals of the test item group macroscopic abscess like reactions in the surrounding tissue were present[217] which was identified to correlate microscopical with a pyogranulomatous necrotic reaction, characterized by a high number of foamy macrophages, polymorphonuclear cells, necrosis, cellular debris and fibrin, surrounded by fibrous connective tissue and macrophages.[218] Additionally gelatinous and filamentous tissue was identified in the HYGEL group.

Macroscopic results from the HYGEL test group regarding postoperative adhesions are listed in Table 48[217], including the occurrence of postoperative adhesions, the extent and the rating according to Zülke and Bigatti.

Table 48 Adhesion between abdominal structures and abdominal wall defect, describing adhesions present, adhesion free, the extent of adhesions, the tenacity, the respective type and the Zühlke score for the HYGEL groups. Results are reported in Ref.[217]

Animal No.	Adhesive structure	Adhesion [%]	Free [%]	Extent [%]	Tenacity	Type	Zühlke score	Zühlke Score (musle suture)
1	caecum	100	0	>75	4	V	IV	-
2	-	0	100	0	1	I	-	-
3	Caecum/duodendum	100	0	>75	4	V	IV	IV
4	-	0	100	0	1	I	-	-
5	Caecum	45	55	25-50	3-4	V	III	II
				<25	3-4	V	III	
6	-	0	100	<25	1	I	-	-
7	Caecum			0	3-4	V	II	II
	Colon	80	20	25-50	3-4	V	II	
	Basis caeci			25-50	3-4	V	II	
8	-	0	100	<25	1	I	-	-
Average		~ 41	~59	0				
sum					4x1	4xI	3xII	2xII
					5x3-4	7xV	2xIII	1xIV
					2x4		2xIV	

The positive control and the negative control were evaluated in the same way and subsequently all three groups were compared regarding the average area of adhesion, which is reported in Table 49. Herein the HYGEL groups revealed the largest percentage of adhesive areas (41%) followed by the positive control (36%). In the negative control no adhesion formation was detected.

Table 49 Average area of detected adhesion between abdominal structures and the abdominal wall defect of the HYGEL group in comparison to the positive control (NaCl rinsing) and the negative control (Seprafilm).

Group	Average area of adhesion [%]	Average area free from adhesion [%]
HYGEL test group	~41	~59
Positive control	~36	~64

Negative control	0	100

Comparing the adhesion free abdominal wall defects of the HYGEL test item group to the adhesion free abdominal wall defects of the other treatment groups (Seprafilm and NaCl), morphological differences in coloration and connective tissue formation were detected macroscopically. The differences between the treatments groups were associated with the higher amount of granulation tissue, which was observed histologically in the internal part of the wall defect of the HYGEL test item treated samples. Histologically the HYGEL test item and the reference item were not visible in any of the examined samples.[218]

Regarding the obtained result of macroscopic findings, local biocompatibility as well as adhesion prophylaxis potential of the applied hydrogel in the HYGEL test group is questionable.

Since the cytotoxicity of the herein used hydrogel system has been investigated in detail, as presented in chapter 4.2.5, before the proof of concept *in vivo* study, results which indicate a non-biocompatibility have not been expected. Moreover, postoperative adhesions were still present in the HYGEL test item group, which may be caused by a strongly accelerated degradation of the hydrogel network. Previous investigation of degradability were limited to incubation without enzymatically active ingredients like hydrolases, which are reported to accelerate degradation processes *in vivo*.[219] By not taking these into account, a degradation of the network could have been proceeded in <7 days, which could lead to formation of postoperative adhesions due to the critical wound healing period of 7 days.[16,107] The network size was previously determined *via* DMA measurements indicating a sufficient mesh size for the prevention of cell migration through the polymer hydrogel network maintained for ≥7 days. Investigations of cell migration behavior from chapter 4.2.5 support this assumption. A second option for the fast biodegradation of the hydrogel is the presence of an inflammatory surrounding which is associated with alkaline pH values.[121] The hydrogels exhibit a pH dependent degradation as already demonstrated in chapter 4.2.3. The presence of a more alkaline milieu may support the degradation process of ester units in the dilactide groups of the hydrogels, either by a higher presence of OH^- species or by enzymatic milieu present under alkaline conditions. Especially matrix-metalloproteases (MMPs) are reported to occur at higher concentrations in chronic wounds, comprising pH values of 7.5-8.9 while the pH optimum for matrix-metalloprotease-2 (MMP-2) is reported at pH=8.0.[220] Proteolytic enzymes, like serine protease α-chymotrypsin, are reported to hydrolyze ester groups of PLA.[132] If MMPs are able to accelerate hydrolysis of ester groups is not reported yet. If this is applicable, the presence of a higher MMP concentration could directly impact the biodegradation rate of the hydrogel. Both mechanisms, regarding OH^- concentration and enzymatic activity might interfere in the present situation *in vivo* and influence the efficacy as an adhesion barrier by accelerating degradation process of the hydrogel network. However, detailed reasons for the accelerated biodegradation process are hardly comprehensible. Explanations of possible effects are limited to assumptions.

Two major conclusions can be summed up by the results of the proof of concept *in vivo* study:

1.) A lack of biocompatibility seems to be present, which was macroscopically identified by abscess like formation in two animals treated with the test item and a microscopic correlation of necrotic tissue behavior in the same animals.

2.) Efficacy of HYGEL as an adhesion barrier is not given, probably caused by too fast biodegradation of the hydrogel, whereby formation of postoperative adhesions is still possible.

Adaptions of the hydrogel system are necessary and will be described in chapter 4.3.2 addressing the major defects of the system carried out by the *in vivo* proof of concept study.

4.3.2 Investigation of Applicator Defects and Optimization of the System

Addressing the biocompatibility, it is questionable why a formation of abscesses did appear in two of the eight rabbits from the test item group. Chronic or infected wounds exist at a more alkaline pH environment which is more conducive to bacterial burden, as reported by Schneider, Korber *et al*..[121]

At this point in time, only assumptions can be made but discussion on pH of chronic wounds might give a hint on possible reasons for *in vivo* testing failure. To investigate occurring pH values during the spray process the hydrogel system used for the *in vivo* proof of concept was applied on a cellulose sheet, coated with a solution of 1wt.-% phenolphthalein indicator in acetone. Phenolphthalein occurs colorless at a pH of 0-8.2, above 8.2 it turns violet, which makes it a suitable indicator for the detection of deviating pH values from physiological values. After conducting the spray experiment on the cellulose sheet, it was identified that higher pH values of >8.2 are present in the hydrogel, as some regions turned violet. PH values of >8.2 depict substantial deviations from physiological pH levels, which can be interpreted as an indicator for unequal mixing of the components.

Figure 100 illustrates the distribution patterns of different color zones obtained from the spray experiment. The colorless region may represent a properly crosslinked hydrogel network, while the violet regions indicate areas with higher pH values, likely caused by insufficient mixing and residual unreacted NH_2 component. Notably, the violet color is especially detected at the borders of the spray nebula, suggesting that the spray nebulas did not fully overlap at the edges, leaving NCO and NH_2 unreacted. NCO groups might undergo self-reaction during NCO hydrolysis, induced by included water, leading to minor changes in pH values. The NH_2 crosslinking component will not be converted to urea and will remain unreacted. Residual un-crosslinked NH_2 groups will likely strongly affect local pH values.

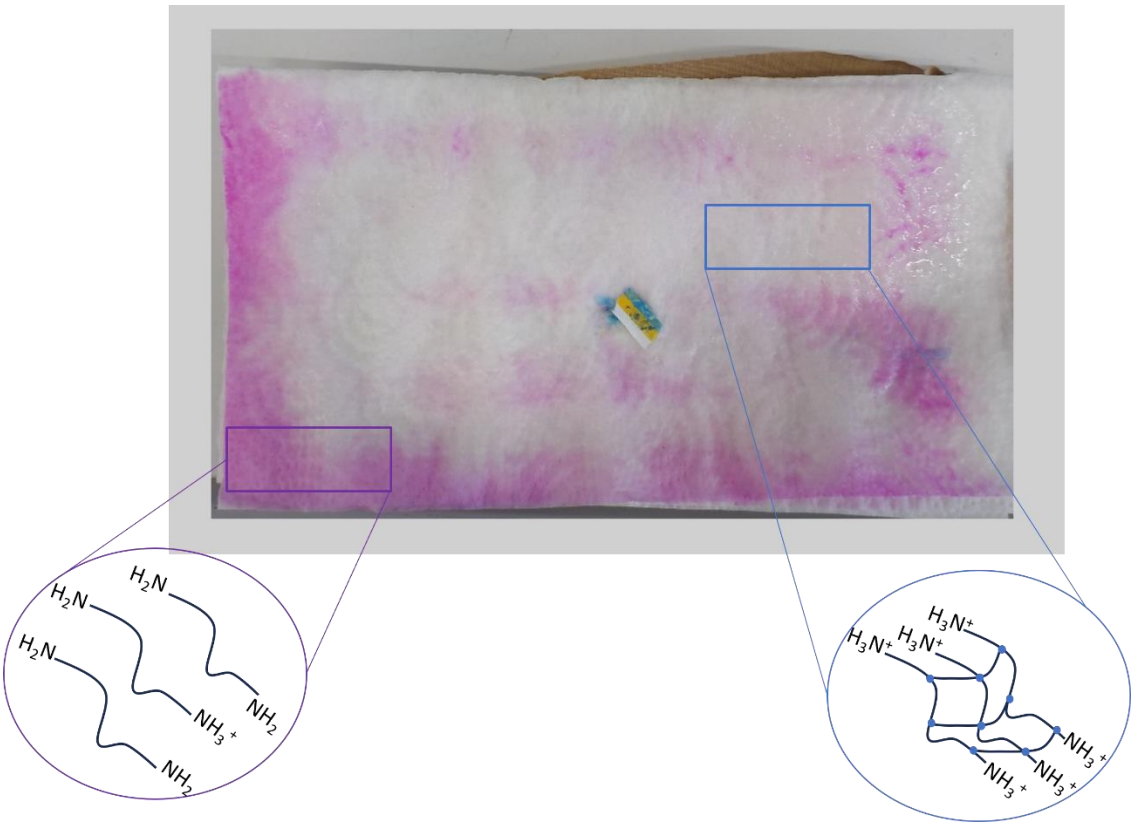

Figure 100 Spray experiment of a CO_2 sprayable hydrogel formulation, using the spray applicator concept from Figure 4, on a cellulose sheet coated with a 1wt.-% phenolphthalein solution. Color patterns indicate insufficient mixing of both components. The colorless region represents a proper cured hydrogel network, while the violet region might be caused by an excess of unreacted NH_2 groups.

Possibilities how to arrange spray nozzles that 100% of spray nebulas from the single components will overlap are depicted by adjustments of the angle of the spray nozzles. This concept still bears the risk of unequal mixing, if for example one side is hindered by surrounding tissues. It was discarded for safety concerns.

The spray applicator type was changed to an inner mixing system, as schematically presented in Figure 101. Herein both single components are provided by single channels to avoid blockages. At the end of the spray applicator a static mixer unit is embedded, wherein both single solutions are mixed before being sprayed on the surface. Hereby, the mixing system is independent of surrounding disruptive factors like barriers or uneven tissue. The contact between the carrier gas and the aqueous solution is still present in the inner mixing system.

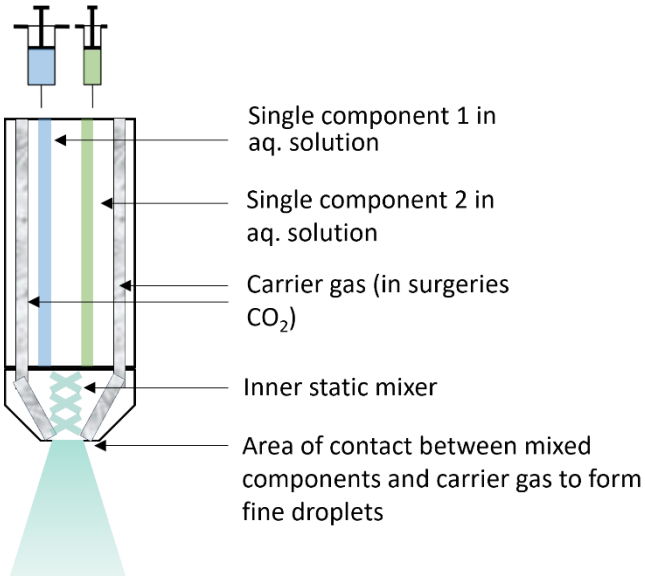

Figure 101 Adapted spray applicator concept encompassing an internal mixing unit.

When using this type of spray applicator, a decrease of the gas flow to 2 NL/min CO_2 is required, which leads to a reduced buffering effect by the reduced amount of introduced CO_2. A decrease of the buffer solution NaOH to 0.02M was identified as suitable *via* pH measurements. A repetition of the phenolphthalein spray experiment revealed that mixing of both components is even, since no area was detected in violet.

Addressing the degradation speed of the hydrogel, it is unclear if the effect of too fast hydrolysis occurs by a general rapid increase of degradation speed under living conditions or if it was triggered by an insufficient mixing of the spray system leading to partially higher pH values, or by higher pH values due to inflammatory reactions and increased enzyme activities. Since a general rapid increase of degradation speed under living conditions can't be excluded, dilactide units are reduced for repetition of an *in vivo* study. As described in chapter 4.2.4 the parameter *dilactide content* exhibits the largest influence on the degradation speed. For further *in vivo* testing **prepolymer-3** was used for hydrogel manufacturing, featuring **polyol-2** in its backbone with a dilactide content of 2.5wt.-% (weight of starter not included).

4.3.3 Results of the Biocompatibility *in vivo* Study

As described in chapter 4.3.2, indicators for the lack of biocompatibility were identified as an unequal mixing of the outer mixing system, resulting in partially alkaline pH areas, being associated with inflammatory tissue reactions.[121] Regarding the fast biodegradation process, it is unclear whether the effect arises from deviation in pH values to alkaline milieu or by a general increase in degradation speed under live conditions in comparison to laboratory *in vitro* experiments. Since the latter can't be excluded adaptions to lower dilactide content of the prepolymer backbone were conducted.

The design of the second *in vivo* study focused on assessing the general biocompatibility of the hydrogel system and no evaluation of its efficacy as an adhesion prophylaxis was performed.

Since formulations using CO_2 as a carrier gas need larger time intervals to obtain physiological pH values ≤7.4, as demonstrated in chapter 4.2.6, basic formulation from previous chapters using HCl as buffering agent and inert gases like compressed air for the spray application, have been investigated additionally to exclude this as a source of *in vivo* failure. Additionally, the risk of spraying an NCO-reactive system into a living organism needs to be analyzed as possible source of harm. It was decided to test the direct sprayed system, as being described previously and a prehardened hydrogel, being implanted after the curing reaction. Two time intervals have been analyzed. Animals were reopened 8 days and 21 days *post operationem*. The study design is illustrated in Figure 102.

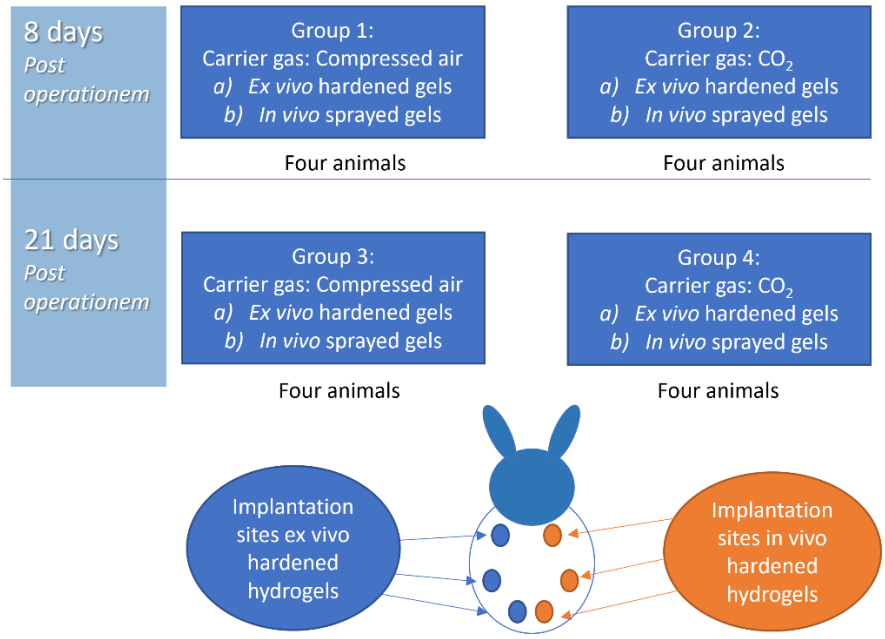

Figure 102 Study design of the second *in vivo* study. 16 rabbits were included and divided in four groups. Group 1) uses a formulation adapted to be sprayed with compressed air. On the right side of each animal the hydrogel is applied on three areas *via* spray application. On the left body side of each animal, prehardened hydrogels are implanted after ~5 min. curing time. These animals were analyzed after 8 days. Group 3) identical to group 1 while analyses of the animals will be conducted after 21 days. Group 2) uses a formulation adapted to be sprayed with CO_2. On the right side of each animal the hydrogel is applied on three areas *via* spray application. On the left body side of each animal, prehardened hydrogels are implanted after ~5 min. curing time. These animals were analyzed after 8 days. Group 4) identical to group 2 while analyses of the animals will be conducted after 21 days.

For the spray application the applicator concept from Figure 101 was utilized. The gas flow was reduced to 2 NL/min for both CO_2 and compressed air. Formulations used for the study are presented in Table 50.

Table 50 Summary of the analyzed formulations in the second *in vivo* study. Two formulations have been analyzed, wherein the first, tested in group 1 and 3, is applicable for an application *via* CO_2 as carrier gas at a gas flow of 2 L/min, while the second, tested in group 2 and 4, is applicable for compressed air as carrier gas, independent of the gas flow.

Testing Group	Component	Applied Volume	Substance	Concentration	Concentration in resulting hydrogel
Group 1, Group 3	Component A	10 mL	Prepolymer-3	15.0wt.-%	10.0wt.-%
			dH_2O	85.0wt.-%	56.7wt.-%
	Component B	5 mL	Jeffamine ED2003	15.3wt.-%	5.1wt.-%
			NaOH 0.02M	84.7wt.-%	28.2wt.-%
Group 2, Group 4	Component A	10 mL	Prepolymer-3	15.0wt.-%	10.0wt.-%
			dH_2O	85.0wt.-%	56.7wt.-%
	Component B	5 mL	Jeffamine ED2003	15.3wt.-%	5.1wt.-%
			HCl 0.02M	84.7wt.-%	28.2wt.-%

Animals were treated according to the respective test group and reopened after 8 or 21 days to evaluate findings regarding biocompatibility. Results for all analyzed groups are summarized in Table 51. Connective tissue embedding of the test item (TI), vascular growth around TI, vascular growth within situs surrounding and presence of white- yellowish substance (most probably pus) were used for the assessment of the biocompatibility.

Table 51 Summary of the macroscopic results of the *in vivo* biocompatibility study regarding connective tissue embedding, vascular growth around test item (TI) and vascular growth within situs surroundings as indicators for local biocompatibility. 12 TIs were present per group. Results are reported in Ref.[221]

	8 days post operationem				21 days post operationem			
	Sprayed TI		Pre-hardened TI		Sprayed TI		Pre-hardened TI	
	CO_2	Air	CO_2	Air	CO_2	Air	CO_2	Air
	Connective tissue embedding							
Slight	-	-	1	3	-	-	-	-
Mild	-	-	2	3	-	-	-	-
Mild to moderate	3	-	-	-	-	-	-	-
Capsule formation	6	12	9	6	3	12	9	12
Implantation pocket	3	-	-	-	9	-	3	-
	Vascular growth around TI							
None	-	-	-	1	-	-	3	4
Slight	-	-	1	3	1	1	4	2
Mild	7	4	5	2	1	4	-	4
Mild to moderate	3	2	1	1	4	3	1	1
Moderate	1	5	5	2	5	3	4	1
Moderate to severe	1	1	-	3	1	1	-	-
	Vascular growth within situs surrounding							
None	-	-	-	-	-	-	-	1
Slight	-	-	-	6	2	1	-	1
Mild	7	2	3	1	2	6	1	4
Mild to moderate	4	1	5	0	8	4	-	2
Moderate	1	7	4	4	-	1	4	2
Moderate to severe	-	2	-	1	-	-	3	-
severe	-	-	-	-	-	-	4	2
	Presence of white- yellowish substance							
missing	5	-	2	6	-	-	-	-
slight	2	-	5	1	12	4	7	8
prominent	5	12	5	5	-	8	5	4

Overall, in approximately 86% of cases (83 out of 96, Table 51) varying amounts of white-yellowish substance was detected within the subcutaneous implantation sites with a varying distribution pattern of the white-yellowish substance ranging from haze-like to flaky conflated. In

92% of cases (88 of 96, Table 51) vascular growth around the TI, and in 99% of cases (95 out of 96, Table 51) vascular growth in the situs surroundings were detected. Moreover, 91% of cases displayed at least a mild to moderate embedding of the TI in connective tissue.

Thus, a specific reaction of the treated tissue against the TI can be presumed. A surgical introduction of germs can most probably be excluded as the animals displayed no clinical alterations characterized by general well-being, no signs of automutilation and continued weight gain.[221]

Summarizing all results of the *in vivo* biocompatibility study, missing biocompatibility of HYGEL can be assumed due to body reactions at most implantation sites, irrespective of the carrier gas (CO_2 vs. compressed air) and the application technique (sprayed vs. prehardened).

4.3.4 Summary and Outlook

The results from the first *in vivo* study lead to two major conclusions:

1.) A lack of biocompatibility seems to be present, which was macroscopically identified by abscess like formation in two animals treated with the test item and a microscopic correlation of necrotic tissue behavior in the same animals.

2.) Efficacy of HYGEL as an adhesion barrier is not given, probably caused by too fast biodegradation of the hydrogel, whereby formation of postoperative adhesions is still possible.

Both concerns were addressed in chapter 4.3.2, wherein the lack of biocompatibility was associated with an identified mixing problem of the spray applicator leading to partially alkaline pH areas in the hydrogel. The spray applicator was changed to an inner mixing system and the mixing became equal. PH deviations to alkaline values have not been detected. It can be assumed that the observed fast biodegradation, as described in point 2 above, can be attributed to the physiological conditions in an organism. **Prepolymer-3** with a reduced dilactide content of the polyol in the backbone of 2.5wt.-% was chosen for the second *in vivo* test, as dilactide content represents the formulation parameter with the highest influence on degradation speed, as identified in chapter 4.2.4.

For investigations of general biocompatibility of the hydrogel system, the study design was adapted and further evaluation was assessed for two distinct formulation variants, wherein one was designed for delivery employing CO_2 as the carrier gas, while the other was formulated for administration using compressed air. Formulations were a) directly sprayed into animals and b) prehardened and after a curing time of ~5 min. implanted. Macroscopic findings indicate foreign body response to the implanted hydrogels, including encapsulation processes, vascular growth around the TI, vascular growth within the situs surround and the presence of a white-yellowish substance in most cases. Overall, the conducted *in vivo* studies demonstrated a lack of biocompatibility of the implanted hydrogels irrespective of the carrier gas (CO_2 vs. compressed air) and of the method of application (sprayed vs. prehardened). The results indicate that missing

biocompatibility is caused in general by the hydrogel system itself, or by degradation products thereof of the hydrogel.

To investigate if these effects occurred from degradation products, cytotoxicity analyses of hydrogels at different degradation degrees were conducted. Herein the formulation from the *in vivo* studies, based on **prepolymer-3** and on **prepolymer-4** was used for the hydrogel preparation. Samples were incubated at 37°C in PBS and were analyzed at each timepoint in a triple determination. Herein the supernatant, which contains degradation products of the hydrogel and the remaining hydrogel as bulk, were analyzed. The results are presented in Figure 103, demonstrating a cytotoxic effect in 5wt.-% dilactide (**prepolymer-4**) on day 6 in the hydrogel and at day 14 day in the gel extracts, containing degradation products of the hydrogel. The 2.5wt.-% dilactide (**prepolymer-3**) formulation showed no cytotoxic effect of the hydrogel (except day 14 and 35) but comprises cytotoxic potential in gel extracts at day 8.

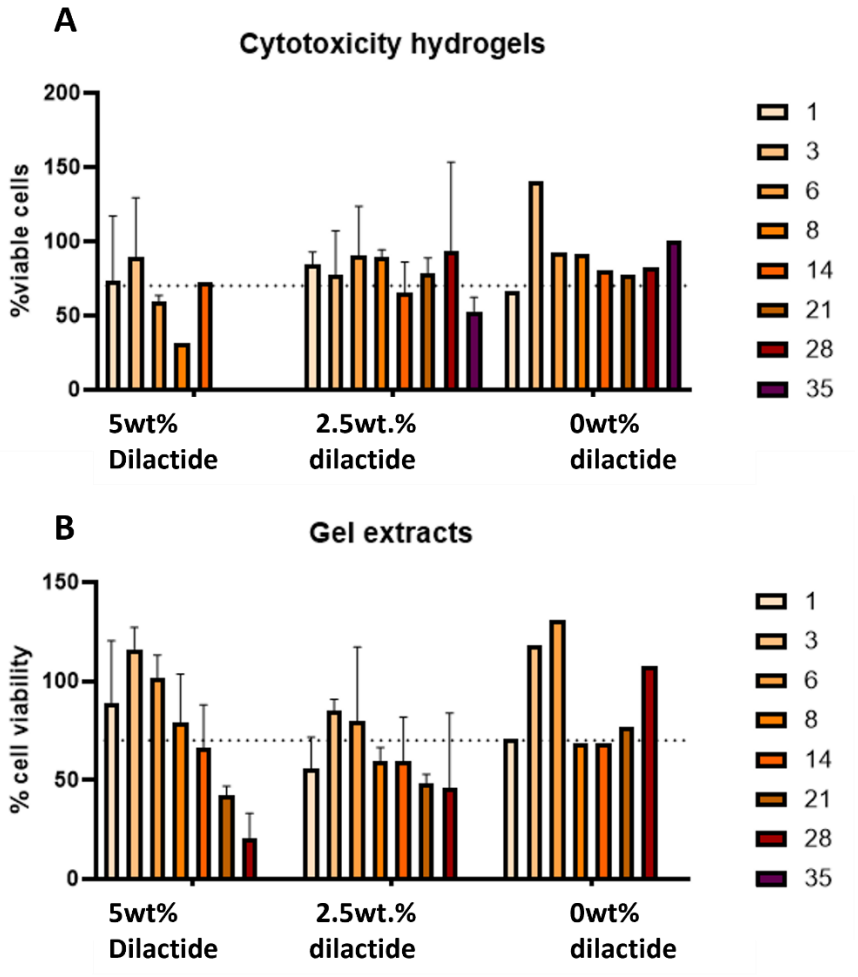

Figure 103 Cytotoxic analyses of the CO_2 formulation from *in vivo* testing of chapter 4.3.3, using **prepolymer-4** (5wt.-% dilactide), **prepolymer-3** (2.5wt.-% dilactide) and **prepolymer-1** (0wt.-% dilactide)

The results from the cytotoxicity tests of the degradation series indicate that a cytotoxic potential is given especially for the gel extracts, indicating that effects may be caused by degradation products of the hydrogels. This effect was not expected, since the cytotoxic potential behavior

was investigated until day 14 of degradation experiments previously in chapter 4.2.5. Additionally, the degradation process of ester units is a well-established procedure for the implementation of degradable sites into an artificial material.[36,222]

Ester groups were limited to dilactide units. If an exchange of dilactide to other degradable esters like caprolactone or glycolide would reduce cytotoxic potential is questionable. It is necessary to identify the source of cytotoxic potential, which could occur from a direct impact of a specified degradation product or by subsequent parameter like a decrease in local pH values, caused by a constant release of carboxylic acids. Other sources may also apply.

5 Summary and Outlook

In this thesis a chemical concept for the development of a sprayable, fast curing, polyurethane based hydrogel has been investigated. Four different concepts for crosslinking were analyzed in chapter 4.1 focusing on a fast reaction kinetics and on adaptions to a sprayable system, exclusively. Herein the required viscosity of 9 mPa*s was identified as the main issue for failure. Most promising results were obtained in approach HYGEL-3, wherein an NCO capped prepolymer with *f*=3 reacts with a macromolecular diamine *f*=2 within the required viscosity limitations in <60 sec. This concept was chosen as the basic crosslinking reaction for further development as it already fulfilled the key requirements *viscosity* and *curing time*. In chapter 4.2.3 preliminary restrictions were identified regarding the viscosity, degradability and biocompatibility (expressed by the pH).

The key identified chemical crosslinking concept is illustrated in Figure 104, wherein the degradable sites, arising from the incorporation of dilactide units into the prepolymer backbone, were already introduced.

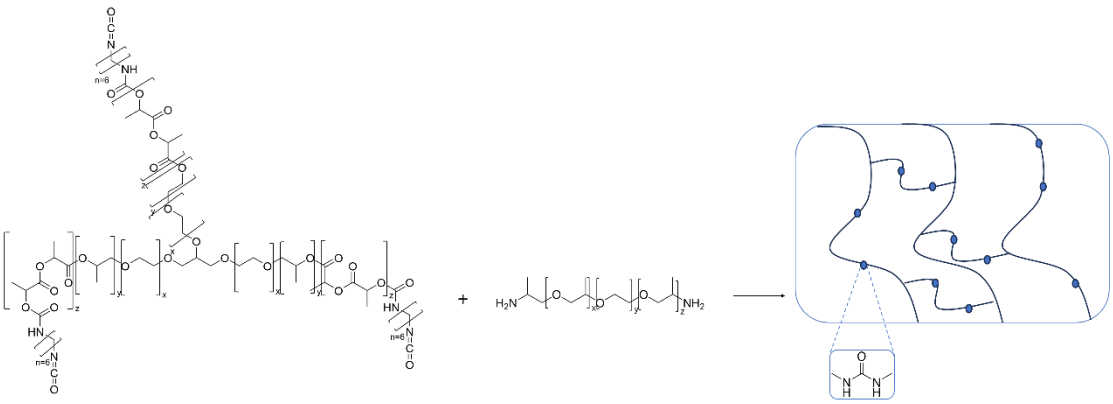

Figure 104 Basic crosslinking reaction of the identified suitable approach HYGEL-3. **Prepolymer-x** contains in addition to EO and PO units dilactide units in its backbone to implement degradable sites. X stands for number 2-5. By crosslinking with **Jeffamine ED2003**, **network-3** is obtained with urea groups as crosslinks.

Degradability was implemented into the prepolymer backbone *via* co-polymerization of EO/PO and dilactide units during the polyol synthesis as demonstrated in chapter 4.2.3 *via* pH measurements of the degradation process and *via* ^{13}C NMR of degradation products.

The initial reaction of a prepolymer with the chosen crosslinker **Jeffamine ED2003** yielded an alkaline hydrogel. Using buffering substances like acetic acid/acetate buffer or HCl, in a concentration that 65-85mol.% NH_2 groups are left unprotonated, hydrogels comprise neutral to slightly acidic pH values which are suitable for the targeted application. This concept neglected a buffering effect coming from the tissue itself, resulting most probably in a lower degree of crosslinks in the networks as a result of a higher protonation degree of NH_2 groups, as demonstrated *via* pH measurements. As a result, curing is hindered and the hydrogel did not adhere to

the surface of the organ. By reducing the buffering effect to 85mol.% free NH_2 groups in addition with a 20mol.% NCO excess, the hydrogel cures and adheres to the organ surfaces.

A DoE was conducted to investigate the structure activity relationship of different parameters within the hydrogel formulation. Factors in the formulation with the highest impact have been identified and are presented in Figure 105. The analyzed responses illustrate the requirement profile for the targeted application as adhesion prophylaxis.

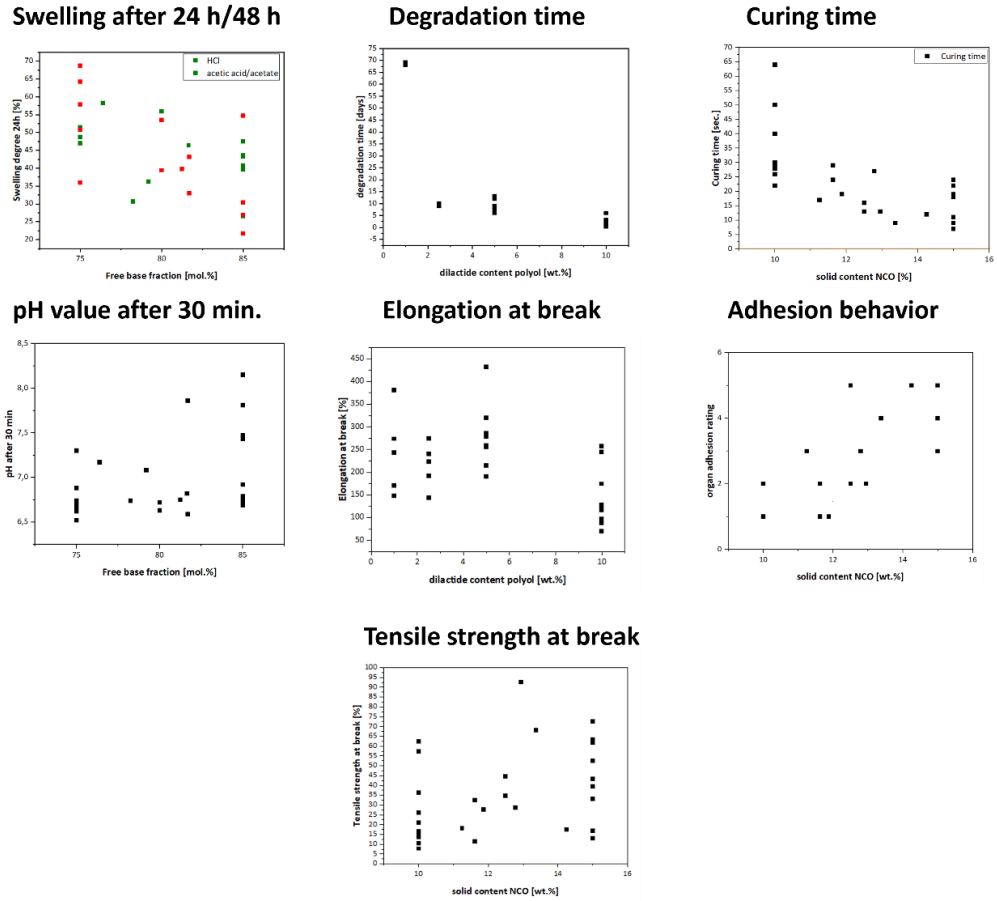

Figure 105 Summary of the DoE. Each response as a function of the identified formulation factor with the highest impact.

A highlight of the DoE was the identification of the solid content as a crucial parameter to enhance adhesion on the organ surface. Without employing the DoE approach, this effect could have been easily overseen. Herein, it becomes evident that formulations with a solid content of the NCO component ≥13.38wt.-% exhibit favorable adhesion to the organ surface upon application. As a consequence of the DoE, a final hydrogel formulation was identified, which was characterized in detail in chapter 4.2.5 concerning the NCO conversion, hydrolytic degradation, viscoelastic properties, mechanical properties and biochemical characterization. Herein, the application test for cytotoxicity as an indicator for biocompatibility was conducted, demonstrating that the hydrogel was identified as non-cytotoxic. An additional key milestone were the results of cell adhesion and cell migration, showing that cells do not migrate through the polymeric network. Thus, it was deducted that the hydrogel could serve as a potential adhesion barrier, maintaining this effect for a minimum of 7 days. Degradation experiments have been prepared

to analyze the resulting molecular weight between two crosslinks as a function of time, and moreover, the resulting mesh size, exhibiting that the experimental determination of M_c and cell migration application tests with M_c as a subordinate parameter corroborate each other. In summary, the mesh size calculations and the cell migration experiment consistently demonstrated that the polymeric network comprises a mesh size significantly smaller than the dimensions of a cell (~10 nm vs. ~10,000 nm). Consequently, the network should act as an effective barrier, preventing cellular migration into the material for at least 7 days, as illustrated in Figure 106.

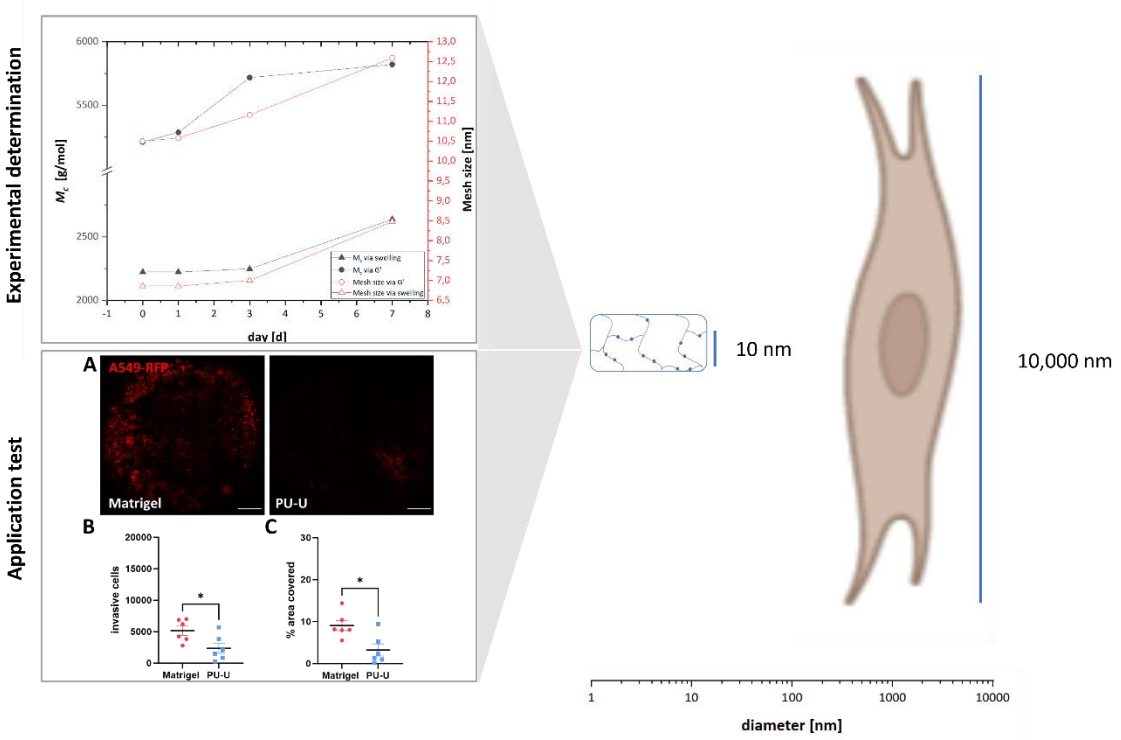

Figure 106 Determination of the mesh size and corroborative application test thereof. Above: The experimental determination of M_c and the subsequent calculations of mesh size revealed that the mesh size of the polymeric network is approximately by factor 10^3 smaller than the size of a typical cell. Below: The application tests, involving cell migration experiments into the polymeric network, confirmed the barrier effect for cells. This barrier effect was maintained for a minimum period of 7 days, indicating that the polymeric network effectively prevented cellular infiltration during this timeframe. Fibroblast illustration was taken from BioRender.

Moreover, the hydrogel formulation was adapted for the utilization of CO_2 as a carrier gas by a substitution of the acidic buffering component with NaOH, which facilitated the obtainment of pH neutral to slightly acidic hydrogels. As a result, two final formulations were achieved, as illustrated in Figure 107. In laparoscopic surgeries CO_2 is used exclusively since it is reported to reduce the formation of embolism. A formulation for the use as an adhesion prophylaxis is therefore restricted to the use of CO_2 as a carrier gas.

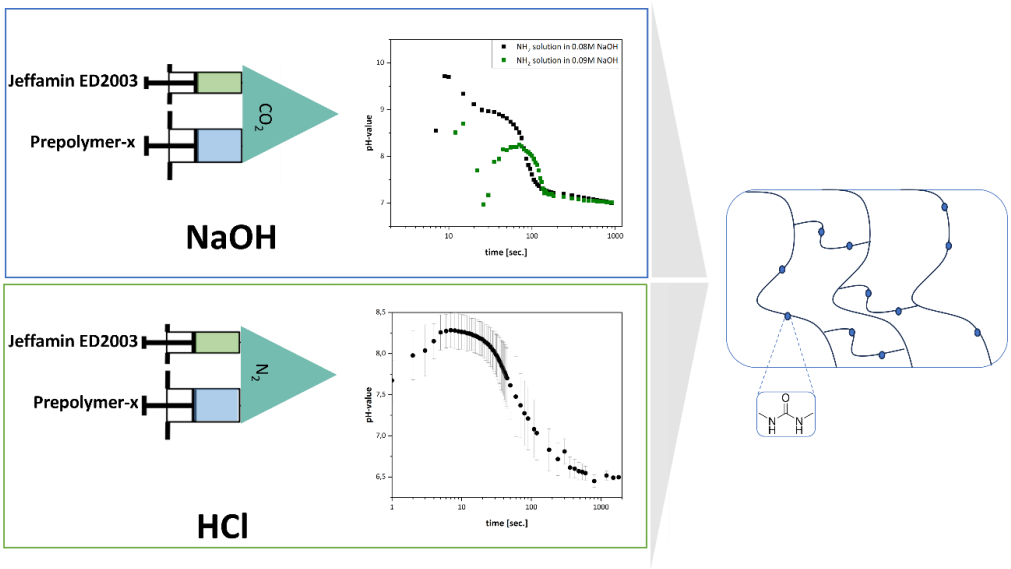

Figure 107 Hydrogel formulation for different carrier gases. Above: formulation adapted to the use of CO_2 as a carrier gas, leading to pH neutral PU-U-hydrogels. Below: formulation adapted to the use with inert gases like N_2 or compressed air, leading to pH neutral to slightly acidic PU-U-hydrogels.

The adapted hydrogel formulation, designed for the use with CO_2 as a carrier gas, was evaluated in an *in vivo* proof of concept study. Two major problems were identified: 1.) The hydrogel network exhibited an accelerated degradation rate *in vivo*, likely occurring within less than 7 days. This rapid degradation probably led to the formation of postoperative adhesions. 2.) Unequal mixing of the NCO and NH_2 components in the spray applicator, as demonstrated through indicator experiments with phenolphthalein. The system was adapted and subsequently analyzed in a second *in vivo* study, focusing exclusively on biocompatibility. Herein, the formulation for CO_2 and the formulation for inert gases have been investigated by reactive spraying and *via* implantation of pre-hardened hydrogels. Results indicate a lack of biocompatibility in all hydrogel formulations irrespective of the carrier gas and the application technique. Later investigations indicate a non-biocompatibility likely caused by toxicological potential of degradation products. The results indicate a non-conformability of the developed degradable hydrogels for implantation. A brief summary from the obtained macroscopic results of the *in vivo* biocompatibility and respective cytotoxicity analyses is presented in Figure 108.

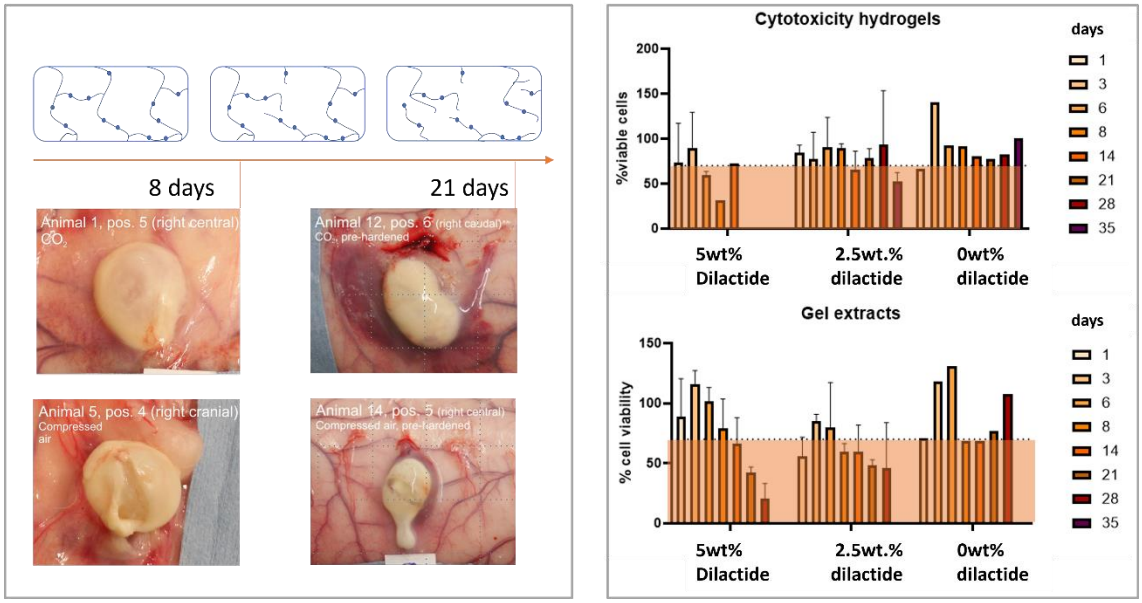

Figure 108 Illustration of toxicological findings of the hydrogel system. Left: macroscopic results *in vivo* after 8 days and 21 days. Right: cytotoxic investigation of degraded hydrogels as such and of degradation products containing extracts thereof, indicating a potential cytotoxic effect at day 8 in 2.5wt.-% dilactide, gel extracts.

However, in this research work a fast room temperature curable 2K formulation was developed which features all requirements for such a sensitive application, which addresses *viscoelastic properties*, *mechanical properties*, (limited) *biocompatibility* and *degradability*. The obtained fast cured hydrogel network serves *in vitro* as an adhesion prophylaxis as shown in experimental determination of the mesh size and in experiments with cells but have been examined less effectively *in vivo* due to accelerated degradation. Unfortunately, cytotoxicity of degradation products indicates toxicological potential thereof, which was confirmed by the *in vivo* studies. The detailed mechanism which induces toxicological reactions *in vivo* needs to be addressed in a detailed evaluation study of degradation products. Hereby information on toxicological substances could be obtained. A deeper analysis of the degradation products needs to be conducted to understand the mechanisms behind indicated cytotoxicity. Therefore, gel extracts should be analyzed regarding their chemical structure. With these information other degradable groups could be incorporated into the polymer backbone to avoid the formation of potential toxic degradation products.

The non-degradable hydrogel system, using **prepolymer-1**, could be of interest for medical application wherein degradation is not required, like medical device coating for long term application[223] or tissue engineering.[224] The suitability of the hydrogel system for various applications requires a more comprehensive evaluation. Properties, useful for a potential application, of the non-degradable hydrogel system, which are tunable by parameters within the formulation were: viscosity of single solutions, curing time, mechanical properties (elongation at break, tensile strength at break), pH values of the resulting hydrogel, swelling behavior and adhesion to organ substrate, investigated *via* the DoE concept transferable on **prepolymer-1**.

6 Experimental Section

6.1 List of Chemicals

The raw materials used for the experimental part of this research work are listed in Table 52.

Table 52 Raw materials used for the experimental section.

Name	CAS	Purity	Supplier
Jeffamines *f>1*			
Jeffamine ED2003	65605-36-9	n.d.	Huntsman
Jeffamine ED900	65605-36-9	n.d.	Huntsman
Jeffamine ED600	65605-36-9	n.d.	Huntsman
Jeffamine EDR148	929-59-9	n.d.	Huntsman
Jeffamine T403	39423-51-3	n.d.	Huntsman
NCO inactivation agents			
Amino acetaldehyde di-ethyl acetal	645-36-3	98%	Sigma-Aldrich
Geniosil XL926	26495-91-0	n.d.	Wacker Chemie AG
Polyether 25	-	n.d.	Covestro Deutschland AG
Polyether 34	-	n.d.	Covestro Deutschland AG
Jeffamine M2005	83713-01-3	n.d.	Huntsman
Diisocyanates			
Hexamethylene diisocya-nate	822-06-0	n.d.	Covestro Deutschland AG
Starters and monomers for polyol synthesis			
Polyether 1	-	n.d.	Covestro Deutschland AG
Polyether 2	-	n.d.	Covestro Deutschland AG
Ethylene oxide	75-21-8	n.d.	GHC Gerling Holz
Propylene oxide	75-56-9	n.d.	Chemogas
Dilactide	95-96-5	>99%	Sigma-Aldrich
Polyols			
Polyether 3	-	n.d.	Covestro Deutschland AG
Polyether-thermo	-	n.d.	Covestro Deutschland AG
Catalysts			
dibutyl phosphate	107-66-4	≥ 97.0%	Sigma-Aldrich
Buffer agents			
Hydrochloric acid 0.1M	7647-01-0	n.d.	Honeywell Fluka
Sodium acetate	127-09-3	ACS reagent, ≥99.0%	Sigma-Aldrich
Acetic acid, glacial	64-19-7	ACS reagent, ≥99.7%	Sigma-Aldrich
Sodium chloride	7647-14-5	+80 mesh, ≥98%	Sigma-Aldrich
Potassium chloride	7447-40-7	ACS reagent, 99.0-100.5%	Sigma-Aldrich
Potassium phosphate monobasic, anhydrous	7778-77-0	ACS reagent, ≥99.0%	Sigma-Aldrich
di-Sodium hydrogen phosphate heptahydrate	7782-85-6	EMPROVE® EXPERT, DAC, USP	Merck
Sodium dihydrogen phos-phate monohydrate	10049-21-5	EMPROVE® EXPERT, BP, USP	Merck
Sodium hydroxide 0.1M	1310-73-2	n.d.	Honeywell Fluka

6.2 Characterization Methods

Hydroxy Value

The hydroxy number (OHZ) was determined in accordance with DIN EN ISO 4629-2. This method involves the acetylation of all hydroxy groups present in the sample with acetic anhydride, followed by titration with a potassium hydroxide (KOH) solution to hydrolyze the acetylated OH groups, thereby regenerating free OH groups. The OHZ is expressed in units of [mg KOH/1 g product]. The OHZ is calculated according to equation 6.2.1.

$$OHZ = \frac{(V_0 - V_{sample}) * c_{KOH} * 56.1}{m_{sample}} + \mathrm{AV} \tag{6.2.1}$$

Where V_o being the volume of KOH solution for the blank sample, V_{sample} being the volume of KOH solution for the sample, c_{KOH} being the concentration of the KOH solution in mol/L, 56.1 being the factor for converting mL KOH to mg (molar mass KOH), $m_{sample}$is the mass of the sample and AV being the acidic value.

The eq. weight of the OH-group containing substance can be calculated according to equation 6.2.2.

$$\mathrm{eq.}\, weight\ R-OH = \frac{56{,}1 * 1000}{OHZ} \tag{6.2.2}$$

Total Acidic Values

The total acidic value (TAV) was determined according to DIN EN ISO 2114:2000. A sample was weighed into an Erlenmeyer flask. 60 mL of a solvent mixture containing pyridine, methyl ethyl ketone and water were added and the sample was stirred until it was fully dissolved and for additional 20 min. The solution is titrated with a KOH solution (0.1M) either by potentiometric determination or by colorimetric methods. TAV is calculated according to equation 6.2.3:

$$TAV = \frac{56{,}1 * (V_1 - V_2) * c}{m_1} \tag{6.2.3}$$

Wherein 56.1 is a constant representative for the molar mass KOH in g=mol, m_1 being the mass of the analyzed sample, V_1 is the consumption of KOH solution to neutralize the resin solution in mL, V_2 is the consumption of KOH solution in the blank test in mL, c is the concentration of the KOH solution in mol/L.

Amine Value

The amine value (*AV*) represents the quantity of KOH in mg equivalent to one gram of a substance and was determined according to DIN 16945. A sample of 0.5 g is weighed into a conical flask and dissolved in a defined amount of acetic acid. Titration was conducted with 0.1mol/L

perchloric acid ($HClO_4$) by using colorimetric methods. *A* was calculated according to equation 6.2.4:

$$AV = \frac{a * F * 5{,}6}{m_{sample}} \tag{6.2.4}$$

Wherein *a* is the volume of $HClO_4$ used in mL, *F* is the titrimetric factor of $HClO_4$, m_{sample} is the initial sample mass in g.

Isocyanate Content via Titration

The isocyanate content was determined according to DIN EN ISO 14896. Isocyanate groups react with a defined excess of dibutyl amine. The amount of unreacted amine can be determined *via* titration with hydrochloric acid, enabling the back-calculation of the isocyanate content. For this purpose, a defined amount of prepolymer was dissolved in acetone. A prepolymer sample of 1-5 g was dissolved in 80-100 mL of acetone and stirred until fully solved. 10 mL of 1M Dibutyl amine (DBA) in Xylol were added and the solution was stirred for a few more seconds. The un-reacted DBA was titrated with a 1M HCl solution. The NCO content was calculated according to the following equation:

$$NCO\ content_{\%} = \frac{(V_0 - V_1) * 4{,}2}{m_{sample}} * 100\% \tag{6.2.5}$$

The eq. weight was determined according to the following equation:

$$eq.weight = \frac{42 * 100}{NCO\ content\ \%} \tag{6.2.6}$$

Residual Monomer Content

The content of monomeric diisocyanate in isocyanate resins is determined according to DIN EN ISO 10283 by gas chromatography using tetradecane as an internal standard.

Calculation of the content of monomeric diisocyanate $\omega_{DI}$was conducted from the peak areas, using the following equation:

$$\omega_{DI} = \frac{m_1 * A_2 * f}{m_2 * A_1} \tag{6.2.7}$$

Wherein m_1 is the mass of the internal standard in the sample solution, m_2 is the mass of the sample, A_2 is the peak area of the monomeric diisocyanate contained in the sample solution, A_1 is the peak area of the internal standard contained in the sample solution.

The mean value from two determinations whose results (mean values) were corrected with the mean value of the respective calculated area correction factor *f*.

Gel Permeation Chromatography

Gel permeation chromatography (GPC) measurements were performed on four PSS SDV analytical columns (2 x 50 Å, 5 µm; 2 x 100 Å, 5 µm) using an Agilent HP 1100 series pump and an

Agilent 1200 series UV detector (230 nm) with tetrahydrofuran as elution solvent at 35 °C and a flow of 0.6 mL/min. The molar masses were determined by comparing the elution volume to a standard calibration based on polystyrene.

Nuclear Magnetic Resonance Spectroscopy

^{1}H NMR spectra (600 MHz) were recorded in d_6DMSO, $CDCl_3$ or D_2O using a Bruker AV III HD 600.

^{13}C NMR spectra (151 MHz) were recorded in d_6DMSO, $CDCl_3$ or D_2O using a Bruker AV III HD 600.

Rheology/ Viscosity

The viscosity measurements of the raw materials (pure and/or solved in aqueous systems) were conducted according to DIN EN ISO 3219. A rotational viscometer from Anton Paar (MCR301) was used for the determination. Measurements were carried out using a cone-plate geometry (α=5°) configuration with a quartz glass plate and a disposable aluminum stamp (*d*=25 mm).

Method A

The temperature was set to a defined value and waited until temperature consistency. The shear rate γ was set to 50 sec.$^{-1}$, constantly. A sample was applied on the surface of the heater and measurements were started immediately and were carried out for 40 sec. with 2 sec. between each data point. 20 single values were recorded while the last point was chosen as reference for indeed viscosity.

Method B

A temperature gradient was applied from 0-37°C with a heating rate of 1°C/min. The shear rate γ was set at 250 sec.$^{-1}$, constantly.

Preparation of Single Components and Formulations

Example for provision of the amine component (Table 53, formulation 14):

For a preparation of 12.5 mL of amine solution which was used in a ratio of 1/1.2 (NH_2/NCO groups), 1.82 g of **Jeffamine ED2003** were weighed into a flask and added up to 12.50 g with aqueous HCl (0.0260M). Afterwards, the solution was stirred and then filled into a cylinder of a spray applicator.

Example for provision of the isocyanate component:

3.75 g of **prepolymer-4** were weighed into a mixing cup and filled up to 25.00 g with demineralized H_2O. The solution was mixed for 30 seconds. Afterwards the solution was filled into a cylinder of a spray applicator and the spray experiments were conducted immediately.

Table 53 Composition of isocyanate and amine solutions used for the preparation of different hydrogels. Functionalities of the prepolymer and amine are denoted as "*f* (prep.)" and "*f* (amine)", respectively. Viscosity is stated in millipascal*seconds and is listed as "[mPa*s]". The solid content of the used Isocyanate or amine component is given in weight% and is stated as "[wt.-%]". The molar concentrations in mol/L of the basic and acidic fractions are denoted as "[M]".

	Isocyanate component				**Amine component (Jeffamine ED2003)**							
Formulation	Prepolymer used	*f* (prepolymer.)	Solid content of the prepared isocyanate solution [wt.-%]	Viscosity of the obtained isocyanate solution at 21 °C [mPa*s]	Amine used	*f* (amine)	Solid content of the prepared amine solution [wt.-%]	Buffer/ Acid type used as solvent	Concentration of basic fraction in the buffer [M]	Concentration of acidic fraction in the buffer [M]	Viscosity of the obtained amine solution at 23 °C [mPa*s]	Molar ratio NH_2/ NCO
1	1	>2	10.0	n.d.	Jeffamine ED2003	2	11.7	H_2O	-	-	2.53	1:1
2a	1	>2	10.0	3.48	Jeffamine ED2003	2	11.7	Phosphate buffer	0.006	0.006	n.d.	1:1
2b	1	>2	10.0	3.48	Jeffamine ED2003	2	11.7	Phosphate buffer	0.012	0.012	n.d.	1:1
2c	1	>2	10.0	3.48	Jeffamine ED2003	2	11.7	Phosphate buffer	0.017	0.017	2.69	1:1
2d	1	>2	10.0	3.48	Jeffamine ED2003	2	11.7	Phosphate buffer	0.029	0.029	3.22	1:1
2e	1	>2	10.0	3.48	Jeffamine ED2003	2	11.7	Phosphate buffer	0.041	0.041	3.68	1:1
2f	1	>2	10.0	3.48	Jeffamine ED2003	2	11.7	Phosphate buffer	0.046	0.046	n.d.	1:1
2g	1	>2	10.0	3.48	Jeffamine ED2003	2	11.7	Phosphate buffer	0.058	0.058	2.95	1:1
3a	1	>2	10.0	3.48	Jeffamine ED2003	2	11.7	Acetate buffer	0.017	0.017	3.07	1:1

3b	1	>2	10.0	3.48	Jeffamine ED2003	2	11.7	Acetate buffer	0.029	0.029	4.22	1:1
3c	1	>2	10.0	3.48	Jeffamine ED2003	2	11.7	Acetate buffer	0.041	0.041	3.79	1:1
3d	1	>2	10.0	3.48	Jeffamine ED2003	2	11.7	Acetate buffer	0.067	0.067	2.83	1:1
3e	1	>2	10.0	3.48	Jeffamine ED2003	2	11.7	Acetate buffer	0.075	0.075	n.d.	1:1
3f	1	>2	10.0	3.48	Jeffamine ED2003	2	11.7	Acetate buffer	0.087	0.087	n.d.	1:1
3g	1	>2	10.0	3.48	Jeffamine ED2003	2	11.7	Acetate buffer	0.100	0.100	n.d.	1:1
4a	1	>2	10.0	3.48	Jeffamine ED2003	2	11.7	HCl solution	-	0.005775	2.11	1:1
4b	1	>2	10.0	3.48	Jeffamine ED2003	2	11.7	HCl solution	-	0.0173	2.35	1:1
4c	1	>2	10.0	3.48	Jeffamine ED2003	2	11.7	HCl solution	-	0.02882	2.09	1:1
4d	1	>2	10.0	3.48	Jeffamine ED2003	2	11.7	HCl solution	-	0.0404	2.53	1:1
5	1	>2	12.0	n.d.	Jeffamine ED2003	2	11.7	Acetate	0.41	0.41	3.79	1:1.2
6	5	>2	11.3	4.9	Jeffamine ED2003	2	12.2	Acetate	0.0299	0,0299	3.04	1:1.2
6b	5	>2	10.0	n.d.	Jeffamine ED2003	2	12.6	H_2O	-	-	n.d.	1:1
7	5	>2	15.0	4.35	Jeffamine ED2003	2	15.7	HCl	-	0.0276	3.58	1:1.2
8	5	>2	15.0	4.35	Jeffamine ED2003	2	15.7	Acetate	0.0283	0.0283	4.64	1:1.2

9	5	>2	15.0	4.35	Jeffamine ED2003	2	15.7	HCl	-	0.0386	3.69	1:1.2
10	4	>2	11.6	6.56	Jeffamine ED2003	2	11.3	HCl	-	0.0276	3.54	1:1.2
11	4	>2	15.0	9.08	Jeffamine ED2003	2	14.5	HCl	-	0.0260	2.74	1:1.2
12	5	>2	15.0	4.35	Jeffamine ED2003	2	15.7	HCl	-	0.0213	3.82	1:1.2
13	4	>2	13.0	7.48	Jeffamine ED2003	2	12.5	Acetate	0.0256	0.0256	2.34	1:1.2
14	4	>2	15.0	9.08	Jeffamine ED2003	2	14.5	HCl	-	0.0260	3.55	1:1.2
15	5	>2	10.0	3.30	Jeffamine ED2003	2	10.5	HCl	-	0.0257	2.65	1:1.2
16	5	>2	10.0	3.30	Jeffamine ED2003	2	10.5	Acetate	0.0154	0.0154	3.37	1:1.2
17	4	>2	15.0	9.08	Jeffamine ED2003	2	14.5	Acetate	0.0356	0.0356	4.65	1:1.2
18	5	>2	12.8	4.48	Jeffamine ED2003	2	13.4	Acetate	0.0197	0.0197	3.47	1:1.2
19	4	>2	13.4	8.51	Jeffamine ED2003	2	13.00	Acetate	0.0191	0.0191	2.47	1:1.2
20	5	>2	14.3	6.82	Jeffamine ED2003	2	15.0	Acetate	0.0346	0.0346	4.85	1:1.2
21	2	>2	10.0	3.80	Jeffamine ED2003	2	10.7	HCl	-	0.02609	2.64	1:1.2
22	3	>2	12.5	4.82	Jeffamine ED2003	2	13.5	HCl	-	0.01987	3.26	1:1.2
23	3	>2	10.0	3.11	Jeffamine ED2003	2	10.8	Acetate	0.02649	0.02649	2.42	1:1.2

24	3	>2	11.3	4.51	Jeffamine ED2003	2	12.2	Acetate	0.02384	0.02384	2.57	1:1.2
25	2	>2	15.0	7.21	Jeffamine ED2003	2	16.0	Acetate	0.02348	0.02348	4.88	1:1.2
26	3	>2	10.0	3.11	Jeffamine ED2003	2	10.8	Acetate	0.02649	0.02649	2.35	1:1.2
27	3	>2	10.0	3.11	Jeffamine ED2003	2	10.8	HCl	-	0.02119	2.57	1:1.2
28	2	>2	15.0	7.21	Jeffamine ED2003	2	16.0	Acetate	0.02348	0.02348	4.12	1:1.2
29	2	>2	12.5	4.87	Jeffamine ED2003	2	13.3	HCl	-	0.01957	3.19	1:1.2
30	2	>2	15.0	7.21	Jeffamine ED2003	2	16.0	HCl	-	0.03914	3.68	1:1.2
31	2	>2	10.0	3.80	Jeffamine ED2003	2	10.7	HCl	-	0.02087	2.68	1:1.2
32	4	>2	15.0	9.08	Jeffamine ED2003	2	15.5	Acetate	0.0	0.0	2.81	1:1.2
1-CO_2	1	>2	15.0	8.39	Jeffamine ED2003	2	15.5	NaOH	0.1	-	n.d.	1:1.2
2-CO_2	1	>2	15.0	8.39	Jeffamine ED2003	2	15.5	NaOH	0.09	-	n.d.	1:1.2
3-CO_2	1	>2	15.0	8.39	Jeffamine ED2003	2	15.5	NaOH	0.08	-	n.d.	1:1.2
4-CO_2	1	>2	15.0	8.39	Jeffamine ED2003	2	15.5	NaOH	0.06	-	n.d.	1:1.2
5-CO_2	4	>2	15.0	9.04	Jeffamine ED2003	2	15.5	NaOH	0.06	-	n.d.	1:1.2
6-CO_2	3	>2	15.0	8.77	Jeffamine ED2003	2	16.0	NaOH	0.02	-	n.d.	1:1.2

Preparation of Hydrogels

The preparation of hydrogels in this research work can be divided into sprayed and mixed hydrogels. Since there are many parameters in the spraying process, three different procedures were used for the spray experiment.

Preparation of hydrogels via 2K Mixpack with a static mixer

Two cylinders were used for the application. One with a volume of 25 mL (Isocyanate component) and one with a volume of 12.5 mL (amine component). For the mixing process a static mixer MAH 4.0-17S from AdChem was used. Both components were dispensed in a constant volume ratio of 2:1 (isocyanate:amine) within 25 seconds.

Preparation of hydrogels via spray application (spray applicator 1)

Two syringes were used for the application. One with a volume of 10 mL (isocyanate component) and one with a volume of 5 mL (amine component). The spray experiment was conducted with a carrier gas (N_2 or compressed air, or CO_2 depending on the formulation) at a volume flow of 6.0 NL/min. which was adjusted with a flowmeter. All single components were obtained from Erbe Elektromedizin GmbH.

Preparation of hydrogels via spray application (spray applicator 2) with nitrogen or compressed air as carrier gas

Two syringes were used for the application. One with a volume of 10 mL (Isocyanate component) and one with a volume of 5 mL (amine component). The spray experiment were conducted with a carrier gas (N_2 or compressed air, or CO_2 depending on the formulation) at a volume flow of 2.0-2.5 NL/min. which was adjusted with a flowmeter. All single components were obtained from Erbe Elektromedizin GmbH.

FT-IR measurements

FT-IR/ATR spectroscopy was used for the determination of NCO conversion during the curing reaction. Experiments were carried out on a Bruker Vertex 70 with an attenuated total reflection (ATR) zinc selenide crystal. For all spectra a baseline correction (rubber band method with anchor points at 983, 1011, 1192, 1830, 2620 3984 cm^{-1}) was performed, and a normalization method was applied using the peak area between 3050cm^{-1} and 3750cm^{-1}.

Dynamic Light Scattering

Particle size distributions were obtained *via* DLS using a Malvern Zetasizer Nano-S at 90° angle. One drop of a 20wt.-% solution of analyte was diluted in a cuvette with dH_2O and was measured from 20-60 sec. after sample preparation. The respective temperature was held for 120 sec. before measurements started, which were carried out for 80 sec. Viscosity of water was set to 1.5678 mPa*s for 4°C measurements and to 0.6864 mPa*s for 37°C measurements.

Lyophilisation of raw materials/hydrogels

Lyophilisation was conducted using a freeze dryer Alpha 1-2 LDplus from Christ. The drying process was conducted at 0.63 mbar and -70°C for 50 h.

Tensile testing

Tensile tests were carried out using a Zwick Retro with a 2 kN load cell, at a test speed of 200 mm/min and a pre-load of 0.002 N/mm² at 23.6-25.3 °C and 47.9-55.5% relative humidity. Samples were punched out from fresh prepared cured hydrogels and a four-fold measurement was performed.

X-Ray Diffraction Measurements

XRD measurements were carried out on a Bruker D2 Phaser 2nd Gen, equipped with a copper tube (wavelength 1.54184 Å), fixed slit 0.4 mm, 4° grid and a Lynx 1D Modus detector. Using the following settings: beam angle 5° to 40°, Rotation 10 U/min, step size 0.024°, time per step 0.3 sec., scan Type: coupled two Theta/Theta, scan modus: continuous PSD fast. The evaluation of chromatograms was carried out in Profex. Obtained raw data were illustrated using origin.

Dynamic Mechanical Analysis

Dynamic mechanical analyses (DMA) measurements were performed on an Anton Paar MCR 702 space at a frequency of 1 Hz and a temperature of 25°C (tensile experiment)/37°C (compression experiment).

Tensile Experiments:

Measurements were carried out in an amplitude sweep experiment from 0.1% to 10.0% strain in a time interval of 3.68 min.

Compression Experiments:

Measurements were carried out in a force sweep experiment in a range of 0.04 N to 20.3 N in a time interval of 5.9 min. Hydrogels were measured in hydrated state with 15wt.-% solid content.

pH Values

pH measurements over the time were conducted by spraying both components into a beaker with a pH electrode inside. Measurements were conducted for 30 minutes.

For single measurements pH paper stripes were used.

Adhesion to Organ Tissue

A kidney (pig) preheated to 37 °C in a newborn incubator *Caleo* from Dräger with a relative humidity of 70-80%, was used as a substrate for the application. Hydrogels were prepared as described above and applied on the surface of the kidney inside the newborn incubator. A rating

system as described in Table 54 and was used to evaluate the adhesion of each formulation to the kidney.

Table 54 Explanation of an implemented rating system to determine the adhesion of the different hydrogel formulations to tissue samples (porcine kidneys) in a quantitative way.

Rating Score	Adhesion Properties
1	No adhesion
2	Very poor adhesion (hydrogel can be removed without applying mechanical force, e.g., by movement of the kidney)
3	Poor adhesion (hydrogel can be removed by applying light mechanical force, like wiping over the surface with moistened gloves)
4	Good adhesion (hydrogel can be removed by applying stronger mechanical force, like pulling or rubbing)
5	Very good adhesion (hydrogel cannot be removed as a whole by applying strong mechanical force, like pulling or rubbing)

Swelling Testing

The swelling tests were conducted in phosphate buffered saline (PBS) solution. Samples with a weight of 2-5 g were incubated at 37°C in 30 mL PBS each. Swelling was calculated according to equation 6.2.8.

$$Swelling\ degree = \frac{m_{swollen}}{m_{swollen} - m_{initial}} * 100\% \quad (6.2.8)$$

Wherein $m_{swollen}$ is the weight of the swollen sample at a specified point in time and $m_{intital}$ is the weight of the prepared hydrogel sample before swelling.

Degradation Testing

For the determination of the degradation rate hydrogels were prepared as described above but dispensed into 3.9 mL PE molds (thick end of 2 mL type pipettes, V_{total}=5.9 mL by VITLAB®). After curing for 5 min, they were weighed and transferred into a 25 mL glass bottle. 22 mL PBS-solution (pH=7.33) were added and the glass bottles were stored at 37 °C in an incubator with shaking speed of 60 rpm. Every 24 h the hydrogel samples were taken out of the buffer solution to record the weight. Afterwards, the old buffer solution was replaced with fresh buffer solution and the samples were again stored in the incubator. This procedure was repeated every 24 h and the samples were incubated until they were fully dissolved in the medium. The point at which the hydrogels could not be removed from the glass bottles without disintegration into smaller gel particles is described as “Loss of mechanical properties”. Without wishing to be bound by theory it is assumed that there would be no barrier effect of the hydrogel anymore, so this point in time is regarded as an end point.

6.3 Experimental Details for Chapter 4.1

Synthesis of Prepolymer-1

592.00 g of HDI and 0.65 g dibutyl phosphate (DBP) were weighed into a three-neck flask and heated up to 80 °C under constant stirring. 697.50 g of polyether 3 (*f* =3, OHZ=37, Starter (Glycerol): 1.96%; EO: 70.89%, PO: 26.43%) , were added dropwise within 2 hours. After the addition was completed, the reaction was stirred for one additional hour until the residual NCO content reached 21.46%. The reaction mixture was allowed to cool down under constant stirring. Unreacted monomers were removed by short path evaporation (SPE) (p=0.1 mbar; $T_{pre\text{-}evaporator}$=130 °C, $T_{main\text{-}evaporator}$=120 °C) and an NCO-terminated prepolymer with NCO-content=2.49wt.-% was obtained.

Residual Monomer content: 0.03wt.-%

NCO content: 2.49wt.-%

Viscosity: 3950 mPa*s, 23 °C

Average eq. weight: 1686.75 g/eq.

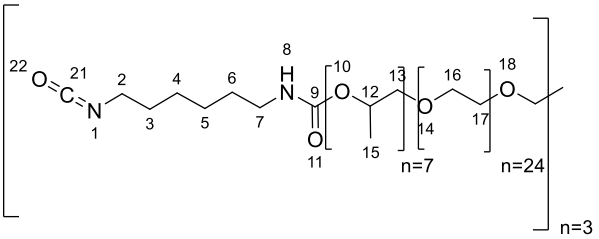

GPC: M_n=7,402 g/mol; M_w= 13,237 g/mol; Đ=1.79

^{1}H NMR (600 MHz, DMSO) δ 7.30 – 6.88 (m, 1H, H-8), 4.04 (t, *J* = 4.7 Hz, 2H, H-2), 3.70 – 3.23 (m, 127H, H-12, H-13, H-16, H-17), 2.96 (q, *J* = 6.7 Hz, 2H, H-7), 1.54 (p, *J* = 6.7 Hz, 2H, H-3), 1.39 (h, *J* = 7.6 Hz, 2H, H-6), 1.34 – 1.21 (m, 5H, H-4, H-5), 1.05 (d, *J* = 6.3 Hz, 21H, H-15).

Synthesis of raw materials used for HYGEL-1

Synthesis of Amine-1

20.0 g of prepolymer-1 were weighed into a beaker and filled off with 980.0 g distilled water. The mixture was stirred for 3 h at RT and afterwards concentrated using a rotary evaporator (~100 mbar, 60°C). The sediment was filtered of and the supernatant was transferred into 20 mL vessels for freeze drying, which was conducted as described in 6.2.

Viscosity: 527,000 mPa*s

AV= 12.7 mg KOH/g

Eq. weight= 4417.3 g/eq.

Synthesis of $(EtOR)_2$-2

The isocyanate content of pre-prepared prepolymer-1 was determined at 2.43%. 328.9 g of prepolymer-1 were weighed into a flask and stirred at RT for 1 h under nitrogen atmosphere. 24.0 g (=0.95 eq.) of amino acetaldehyde were added over 60 min. Temperature is monitored, due to the exothermal reaction behavior. The reaction was monitored *via* FT-IR by tracking of characteristic NCO band at 2265 cm^{-1}. As long as NCO band is visible 0.24 g (0.01 eq.) amino acetaldehyde was added and stirred for an additional 10 min. This procedure was repeated in 0.01 eq. steps until no NCO signal was detected *via* FT-IR measurements at 2265 cm^{-1}.

Viscosity: 18,706 mPa*s

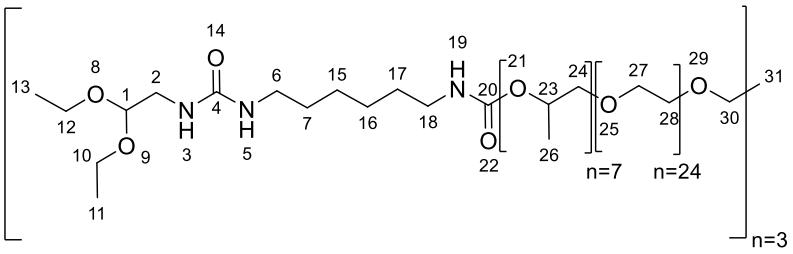

^{1}H NMR (600 MHz, DMSO) δ 7.20 – 6.99 (m, 1H, H-19), 5.93 (t, *J* = 5.7 Hz, 1H, H-5), 5.70 (t, *J* = 6.0 Hz, 1H, H-3), 4.39 (t, *J* = 5.4 Hz, 1H, H-1), 4.04 (t, *J* = 4.7 Hz, 2H, H-6), 3.70 – 3.25 (m, 133H, H-2, H-23, H-24, H-27, -28), 3.06 (t, *J* = 5.7 Hz, 2H, H-10), 3.00 – 2.92 (m, 4H, H-12, H-18), 1.44 – 1.30 (m, 5H, H-7, H-17), 1.24 (h, *J* = 4.5 Hz, 4H, H-15, H-16), 1.12 (t, *J* = 7.0 Hz, 6H, H-11, H-13), 1.05 (d, *J* = 6.3 Hz, 21H, H-26).

GPC: M_n=6,247 g/mol; M_w=10,253 g/mol; Đ=1.64

Synthesis of COO-2

30.3 g of $(EtOR)_2$-2 were weighed into a 250 mL flask with a stir bar. 27.1 mL of 0.1M (=0.1N) aqueous HCl solution is added and the solution is stirred at room temperature for 4 hours. Afterwards the reaction was neutralized using 0.1M aqueous NaOH solution. Neutralization is controlled by pH measurements (paper stripes). The aqueous reaction mixture was freeze dried to remove H_2O and obtain COO-2 as a viscous resin. COO-2 was used without further purification.

Viscosity: 7,667.3 mPa*s

GPC: M_n=3,579 g/mol; M_w= 6,270 g/mol; Đ=1.75

^{1}H NMR (600 MHz, DMSO) δ 9.88 (s, 1H, H-1), 7.22 – 6.96 (m, 1H, H-19), 6.41 (t, *J* = 2.4 Hz, 1H, H-5), 6.30 (t, *J* = 2.6 Hz, 1H, H-3), 4.04 (t, *J* = 4.7 Hz, 1H, H-6), 3.75 – 3.27 (m, 141H, H-2, H-23, H-24, H-27, H-28), 3.18 – 2.86 (m, 2H,H-18), 1.54 (t, *J* = 7.2 Hz, 2H, H-7), 1.37 (dp, *J* = 14.6, 6.4 Hz, 2H, H-17), 1.24 (tt, *J* = 16.6, 6.5 Hz, 4H, H-15, H-16), 1.15 – 1.10 (m, 1H, n.d.), 1.07 – 0.99 (m, 21H, H-26).

Gelation experiments of HYGEL-1

1.) First gelation tests were conducted by weighing 2.5 g of amine-1 into a 50 mL beaker and fill of with distilled water to 10.0 g to obtain a 10wt.-% solution. A 50% solution of aldehyde COO-1 was added dropwise. A gel was obtained within seconds (<60 sec.).

2.) A 25 mL solution of 9wt.-% amine-1 in water (=0.00051 eq. Amin) was prepared and stirred at RT. A solution of 12.5 mL of COO-1 in water was prepared (0.238 g COO-1-50wt.-%-solution ad 12.5 mL distilled H_2O (=0.0048 eq.) and transferred into a syringe. The solution of amine-1 was stirred while the solution of COO-1 was added dropwise. The reaction mixture turned slightly yellow after a few seconds without yielding a gel. A few drops HCl (0.1M) were added and the reaction mixture turned red while a gelation behavior was observed but did not yield a solid-like network

3.) A 16.6wt.-% solution of Jeffamine ED2003 in water was prepared and 10 mL of a 25wt.-% solution of COO-2 were added dropwise. After 72 h no visual gelation reaction could be observed

Synthesis of raw materials used for HYGEL-2

Synthesis of EtOSi-prepolymer-1

The isocyanate content of pre-prepared prepolymer-1 was determined at 2.43%. 484.7 g of pre-polymer-1 were weighed into a flask and stirred at RT for 1 h under nitrogen atmosphere. 73.28 g (=0.95 eq.) of Geniosil XL926 were added over 60 min. Temperature is monitored, due to the exothermal reaction behavior. The reaction as monitored *via* IR measurements by tracking of characteristic NCO band at 2265 cm^{-1}. As long as NCO band is visible 0.77 g (0.01 eq.) of Geniosil XL926 was added and stirred for an additional 10 min. This procedure was repeated in 0.01 eq. steps until no NCO signal was detected *via* FT-IR measurements.

GPC: M_n=7102 g/mol; Mw=14994 g/mol; Đ=2.11

Synthesis of raw materials used for HYGEL-4

Synthesis of Prepolymer-Thermo

500.00 g of HDI and 0.41 g DBP were weighed into a three-neck flask and heated up to 80 °C under constant stirring. 327.18 g of polyether-thermo (*f* =2, OHZ=29.1, Starter (propylene glycol): 1.22wt.-%; EO: 13.05wt.-%, PO: 85.23wt.-%), were added dropwise over a period of 2 hours. After the addition was completed, the reaction was stirred for one additional hour until the residual NCO content reached 18.43%. The reaction mixture was allowed to cool down under constant stirring. Unreacted monomers were removed by SPE (p=0.1 mbar; $T_{pre\text{-}evaporator}$=130 °C, $T_{main\text{-}evaporator}$=120 °C) and an NCO-terminated prepolymer with NCO-content=2.00wt.-% was obtained.

Residual Monomer content: 0.16wt.-%

NCO content: 2.00wt.-%

Viscosity: 2290.3 mPa*s, 23 °C

Average eq. weight: 2100 g/eq.

GPC: M_n=4098 g/mol; M_w=6906 g/mol; Đ=1.68

Synthesis of 809

The isocyanate content of pre-prepared prepolymer-1 was determined at 2.43%. 400 g of prepolymer-1 were weighed into a flask and stirred at RT for 1 h under nitrogen atmosphere. 456.7 g (=0.95 eq.) of Jeffamine M2005 were added over 60 min. Temperature was monitored as indicator for exothermal reaction behavior. The reaction was monitored *via* FT-IR measurements by tracking the characteristic NCO band at 2265 cm^{-1}. As long as NCO band is visible 4.8 g (0.01 eq.) of Jeffamine M2005 was added and stirred for additional 10 min. This procedure was repeated in 0.01 eq. steps until no NCO signal was detected *via* FT-IR measurements at 2265 cm^{-1}.

Viscosity: 3,253,300 mPa*s

GPC: M_n=13,794 g/mol; M_w=27,319 g/mol ; Đ=1.98

Synthesis of 1372

The isocyanate content of pre-prepared prepolymer-1 was determined at 2.55%. 100 g of prepolymer-1 were weighed into a flask and heated to 80°C under nitrogen atmosphere. 126.5 g (1.0 eq.) of polyether 25 were added over 60 min. The reaction was monitored *via* FT-IR measurements by tracking of the characteristic NCO band at 2265 cm^{-1}. As long as NCO band was present, stirring at 80°C was continued. The reaction was stirred for 24.5 h until full NCO conversion was reached.

Viscosity: 3,290,400 mPa*s

GPC: M_n=9,026 g/mol ; M_w= 27,528 g/mol ; Đ=3.05

Synthesis of 1373

The isocyanate content of pre-prepared prepolymer-1 was determined at 2.55%. 100 g of prepolymer-1 were weighed into a flask and heated to 80°C under nitrogen atmosphere. 95.7 g (1.0 eq.) of polyether 34 were added over 60 min. The reaction was monitored *via* FT-IR measurements by tracking the characteristic NCO band at 2265 cm^{-1}. As long as NCO band was present, stirring at 80°C was continued. The reaction was stirred for 23 h until full NCO conversion was reached.

Viscosity: 3,251,100 mPa*s

GPC: M_n=9,658 g/mol; M_w=28,221 g/mol; Đ=2.92

Synthesis of 1318

The isocyanate content of pre-prepared prepolymer-thermo was determined at 1.83%. 50 g of prepolymer-thermo were weighed into a flask and stirred for 1 h under nitrogen atmosphere. 46.92 g (1.0 eq.) of Jeffamine M2005 were added over 60 min. The temperature was monitored as an indicator for exothermal reaction behavior. The reaction was monitored *via* FT-IR measurements by tracking the characteristic NCO band at 2265 cm^{-1}. The reaction was stirred for 1.67 h until full NCO conversion was reached.

Viscosity: 3,290,200 mPa*s

M_n=10,122 g/mol; M_w=18,678 g/mol; Đ=1.85

Synthesis of 1206

The isocyanate content of pre-prepared prepolymer-thermo was determined at 1.83%. 50 g of prepolymer-thermo were weighed into a flask and heated to 80°C under nitrogen atmosphere. 48.88 g (1.0 eq.) of polyether 25 were added over 60 min. The reaction was monitored *via* FT-IR measurements by tracking characteristic NCO band at 2265 cm^{-1}. As long as NCO band was present, stirring at 80°C was continued. The reaction was stirred for 42 h until full NCO conversion was reached.

Viscosity: 16,239 mPa*s

GPC: M_n=8,049 g/mol; M_w=17,000 g/mol; Đ=2.11

Synthesis of 1195

The isocyanate content of pre-prepared prepolymer-thermo was determined at 1.83%. 50 g of prepolymer-thermo were weighed into a flask and heated to 80°C under nitrogen atmosphere. 35.05 g (1.0 eq.) of polyether 34 were added over 60 min. The reaction was monitored *via* FT-IR measurements by tracking characteristic NCO band at 2265 cm^{-1}. As long as NCO band was present, stirring at 80°C was continued. The reaction was stirred for 16 h until full NCO conversion was reached.

Viscosity: 3,300,500 mPa*s

GPC: M_n= 6,787 g/mol; M_w= 20,884 g/mol; Đ=3.08

6.4 Experimental Details for Chapter 4.2

Synthesis of raw materials used for chapter 4.2

Synthesis of Polyol-2

1645.00 g of a glycerol (*f*=3) started polyoxypropylene triol (Polyether 1; OHZ=233 mg KOH/g), 83.50 g of dilactide (Aldrich, LOT BCBV8611) and 2.00 g of a DMC-catalyst (prepared as stated in WO 01/80994 A1, example 6[225]) were weighed into a 20l stainless-steel pressure reactor under nitrogen atmosphere. After stripping with nitrogen for 30 min. at 100 °C and 0.1 bar, the temperature of the reactor was set to 130 °C. 2215.00 g of propylene oxide (Chemogas) and 6058.00 g of ethylene oxide (GHC Gerling Holz) were dosed within 135 min. to the reaction mixture and were reacted for further 45 min at 130 °C. Afterwards the reaction was cooled to 90 °C and volatile compounds were distilled off for 30 min. at <0.01 bar. The reaction mixture was stabilized with 6.00 g of Irganox 1076.

Ethylene oxide content: 60.57wt.-%

OH number: 39.90 mg KOH/g

Acidic number: 0.01 mg KOH/g

Viscosity: 1010 mPa*s, 25 °C

PO/EO/dilactide amount ratios: 26.5%/72.5%/1%

Synthesis of Polyol-3

1645.00 g of a glycerol (*f*=3) started polyoxypropylene triol (Polyether 1; OHZ=233 mg KOH/g), 209.00 g of dilactide (Aldrich, LOT BCBV8611) and 2.00 g of a DMC-catalyst (prepared as stated in WO 01/80994 A1, example 6[225]) were weighed into a 20l stainless-steel pressure reactor under nitrogen atmosphere. After stripping with nitrogen for 30 min. at 100 °C and 0.1 bar, the temperature of the reactor was set to 130 °C. 2069.00 g of propylene oxide (Chemogas) and 6058.00 g of ethylene oxide (GHC Gerling Holz) were dosed within 135 min. to the rection mixture and were reacted for further 45 min at 130 °C. Afterwards the reaction was cooled to 90 °C and volatile compounds were distilled off for 30 min. at <0.01 bar. The reaction mixture was stabilized with 6.00 g of Irganox 1076.

Ethylene oxide content: 60.70wt.-%

OH number: 39.7 mg KOH/g

Acidic number: 0.01 mg KOH/g

Viscosity: 1040 mPa*s, 25 °C

PO/EO/dilactide amount ratios: 25.0%/72.5%/2.5%

Synthesis of Polyol-4

1194.70 g of a glycerol (*f*=3) started polyoxypropylene triol (Polyether 1; OHZ=233 mg KOH/g), 300.70 g of dilactide (Aldrich, LOT BCBV8611) and 0.75 g of a DMC-catalyst (prepared as stated in WO 01/80994 A1, example 6[225]) were weighed into a 20l stainless-steel pressure reactor under nitrogen atmosphere. After stripping with nitrogen for 30 min. at 100 °C and 0.1 bar, the temperature of the reactor was set to 130 °C and the pressure to 2.21 bar with nitrogen. 1353.40 g of propylene oxide (Chemogas) and 4361.00 g of ethylene oxide (GHC Gerling Holz) were dosed within 135 min. to the rection mixture and were reacted for further 45 min at 130 °C. Afterwards the reaction was cooled to 90 °C and volatile compounds were distilled off for 30 min. at <0.01 bar. The reaction mixture was stabilized with 6.00 g of Irganox 1076.

Ethylene oxide content: 60.48wt.-%

OH number: 38.5 mg KOH/g

Acidicic number: 0.02 mg KOH/g

Viscosity: 1145 mPa*s, 25 °C

PO/EO/dilactide amount ratios (wt.-%): 22.5%/72.5%/5%

Synthesis of Polyol-5

1643.00 g of a glycerol (*f*=3) started polyoxypropylene triol (Polyether 1; OHZ=233 mg KOH/g), 833.0 g of dilactide (Aldrich, LOT BCBV8611) and 2.0 g of a DMC-catalyst (prepared as stated in WO 01/80994 A1, example 6[225]) were weighed into a 20 L stainless-steel pressure reactor under nitrogen atmosphere. After stripping with nitrogen for 30 min. at 100 °C and 0.1 bar, the temperature of the reactor was set to 130 °C. 1450.00 g of propylene oxide (Chemogas) and 6058.00 g of ethylene oxide (GHC Gerling Holz) were dosed within 135 min. to the rection mixture and were reacted for further 45 min at 130 °C. Afterwards the reaction was cooled to 90 °C and volatile compounds were distilled off for 30 min. at <0.01 bar. The reaction mixture was stabilized with 6.00 g of Irganox 1076.

Ethylene oxide content: 60.68wt.-%

OH number: 37.20 mg KOH/g

Acidic number: 0.02 mg KOH/g

Viscosity: 1400 mPa*s, 25 °C

PO/EO/dilactide amount ratios: 17.5%/72.5%/10%

Synthesis of Prepolymer-2

628.05 g of HDI and 0.66 g DBP were weighed into a three-neck flask and heated up to 80 °C under constant stirring under nitrogen atmosphere. 700.00 g of polyol-1 were added dropwise within 2 hours. After the addition was completed, the reaction was stirred for one additional hour until residual NCO content reached 22.06%. The reaction mixture was allowed to cool down under constant stirring. Unreacted monomer was removed by SPE (p=0.1 mbar; $T_{pre\text{-}evaporator}$=130 °C, $T_{main\text{-}evaporator}$=120 °C) and an NCO-terminated prepolymer with NCO content= 2.63wt.-% was obtained.

Residual Monomer content: 0.03wt.-%

NCO content: 2.63wt.-%

Viscosity: 3504 mPa*s, 23°C

Average eq. weight: 1596.96 g/eq.

GPC: M_n=5437.4 g/mol ;M_w=8325.0 g/mol ; PDI=1.53

Synthesis of Prepolymer-3

625.64 g of HDI and 0.66 g DBP were weighed into a three-neck flask and heated up to 80 °C under constant stirring under nitrogen atmosphere. 700.00 g of polyol-2, were added dropwise within 2 hours. After the addition was completed, the reaction was stirred for one additional hour until residual NCO content reached 19.41%. The reaction mixture was allowed to cool down under constant stirring. Unreacted monomer was removed by SPE (p=0.1 mbar; $T_{pre\text{-}evaporator}$=130 °C, $T_{main\text{-}evaporator}$=120 °C) and an NCO-terminated prepolymer with NCO content= 2.67wt.-% was obtained.

Residual Monomer content: 0.02wt.-%

NCO content: 2.67wt.-%

Viscosity: 3510 mPa*s, 23°C

Average eq. weight: 1573.03 g/eq.

GPC: M_n=5283.8 g/mol ;M_w=8421.4 g/mol ; PDI=1.59

Synthesis of Prepolymer-4

592.00 g of HDI and 0.61 g DBP were weighed into a three-neck flask and heated up to 80 °C under constant stirring under nitrogen atmosphere. 632.92 g of polyol-3 were added dropwise within 2 hours. After the addition was completed, the reaction was stirred for one additional hour until residual NCO content reached 22.56%. The reaction mixture was allowed to cool down under constant stirring. Unreacted monomer was removed by SPE (p=0.1 mbar; $T_{pre\text{-}evaporator}$=130 °C, $T_{main\text{-}evaporator}$=120 °C) and an NCO-terminated prepolymer with NCO content= 2.55wt.-% was obtained.

Residual Monomer content: >0.01wt.-%

NCO content: 2.53wt.-%

Viscosity: 3990 mPa*s, 23 °C

Average eq. weight: 1647.06 g/eq.

GPC: M_n=4598.6 g/mol ;M_w=7919.8 g/mol ; Đ=1.72

Synthesis of Prepolymer-5

592.00 g of HDI and 0.65 g DBP were weighed into a three-neck flask and heated up to 80 °C under constant stirring. 703.92 g of polyol-4 were added dropwise within 2 hours. After the addition was completed, the reaction was stirred for one additional hour until residual NCO content reached 21.30%. The reaction mixture was allowed to cool down under constant stirring. Unreacted monomer was removed by SPE (p=0.1 mbar; $T_{pre\text{-}evaporator}$=130 °C, $T_{main\text{-}evaporator}$=120 °C) and an NCO-terminated prepolymer with NCO content= 2.59wt.-% was obtained.

Residual Monomer content: 0.03wt.-%

NCO content: 2.59wt.-%

Viscosity: 9451 mPa*s, 23 °C

Average eq. weight: 1621.62 g/eq.

GPC: M_n=5242.3 g/mol ;M_w=8860.6 g/mol ; Đ =1.69

Design of Experiments

The design of experiments was conducted using Design-Expert13 as a Software. The formulations which were tested are listed in Table 55.

Table 55 Analyzed formulations of the design of experiments with the four different factors: *dilactide content*, *solid content* $_{NCO}$, *free base fraction* and *buffer/acid type*.

Run	Dilactide content [%]	Solid content NCO [%]	Buffering degree of NH_2 [%]	Buffer/acide type
1	10	11.63	75	Acetic acid/acetate
2	5	10	78.25	Acetic acid/acetate
3	10	15	75	HCl
4	10	15	81.65	Acetic acid/acetate
5	10	15	75	HCl
6	5	10	85	HCl
7	5	10	85	HCl
8	10	11.88	81.25	HCl
9	5	11.63	75	HCl
10	5	15	81.7	HCl
11	10	15	85	HCl
12	5	12.95	79.2	Acetic acid/acetate
13	5	15	81.7	HCl
14	10	10	75	HCl
15	10	10	85	Acetic acid/acetate
16	5	15	75	Acetic acid/acetate
17	10	12.79	85	Acetic acid/acetate
18	5	13.38	85	Acetic acid/acetate
19	10	14.25	76.4	Acetic acid/acetate
20	1	10	85	Acetic acid/acetate
21	1	10	75	HCl
22	2.5	12.5	85	HCl

23	2.5	10	75	Acetic acid/acetate
24	2.5	11.25	80	Acetic acid/acetate
25	1	15	85	Acetic acid/acetate
26	2.5	10	75	Acetic acid/acetate
27	2.5	10	80	HCl
28	1	15	85	Acetic acid/acetate
29	1	12.5	85	HCl
30	1	15	75	HCl
31	1	10	80	HCl

6.5 Experimental Details for Chapter 4.3.

In vivo proof of concept study from chapter 4.3.1

The animal study *HYGEL4MIC; Examination of local intraabdominal adhesion prophylaxis and biocompatibility in rabbit* was designed in accordance with ISO 10993-6* and ISO 10993-2 and conducted as a non-GLP-study by FREY-TOX GmbH as an accredited laboratory according to EN ISO/IEC 17025. The study was accomplished as a NON-GLP study with 24 female SPF albino rabbits of the stock New Zealand White with a bodyweight from 3.4 to 4.3 kg. Determination of occurrence and extent of postoperative adhesions was analyzed according to modified Diamond Score by Bigatti *et al*.[215] , as being described in Table 56, and according to Zühlke adhesion rating score[216], Table 57.

Sterilization of the hydrogel system was carried out *via* gamma-ray treatment at a dosing of 25 kGy.

Table 56 Modified diamonds adhesion rating score according to Bigatti *et al*.[215].

Extent [%]	Tenacity	Grade	Type	Grade
0	None	1	None	I
<25	Adhesions essentially fell apart	2	Filmy, no vessels (transparent)	II
25-50	Adhesions lysed with traction	3	Opaque, no vessels (translucent)	III
50-75	Adhesions required sharp dissesction	4	Opaque, small vessels	IV
>75	-	-	Opaque, large vessels	V

Table 57 Adhesion rating Score according to Zühlke *et al*.[216].

Grade	Description
0	No adhesions
I	Filament-like adhesions
	Blunt detachment
II	Strand-like adhesions with partial vascularization
	Blunt to blunt-sharp detachment
III	Strand-like adhesions with distinct vascularization
	sharp detachment
IV	Tight and areal adhesions
	sharp detachment with loss of substance

In vivo biocompatibility study from chapter 4.3.3

The animal study *HYGEL4MIC: Evaluation of local biocompatibility and initial degradation pattern following subcutaneous implantation in rabbit* was designed in accordance with ISO 10993-6* and ISO 10993-2 and conducted as a non-GLP-study by FREY-TOX GmbH as an accredited laboratory according to EN ISO/IEC 17025. A respective study design was chosen for the evaluation of biocompatibility and was accomplished as a NON-GLP study with 16 female albino rabbits of the stock New Zealand White with a bodyweight from 3.7 to 4.55 kg.

7 References

(1) Donati, S.; Caprani, S. M.; Airaghi, G.; Vinciguerra, R.; Bartalena, L.; Testa, F.; Mariotti, C.; Porta, G.; Simonelli, F.; Azzolini, C. Vitreous substitutes: the present and the future. *BioMed research international* **2014**, *2014*, 351804. DOI: 10.1155/2014/351804. Published Online: May. 4, 2014.

(2) Le Goff, M. M.; Bishop, P. N. Adult vitreous structure and postnatal changes. *Eye (London, England)* **2008**, *22* (10), 1214–1222. DOI: 10.1038/eye.2008.21;. Published Online: Feb. 29, 2008.

(3) Mantha, S.; Pillai, S.; Khayambashi, P.; Upadhyay, A.; Zhang, Y.; Tao, O.; Pham, H. M.; Tran, S. D. Smart Hydrogels in Tissue Engineering and Regenerative Medicine. *Materials (Basel, Switzerland)* **2019**, *12* (20). DOI: 10.3390/ma12203323. Published Online: Oct. 12, 2019.

(4) Choudhary, B.; Paul, S. R.; Nayak, S. K.; Qureshi, D.; Pal, K. Synthesis and biomedical applications of filled hydrogels. In *Polymeric Gels*; Elsevier, 2018; pp 283–302. DOI: 10.1016/B978-0-08-102179-8.00011-9.

(5) Huang, C.; Dong, L.; Zhao, B.; Lu, Y.; Huang, S.; Yuan, Z.; Luo, G.; Xu, Y.; Qian, W. Anti-inflammatory hydrogel dressings and skin wound healing. *Clinical and translational medicine* **2022**, *12* (11), e1094. DOI: 10.1002/ctm2.1094.

(6) Haworth, K.; Travis, D.; Abariga, S. A.; Fuller, D.; Pucker, A. D. Silicone hydrogel versus hydrogel soft contact lenses for differences in patient-reported eye comfort and safety. *Cochrane Database of Systematic Reviews* **2021.** DOI: 10.1002/14651858.CD014791.

(7) Vigata, M.; Meinert, C.; Hutmacher, D. W.; Bock, N. Hydrogels as Drug Delivery Systems: A Review of Current Characterization and Evaluation Techniques. *Pharmaceutics* **2020**, *12* (12). DOI: 10.3390/pharmaceutics12121188. Published Online: Dec. 7, 2020.

(8) Siepmann, J.; Siegel, R. A.; Rathbone, M. J. *Fundamentals and Applications of Controlled Release Drug Delivery*; Springer US, 2012. DOI: 10.1007/978-1-4614-0881-9.

(9) Yang, H.; Zhao, M.; Xing, D.; Zhang, J.; Fang, T.; Zhang, F.; Nie, Z.; Liu, Y.; Yang, L.; Li, J.; Wang, D. Contact lens as an emerging platform for ophthalmic drug delivery: A systematic review. *Asian journal of pharmaceutical sciences* **2023**, *18* (5), 100847. DOI: 10.1016/j.ajps.2023.100847. Published Online: Sep. 27, 2023.

(10) Rykowska, I.; Nowak, I.; Nowak, R. Soft Contact Lenses as Drug Delivery Systems: A Review. *Molecules (Basel, Switzerland)* **2021**, *26* (18). DOI: 10.3390/molecules26185577. Published Online: Sep. 14, 2021.

(11) Liu, H.; Wang, C.; Li, C.; Qin, Y.; Wang, Z.; Yang, F.; Li, Z.; Wang, J. A functional chitosan-based hydrogel as a wound dressing and drug delivery system in the treatment of wound healing. *RSC advances* **2018**, *8* (14), 7533–7549. DOI: 10.1039/C7RA13510F. Published Online: Feb. 16, 2018.

(12) Park, H.; Baek, S.; Kang, H.; Lee, D. Biomaterials to Prevent Post-Operative Adhesion. *Materials (Basel, Switzerland)* **2020**, *13* (14). DOI: 10.3390/ma13143056. Published Online: Jul. 8, 2020.

(13) Vrijland, W. W.; Jeekel, J.; van Geldorp, H. J.; Swank, D. J.; Bonjer, H. J. Abdominal adhesions: intestinal obstruction, pain, and infertility. *Surgical endoscopy* **2003**, *17* (7), 1017–1022. DOI: 10.1007/s00464-002-9208-9. Published Online: Mar. 14, 2003.

(14) Lauder, C. I. W.; Garcea, G.; Strickland, A.; Maddern, G. J. Abdominal adhesion prevention: still a sticky subject? *Digestive surgery* **2010**, *27* (5), 347–358. DOI: 10.1159/000314805. Published Online: Sep. 16, 2010.

(15) Weibel, M. A.; Majno, G. Peritoneal adhesions and their relation to abdominal surgery. A postmortem study. *American journal of surgery* **1973**, *126* (3), 345–353. DOI: 10.1016/S0002-9610(73)80123-0.

(16) Fatehi Hassanabad, A.; Zarzycki, A. N.; Jeon, K.; Dundas, J. A.; Vasanthan, V.; Deniset, J. F.; Fedak, P. W. M. Prevention of Post-Operative Adhesions: A Comprehensive Review of Present and Emerging Strategies. *Biomolecules* **2021**, *11* (7). DOI: 10.3390/biom11071027. Published Online: Jul. 14, 2021.

(17) Hong, M.-K.; Ding, D.-C. Seprafilm® Application Method in Laparoscopic Surgery. *JSLS : Journal of the Society of Laparoendoscopic Surgeons* **2017**, *21* (1). DOI: 10.4293/JSLS.2016.00097.

(18) Diamond, M. P.; Freeman, M. L. Clinical implications of postsurgical adhesions. *Human reproduction update* **2001**, *7* (6), 567–576. DOI: 10.1093/humupd/7.6.567.

(19) Fatehi Hassanabad, A.; Zarzycki, A. N.; Jeon, K.; Deniset, J. F.; Fedak, P. W. M. Post-Operative Adhesions: A Comprehensive Review of Mechanisms. *Biomedicines* **2021**, *9* (8). DOI: 10.3390/biomedicines9080867. Published Online: Jul. 22, 2021.

(20) Tittel, A.; Schippers, E.; Treutner, K. H.; Anuroff, M.; Polivoda, M.; Ottinger, A.; Schumpelick, V. Laparoskopie versus Laparotomie. Eine tierexperimentelle Studie zum Vergleich der Adhäsionsbildung im Hund. *Langenbecks Archiv fur Chirurgie* **1994**, *379* (2), 95–98. DOI: 10.1007/BF00195870.

(21) ETHICON. *DRINGENDE SICHERHEITSINFORMATION GYNECARE INTERCEED™ – Klinische Studienergebnisse*. https://www.bfarm.de/SharedDocs/Kundeninfos/DE/11/2021/12986-21_kundeninfo_de.html (accessed 2024-01-04).

(22) Boretos, J. W.; Pierce, W. S. Segmented polyurethane: a polyether polymer. An initial evaluation for biomedical applications. *J. Biomed. Mater. Res.* **1968**, *2* (1), 121–130. DOI: 10.1002/jbm.820020109.

(23) Brash, J. L.; Fritzinger, B. K.; Bruck, S. D. Development of block copolyether-urethane intra-aortic balloons and other medical devices. *J. Biomed. Mater. Res.* **1973**, *7* (4), 313–334. DOI: 10.1002/jbm.820070405.

(24) Lyman, D. J.; Kwan-Gett, C.; Zwart, H. H.; Bland, A.; Eastwood, N.; Kawai, J.; Kolff, W. J. The development and implantation of a polyurethane hemispherical artificial heart. *Transactions - American Society for Artificial Internal Organs* **1971**, *17*, 456–463.

(25) Park, B.-D.; Lee, Y.-S. The effect of PEG groups on swelling properties of PEG-grafted-polystyrene resins in various solvents. *Reactive and Functional Polymers* **2000**, *44* (1), 41–46. DOI: 10.1016/S1381-5148(99)00075-9.

(26) Gheni, S. A.; Ali, M. M.; Ta, G. C.; Harbin, H. J.; Awad, S. A. Toxicity, Hazards, and Safe Handling of Primary Aromatic Amines. *ACS Chem. Health Saf.* **2024**, *31* (1), 8–21. DOI: 10.1021/acs.chas.3c00073.

(27) Barnard, J.; Speake, D. In open heart surgery is there a role for the use of carbon dioxide field flooding techniques to reduce the level of post-operative gaseous emboli? *Interactive cardiovascular and thoracic surgery* **2004**, *3* (4), 599–602. DOI: 10.1016/j.icvts.2004.07.004.

(28) Chao, H.-H.; Torchiana, D. F. BioGlue: albumin/glutaraldehyde sealant in cardiac surgery. *Journal of cardiac surgery* **2003**, *18* (6), 500–503. DOI: 10.1046/j.0886-0440.2003.00304.x.

(29) LoPachin, R. M.; Gavin, T. Molecular mechanisms of aldehyde toxicity: a chemical perspective. *Chemical research in toxicology* **2014**, *27* (7), 1081–1091. DOI: 10.1021/tx5001046. Published Online: Jun. 17, 2014.

(30) Negrell, C.; Voirin, C.; Boutevin, B.; Ladmiral, V.; Caillol, S. From monomer synthesis to polymers with pendant aldehyde groups. *European Polymer Journal* **2018**, *109*, 544–563. DOI: 10.1016/j.eurpolymj.2018.10.039.

(31) Gadhave, R. V.; Gadhave, C. R.; Dhawale, P. V. Silane Terminated Prepolymers: An Alternative to Silicones and Polyurethanes. *OJPChem* **2021**, *11* (03), 31–54. DOI: 10.4236/ojpchem.2021.113003.

(32) Delebecq, E.; Pascault, J.-P.; Boutevin, B.; Ganachaud, F. On the versatility of urethane/urea bonds: reversibility, blocked isocyanate, and non-isocyanate polyurethane. *Chemical reviews* **2013**, *113* (1), 80–118. DOI: 10.1021/cr300195n. Published Online: Oct. 19, 2012.

(33) Soliman, K. A.; Ullah, K.; Shah, A.; Jones, D. S.; Singh, T. R. R. Poloxamer-based in situ gelling thermoresponsive systems for ocular drug delivery applications. *Drug discovery today* **2019**, *24* (8), 1575–1586. DOI: 10.1016/j.drudis.2019.05.036. Published Online: Jun. 5, 2019.

(34) Salinas, Y.; Kneidinger, M.; Fornaguera, C.; Borrós, S.; Brüggemann, O.; Teasdale, I. Dual stimuli-responsive polyphosphazene-based molecular gates for controlled drug delivery in lung cancer cells. *RSC Adv.* **2020**, *10* (46), 27305–27314. DOI: 10.1039/d0ra03210g. Published Online: Jul. 21, 2020.

(35) Cai, Q.; Shi, G.; Bei, J.; Wang, S. Enzymatic degradation behavior and mechanism of poly(lactide-co-glycolide) foams by trypsin. *Biomaterials* **2003**, *24* (4), 629–638. DOI: 10.1016/s0142-9612(02)00377-0.

(36) Tokiwa, Y.; Calabia, B. P. Biodegradability and biodegradation of poly(lactide). *Applied microbiology and biotechnology* **2006**, *72* (2), 244–251. DOI: 10.1007/s00253-006-0488-1. Published Online: Jul. 6, 2006.

(37) Manoukian, O. S.; Sardashti, N.; Stedman, T.; Gailiunas, K.; Ojha, A.; Penalosa, A.; Mancuso, C.; Hobert, M.; Kumbar, S. G. Biomaterials for Tissue Engineering and Regenerative

Medicine. In *Encyclopedia of Biomedical Engineering*; Elsevier, 2019; pp 462–482. DOI: 10.1016/B978-0-12-801238-3.64098-9.

(38) Thakur, M.; Majid, I.; Hussain, S.; Nanda, V. Poly(ε-caprolactone): A potential polymer for biodegradable food packaging applications. *Packag Technol Sci* **2021**, *34* (8), 449–461. DOI: 10.1002/pts.2572.

(39) Kim, G.; Gavande, V.; Shaikh, V.; Lee, W.-K. Degradation Behavior of Poly(Lactide-Co-Glycolide) Monolayers Investigated by Langmuir Technique: Accelerating Effect. *Molecules (Basel, Switzerland)* **2023**, *28* (12). DOI: 10.3390/molecules28124810. Published Online: Jun. 16, 2023.

(40) Park, J. H.; Lee, B. K.; Park, S. H.; Kim, M. G.; Lee, J. W.; Lee, H. Y.; Lee, H. B.; Kim, J. H.; Kim, M. S. Preparation of Biodegradable and Elastic Poly(ε-caprolactone-co-lactide) Copolymers and Evaluation as a Localized and Sustained Drug Delivery Carrier. *International journal of molecular sciences* **2017**, *18* (3). DOI: 10.3390/ijms18030671. Published Online: Mar. 21, 2017.

(41) Makadia, H. K.; Siegel, S. J. Poly Lactic-co-Glycolic Acid (PLGA) as Biodegradable Controlled Drug Delivery Carrier. *Polymers* **2011**, *3* (3), 1377–1397. DOI: 10.3390/polym3031377. Published Online: Aug. 26, 2011.

(42) Auras, R.; Harte, B.; Selke, S. An overview of polylactides as packaging materials. *Macromolecular bioscience* **2004**, *4* (9), 835–864. DOI: 10.1002/mabi.200400043.

(43) Chafran, L. S.; Paiva, M. F.; Freitas, J. O. C.; Sales, M. J. A.; Dias, S. C. L.; Dias, J. A. Preparation of PLA blends by polycondensation of D,L-lactic acid using supported 12-tungstophosphoric acid as a heterogeneous catalyst. *Heliyon* **2019**, *5* (5), e01810. DOI: 10.1016/j.heliyon.2019.e01810. Published Online: May. 28, 2019.

(44) Heckroth, H.; Eggert, C.; Hofmann, Jörg, Lorenz, Klaus. Isocyanate-Functional Prepolymer for a Biologically Degradable Fabric Adhesive.

(45) Sperling, L. H. *Introduction to physical polymer science*, 4. ed.; Wiley, 2006.

(46) WICHTERLE, O.; Lim, D. Hydrophilic Gels for Biological Use. *Nature* **1960**, *185* (4706), 117–118. DOI: 10.1038/185117a0.

(47) Mahinroosta, M.; Jomeh Farsangi, Z.; Allahverdi, A.; Shakoori, Z. Hydrogels as intelligent materials: A brief review of synthesis, properties and applications. *Materials Today Chemistry* **2018**, *8*, 42–55. DOI: 10.1016/j.mtchem.2018.02.004.

(48) Correa, S.; Grosskopf, A. K.; Lopez Hernandez, H.; Chan, D.; Yu, A. C.; Stapleton, L. M.; Appel, E. A. Translational Applications of Hydrogels. *Chemical reviews* **2021**, *121* (18), 11385–11457. DOI: 10.1021/acs.chemrev.0c01177. Published Online: May. 3, 2021.

(49) Chen, Y.; Zhang, S.; Cui, Q.; Ni, J.; Wang, X.; Cheng, X.; Alem, H.; Tebon, P.; Xu, C.; Guo, C.; Nasiri, R.; Moreddu, R.; Yetisen, A. K.; Ahadian, S.; Ashammakhi, N.; Emaminejad, S.; Jucaud, V.; Dokmeci, M. R.; Khademhosseini, A. Microengineered poly(HEMA) hydrogels for wearable contact lens biosensing. *Lab on a chip* **2020**, *20* (22), 4205–4214. DOI: 10.1039/D0LC00446D.

(50) Ansari, M. J.; Rajendran, R. R.; Mohanto, S.; Agarwal, U.; Panda, K.; Dhotre, K.; Manne, R.; Deepak, A.; Zafar, A.; Yasir, M.; Pramanik, S. Poly(N-isopropylacrylamide)-Based Hydrogels for

Biomedical Applications: A Review of the State-of-the-Art. *Gels (Basel, Switzerland)* **2022**, *8* (7). DOI: 10.3390/gels8070454. Published Online: Jul. 20, 2022.

(51) Seuring, J.; Agarwal, S. First Example of a Universal and Cost-Effective Approach: Polymers with Tunable Upper Critical Solution Temperature in Water and Electrolyte Solution. *Macromolecules* **2012**, *45* (9), 3910–3918. DOI: 10.1021/ma300355k.

(52) Augé, A.; Zhao, Y. What determines the volume transition temperature of UCST acrylamide–acrylonitrile hydrogels? *RSC Adv.* **2016**, *6* (74), 70616–70623. DOI: 10.1039/C6RA12720G.

(53) Liang, W.; Ni, N.; Huang, Y.; Lin, C. An Advanced Review: Polyurethane-Related Dressings for Skin Wound Repair. *Polymers* **2023**, *15* (21). DOI: 10.3390/polym15214301. Published Online: Nov. 1, 2023.

(54) Kamaci, M. Polyurethane-based hydrogels for controlled drug delivery applications. *European Polymer Journal* **2020**, *123*, 109444. DOI: 10.1016/j.eurpolymj.2019.109444.

(55) Peppas, N. A. Physiologically Responsive Hydrogels. *Journal of Bioactive and Compatible Polymers* **1991**, *6* (3), 241–246. DOI: 10.1177/088391159100600303.

(56) Wang, S.; Chen, Y.; Sun, Y.; Qin, Y.; Zhang, H.; Yu, X.; Liu, Y. Stretchable slide-ring supramolecular hydrogel for flexible electronic devices. *Commun Mater* **2022**, *3* (1). DOI: 10.1038/s43246-022-00225-7.

(57) Liu, W.; Duan, H.; Zhang, D.; Zhang, X.; Luo, Q.; Xie, T.; Yan, H.; Peng, L.; Hu, Y.; Liang, L.; Zhao, G.; Xie, Z.; Hu, J. Concepts and Application of DNA Origami and DNA Self-Assembly: A Systematic Review. *Applied bionics and biomechanics* **2021**, *2021*, 9112407. DOI: 10.1155/2021/9112407. Published Online: Nov. 16, 2021.

(58) Anderson, J. M.; Andukuri, A.; Lim, D. J.; Jun, H.-W. Modulating the gelation properties of self-assembling peptide amphiphiles. *ACS nano* **2009**, *3* (11), 3447–3454. DOI: 10.1021/nn900884n.

(59) Wang, Y.; Chen, Q.; Chen, M.; Guan, Y.; Zhang, Y. PHEMA hydrogel films crosslinked with dynamic disulfide bonds: synthesis, swelling-induced mechanical instability and self-healing. *Polym. Chem.* **2019**, *10* (35), 4844–4851. DOI: 10.1039/C9PY00670B.

(60) Ji, N.; Luo, J.; Zhang, W.; Sun, J.; Wang, J.; Qin, C.; Zhuo, Q.; Dai, L. A Novel Polyvinyl Alcohol-Based Hydrogel with Ultra-Fast Self-Healing Ability and Excellent Stretchability Based on Multi Dynamic Covalent Bond Cross-Linking. *Macro Materials & Eng* **2023**, *308* (3). DOI: 10.1002/mame.202200525.

(61) Dodero, A.; Pianella, L.; Vicini, S.; Alloisio, M.; Ottonelli, M.; Castellano, M. Alginate-based hydrogels prepared via ionic gelation: An experimental design approach to predict the cross-linking degree. *European Polymer Journal* **2019**, *118*, 586–594. DOI: 10.1016/j.eurpolymj.2019.06.028.

(62) Abasalizadeh, F.; Moghaddam, S. V.; Alizadeh, E.; Akbari, E.; Kashani, E.; Fazljou, S. M. B.; Torbati, M.; Akbarzadeh, A. Alginate-based hydrogels as drug delivery vehicles in cancer

treatment and their applications in wound dressing and 3D bioprinting. *Journal of biological engineering* **2020**, *14*, 8. DOI: 10.1186/s13036-020-0227-7. Published Online: Mar. 13, 2020.

(63) Ino, K.; Fukuda, M. T.; Hiramoto, K.; Taira, N.; Nashimoto, Y.; Shiku, H. Fabrication of three-dimensional calcium alginate hydrogels using sacrificial templates of sugar. *Journal of bioscience and bioengineering* **2020**, *130* (5), 539–544. DOI: 10.1016/j.jbiosc.2020.06.014. Published Online: Aug. 2, 2020.

(64) van Tran, T. Anisotropic Ca-alginate Hydrogels with Superior Mechanical Properties and Excellent Stability for Underwater Applications. *J Polym Environ* **2023.** DOI: 10.1007/s10924-023-02974-z.

(65) Fadler, R. E.; Flood, A. H. Rigidity and Flexibility in Rotaxanes and Their Relatives; On Being Stubborn and Easy-Going. *Frontiers in chemistry* **2022**, *10*, 856173. DOI: 10.3389/fchem.2022.856173. Published Online: Apr. 7, 2022.

(66) Hart, L. F.; Hertzog, J. E.; Rauscher, P. M.; Rawe, B. W.; Tranquilli, M. M.; Rowan, S. J. Material properties and applications of mechanically interlocked polymers. *Nat Rev Mater* **2021**, *6* (6), 508–530. DOI: 10.1038/s41578-021-00278-z.

(67) Iijima, K.; Aoki, D.; Otsuka, H.; Takata, T. Synthesis of rotaxane cross-linked polymers with supramolecular cross-linkers based on γ-CD and PTHF macromonomers: The effect of the macromonomer structure on the polymer properties. *Polymer* **2017**, *128*, 392–396. DOI: 10.1016/j.polymer.2017.01.024.

(68) Takata, T. Polyrotaxane and Polyrotaxane Network: Supramolecular Architectures Based on the Concept of Dynamic Covalent Bond Chemistry. *Polym J* **2006**, *38* (1), 1–20. DOI: 10.1295/polymj.38.1.

(69) Aseyev, V.; Tenhu, H.; Winnik, F. M. Non-ionic Thermoresponsive Polymers in Water. In *Self Organized Nanostructures of Amphiphilic Block Copolymers II*; Müller, A. H., Borisov, O., Eds.; Advances in Polymer Science; Springer Berlin Heidelberg, 2011; pp 29–89. DOI: 10.1007/12_2010_57.

(70) Seuring, J.; Agarwal, S. Polymers with upper critical solution temperature in aqueous solution. *Macromolecular rapid communications* **2012**, *33* (22), 1898–1920. DOI: 10.1002/marc.201200433. Published Online: Sep. 7, 2012.

(71) Howard G. Schild, David A. Tirrell. Microcalorimetric Detection of Lower Critical Solution Temperatures in Aqueous Polymer Solutions. *J. Phys. Chem*, 4352–4356.

(72) Heskins, M.; Guillet, J. E. Solution Properties of Poly(N-isopropylacrylamide). *Journal of Macromolecular Science: Part A - Chemistry* **1968**, *2* (8), 1441–1455. DOI: 10.1080/10601326808051910.

(73) Anghelache, A.; Teodorescu, M.; Stănescu, P. O.; Drăghici, C.; Vuluga, D. M. Novel cross-linked thermoresponsive hydrogels with controlled poly(ethylene glycol)—poly(propylene glycol) multiblock copolymer structure. *Colloid Polym Sci* **2014**, *292* (4), 829–838. DOI: 10.1007/s00396-013-3128-1.

(74) Aulton, M. E., Ed. *Aulton's pharmaceutics*:*The design and manufacture of medicines*, 3rd ed.; Churchill Livingstone, 2007.

(75) Oparaji, O.; Minelli, M.; Zhu, C.; Schaible, E.; Hexemer, A.; Hallinan, D. T. Effect of block copolymer morphology on crystallization and water transport. *Polymer* **2017**, *120*, 209–216. DOI: 10.1016/j.polymer.2017.05.055.

(76) St-Onge, V.; Cui, M.; Rochon, S.; Daigle, J.-C.; Claverie, J. P. Reducing crystallinity in solid polymer electrolytes for lithium-metal batteries via statistical copolymerization. *Commun Mater* **2021**, *2* (1). DOI: 10.1038/s43246-021-00187-2.

(77) Chang, C.; Duan, B.; Cai, J.; Zhang, L. Superabsorbent hydrogels based on cellulose for smart swelling and controllable delivery. *European Polymer Journal* **2010**, *46* (1), 92–100. DOI: 10.1016/j.eurpolymj.2009.04.033.

(78) Hong, B. T.; Roh, S. S.; Kim, D. S. Chemorheological studies on a dicyanate resin modified with polyethersulfone. *Polymer International* **2004**, *53* (6), 640–645. DOI: 10.1002/pi.1320.

(79) Mortimer, S.; Ryan, A. J.; Stanford, J. L. Rheological Behavior and Gel-Point Determination for a Model Lewis Acid-Initiated Chain Growth Epoxy Resin. *Macromolecules* **2001**, *34* (9), 2973–2980. DOI: 10.1021/ma001835x.

(80) Tung, C.-Y. M.; Dynes, P. J. Relationship between viscoelastic properties and gelation in thermosetting systems. *J of Applied Polymer Sci* **1982**, *27* (2), 569–574. DOI: 10.1002/app.1982.070270220.

(81) Hopkins, E.; Sanvictores, T.; Sharma, S. *StatPearls*:*Physiology, Acid Base Balance*, 2024.

(82) Mortimer, C. E.; Müller, U. *Chemie*:*Das Basiswissen der Chemie*, 12., korrigierte und aktualisierte Auflage; Georg Thieme Verlag, 2015.

(83) Yuan, Y.; Raheja, K.; Milbrandt, N. B.; Beilharz, S.; Tene, S.; Oshabaheebwa, S.; Gurkan, U. A.; Samia, A. C. S.; Karayilan, M. Thermoresponsive polymers with LCST transition: synthesis, characterization, and their impact on biomedical frontiers. *RSC Appl. Polym.* **2023**, *1* (2), 158–189. DOI: 10.1039/D3LP00114H.

(84) Lin, X.; Zhao, X.; Xu, C.; Wang, L.; Xia, Y. Progress in the mechanical enhancement of hydrogels: Fabrication strategies and underlying mechanisms. *Journal of Polymer Science* **2022**, *60* (17), 2525–2542. DOI: 10.1002/pol.20220154.

(85) Petersen, J.; Geier, S.; Wierach, P.; Wiedemann, M. In situ mechanical and electrical characterization of composite-integrated thin film-supercapacitors. *MATEC Web Conf.* **2018**, *188*, 1028. DOI: 10.1051/matecconf/201818801028.

(86) Grellmann, W., Ed. *Polymer testing*:*= Kunststoffprüfung engl*, 2. ed.; Hanser, 2013.

(87) Menard, K. P.; Menard, N. R. *Dynamic Mechanical Analysis*; CRC Press, 2020. DOI: 10.1201/9780429190308.

(88) Wu, Y.; Joseph, S.; Aluru, N. R. Effect of cross-linking on the diffusion of water, ions, and small molecules in hydrogels. *The journal of physical chemistry. B* **2009**, *113* (11), 3512–3520. DOI: 10.1021/jp808145x.

(89) Rehmann, M. S.; Skeens, K. M.; Kharkar, P. M.; Ford, E. M.; Maverakis, E.; Lee, K. H.; Kloxin, A. M. Tuning and Predicting Mesh Size and Protein Release from Step Growth Hydrogels. *Biomacromolecules* **2017**, *18* (10), 3131–3142. DOI: 10.1021/acs.biomac.7b00781. Published Online: Sep. 14, 2017.

(90) Pósfalvi, Ö. ÜBER DAS ELASTIZITÄTSGESETZ UND DIE POISSONSCHE ZAHL VON GUMMIELASTISCHEN WERKSTOFFEN. *Periodica Polytechnica. Transportation Engineering* **1982**, *10* (1), 61–66.

(91) Flory, P. J.; Rehner, J. Statistical Mechanics of Cross-Linked Polymer Networks II. Swelling. *The Journal of Chemical Physics* **1943**, *11* (11), 521–526. DOI: 10.1063/1.1723792.

(92) Kong, D.; Meng, Y.; McKenna, G. B. Determination of the molecular weight between cross-links for different ambers: Viscoelastic measurements of the rubbery plateau*. *Polymer Engineering & Sci* **2022**, *62* (4), 1023–1040. DOI: 10.1002/pen.25903.

(93) Adams, D. J. Does Drying Affect Gel Networks? *Gels (Basel, Switzerland)* **2018**, *4* (2). DOI: 10.3390/gels4020032. Published Online: Apr. 3, 2018.

(94) Ionescu, M. *Chemistry and Technology of Polyols for Polyurethanes, 2nd Edition, Volume 1*; Smithers Rapra, 2016.

(95) Park, S.-J.; Seo, M.-K. Element and Processing. In *Interface Science and Composites*; Interface Science and Technology; Elsevier, 2011; pp 431–499. DOI: 10.1016/B978-0-12-375049-5.00006-2.

(96) Li, X.; Lu, Y.; Wang, H.; Pöselt, E.; Eling, B.; Men, Y. Crystallization of hard segments in MDI/BD-based polyurethanes deformed at elevated temperature and their dependence on the MDI/BD content. *European Polymer Journal* **2017**, *97*, 423–436. DOI: 10.1016/j.eurpolymj.2017.10.014.

(97) Mahmood, S.; Khan, A.; Kant, C.; Chu, C. W.; Katiyar, M.; Lin, H.-C. Transparent, Stretchable, and Self-Healable Gas Barrier Films with 2D Nanoplatelets for Flexible Electronic Device Packaging Applications. *Adv Materials Inter* **2023**, *10* (5). DOI: 10.1002/admi.202202093.

(98) Askeland, D. R. Polymers. In *The Science and Engineering of Materials*; Askeland, D. R., Ed.; Springer US, 1996; pp 488–548. DOI: 10.1007/978-1-4899-2895-5_15.

(99) Sastri, V. R. Materials Used in Medical Devices. In *Plastics in Medical Devices*; Elsevier, 2022; pp 41–64. DOI: 10.1016/B978-0-323-85126-8.00015-1.

(100) Mark, J. E.; Erman, B. *Rubberlike Elasticity*; Cambridge University Press, 2009. DOI: 10.1017/CBO9780511541322.

(101) Fernando, S.; McEnery, M.; Guelcher, S. A. Polyurethanes for bone tissue engineering. In *Advances in Polyurethane Biomaterials*; Elsevier, 2016; pp 481–501. DOI: 10.1016/B978-0-08-100614-6.00016-0.

(102) Engels, H.-W.; Pirkl, H.-G.; Albers, R.; Albach, R. W.; Krause, J.; Hoffmann, A.; Casselmann, H.; Dormish, J. Polyurethanes: versatile materials and sustainable problem solvers for today's challenges. *Angewandte Chemie (International ed. in English)* **2013**, *52* (36), 9422–9441. DOI: 10.1002/anie.201302766. Published Online: Jul. 24, 2013.

(103) Szycher, P. M. *Szycher's Handbook of Polyurethanes, Second Edition*, 2nd ed.; Taylor and Francis, 2013.

(104) Flory, P. J. Molecular Size Distribution in Linear Condensation Polymers 1. *J. Am. Chem. Soc.* **1936**, *58* (10), 1877–1885. DOI: 10.1021/ja01301a016.

(105) Baek, S.; Park, H.; Park, Y.; Kang, H.; Lee, D. Development of a Lidocaine-Loaded Alginate/CMC/PEO Electrospun Nanofiber Film and Application as an Anti-Adhesion Barrier. *Polymers* **2020**, *12* (3). DOI: 10.3390/polym12030618. Published Online: Mar. 8, 2020.

(106) Brown, C. B.; Luciano, A. A.; Martin, D.; Peers, E.; Scrimgeour, A.; diZerega, G. S. Adept (icodextrin 4% solution) reduces adhesions after laparoscopic surgery for adhesiolysis: a double-blind, randomized, controlled study. *Fertility and sterility* **2007**, *88* (5), 1413–1426. DOI: 10.1016/j.fertnstert.2006.12.084. Published Online: Mar. 26, 2007.

(107) Boland, G. M.; Weigel, R. J. Formation and prevention of postoperative abdominal adhesions. *The Journal of surgical research* **2006**, *132* (1), 3–12. DOI: 10.1016/j.jss.2005.12.002. Published Online: Feb. 2, 2006.

(108) Haensig, M.; Mohr, F. W.; Rastan, A. J. Bioresorbable adhesion barrier for reducing the severity of postoperative cardiac adhesions: Focus on REPEL-CV(®). *Medical devices (Auckland, N.Z.)* **2011**, *4*, 17–25. DOI: 10.2147/MDER.S7957. Published Online: Jan. 12, 2011.

(109) Johnson & Johnson Patient Care Inc. Prevention of postsurgical adhesions by INTERCEED(TC7), an absorbable adhesion barrier: a prospective randomized multicenter clinical study. INTERCEED(TC7) Adhesion Barrier Study Group. *Fertility and sterility* **1989**, *51* (6), 933–938.

(110) Haney, A. F.; Doty, E. A barrier composed of chemically cross-linked hyaluronic acid (Incert) reduces postoperative adhesion formation. *Fertility and sterility* **1998**, *70* (1), 145–151. DOI: 10.1016/S0015-0282(98)00116-2.

(111) Ahmad, M.; Crescenti, F. Significant Adhesion Reduction with 4DryField PH after Release of Adhesive Small Bowel Obstruction. *Surgery journal (New York, N.Y.)* **2019**, *5* (1), e28-e34. DOI: 10.1055/s-0039-1687857. Published Online: May. 10, 2019.

(112) Capella-Monsonís, H.; Kearns, S.; Kelly, J.; Zeugolis, D. I. Battling adhesions: from understanding to prevention. *BMC biomedical engineering* **2019**, *1*, 5. DOI: 10.1186/s42490-019-0005-0. Published Online: Feb. 27, 2019.

(113) Ge, L.; Chen, S. Recent Advances in Tissue Adhesives for Clinical Medicine. *Polymers* **2020**, *12* (4). DOI: 10.3390/polym12040939. Published Online: Apr. 18, 2020.

(114) Murdock, M. H.; Chang, J. T.; Luketich, S. K.; Pedersen, D.; Hussey, G. S.; D'Amore, A.; Badylak, S. F. Cytocompatibility and mechanical properties of surgical sealants for cardiovascular applications. *The Journal of thoracic and cardiovascular surgery* **2019**, *157* (1), 176–183. DOI: 10.1016/j.jtcvs.2018.08.043. Published Online: Sep. 1, 2018.

(115) Wallwiener, M.; Brucker, S.; Hierlemann, H.; Brochhausen, C.; Solomayer, E.; Wallwiener, C. Innovative barriers for peritoneal adhesion prevention: liquid or solid? A rat uterine

horn model. *Fertility and sterility* **2006**, *86* (4 Suppl), 1266–1276. DOI: 10.1016/j.fertnstert.2006.05.023.

(116) Banasiewicz, T.; Horbacka, K.; Karoń, J.; Malinger, S.; Antos, F.; Rudzki, S.; Kala, Z.; Stojcev, Z.; Kössi, J.; Krokowicz, P. Preliminary study with SprayShield™ Adhesion Barrier System in the prevention of abdominal adhesions. *Wideochirurgia i inne techniki maloinwazyjne = Videosurgery and other miniinvasive techniques* **2013**, *8* (4), 301–309. DOI: 10.5114/wiitm.2011.34884. Published Online: May. 6, 2013.

(117) Liu, Y.; Shu, X. Z.; Prestwich, G. D. Reduced postoperative intra-abdominal adhesions using Carbylan-SX, a semisynthetic glycosaminoglycan hydrogel. *Fertility and sterility* **2007**, *87* (4), 940–948. DOI: 10.1016/j.fertnstert.2006.07.1532. Published Online: Dec. 8, 2006.

(118) Junge, K.; Klinge, U.; Prescher, A.; Giboni, P.; Niewiera, M.; Schumpelick, V. Elasticity of the anterior abdominal wall and impact for reparation of incisional hernias using mesh implants. *Hernia : the journal of hernias and abdominal wall surgery* **2001**, *5* (3), 113–118. DOI: 10.1007/s100290100019.

(119) Soucasse, A.; Jourdan, A.; Edin, L.; Gillion, J.-F.; Masson, C.; Bege, T. A better understanding of daily life abdominal wall mechanical solicitation: Investigation of intra-abdominal pressure variations by intragastric wireless sensor in humans. *Medical engineering & physics* **2022**, *104*, 103813. DOI: 10.1016/j.medengphy.2022.103813. Published Online: Apr. 27, 2022.

(120) Power, G.; Moore, Z.; O'Connor, T. Measurement of pH, exudate composition and temperature in wound healing: a systematic review. *Journal of wound care* **2017**, *26* (7), 381–397. DOI: 10.12968/jowc.2017.26.7.381.

(121) Schneider, L. A.; Korber, A.; Grabbe, S.; Dissemond, J. Influence of pH on wound-healing: a new perspective for wound-therapy? *Archives of dermatological research* **2007**, *298* (9), 413–420. DOI: 10.1007/s00403-006-0713-x. Published Online: Nov. 8, 2006.

(122) Erdi, M.; Rozyyev, S.; Balabhadrapatruni, M.; Saruwatari, M. S.; Daristotle, J. L.; Ayyub, O. B.; Sandler, A. D.; Kofinas, P. Sprayable tissue adhesive with biodegradation tuned for prevention of postoperative abdominal adhesions. *Bioengineering & translational medicine* **2023**, *8* (1), e10335. DOI: 10.1002/btm2.10335. Published Online: May. 23, 2022.

(123) Lang, J.; Ma, D.; Xiang, Y.; Hua, K.; Liu, K.; Pan, L.; Wang, P.; Yao, S.; Zhao, F.; Cheng, W.; Cui, M.; Guo, H.; Guo, R.; Hong, L.; Li, P.; Liu, M.; Meng, Y.; Wang, H.; Wang, J.; Wang, W.; Wu, M.; Yang, X.; Zhang, J. Chinese expert consensus on the prevention of abdominal pelvic adhesions after gynecological tumor surgeries. *Annals of translational medicine* **2020**, *8* (4), 79. DOI: 10.21037/atm.2020.02.53.

(124) Betro, G. A.; Kaplan, L. J. Abdominal Compartment Syndrome. In *Critical Care Nephrology*; Elsevier, 2009; pp 345–350. DOI: 10.1016/B978-1-4160-4252-5.50065-4.

(125) Deeken, C. R.; Lake, S. P. Mechanical properties of the abdominal wall and biomaterials utilized for hernia repair. *Journal of the mechanical behavior of biomedical materials* **2017**, *74*, 411–427. DOI: 10.1016/j.jmbbm.2017.05.008. Published Online: May. 6, 2017.

(126) Bártolo, P.; Bidanda, B., Eds. *Bio-Materials and Prototyping Applications in Medicine*; Springer US, 2008. DOI: 10.1007/978-0-387-47683-4.

(127) Wang, W.; Wang, C. Polyurethane for biomedical applications: A review of recent developments. In *The Design and Manufacture of Medical Devices*; Elsevier, 2012; pp 115–151. DOI: 10.1533/9781908818188.115.

(128) Kolb, H. C.; Finn, M. G.; Sharpless, K. B. Click Chemistry: Diverse Chemical Function from a Few Good Reactions. *Angewandte Chemie (International ed. in English)* **2001**, *40* (11), 2004–2021. DOI: 10.1002/1521-3773(20010601)40:11<2004:AID-ANIE2004>3.0.CO;2-5.

(129) Yu, F.; Cao, X.; Zeng, L.; Zhang, Q.; Chen, X. An interpenetrating HA/G/CS biomimic hydrogel via Diels-Alder click chemistry for cartilage tissue engineering. *Carbohydrate polymers* **2013**, *97* (1), 188–195. DOI: 10.1016/j.carbpol.2013.04.046. Published Online: Apr. 26, 2013.

(130) Jiang, H.; Qin, S.; Dong, H.; Lei, Q.; Su, X.; Zhuo, R.; Zhong, Z. An injectable and fast-degradable poly(ethylene glycol) hydrogel fabricated via bioorthogonal strain-promoted azide-alkyne cycloaddition click chemistry. *Soft matter* **2015**, *11* (30), 6029–6036. DOI: 10.1039/C5SM00508F. Published Online: Jul. 1, 2015.

(131) Frayne, S. H.; Murthy, R. R.; Northrop, B. H. Investigation and Demonstration of Catalyst/Initiator-Driven Selectivity in Thiol-Michael Reactions. *J. Org. Chem.* **2017**, *82* (15), 7946–7956. DOI: 10.1021/acs.joc.7b01200. Published Online: Jul. 25, 2017.

(132) Srividhya, M.; Lakshmi, M. S.; Reddy, B. S. R. Chemistry of Siloxane Amide as a New Curing Agent for Epoxy Resins: Material Characterization and Properties. *Macro Chemistry & Physics* **2005**, *206* (24), 2501–2511. DOI: 10.1002/macp.200500143.

(133) Tasdelen, M. A. Diels–Alder “click” reactions: recent applications in polymer and material science. *Polym. Chem.* **2011**, *2* (10), 2133. DOI: 10.1039/C1PY00041A.

(134) Clayden, J.; Greeves, N.; Warren, S. G. *Organische Chemie*, 2. Aufl.; Lehrbuch; Springer Spektrum, 2013.

(135) Giofrè, S. V.; Tiecco, M.; Ferlazzo, A.; Romeo, R.; Ciancaleoni, G.; Germani, R.; Iannazzo, D. *Investigation of Base-free Copper-Catalysed Azide–Alkyne Click Cycloadditions (CuAAc) in Natural Deep Eutectic Solvents as Green and Catalytic Reaction Media*, 2021. DOI: 10.26434/chemrxiv.13372574.v4.

(136) Presolski, S. I.; Hong, V. P.; Finn, M. G. Copper-Catalyzed Azide-Alkyne Click Chemistry for Bioconjugation. *Current protocols in chemical biology* **2011**, *3* (4), 153–162. DOI: 10.1002/9780470559277.ch110148. Published Online: Dec. 1, 2011.

(137) Worrell, B. T.; Malik, J. A.; Fokin, V. V. Direct evidence of a dinuclear copper intermediate in Cu(I)-catalyzed azide-alkyne cycloadditions. *Science (New York, N.Y.)* **2013**, *340* (6131), 457–460. DOI: 10.1126/science.1229506. Published Online: Apr. 4, 2013.

(138) Wu, Z.-G.; Liao, X.-J.; Yuan, L.; Wang, Y.; Zheng, Y.-X.; Zuo, J.-L.; Pan, Y. Visible-Light-Mediated Click Chemistry for Highly Regioselective Azide-Alkyne Cycloaddition by a Photoredox Electron-Transfer Strategy. *Chemistry (Weinheim an der Bergstrasse, Germany)* **2020**, *26* (25), 5694–5700. DOI: 10.1002/chem.202000252. Published Online: Apr. 17, 2020.

(139) Han, S.-S.; Yoon, H. Y.; Yhee, J. Y.; Cho, M. O.; Shim, H.-E.; Jeong, J.-E.; Lee, D.-E.; Kim, K.; Guim, H.; Lee, J. H.; Huh, K. M.; Kang, S.-W. In situ cross-linkable hyaluronic acid hydrogels using copper free click chemistry for cartilage tissue engineering. *Polym. Chem.* **2018**, *9* (1), 20–27. DOI: 10.1039/c7py01654a.

(140) Schrag, M.; Mueller, C.; Oyoyo, U.; Smith, M. A.; Kirsch, W. M. Iron, zinc and copper in the Alzheimer's disease brain: a quantitative meta-analysis. Some insight on the influence of citation bias on scientific opinion. *Progress in neurobiology* **2011**, *94* (3), 296–306. DOI: 10.1016/j.pneurobio.2011.05.001. Published Online: May. 11, 2011.

(141) Hatano, R.; Ebara, M.; Fukuda, H.; Yoshikawa, M.; Sugiura, N.; Kondo, F.; Yukawa, M.; Saisho, H. Accumulation of copper in the liver and hepatic injury in chronic hepatitis C. *Journal of gastroenterology and hepatology* **2000**, *15* (7), 786–791. DOI: 10.1046/j.1440-1746.2000.02199.x.

(142) Hoyle, C. E.; Bowman, C. N. Thiol-ene click chemistry. *Angewandte Chemie (International ed. in English)* **2010**, *49* (9), 1540–1573. DOI: 10.1002/anie.200903924.

(143) Chen, J.; Nichols, B. L. B.; Norris, A. M.; Frazier, C. E.; Edgar, K. J. All-Polysaccharide, Self-Healing Injectable Hydrogels Based on Chitosan and Oxidized Hydroxypropyl Polysaccharides. *Biomacromolecules* **2020**, *21* (10), 4261–4272. DOI: 10.1021/acs.biomac.0c01046. Published Online: Sep. 8, 2020.

(144) Dorfman, L. M. Fast Reaction Studies of Organic Ions in Solution. In *Fast Reactions in Energetic Systems*; Capellos, C., Walker, R. F., Eds.; Springer Netherlands, 1981; pp 95–109. DOI: 10.1007/978-94-009-8511-7_7.

(145) Kleppmann, W. *Taschenbuch Versuchsplanung*:*Produkte und Prozesse optimieren*, 7., aktualisierte u. erw. Aufl.; Praxisreihe Qualitätswissen; Hanser, 2011.

(146) Wasserstein, R. L.; Lazar, N. A. The ASA Statement on p -Values: Context, Process, and Purpose. *The American Statistician* **2016**, *70* (2), 129–133. DOI: 10.1080/00031305.2016.1154108.

(147) Stat-Ease. *Design Expert V11*:*ANOVA Output*. https://www.statease.com/docs/v11/contents/analysis/anova-output/ (accessed 2024-02-20).

(148) Anderson, M. J.; Whitcomb, P. J. *DOE simplified*:*Practical tools for effective experimentation*, Third edition; Productivity Press, 2017.

(149) Stat-Ease. *Design Expert V11*:*Box Cox Plot*. https://www.statease.com/docs/v11/contents/analysis/box-cox-plot/#box-cox-plot (accessed 2024-02-20).

(150) Stat-Ease. *Design Expert V11*:*Response Transformations*. https://www.statease.com/docs/v11/contents/analysis/response-transformations/ (accessed 2024-02-20).

(151) Flory, P. J. Molecular Size Distribution in Three Dimensional Polymers. II. Trifunctional Branching Units. *J. Am. Chem. Soc.* **1941**, *63* (11), 3091–3096. DOI: 10.1021/ja01856a062.

(152) Macosko, C. W.; Miller, D. R. A new derivation of average molecular weights of nonlinear polymers. *Macromolecules* **1976**, *9* (2), 199–206. DOI: 10.1021/ma60050a003.

(153) Rimdusit, S.; Bangsen, W.; Kasemsiri, P. Chemorheology and thermomechanical characteristics of benzoxazine-urethane copolymers. *J of Applied Polymer Sci* **2011**, *121* (6), 3669–3678. DOI: 10.1002/app.34170.

(154) Rufino, V. C.; Pliego, J. R. Carboxylic acid catalysis on the imine formation versus aza-Michael reaction in apolar aprotic solvent. *J of Physical Organic Chem* **2023**, *36* (3). DOI: 10.1002/poc.4467.

(155) Sayer, J. M.; Peskin, M.; Jencks, W. P. Imine-Forming Elimination Reactions. I. General Base Acid Catalysis and Influence of the Nitrogen Substituent on Rates and Equilibria for Carbinolamine Dehydration. *J. Am. Chem. Soc.* **1973**, *95* (13), 4277–4287. DOI: 10.1021/ja00794a600.

(156) Yang, H.; Fustin, C.-A. Design and Applications of Dynamic Hydrogels Based on Reversible C═N Bonds. *Macro Chemistry & Physics* **2023**, *224* (20). DOI: 10.1002/macp.202300211.

(157) Nielsen, A. T.; Lawrence, G. W. 1,2-Bis(2-hydroxyethyl)hydrazine and derivatives. *J. Org. Chem.* **1977**, *42* (17), 2900–2902. DOI: 10.1021/jo00437a026.

(158) Pannone, M. C.; Macosko, C. W. Kinetics of isocyanate amine reactions. *J of Applied Polymer Sci* **1987**, *34* (7), 2409–2432. DOI: 10.1002/app.1987.070340707.

(159) Smith, B. C. Infrared Spectroscopy of Polymers XIII: Polyurethanes. *Spectroscopy* **2023**, 14–16. DOI: 10.56530/spectroscopy.fn3378a3.

(160) Wenhao, Z. Influence of Temperature and Concentration on Viscosity of Complex Fluids. *J. Phys.: Conf. Ser.* **2021**, *1965* (1), 12064. DOI: 10.1088/1742-6596/1965/1/012064.

(161) Dulong, V.; Mocanu, G.; Picton, L.; Le Cerf, D. Amphiphilic and thermosensitive copolymers based on pullulan and Jeffamine®: Synthesis, characterization and physicochemical properties. *Carbohydrate polymers* **2012**, *87* (2), 1522–1531. DOI: 10.1016/j.carbpol.2011.09.049.

(162) Madau, M.; Le Cerf, D.; Dulong, V.; Picton, L. Hyaluronic Acid Functionalization with Jeffamine® M2005: A Comparison of the Thermo-Responsiveness Properties of the Hydrogel Obtained through Two Different Synthesis Routes. *Gels (Basel, Switzerland)* **2021**, *7* (3). DOI: 10.3390/gels7030088. Published Online: Jul. 9, 2021.

(163) Agrawal, C. M.; Athanasiou, K. A. Technique to control pH in vicinity of biodegrading PLA-PGA implants. *J. Biomed. Mater. Res.* **1997**, *38* (2), 105–114. DOI: 10.1002/(SICI)1097-4636(199722)38:2<105:AID-JBM4>3.0.CO;2-U.

(164) Huber, T.; Starling, K.; Cen, W.; Fee, C.; Dimartino, S. Effect of Urea Concentration on the Viscosity and Thermal Stability of Aqueous NaOH/Urea Cellulose Solutions. *Journal of Polymers* **2016**, *2016*, 1–9. DOI: 10.1155/2016/2658747.

(165) Bennison LR, Miller CN, Summers RJ, Minnis AMB, Sussman G & McGuiness W. The pH of wounds during healing and infection: a descriptive literature review. *Wound Practice & Research: Journal of the Australian Wound Management Association,* **2017** (Vol. 25, No. 2), 63-39.

(166) BULL, H. B.; BREESE, K.; FERGUSON, G. L.; SWENSON, C. A. THE PH OF UREA SOLUTIONS. *Archives of biochemistry and biophysics* **1964**, *104*, 297–304. DOI: 10.1016/S0003-9861(64)80017-5.

(167) Karakyriazis, K.; Lührs, V.; Stößlein, S.; Grunwald, I.; Hartwig, A. Synthesis and characterization of a Schiff base crosslinked hydrogel based on hyperbranched polyglycerol. *Mater. Adv.* **2023**, *4* (7), 1648–1655. DOI: 10.1039/D2MA01050J.

(168) Sheng, J. J.; McNamara, D. P.; Amidon, G. L. Toward an in vivo dissolution methodology: a comparison of phosphate and bicarbonate buffers. *Molecular pharmaceutics* **2009**, *6* (1), 29–39. DOI: 10.1021/mp800148u.

(169) Naito, T.; Shinagawa, T.; Nishimoto, T.; Takanabe, K. Water Electrolysis in Saturated Phosphate Buffer at Neutral pH. *ChemSusChem* **2020**, *13* (22), 5921–5933. DOI: 10.1002/cssc.202001886. Published Online: Sep. 17, 2020.

(170) Samuelsen, L.; Holm, R.; Lathuile, A.; Schönbeck, C. Buffer solutions in drug formulation and processing: How pKa values depend on temperature, pressure and ionic strength. *International journal of pharmaceutics* **2019**, *560*, 357–364. DOI: 10.1016/j.ijpharm.2019.02.019. Published Online: Feb. 22, 2019.

(171) Junginger, M.; Horny, J. Hydrogel Matrix Having Increased Absorption Capacity for Liquids.

(172) Prasad, K. Peripheral Circulation and Its Control Mechanism. In *Textbook of Angiology*; Chang, J. B., Ed.; Springer New York, 2000; pp 39–45. DOI: 10.1007/978-1-4612-1190-7_3.

(173) Lazzari, S.; Codari, F.; Storti, G.; Morbidelli, M.; Moscatelli, D. Modeling the pH-dependent PLA oligomer degradation kinetics. *Polymer Degradation and Stability* **2014**, *110*, 80–90. DOI: 10.1016/j.polymdegradstab.2014.08.012.

(174) Cornish-Bowden, A. *Fundamentals of Enzyme Kinetics*, 4. Auflage; Wiley-VCH, 2013.

(175) Cretu, A.; Kuckling, D.; Adler, H.-J. Hydrophilic – Hydrophobic Polymers Based on Poly(L-lactide) and Poly(2-Hydroxyethyl Methacrylate). *MSF* **2004**, *455-456*, 425–428. DOI: 10.4028/www.scientific.net/MSF.455-456.425.

(176) Seera, S. D. K.; Kundu, D.; Banerjee, T. Physical and chemical crosslinked microcrystalline cellulose-polyvinyl alcohol hydrogel: freeze–thaw mediated synthesis, characterization and in vitro delivery of 5-fluorouracil. *Cellulose* **2020**, *27* (11), 6521–6535. DOI: 10.1007/s10570-020-03249-9.

(177) Ostroha, J.; Pong, M.; Lowman, A.; Dan, N. Controlling the collapse/swelling transition in charged hydrogels. *Biomaterials* **2004**, *25* (18), 4345–4353. DOI: 10.1016/j.biomaterials.2003.11.019.

(178) Liparoti, S.; Iozzino, V.; Speranza, V.; Pantani, R. Modulating poly(lactic acid) degradation rate for environmentally sustainable applications. *Waste management (New York, N.Y.)* **2024**, *175*, 215–224. DOI: 10.1016/j.wasman.2024.01.004. Published Online: Jan. 12, 2024.

(179) Iglesias-Martinez, E.; Brandariz, I.; Penedo, F. Ester hydrolysis and nitrosative deamination of novocaine in aqueous solutions. *Chemical research in toxicology* **2006**, *19* (4), 594–600. DOI: 10.1021/tx060013b.

(180) Lau, C. M. L.; Jahanmir, G.; Chau, Y. Local environment-dependent kinetics of ester hydrolysis revealed by direct 1H NMR measurement of degrading hydrogels. *Acta biomaterialia* **2020**, *101*, 219–226. DOI: 10.1016/j.actbio.2019.10.030. Published Online: Oct. 25, 2019.

(181) Liao, X.; Li, H.; Cheng, Y.; Chen, N.; Li, C.; Yang, Y. Process performance of high-solids batch anaerobic digestion of sewage sludge. *Environmental technology* **2014**, *35* (21-24), 2652–2659. DOI: 10.1080/09593330.2014.916756. Published Online: May. 20, 2014.

(182) Zengwen, C.; Pan, H.; chen, Y.; Bian, J.; Han, L.; Zhang, H.; Dong, L.; Yang, Y. Transform poly (lactic acid) packaging film from brittleness to toughness using traditional industrial equipments. *Polymer* **2019**, *180*, 121728. DOI: 10.1016/j.polymer.2019.121728.

(183) El-Hadi, A. M. Increase the elongation at break of poly (lactic acid) composites for use in food packaging films. *Scientific reports* **2017**, *7*, 46767. DOI: 10.1038/srep46767. Published Online: May. 3, 2017.

(184) Feng, L.; Bian, X.; Li, G.; Chen, Z.; Cui, Y.; Chen, X. Determination of ultra-low glass transition temperature via differential scanning calorimetry. *Polymer Testing* **2013**, *32* (8), 1368–1372. DOI: 10.1016/j.polymertesting.2013.08.015.

(185) Zhang, H.; Huang, X.; Jiang, J.; Shang, S.; Song, Z. Hydrogels with high mechanical strength cross-linked by a rosin-based crosslinking agent. *RSC Adv.* **2017**, *7* (67), 42541–42548. DOI: 10.1039/c7ra08024g.

(186) Choi, W. S.; Patel, D.; Han, J. H. Effects of pH and Salts on Physical and Mechanical Properties of Pea Starch Films. *Journal of Food Science* **2016**, *81* (7). DOI: 10.1111/1750-3841.13342.

(187) Li, F.-J.; Liang, J.-Z.; Zhang, S.-D.; Zhu, B. Tensile Properties of Polylactide/Poly(ethylene glycol) Blends. *J Polym Environ* **2015**, *23* (3), 407–415. DOI: 10.1007/s10924-015-0718-7.

(188) Yang, J.; Bai, R.; Chen, B.; Suo, Z. Hydrogel Adhesion: A Supramolecular Synergy of Chemistry, Topology, and Mechanics. *Adv Funct Materials* **2020**, *30* (2). DOI: 10.1002/adfm.201901693.

(189) Kortenbrede, L.; Heider, J.; Heckroth, H.; Leimenstoll, M.; Steuer, H.; Sütterlin, J.; Weise, F.; Hokamp, T. Development and Characterization of Biodegradable Polyurethane-Urea-based Hydrogels for the Prevention of Postoperative Peritoneal Adhesions. *ACS Omega* **2024**, (submitted).

(190) Stockmayer, W. H. Molecular distribution in condensation polymers. *J. Polym. Sci.* **1952**, *9* (1), 69–71. DOI: 10.1002/pol.1952.120090106.

(191) Simões, A.; Miranda, M.; Cardoso, C.; Vitorino, F. V. a. Rheology by Design: A Regulatory Tutorial for Analytical Method Validation. *Pharmaceutics* **2020**, *12* (9). DOI: 10.3390/pharmaceutics12090820. Published Online: Aug. 28, 2020.

(192) Brandes, R.; Lang, F.; Schmidt, R. F. *Physiologie des Menschen*; Springer Berlin Heidelberg, 2019. DOI: 10.1007/978-3-662-56468-4.

(193) Roksnoer, L. C. W.; Heijnen, B. F. J.; Nakano, D.; Peti-Peterdi, J.; Walsh, S. B.; Garrelds, I. M.; van Gool, J. M. G.; Zietse, R.; Struijker-Boudier, H. A. J.; Hoorn, E. J.; Danser, A. H. J. On the Origin of Urinary Renin: A Translational Approach. *Hypertension (Dallas, Tex. : 1979)* **2016**, *67* (5), 927–933. DOI: 10.1161/HYPERTENSIONAHA.115.07012. Published Online: Feb. 29, 2016.

(194) Peppas, N. A.; Bures, P.; Leobandung, W.; Ichikawa, H. Hydrogels in pharmaceutical formulations. *European journal of pharmaceutics and biopharmaceutics : official journal of Arbeitsgemeinschaft fur Pharmazeutische Verfahrenstechnik e.V* **2000**, *50* (1), 27–46. DOI: 10.1016/s0939-6411(00)00090-4.

(195) Allen, F. H.; Kennard, O.; Watson, D. G.; Brammer, L.; Orpen, A. G.; Taylor, R. Tables of bond lengths determined by X-ray and neutron diffraction. Part 1. Bond lengths in organic compounds. *J. Chem. Soc., Perkin Trans. 2* **1987** (12), S1. DOI: 10.1039/P298700000S1.

(196) Brandl, F.; Kastner, F.; Gschwind, R. M.; Blunk, T.; Tessmar, J.; Göpferich, A. Hydrogel-based drug delivery systems: comparison of drug diffusivity and release kinetics. *Journal of controlled release : official journal of the Controlled Release Society* **2010**, *142* (2), 221–228. DOI: 10.1016/j.jconrel.2009.10.030. Published Online: Nov. 1, 2009.

(197) an Gong; Min, M. Measuring the size and growth of single cells. *Biophysics reports* **2022**, *8* (3), 150–157. DOI: 10.52601/bpr.2022.210036.

(198) Vander, A. J.; Sherman, J. H.; Luciano, D. S. *Human physiology*:*The mechanisms of body function, 6th ed*, 6th ed.; New York; McGraw-Hill, 1994.

(199) Robert A. Freitas Jr. *Nanomedicine, Volume I: Basic Capabilities*; Landes Bioscience, 1999.

(200) Riedel, E.; Janiak, C. *Anorganische Chemie*, 10. Auflage; De Gruyter Studium; De Gruyter, 2022. DOI: 10.1515/9783110694444.

(201) Huntsman. *The JEFFAMINE® Polyetheramines*. https://www.yumpu.com/en/document/view/148618/jeffaminer-polyetheramines (accessed 2024-05-07).

(202) Aslan, M.; Hsu, E.-C.; Liu, S.; Stoyanova, T. Quantifying the invasion and migration ability of cancer cells with a 3D Matrigel drop invasion assay. *Biology methods & protocols* **2021**, *6* (1), bpab014. DOI: 10.1093/biomethods/bpab014. Published Online: Jul. 21, 2021.

(203) Lih, E.; Oh, S. H.; Joung, Y. K.; Lee, J. H.; Han, D. K. Polymers for cell/tissue anti-adhesion. *Progress in Polymer Science* **2015**, *44*, 28–61. DOI: 10.1016/j.progpolymsci.2014.10.004.

(204) Singh, A. K. Structure, Synthesis, and Application of Nanoparticles. In *Engineered Nanoparticles*; Elsevier, 2016; pp 19–76. DOI: 10.1016/B978-0-12-801406-6.00002-9.

(205) Xiao, K.; Wang, Z.; Wu, Y.; Lin, W.; He, Y.; Zhan, J.; Luo, F.; Li, Z.; Li, J.; Tan, H.; Fu, Q. Biodegradable, anti-adhesive and tough polyurethane hydrogels crosslinked by triol crosslinkers. *Journal of biomedical materials research. Part A* **2019**, *107* (10), 2205–2221. DOI: 10.1002/jbm.a.36730. Published Online: Jun. 6, 2019.

(206) Yu, H. C.; Zhang, H.; Ren, K.; Ying, Z.; Zhu, F.; Qian, J.; Ji, J.; Wu, Z. L.; Zheng, Q. Ultrathin κ-Carrageenan/Chitosan Hydrogel Films with High Toughness and Antiadhesion Property. *ACS applied materials & interfaces* **2018**, *10* (10), 9002–9009. DOI: 10.1021/acsami.7b18343. Published Online: Feb. 28, 2018.

(207) Chou, P.-Y.; Chen, S.-H.; Chen, C.-H.; Chen, S.-H.; Fong, Y. T.; Chen, J.-P. Thermo-responsive in-situ forming hydrogels as barriers to prevent post-operative peritendinous adhesion. *Acta biomaterialia* **2017**, *63*, 85–95. DOI: 10.1016/j.actbio.2017.09.010. Published Online: Sep. 12, 2017.

(208) Solbu, A. A.; Caballero, D.; Damigos, S.; Kundu, S. C.; Reis, R. L.; Halaas, Ø.; Chahal, A. S.; Strand, B. L. Assessing cell migration in hydrogels: An overview of relevant materials and methods. *Materials today. Bio* **2023**, *18*, 100537. DOI: 10.1016/j.mtbio.2022.100537. Published Online: Dec. 29, 2022.

(209) Lv, B.; Guo, B.; Zhou, Z.; Jing, G. Mechanisms of CO2 Capture into Monoethanolamine Solution with Different CO2 Loading during the Absorption/Desorption Processes. *Environmental science & technology* **2015**, *49* (17), 10728–10735. DOI: 10.1021/acs.est.5b02356. Published Online: Aug. 13, 2015.

(210) Lee, A. S.; Kitchin, J. R. Chemical and Molecular Descriptors for the Reactivity of Amines with CO 2. *Ind. Eng. Chem. Res.* **2012**, *51* (42), 13609–13618. DOI: 10.1021/ie301419q.

(211) Perinu, C.; Arstad, B.; Jens, K.-J. 13C NMR Experiments and Methods used to Investigate Amine-CO2-H2O Systems. *Energy Procedia* **2013**, *37*, 7310–7317. DOI: 10.1016/j.egypro.2013.06.669.

(212) Görög, S. Derivatization of Analytes. In *Encyclopedia of Analytical Science*; Elsevier, 2005; pp 263–273. DOI: 10.1016/B0-12-369397-7/00739-1.

(213) Mulana, F.; Munawar, E.; Heldiana, H.; Rahmi, M. The effect of carbon dioxide gas pressure on solubility, density and pH of carbon dioxide – Water mixtures. *Materials Today: Proceedings* **2022**, *63*, S46-S49. DOI: 10.1016/j.matpr.2022.01.033.

(214) Bello, D.; Herrick, C. A.; Smith, T. J.; Woskie, S. R.; Streicher, R. P.; Cullen, M. R.; Liu, Y.; Redlich, C. A. Skin exposure to isocyanates: reasons for concern. *Environmental health perspectives* **2007**, *115* (3), 328–335. DOI: 10.1289/ehp.9557. Published Online: Nov. 28, 2006.

(215) Bigatti, G.; Segers, N.; Boeckx, W.; Gruft, L.; Mariani, A.; Brosens, I. Evaluation of recombinant tissue-type plasminogen activator in adhesion prevention and neoangiogenesis in a rat experimental adhesion model. *Gynecol Surg* **2006**, *3* (3), 175–179. DOI: 10.1007/s10397-005-0170-0.

(216) Zühlke, H. V.; Lorenz, E. M.; Straub, E. M.; Savvas, V. Pathophysiologie und Klassifikation von Adhäsionen. *Langenbecks Archiv fur Chirurgie. Supplement II, Verhandlungen der Deutschen Gesellschaft fur Chirurgie. Deutsche Gesellschaft fur Chirurgie. Kongress* **1990**, 1009–1016.

(217) Henriette Jülke. *HYGEL4MIC Examination of local intraabdominal adhesion prophylaxis and biocompatibility in rabbit*:*NON-GLP study*.

(218) Raquel Vallejo Garcia. *HYGEL4MIC Examination of local intraabdominal adhesion prophylaxis and biocompatibility in rabbit*:*Histopathology Examination*.

(219) Huang, Q.-S.; Yan, Z.-F.; Chen, X.-Q.; Du, Y.-Y.; Li, J.; Liu, Z.-Z.; Xia, W.; Chen, S.; Wu, J. Accelerated biodegradation of polyethylene terephthalate by Thermobifida fusca cutinase mediated by Stenotrophomonas pavanii. *The Science of the total environment* **2022**, *808*, 152107. DOI: 10.1016/j.scitotenv.2021.152107. Published Online: Dec. 2, 2021.

(220) Greener, B.; Hughes, A. A.; Bannister, N. P.; Douglass, J. Proteases and pH in chronic wounds. *Journal of wound care* **2005**, *14* (2), 59–61. DOI: 10.12968/jowc.2005.14.2.26739.

(221) Henriette Jülke. *HYGEL4MIC Evaluation of local biocompatibility and initial degradation pattern following subcutaneous implantation in rabbit*:*NON-GLP study*.

(222) Da Silva, D.; Kaduri, M.; Poley, M.; Adir, O.; Krinsky, N.; Shainsky-Roitman, J.; Schroeder, A. Biocompatibility, biodegradation and excretion of polylactic acid (PLA) in medical implants and theranostic systems. *Chemical engineering journal (Lausanne, Switzerland : 1996)* **2018**, *340*, 9–14. DOI: 10.1016/j.cej.2018.01.010. Published Online: Jan. 3, 2018.

(223) Peng, T.; Shi, Q.; Chen, M.; Yu, W.; Yang, T. Antibacterial-Based Hydrogel Coatings and Their Application in the Biomedical Field-A Review. *Journal of functional biomaterials* **2023**, *14* (5). DOI: 10.3390/jfb14050243. Published Online: Apr. 25, 2023.

(224) Geevarghese, R.; Sajjadi, S. S.; Hudecki, A.; Sajjadi, S.; Jalal, N. R.; Madrakian, T.; Ahmadi, M.; Włodarczyk-Biegun, M. K.; Ghavami, S.; Likus, W.; Siemianowicz, K.; Łos, M. J. Biodegradable and Non-Biodegradable Biomaterials and Their Effect on Cell Differentiation. *International journal of molecular sciences* **2022**, *23* (24). DOI: 10.3390/ijms232416185. Published Online: Dec. 19, 2022.

(225) Hofmann, J.; Ehlers, S.; Klinksiek, B.; Fechtel, T.; Ruhland, M.; Scholz, J.; Föhles, F.; Esser, U. Method for Producing Double Metal Cyanide (DMC) Catalysts.

Appendix

Prepolymer-1

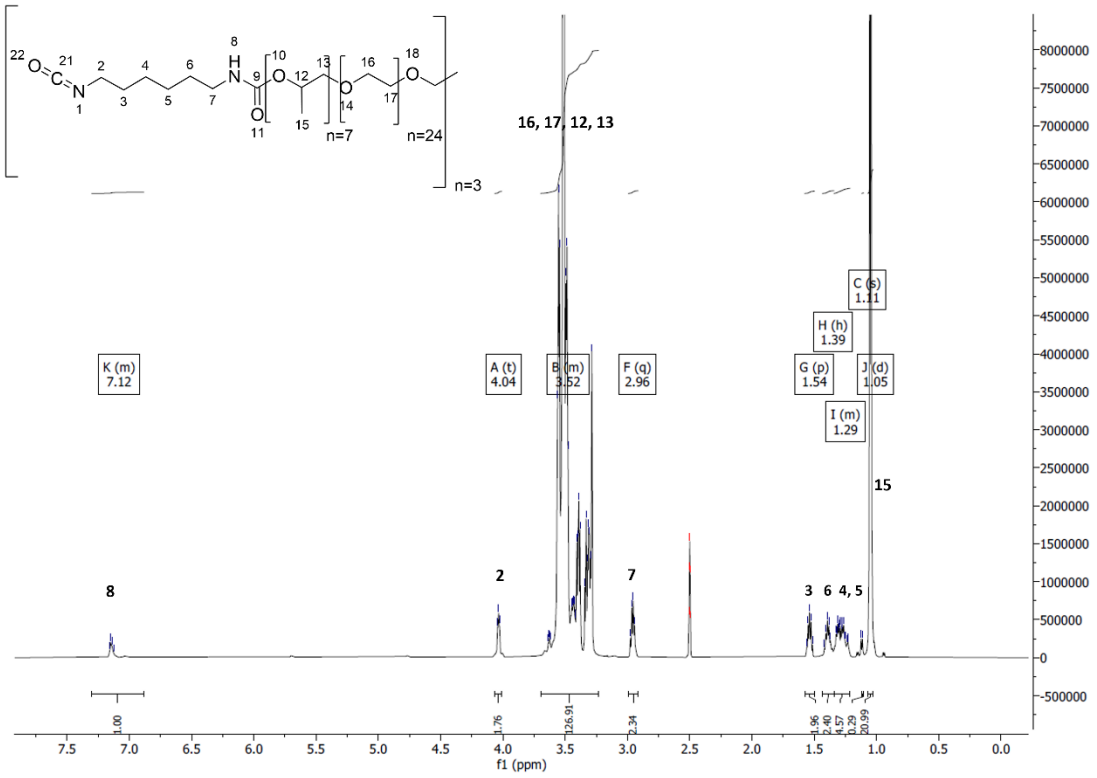

Figure-Appendix 1 ^{1}H NMR spectra of **prepolymer-1** in d_6DMSO.

(EtOR)$_2$-2

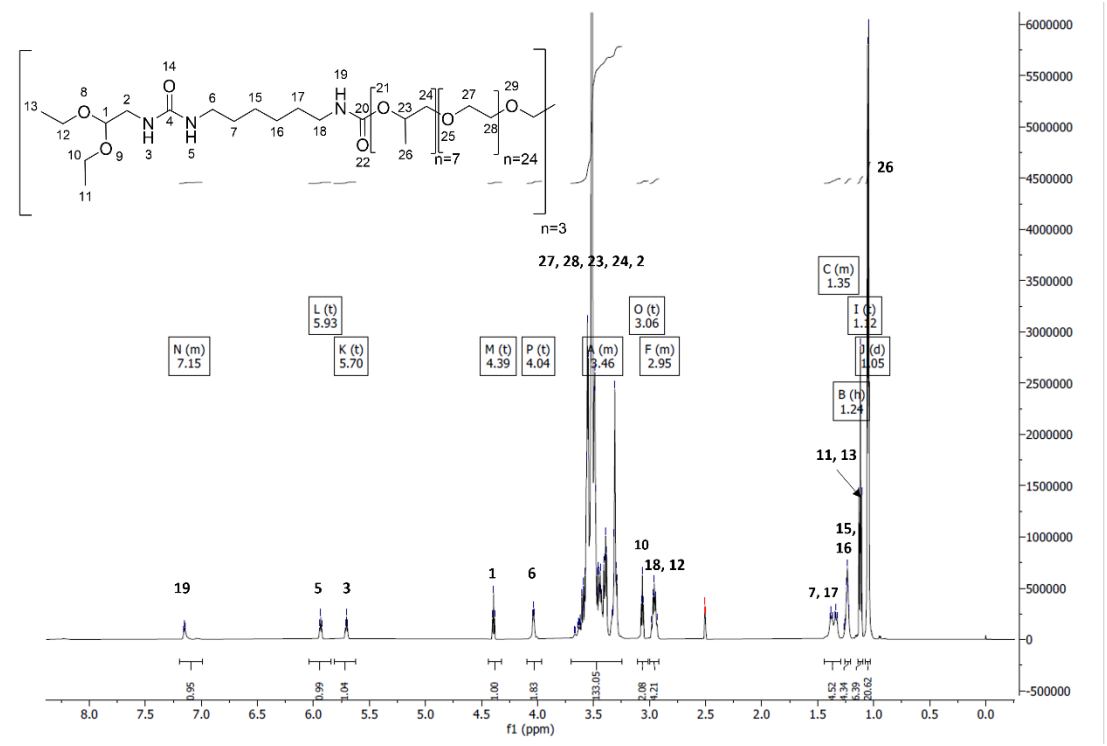

Figure-Appendix 2 ^{1}H NMR spectra of **(EtOR)$_2$-2** in d_6DMSO.

COO-2

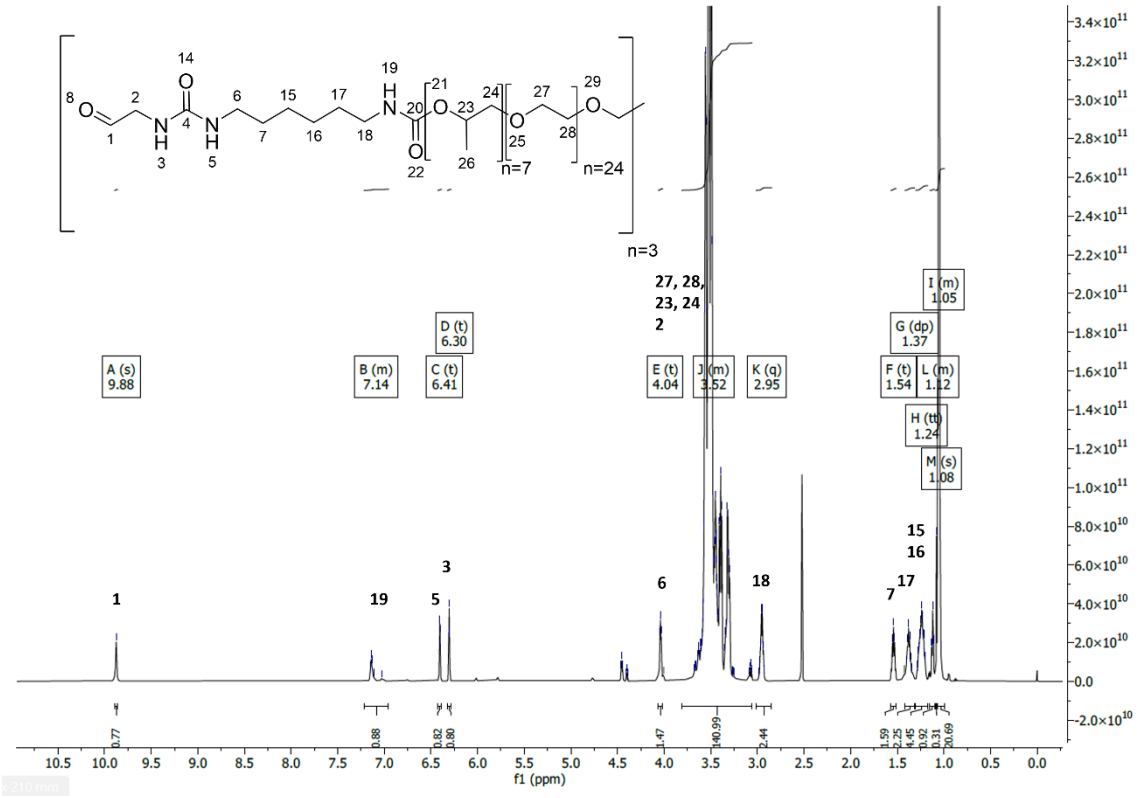

Figure-Appendix 3 ^{1}H NMR spectra of **COO-2** in d_6DMSO.

Erklärung zur Dissertation

Hiermit versichere ich an Eides statt, dass ich die vorliegende Dissertation selbstständig und ohne die Benutzung anderer als der angegebenen Hilfsmittel und Literatur angefertigt habe. Alle Stellen, die wörtlich oder sinngemäß aus veröffentlichten und nicht veröffentlichten Werken dem Wortlaut oder dem Sinn nach entnommen wurden, sind als solche kenntlich gemacht. Ich versichere an Eides statt, dass diese Dissertation noch keiner anderen Fakultät oder Universität zur Prüfung vorgelegen hat; dass sie - abgesehen von unten angegebenen Teilpublikationen und eingebundenen Artikeln und Manuskripten - noch nicht veröffentlicht worden ist sowie, dass ich eine Veröffentlichung der Dissertation vor Abschluss der Promotion nicht ohne Genehmigung des Promotionsausschusses vornehmen werde. Die Bestimmungen dieser Ordnung sind mir bekannt. Darüber hinaus erkläre ich hiermit, dass ich die Ordnung zur Sicherung guter wissenschaftlicher Praxis und zum Umgang mit wissenschaftlichem Fehlverhalten der Universität zu Köln gelesen und sie bei der Durchführung der Dissertation zugrundeliegenden Arbeiten und der schriftlich verfassten Dissertation beachtet habe und verpflichte mich hiermit, die dort genannten Vorgaben bei allen wissenschaftlichen Tätigkeiten zu beachten und umzusetzen. Ich versichere, dass die eingereichte elektronische Fassung der eingereichten Druckfassung vollständig entspricht.

Publications and Patents

- Kortenbrede, L.; Heider, J.; Heckroth, H.; Leimenstoll, M.; Steuer, H.; Sütterlin, J.; Weise, F.; Hokamp, T. Development and Characterization of Biodegradable Polyurethane-Urea-based Hydrogels for the Prevention of Postoperative Peritoneal Adhesions. ACS Omega 2024 Jul 25;9(31):34008-34020. DOI: 10.1021/acsomega.4c04577.
- Kortenbrede, L., Heckroth, H. & Sütterlin, J. Method of manufacturing a hydrogel useful for preventing post-surgical adhesions, WO2024132836 A1.

Conferences

- Kortenbrede, L., presentation of “Fast-curing, sprayable polyurethane-urea hydrogels as postoperative adhesion barriers- a journey from bench to kidney”, Covestro TechDay, 13.12.2021 (online).
- Kortenbrede, L., Sütterlin, J., Heckroth, H., Griesbeck, A. & Leimenstoll, M. Poster presentation of “Development of a requirement profile for *in situ* crosslinking hydrogels as adhesion prophylaxis and possible reaction types to fulfill these, Poster Symposium Cologne Graduated School Chemistry, Köln 24.05.2022.
- Kortenbrede, L., presentation of „Hydrogel-Werkstoffe für die minimal invasive Chirugie zur Vermeidung von Adhäsionen“. At BMBF Technologiegespräch: „Materialinnovationen für die Medizintechnik 2023“, Düsseldorf 14.11.2023.

Die Primärdaten dieser Arbeit sind auf dem Server der Covestro Deutschland AG abgesichert.

Köln, 30.06.2024

Curriculum Vitae

Lana Kortenbrede

*02.06.1993

EDUCATION

03/2021-08/2024	**PhD Student in the group of Prof. Dr. Axel Griesbeck, University of Cologne in cooperation with Cologne University of Applied Science and Covestro Deutschland AG** Development of *in situ* fast curing polyurethane-urea hydrogels for medical applications
09/2018-02/2021	**M.Sc. Drug Discovery and Development at University of Cologne and Cologne University of Applied Science** Master thesis: Investigation of thermoplastic polyurethanes for medical implants
09/2014-08/2018	**B.Sc. Pharmaceutical Chemistry at Cologne University of Applied Science** Bachelor thesis: Optimization of a Diels-Alder based synthesis approach for derivatives of ketamine
08/2011-07/2014	**Berufskolleg Ehrenfeld, Cologne** Advanced technical college certificate, focus: chemistry and home economics

EXPERIENCE

Since 09/2024	**Head of Product Development at LANXESS Deutschland GmbH, Leverkusen** Laboratory Head for ion exchangers and adsorbers
03/2021-08/2024	**PhD Student at Covestro Deutschland AG, Leverkusen** Medical implants, fast crosslinking hydrogels
09/2020-02/2021	**Master Thesis at Covestro Deutschland AG, Dormagen** Development of thermoplastic polyurethanes for active ingredient containing implants (drug delivery approaches)
09/2019-11/2019	**Internship at ClinAssess GmbH** Insights into a clinical research organization: monitoring, data management, biometrics, pharmacovigilance